



UNIL | Université de Lausanne

Unicentre

CH-1015 Lausanne

<http://serval.unil.ch>

---

Year : 2021

## Molecular mechanisms underlying PIFmediated growth responses

Ince Yetkin Çaka

Ince Yetkin Çaka, 2021, Molecular mechanisms underlying PIFmediated growth responses

Originally published at : Thesis, University of Lausanne

Posted at the University of Lausanne Open Archive <http://serval.unil.ch>

Document URN : urn:nbn:ch:serval-BIB\_8D2A12541D7B1

### **Droits d'auteur**

L'Université de Lausanne attire expressément l'attention des utilisateurs sur le fait que tous les documents publiés dans l'Archive SERVAL sont protégés par le droit d'auteur, conformément à la loi fédérale sur le droit d'auteur et les droits voisins (LDA). A ce titre, il est indispensable d'obtenir le consentement préalable de l'auteur et/ou de l'éditeur avant toute utilisation d'une oeuvre ou d'une partie d'une oeuvre ne relevant pas d'une utilisation à des fins personnelles au sens de la LDA (art. 19, al. 1 lettre a). A défaut, tout contrevenant s'expose aux sanctions prévues par cette loi. Nous déclinons toute responsabilité en la matière.

### **Copyright**

The University of Lausanne expressly draws the attention of users to the fact that all documents published in the SERVAL Archive are protected by copyright in accordance with federal law on copyright and similar rights (LDA). Accordingly it is indispensable to obtain prior consent from the author and/or publisher before any use of a work or part of a work for purposes other than personal use within the meaning of LDA (art. 19, para. 1 letter a). Failure to do so will expose offenders to the sanctions laid down by this law. We accept no liability in this respect.



UNIL | Université de Lausanne

Faculté de biologie  
et de médecine

Centre Intégréatif de Génomique

# Molecular mechanisms underlying PIF-mediated growth responses

Thèse de doctorat

présentée à la

Faculté de biologie et de médecine de l'Université de Lausanne

pour l'obtention du grade de

Docteur ès sciences de la vie (PhD)

par

**Yetkin Çaka INCE**

Master of Science, Middle East Technical University, Turquie

**Directeur de thèse**

Prof. Christian Fankhauser

**Jury**

Prof. Nicolas Salamin, Président

Prof. Miguel A. Blázquez, Expert

Prof. Christian Hardtke, Expert

Lausanne 2021



# Imprimatur

Vu le rapport présenté par le jury d'examen, composé de

<b>Président·e</b>	Monsieur	Prof.	Nicolas	<b>Salamin</b>
<b>Directeur·trice de thèse</b>	Monsieur	Prof.	Christian	<b>Fankhauser</b>
<b>Expert·e·s</b>	Monsieur	Prof.	Miguel A.	<b>Blázquez</b>
	Monsieur	Prof.	Christian	<b>Hardtke</b>

le Conseil de Faculté autorise l'impression de la thèse de

## **Monsieur Yetkin Çaka Ince**

Master of Science, Middle East Technical University, Turquie

intitulée

## **Molecular mechanisms underlying PIF-mediated growth responses**

Lausanne, le 14 janvier 2021

pour le Doyen  
de la Faculté de biologie et de médecine

Prof. Niko GELDNER  
Directeur de l'Ecole Doctorale

# THANK YOU

I would like to express my deepest gratitude to my thesis supervisor, Christian Fankhauser for his guidance, teaching, and advices throughout this thesis. He has been a great supervisor and always found the time to help me even with the smallest details. Besides being an amazing role model for me as a scientist, he is a great group leader who provided me and all lab members a very peaceful and friendly work environment.

I would like to thank the members of thesis examining committee; Miguel Blázquez, Christian Hardtke, and Nicolas Salamin, for their suggestions and evaluation of this thesis. Their suggestions especially in the mid-thesis exam greatly helped me to make this thesis better.

Special thanks to Mieke de Wit who was a go-to person for me when I first started in the lab and she taught me a lot both experimentally and theoretically. Her advices, comments, and encouragements were valuable for me throughout this study.

I would like to thank my mentor Vincent Dion whose advices especially helped me to establish better communication skills in academic life.

I also would like to thank all past and present members of Fankhauser lab. Anne-Sophie was a great lab mate and collaborator. She was always ready to help with anything. She translated the thesis summary to French and her comments on the thesis manuscript were too valuable. Vinicius is and will always be a great example of organisation and meticulous work in research. Martina, Alessandra, Ana, Ganesh, Olivier, Johanna, Geoffrey, Bogna, Anupama, Paolo, Prashant, Markus, Perrine, Antoine, Cécile, Marion, Sara; thank you all for your helps, discussions and the great and friendly work environment. Special thanks to Martine and Laure for keeping everything well organised and being a life saver anytime needed. Thanks to Nathalie and Corrine whose excellent work makes everything smoothly functional. Finally all the people that I had the

pleasure to know, exchange ideas and participate in great discussions during the courses, conferences and seminars that I attended.

Our collaborators Sebastien Mongrand and Julijana Ivanisevic not only analysed very crucial data but also guided me with their valuable suggestions during my work. I would like to many thanks to them and their lab members for the impeccable work.

I also would like to thank researchers in GTF; Johann Weber, Julien Marquis, Hannes Richter, Sylvain Pradervand, Leonore Wigger and all others who did the RNA-seq analysis and helped me with RT-qPCR analyses.

I am also thankful to my friends Soner, Sinem, and Ersin with whom I had great moments in our little trips all around Switzerland and Europe. Ezgi, Anil, Tugba, Toygar, Cansaran, Mustafa, Fanny, Efe, Fatma, Eda, and Ebru, whose accompany kept me sane and well missed during the lockdown. Kutalmis, Mine, Ahmet, Bülent, Cevahir, Tolga, Mete, Ilyas, and Eren for the lovely video calls that we had during lockdown. And Deirdre who has appeared in my life during the heat of writing period and become a great source of joy and happiness.

Finally, I would like to thank my parents, brothers, and sister for believing in me; and my nieces and nephew for their presence.

# SUMMARY

Plants finely tune their development using external cues such as light and temperature. Phytochrome-interacting factors (PIFs) are the transcription factors promoting hypocotyl elongation in vegetative shade, neighbour proximity, and elevated temperature.

PIF4 is known to induce hypocotyl elongation in elevated temperature. Proximity and elevated temperature largely share molecular mechanisms to regulate hypocotyl elongation. PIF7 is the major regulator of plant proximity responses, yet little is known about its role in elevated temperature. Here, we identified PIF7 as a novel player for elevated temperature responses. PIF7 protein levels increase rapidly in elevated temperature and it induces expression of auxin biosynthetic and signalling genes.

CO<sub>2</sub> fixation mainly occurs in the source organ (cotyledons) and supplies necessary resources to the sink organs including hypocotyls. We showed that CO<sub>2</sub> fixation rate remains unaffected in *B. rapa* cotyledons sensing neighbour proximity. Furthermore, the partition of fixed CO<sub>2</sub> increases in all downstream carbon pools within hypocotyls. We also showed that sucrose transport from cotyledons is indispensable for neighbour-proximity induced hypocotyl elongation. Moreover, hypocotyl elongation is mediated by a metabolic response which depends on PIF7.

Fixed CO<sub>2</sub> provides the material required for cell elongation. Although shade and neighbour proximity both induce hypocotyl elongation, decreased light in shade reduces CO<sub>2</sub> fixation while neighbour proximity does not. Using organ-specific transcriptome responses and genetic approaches, we showed that proximity and shade promotes biosynthesis and recycling processes, respectively to obtain the materials required for cell elongation. Autophagy is induced in shade, whereas proximity promotes biosynthetic mechanisms, including biosynthesis of plasma membrane (PM) lipids. We identified a novel role for PIFs, which induce sterol biosynthetic genes in the hypocotyl, likely contributing to PM and cell elongation in response to neighbour proximity.

# RÉSUMÉ

Les plantes ajustent finement leur développement en réponse à des signaux de l'environnement comme la lumière ou la température. Les PIF (Phytochrome-Interacting Factors) sont des facteurs de transcription qui promeuvent l'élongation de l'hypocotyle dans les réponses d'évitement de l'ombre (détection de plantes voisines ou sous une canopée) ou sous une température élevée.

Le facteur PIF4 a un rôle majeur dans l'élongation de l'hypocotyle en réponse à une température élevée. La détection des plantes voisines et la perception d'une élévation de température reposent sur des mécanismes moléculaires très similaires. Bien que PIF7 soit le principal facteur régulant les réponses de proximité, il n'avait jusqu'à présent pas de rôle connu dans les réponses à la température. Dans cette étude, nous avons montré que PIF7 intervient également dans les réponses à une élévation de température. Le niveau de protéines PIF7 augmente rapidement quand la température ambiante monte et PIF7 induit directement l'expression de gènes des voies de biosynthèse et de signalisation de l'auxine.

La fixation du CO<sub>2</sub> atmosphérique par la photosynthèse a lieu principalement dans les organes sources (cotylédons) qui approvisionnent les organes puits (hypocotyle) en ressources carbonées. Nous avons montré que le taux de fixation du CO<sub>2</sub> est inchangé dans les cotylédons de *Brassica rapa* en conditions d'ombre mimant la présence de plantes voisines. De plus la répartition du CO<sub>2</sub> fixé augmente dans tous les pools carbonés au sein de l'hypocotyle. Nous avons également montré que le transport du saccharose depuis les cotylédons est indispensable à l'élongation de l'hypocotyle induite par la détection du voisin. Enfin, cette élongation de l'hypocotyle est médiée par une réponse métabolique dépendant de PIF7.

Le CO<sub>2</sub> fixé fournit le matériel organique nécessaire à l'allongement des cellules. Les réponses à la proximité des plantes voisines et à la présence d'une canopée induisent toutes deux une élongation de l'hypocotyle. Pourtant, sous une canopée, la quantité de lumière diminue, et avec elle la fixation du CO<sub>2</sub>, ce qui n'est pas le cas dans la détection du voisin. En utilisant des données transcriptomiques obtenues sur des organes spécifiques combinées à une approche génétique, nous avons montré que les deux types de réponses à l'ombre, détection du voisin et canopée, induisent respectivement la biosynthèse et le recyclage, permettant d'obtenir le matériel nécessaire à l'élongation cellulaire. L'autophagie est induite dans les conditions mimant une canopée. Dans les conditions mimant la présence de plantes voisines, ce sont les mécanismes de biosynthèse des lipides qui sont favorisés, en particulier des lipides constituant la membrane plasmique. Nous avons identifié un rôle encore méconnu des PIF, qui induisent l'expression des gènes de biosynthèse des stérols dans l'hypocotyle. Cela contribue certainement à la formation de la membrane plasmique et à l'élongation des cellules dans le contexte de détection du voisin.

# TABLE OF CONTENTS

<b>THANK YOU .....</b>	<b>2</b>
<b>SUMMARY .....</b>	<b>4</b>
<b>RÉSUMÉ .....</b>	<b>5</b>
<b>TABLE OF CONTENTS .....</b>	<b>7</b>
<b>LIST OF FIGURES AND TABLES .....</b>	<b>11</b>
<b>GENERAL INTRODUCTION.....</b>	<b>14</b>
Light is a source of information for plants.....	14
Photoreceptors perceive changes in light cues .....	14
Phytochromes .....	15
Cryptochromes.....	19
UVR8 .....	20
PIFs are the key regulators of SAS and thermomorphogenesis.....	21
Perception of Shade and Elevated Temperature .....	22
Overview of PIFs and PIF-regulated morphological responses .....	25
Regulation of PIF abundance and activity.....	26
Shade and thermomorphogenesis regulate auxin pathway through PIF proteins.....	33
Auxin Production.....	35
Auxin transport.....	36
Auxin response.....	36
Brassinosteroids .....	38
Gibberellins .....	39
Ethylene .....	40
Regulation of cellular elongation .....	42

Cell wall extension is the key for the cellular elongation .....	42
PIFs and hormonal responses regulate cell elongation .....	44
<b>Aim of the study .....</b>	<b>48</b>
<b>RESULTS .....</b>	<b>50</b>
<b>Chapter 1. PHYTOCHROME INTERACTING FACTOR 7 is important for early responses to elevated temperature in Arabidopsis seedlings.....</b>	<b>50</b>
OVERVIEW .....	51
PUBLICATION .....	51
<b>Chapter 2. Changes in resource partitioning between and within organs support growth adjustment to neighbour proximity in Brassicaceae seedlings .....</b>	<b>70</b>
OVERVIEW .....	71
PUBLICATION .....	72
<b>Chapter 3. Distinct mechanisms underlying hypocotyl growth promotion in response to neighbour proximity and vegetative shade .....</b>	<b>88</b>
OVERVIEW .....	89
ABSTRACT .....	90
INTRODUCTION .....	91
RESULTS .....	99
LRFR-induced hypocotyl elongation requires PIFs for more than induction of auxin biosynthesis in cotyledons .....	99
PIFs induce SMT2 and SMT3 expression in LRFR .....	99
SMT2 is required for LRFR-induced hypocotyl elongation .....	103
SMT2 is not required for LB-induced hypocotyl elongation .....	105
LRFR and LB induces different transcriptome changes.....	107
PIFs also induce other hormone responses and cell wall organisation in LRFR.....	115
The potential roles of PIFs and YUCCAs in LB-induced hypocotyl elongation.....	119

Auxin biosynthesis, transport and response are not impaired in <i>smt2</i> mutant in LRFR ....	
121	
Sucrose transport is not altered in <i>smt2</i> mutant in LRFR .....	123
The ratio between campesterol to sitosterol in <i>Brassica rapa</i> hypocotyls does not change rapidly in LRFR.....	125
Lipid profile of <i>Brassica rapa</i> hypocotyls changes in response to LRFR .....	127
LRFR decreases PM fluidity in hypocotyls .....	130
Low blue light induces autophagy .....	133
DISCUSSION.....	138
PIFs induce SMT2 and SMT3 expression that are required for hypocotyl elongation in LRFR .....	138
LRFR promotes accumulation of PM lipids and degradation of storage and chloroplast lipids.....	140
The individual and combined functions of PIFs and YUCCAs in LRFR.....	144
PIFs and YUCCAs are required in LB-induced hypocotyl elongation .....	145
Metabolic pathways to obtain new material for elongating hypocotyls differ in LB and LRFR .....	146
MATERIALS AND METHODS.....	149
Plant material and growth conditions .....	149
Constructs cloning .....	151
RNA isolation, quantitative RT-PCR and RNA-sequencing .....	151
Gene set enrichment analysis for Gene Ontology .....	156
ChIP-qPCR.....	157
Western-blot analysis .....	157
Microscopy and GUS Staining .....	158
Sterol measurements .....	159

Lipidomics.....	159
Statistical analysis.....	162
SUPPLEMENTARY FIGURES.....	163
ACKNOWLEDGEMENTS.....	185
<b>GENERAL DISCUSSION AND OUTLOOK.....</b>	<b>186</b>
<b>BIBLIOGRAPHY.....</b>	<b>191</b>

# LIST OF FIGURES AND TABLES

<b>GENERAL INTRODUCTION</b> .....	<b>14</b>
Figure 1. Photoreceptors perceive changes in light cues to regulate plant development. ....	16
Figure 2. The photocycle of photoreceptors. ....	18
Figure 3. Shade changes the quality and the quantity of the light reaching to plants. ....	23
Figure 4. Mechanisms regulating PIF abundance. ....	27
Figure 5. LRFR- and elevated temperature-induced auxin signaling model in Arabidopsis seedlings. ....	34
Figure 6. The model for cell wall biosynthesis and structure. ....	41
<b>RESULTS</b> .....	<b>50</b>
<b>Chapter 1. PHYTOCHROME INTERACTING FACTOR 7 is important for early responses to elevated temperature in Arabidopsis seedlings</b> .....	<b>50</b>
Given as in the publication	
<b>Chapter 2. Changes in resource partitioning between and within organs support growth adjustment to neighbour proximity in Brassicaceae seedlings</b> .....	<b>70</b>
Given as in the publication	
<b>Chapter 3. Distinct mechanisms underlying hypocotyl growth promotion in response to neighbour proximity and vegetative shade</b> .....	<b>88</b>
<b>INTRODUCTION</b> .....	<b>91</b>
Figure 1. The current model for PIF-mediated hypocotyl elongation in LRFR.....	97
<b>RESULTS</b> .....	<b>99</b>
Figure 2. PIFs are required for more than induction of auxin biosynthesis in cotyledons during LRFR-induced hypocotyl elongation. ....	100

Figure 3. PIFs regulate expression of SMT encoding genes in hypocotyls in response to LRFR treatment. ....	101
Figure 4. SMT2 is required for LRFR-induced hypocotyl elongation. ....	104
Figure 5. SMT2 is not required for LB-induced hypocotyl elongation. ....	106
Figure 6. LB and LRFR induces transcriptome changes in cotyledons and hypocotyls. ...	110
Figure 7. Similarities and differences LB and LRFR transcriptome. ....	114
Figure 8. PIFs induce hormone responses and cell wall organisation in LRFR. ....	118
Figure 9. Auxin biosynthesis, transport and response are not impaired in <i>smt2</i> mutant in LRFR. ....	122
Figure 10. Sucrose transport is not altered in <i>smt2</i> mutant in LRFR. ....	124
Figure 11. Sterol composition of <i>Brassica rapa</i> hypocotyls does not change rapidly in LRFR. ....	126
Figure 12. Lipid profile of <i>Brassica rapa</i> hypocotyls changes in response to LRFR. ...	128
Figure 13. LRFR decreases plasma membrane (PM) fluidity. ....	132
Figure 14. Low blue light induces autophagy. ....	136
MATERIALS AND METHODS. ....	149
Figure M1. Light spectra of the conditions used in this study. ....	150
Table M1. List of oligonucleotides used for genotyping. ....	152
Table M2. List of oligonucleotides used in cloning. ....	153
Table M3. List of oligonucleotides used in RT-qPCR. ....	154
Table M4. List of oligonucleotides used in ChIP-qPCR. ....	155
SUPPLEMENTARY FIGURES. ....	163
Figure S1. Sterol biosynthesis related genes are induced in LRFR in hypocotyls. ....	163
Figure S2. Organ-specific expression of shade control genes. ....	164

Figure S3. PIFs bind to SMT2 and SMT3 promoters.....	165
Figure S4. Hypocotyl elongation of <i>smt</i> mutants in LRFR and in BR. ....	166
Figure S5. Hypocotyl specific complementation of SMT2 rescues <i>smt2-1</i> mutant hypocotyl elongation in LRFR. ....	167
Figure S6. Hypocotyl elongation of <i>smt</i> mutants are not impaired in cFR. ....	168
Figure S7. Hypocotyl elongation of <i>smt</i> mutants are not impaired in LB. ....	169
Figure S8. Phenotypic evaluation of genotypes used in RNA-seq analysis. ....	170
Figure S9. Principle component analysis of hypocotyl and cotyledon transcriptomes. ....	171
Figure S10. Validation of RNA-seq data. ....	172
Figure S11. Similarities and differences in LB and LRFR transcriptomes (downregulated genes).....	174
Figure S12. Determining the PIF- and YUC- dependently and independently LRFR- regulated genes in hypocotyls. ....	175
Figure S13. Identification of transcriptome changes in mutants and Col-0 in WL. ....	177
Figure S14. Comparison of LB and picloram regulated genes in hypocotyls. ....	178
Figure S15. Sucrose transport is not indispensable in LB light. ....	179
Figure S16. Composition of other sterols and expression of control genes in LRFR in <i>B. rapa</i> hypocotyls.....	180
Figure S17. Lipid profile of <i>B. rapa</i> hypocotyls changes in response to LRFR (MS1). .	181
Figure S18. LRFR expression of FAD family genes in cotyledons and PM fluidity in LB. ...	182
Figure S19. Low blue light treatment induces autophagy in cotyledons and hypocotyls.....	183

# **GENERAL INTRODUCTION**

## **Light is a source of information for plants**

Plants are predominantly photosynthetic organisms that obtain most of their energy from sunlight. Yet, the sunlight is not only the source of energy but also a source of information modulating plant development from germination to flowering. Plants spend their entire life at the location where they first germinated. However, this sessile characteristic is compensated by their phenotypic plasticity that enables them to finely tune their development in order to rapidly respond to changing environmental cues like temperature and light. The phenotypic plasticity allows plants to cope with biotic and abiotic factors surrounding them, increasing their chance of survival. As the ultimate source of energy via photosynthesis, light is one of the most important cues among the abiotic factors. Therefore, plants optimise their development in response to changes in physical parameters of light, such as wavelength, intensity, direction, and duration via various physiological adaptations, to catch the necessary light for photosynthesis (Casal, 2012, Fiorucci & Fankhauser, 2017).

## **Photoreceptors perceive changes in light cues**

Skotomorphogenesis and photomorphogenesis are two growth strategies where seedling development takes place in darkness and light, respectively. When seeds germinate in the dark, an etiolated growth of the seedling is triggered where the hypocotyl elongates rapidly while cotyledon and root development is inhibited (de Wit et al., 2016a). This strategy enables seedlings to quickly reach the soil surface and light, which is required for photosynthesis. On the contrary, light induces photomorphogenesis that inhibits the hypocotyl elongation whereas it induces the cotyledon expansion. The photomorphogenic growth of the seedling is called de-etiolated growth. Plants possess multiple photoreceptors that accurately detect various wavelengths of sunlight as well as

the changes in physical parameters of light and mediate the physiological adaptations including skotomorphogenesis and photomorphogenesis (Fig. 1). Unlike animals, plant photoreceptors are found throughout the plant organs as well as the different stages of development (Galvao & Fankhauser, 2015). Sunlight is composed of a large spectral range, yet plants are only able to use the solar radiation ranging from 400 to 700 nanometers (nm), called photosynthetically active radiation (PAR), for photosynthesis. There are five different classes of photoreceptors that perceive specific changes in the light spectrum. Mainly, UV RESISTANCE LOCUS 8 (UVR8) absorbs ultraviolet-B (UV-B) (peak at ~280-315 nm); cryptochromes (cry), phototropins (phot) and Zeitlupes (ZTL) absorb UV-A/blue (B) (peak at ~390-500 nm); and phytochromes (phy) absorb red (R) (peak at ~670 nm) and far red (FR) (peak at ~730 nm) (Fiorucci & Fankhauser, 2017). Zeitlupes are mainly involved in the control of floral transition and entrainment of the circadian clock, whereas phototropins perceive the directional UV-A/blue light and induce phototropism (Galvao & Fankhauser, 2015). In the following section, I will further discuss the other three classes of photoreceptors that primarily control elongation and growth responses depending on the light environment.

## **Phytochromes**

Phytochromes are dimeric red/far-red light receptors that are found in bacteria, fungi, algae, and land plants (Legris et al., 2019). They are synthesised in the inactive form Pr that is converted to the active Pfr conformation upon R absorption (Fig. 2a, top). Conversely, FR absorption inactivates Pfr form. Thermal relaxation (i.e., dark relaxation) also converts Pfr back to the inactive Pr form in a temperature dependent manner. The conformational changes between the active and inactive forms occurs through a phytochromobilin tetrapyrrole ring that is covalently attached to the phytochromes and isomerise in response to light cues, changing the protein structure. Although absorption maxima of Pr and Pfr are different, both conformers are present in the light as they largely share the

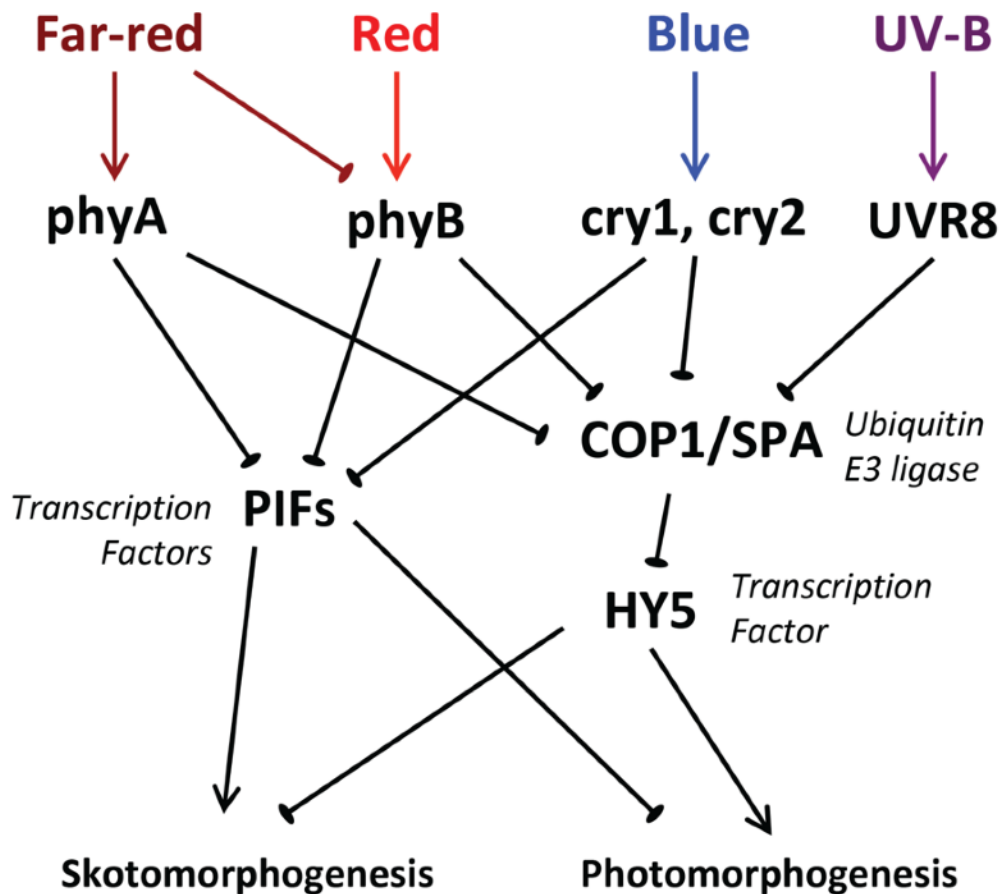


**Figure 1. Photoreceptors perceive changes in light cues to regulate plant development.**

In darkness, E3 ubiquitin ligase COP1/SPA complex leads HY5, a key light signaling TF, to proteasome-mediated degradation. Phytochrome (phy), cryptochrome (cry), and UVR8 photoreceptors perceive the red (R) and far red (FR), blue (B), and ultraviolet (UV-B) light signals, respectively and get activated. Light-activated photoreceptors inhibit COP1/SPA, resulting in accumulation of HY5 protein and consequent induction of gene expression for light-mediated development (*i.e.*, photomorphogenesis) where hypocotyl elongation is repressed. Active form of phytochromes and cryptochromes also interacts with PIFs to inhibit hypocotyl elongation in light, whereas PIFs induce expression of auxin and cell wall related genes to mediate seedling growth in dark (*i.e.*, skotomorphogenesis), as well as shade and elevated temperature conditions where phytochromes and cryptochromes are inactivated (Galvao & Fankhauser, 2015).

overlapping spectra (Fig. 2a, *bottom*). Only prolonged darkness converts all Pfr to Pr.

The phytochrome family in *Arabidopsis* is composed of five members: phyA, phyB, phyC, phyD, and phyE, among which phyA and phyB are the most abundant ones and play the most important roles (Legris et al., 2019). Although they share almost the identical absorption spectra, their action spectra are different due to the different responses to the fluence rates and irradiance of light (Legris et al., 2019). Both phytochromes respond to fluence rates between 1-1000  $\mu\text{M}/\text{m}^2$  that is known as low fluence responses (LFR). The above-mentioned light-mediated reversibility of Pr and Pfr forms is the characteristics of LFR. However, phyA is also able to respond very low fluence rates (0.0001-0.05  $\mu\text{M}/\text{m}^2$ ) that are important for seed germination underground (VLFR). In addition, phyA can mediate high irradiance responses to continuous FR light illumination (FR-HIR). PhyA can initiate downstream responses as a PfrA-PrA heterodimers. Thus, phyA can trigger responses with a much lower fraction of Pfr as in VLFR and FR-HIR. Unlike phyA, phyB can only work as a PfrB-PfrB homodimer, which allows phyB to mediate responses to rapidly changing light and temperature conditions (Legris et al., 2019). Another important key step in light-mediated regulation of phytochromes is the control of their cellular location. Light triggers the translocation of all five phytochromes from cytosol to nucleus in *Arabidopsis*. PhyA nuclear transport depends on the interaction between PfrA and FAR RED ELONGATED HYPOCOTYL 1 (FHY1) and FHY1 LIKE (FHL) (Hiltbrunner et al., 2006). Yet, phyB nuclear localisation is not controlled by FHY1 or FHL and remains poorly understood (Legris et al., 2019).

Phytochromes regulate developmental processes including germination, photomorphogenesis, shade avoidance syndrome (SAS), thermomorphogenesis, stomatal development, and flowering (Pham et al., 2018). Upon light illumination, Pfr interacts with several classes of transcription

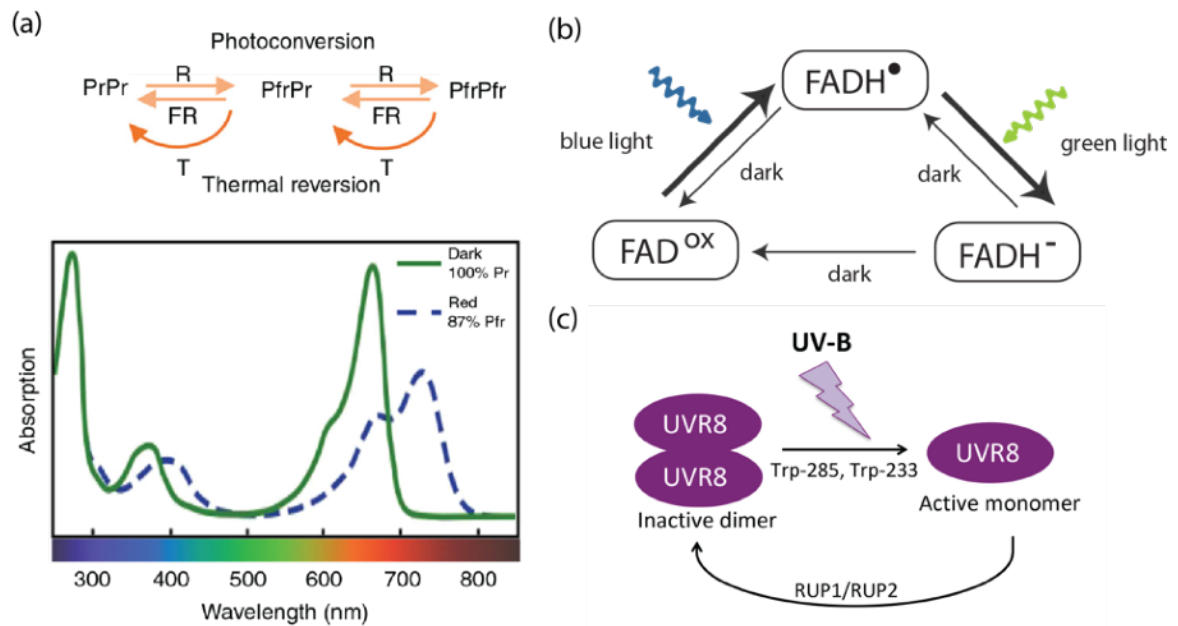


**Figure 2. The photocycle of photoreceptors.**

(a) Phytochromes are dimeric proteins that are activated by red (R) light and inactivated by far red (FR) light or thermal reversion, a process that depends on temperature (T) (top). Absorption spectra of inactive Pr and active Pfr forms of phytochromes (bottom) (Adapted from Legris et al., 2019). (b) Cryptochromes employ FAD as the chromophore. The resting state in dark is FADox that is reduced to radical FADH° upon blue light illumination, activating the cryptochrome via a conformational change. Further blue or green light illumination reduces FADH° to FADH- that is the inactive redox form. Darkness spontaneously re-oxidise the fully reduced FADH- to FADox (Adapted from Ritz, 2011). (c) UV-B monomerize the UVR8 homodimer via a tryptophan-based chromophore. RUP1 and RUP2 re-dimerise UVR8 monomer, inactivating the downstream signalling pathway (Tilbrook et al., 2013).

factors related to hormone signalling pathways and ubiquitin E3 ligases controlling the stability of the transcriptional regulators (Pham et al., 2018, Legris et al., 2019). These interactions regulate a rapid global transcriptional reprogramming. During de-etiolation response, Pfr interact with SUPPRESSOR OF PHYA (SPA) and inhibit CONSTITUTIVE PHOTOMORPHOGENIC 1 (COP1)/SPA complex, leading to ELONGATED HYPOCOTYL 5 (HY5)-mediated transcriptional activation of photomorphogenesis (Fig. 1). It was recently shown

that light induces phyB interaction with ETHYLENE-INSENSITIVE 3 (EIN3), a nuclear ethylene response transcription factor that initiates downstream transcriptional cascades for etiolated growth (Shi et al., 2016). This interaction facilitates EIN3 ubiquitination and degradation. Recent evidences suggest that phyB interacts and inhibits a brassinosteroid signalling transcription factor BRI1-EMS-SUPPRESSOR 1 (BES1)(Wu et al., 2019). PfrA and PfrB also interact with several Aux/IAA proteins that are repressors auxin-controlled gene expression and prevent their degradation (Xu et al., 2018, Yang et al., 2018a). Finally, Pfr interacts with a subfamily of the basic helix-loop-helix (bHLH) transcription factor superfamily, phytochrome-interacting factors (PIFs) and inhibits hypocotyl elongation (Fig. 1) (Pham et al., 2018, Legris et al., 2019). I will further focus on details of molecular mechanisms of PIF-mediated responses in the following sections.

## **Cryptochromes**

Cryptochromes are blue/UV-A light receptors that are found in bacteria, fungi, animals, and plants. Arabidopsis has two phytochromes, cry1 and cry2 that share a common evolutionary ancestor with light activated DNA repair enzymes known as photolyases (Ahmad, 2016, Wang et al., 2018b). In spite of the common structural features and the same FAD cofactor between cryptochromes and photolyases, cryptochromes have novel roles in light signaling (Ahmad, 2016). Cryptochrome photocycle is regulated via a light-absorbing flavin adenine dinucleotide (FAD) that is the chromophore bound to cryptochromes. The flavin cofactor can exist in three redox forms: FADox, FADH<sup>•</sup>, FADH<sup>-</sup> that undergo light-dependent electron transfer. FADox is the resting state in dark and light reduces it first to the radical FADH<sup>•</sup> that triggers conformational change and unfolding of the C-terminal domain to give the activated form of the receptor (Fig. 2b). Further illumination with blue or green light induces the reduction to FADH<sup>-</sup> that is the inactive redox form. The fully reduced FADH<sup>-</sup> is spontaneously re-oxidised within several minutes upon return to darkness (Ahmad, 2016). Upon

blue light irradiation, cry1 and cry2 are phosphorylated, where PHOTOREGULATORY PROTEIN KINASEs (PPKs) and CASEIN KINASEs (CKs) are important (Shalitin et al., 2002, Shalitin et al., 2003, Tan et al., 2013, Liu et al., 2017). Cry2 phosphorylation occurs primarily in the nucleus and enhances its activity by inducing conformational changes (Yu et al., 2007, Yu et al., 2009, Zuo et al., 2012, Wang et al., 2015). BLUE-LIGHT INHIBITOR OF CRYPTOCHROMES (BICs) suppress dimerization, phosphorylation, degradation, and activities of cry2 (Wang et al., 2016).

Cryptochromes control plant developmental processes including seedling de-etiolation, elongation, the initiation of flowering, and entrainment of the circadian clock (Li & Yang, 2007). Although they share partially overlapping functions, cry1 predominantly regulates de-etiolation and cry2 regulates the photoperiodic control of flowering (Liu et al., 2011). B-light induced cry1 and cry2 binding and inhibition of COP1/SPA1 E3 ubiquitin ligase leads to accumulation of HY5, that promotes de-etiolation (Lau et al., 2019, Ponnu et al., 2019) (Fig. 1). Light-activated cry2 interacts with CRYPTOCHROME-INTERACTING bHLHs (CIBs), transcription factors that activates transcription of flowering promotion genes (Liu et al., 2008). Cryptochromes also interact with PIFs and mediate shade-avoidance syndrome and elevated temperature responses (i.e., thermomorphogenesis), which is described in the following sections.

## **UVR8**

UV-B is a part of solar radiation that reaches to the Earth. Instead of fuelling photosynthesis, it is rather a threat to the integrity of plants due to the deleterious effects of high-energy UV light (Yang et al., 2015). Plants employ UVR8 photoreceptor to acclimate to the harmful effects of UV-B. UVR8 does not have a cofactor chromophore unlike phytochromes and cryptochromes. Rather, Trp233 and Trp285 serve as chromophores for UV-B perception. UV-B irradiation induces the monomerization and nuclear accumulation of UVR8 that is found as

inactive homodimers (Fig. 2c) (Kaiserli & Jenkins, 2007, Rizzini et al., 2011). REPRESSOR of UV-B PHOTOMORPHOGENESIS 1 (RUP1) and RUP2 physically interacts with UVR8 and facilitate UVR8 re-dimerization (Gruber et al., 2010, Heijde & Ulm, 2013).

UVR8 mediates morphological adaptations and the biosynthesis of flavonoids that act as UV-B protectant. Furthermore, UVR8 modulates hypocotyl elongation, phototropic bending, stomatal movement, and entraining of the circadian clock (Liang et al., 2019). The photoactivated monomeric UVR8 physically interacts with COP1 that reduces the ubiquitination and degradation of HY5 (Fig. 1) (Oravec et al., 2006, Huang et al., 2013, Lau et al., 2019). Moreover, UVR8 interacts with multiple transcription factors including WRKY DNA-BINDING PROTEIN 36 (WRKY36), BES1 and BES1-INTERACTING MYC-LIKE 1 (BIM1) and directly regulates gene expression. WRKY36 can interact with both dimeric and monomeric UVR8, but the nuclear accumulation of monomeric UVR8- WRKY36 complex is promoted by UV-B irradiation. WRKY36 regulates hypocotyl elongation via inhibiting HY5 expression and UV-B suppresses WRKY36 (Yang et al., 2018b). BR signalling transcription factors BES1 and BIM1 also interact with UVR8, independent of UV-B treatment (Liang et al., 2018). BIM1 interacts with BES1 and they co-ordinately regulate BR-induced gene expression and hypocotyl elongation. UV-B mediated nuclear localisation of monomeric UVR8 promotes accumulation of UVR8-BES1/BIM1, leading to repression of BR signalling to inhibit hypocotyl elongation (Liang et al., 2019). Thus, the photoactive monomeric UVR8 regulates downstream responses via transcriptional cascades.

## **PIFs are the key regulators of SAS and thermomorphogenesis**

Shade decreases both the quality and quantity of light reaching photosynthetic organs of plants (Casal, 2013). Plants have evolved a series of responses

collectively called shade avoidance syndrome (SAS) to consolidate light capture necessary for photosynthesis in canopy environments (Casal, 2013). SAS includes hypocotyl, stem and petiole elongation, hyponastic leaf movement, reduced leaf development and branching, and reduced root development (Franklin, 2008, Casal, 2013). The temperature also regulates plant morphogenesis, which is called thermomorphogenesis (Casal & Balasubramanian, 2019). Although thermomorphogenesis is a broad term that also includes morphological responses to cold and alternating (day/night) temperatures, I will only describe the responses to elevated temperatures that induce changes similar to SAS. Several plant photoreceptors perceive changes in light and temperature cues and regulate the morphological adaptations via a transcriptional cascade where phytochrome-interacting factors (PIFs) are the key modulators.

### **Perception of Shade and Elevated Temperature**

Plant leaves absorb blue (B) and red light (R) and transmit and reflect far-red (FR) light. Thus, in the presence of neighbours, plants are exposed to increased intensity of FR leading to low R/FR (LRFR) whether or not they are shaded (Fig. 3). The level of photosynthetically active radiation (PAR) (400-700 nm), thus the intensity of B light also decreases under vegetational canopy shade (Casal, 2013, Fiorucci & Fankhauser, 2017). Neighbour proximity that is perceived as a signal for future shade, and vegetative shade similarly induce hypocotyl elongation in *Arabidopsis* seedlings (Fig. 3b). LRFR and low B (LB) are often used as model systems to mimic neighbour proximity and vegetative shade, respectively (Pedmale et al., 2016).

As R and FR light photoreceptors, phytochromes perceive the neighbour proximity signal. The R/FR reduction in neighbour proximity and shade shifts the Pr-Pfr photo-equilibrium towards the inactive Pr form, which allows plants to perceive shade. phyB is the major phytochrome regulating SAS in young seedlings (Franklin, 2008, Casal, 2013). Hypocotyl elongation response in B light mainly depends on cryptochromes. Genetic and biochemical evidences suggest

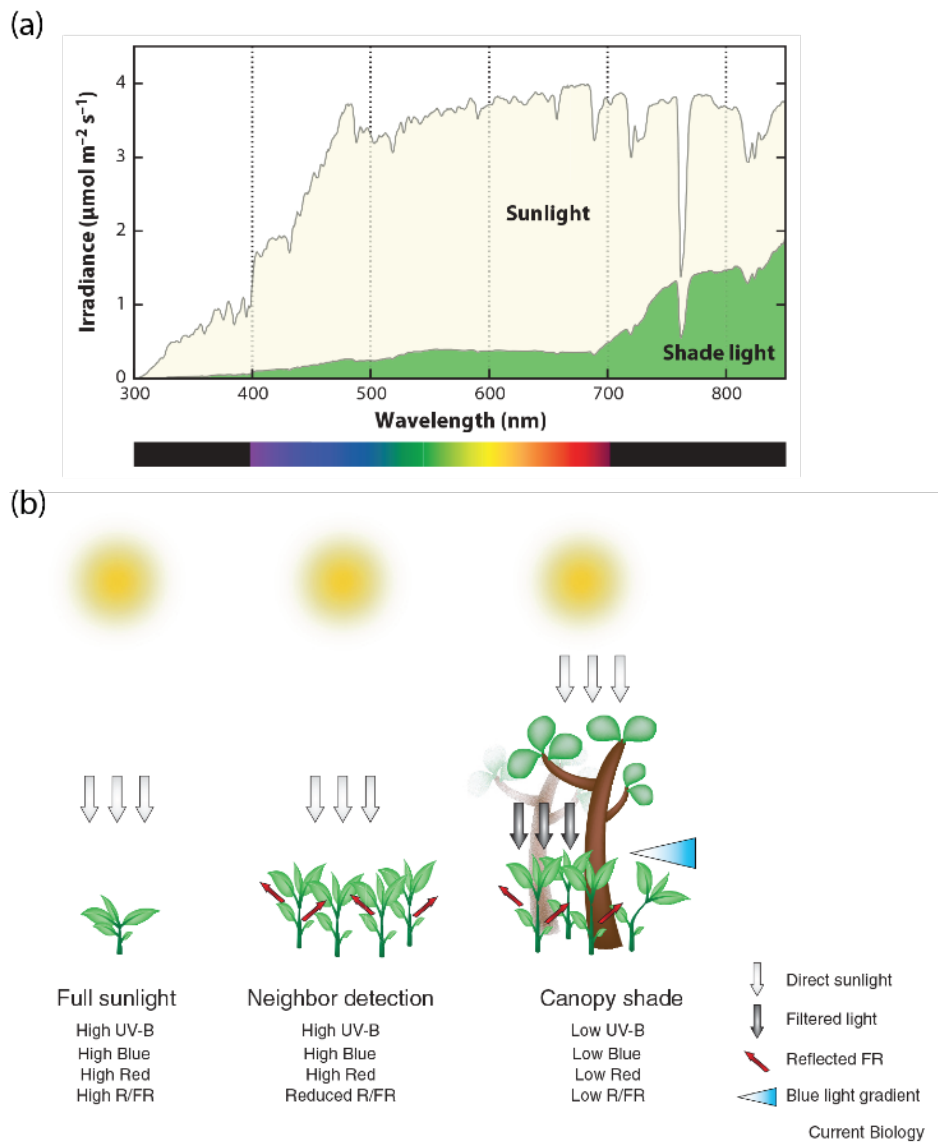


**Figure 3. Shade changes the quality and the quantity of the light reaching to plants.**

(a) Spectra of sunlight and shade are different (Adapted from Casal, 2013). (b) A plant under full sunlight receives high UV-B, blue, and red light, but relatively low amounts of far-red (Spectrum in Fig. 3a). Presence of neighbours increases far-red due to the reflection from the green tissues, whereas plants still receive high quantities of PAR. The decrease in R/FR is an alert for future vegetative shade that induces SAS to get a better access to sunlight. Under canopy shade, light is strongly filtered by the green leaves, decreasing the UV-B, blue and red wavelengths, whereas the relative amount of far-red increases leading to low R/FR. Canopy shade also leads to SAS with a more pronounced phenotypic response than neighbour detection (Adapted from Fiorucci & Fankhauser, 2017).

that LB-induced hypocotyl elongation is regulated by cry1 and cry2 in Arabidopsis seedlings (Pedmale et al., 2016). Therefore, red and blue light photoreceptors function as shade and neighbour proximity sensors. Inactive photoreceptors require the activation energy from light to convert to the active conformer. In other words, the inactive conformer of photoreceptors is thermodynamically favourable. According to Boltzmann–Arrhenius model, as the enthalpy increases with the increasing temperature, more light energy is required to convert inactive photoreceptors to thermodynamically unfavourable active conformations (Casal & Balasubramanian, 2019). Therefore, in theory, any photoreceptor can work as a thermosensor. In line with this model, hypocotyl elongation response to elevated temperature decreases with increasing light intensity (Qiu et al., 2019). Experimentally, phyB has been identified as a sensor for the elevated temperature (Jung et al., 2016, Legris et al., 2016). PfrB-PfrB homodimer is considered to be the active conformer of phyB and the rate of thermal reversion of PfrB-PrB heterodimer is much faster than that of the PfrB-PfrB (Legris et al., 2019). This allows phyB to mediate responses to rapidly changing temperature conditions. In addition, cry1 has been identified to modulate temperature sensitivity for Arabidopsis hypocotyl elongation in blue and white light (Ma et al., 2016, Qiu et al., 2019). It is also shown that UVR8 strongly inhibits elevated temperature-induced hypocotyl elongation in UV-B light (Hayes et al., 2017). The rate of UVR8 active monomer to inactive dimer reversion increases with temperature in Arabidopsis, in line with Boltzmann–Arrhenius model (Findlay & Jenkins, 2016). Finally, warm temperatures reduce the lifetime of the light-activated phototropins in liverwort *Marchantia polymorpha*, suggesting phototropins can also sense temperature (Fujii et al., 2017). However, there are no studies showing phototropins as a thermosensor in Arabidopsis.

## Overview of PIFs and PIF-regulated morphological responses

PIFs are members of a subfamily of the basic helix-loop-helix (bHLH) TF-superfamily, most of which primarily function as negative regulators of photomorphogenesis (Leivar & Monte, 2014). Arabidopsis has eight PIFs (PIF1, PIL1/PIF2, PIF3-PIF8) that regulate a wide range of responses downstream of phytochromes and cryptochromes including seed dormancy, germination, shade and temperature induced responses, diurnal growth, stomata development, flowering, and leaf senescence (Pham et al., 2018).

PIF1 is the key regulator in inhibition of light-dependent seed germination (Oh et al., 2004). Two phytohormones, gibberellin (GA) and abscisic acid (ABA) control the germination downstream of phytochromes (de Wit et al., 2016a). R-light activated phyA and phyB promote GA biosynthesis and induce the germination. In darkness or a pulse of FR, phyB in the endosperm is inactivated, that leads to ABA biosynthesis. ABA is then released to the embryo and inhibits GA biosynthesis stimulated by phyA, which inhibits the germination. However, ABA signal fades out over time and another pulse of FR leads to GA increase via phyA activation and induces the germination (Lee et al., 2012). PIF1 regulates gene expression, leading to low GA but high ABA levels. Furthermore, PIF1 promotes the expression of GA-repressor (DELLA) genes, decreasing GA sensitivity of the seed. PIF1 is also identified as a negative regulator for chlorophyll biosynthesis and plastid development (Huq et al., 2004, Moon et al., 2008, Kim et al., 2016).

As a key negative regulator of photomorphogenesis, PIF3 regulates the abundance of phyB levels (Kim et al., 2003, Monte et al., 2004, Leivar et al., 2008). PIF3 also regulates the diurnal growth of hypocotyl elongation via interacting with TIMING OF CAB EXPRESSION 1 (TOC1) (Soy et al., 2016). Other functions of PIF3 include the repression of chlorophyll biosynthesis (Stephenson et al., 2009), the regulation of ethylene-induced hypocotyl elongation and freezing tolerance (Zhong et al., 2012, Jiang et al., 2017).

PIF4 is one of the main regulators of shade-induced hypocotyl elongation together with PIF5 and PIF7, while PIF1 and PIF3 are considered as modest contributors (Lorrain et al., 2008, Li et al., 2012, Leivar & Monte, 2014). PIF4 and PIF5 are particularly important in response to a reduction in B light, while PIF7 plays a predominant function when the R/FR ratio drops (Pedmale et al., 2016). Similarly, PIF4, PIF7 and to a lesser extent PIF5 regulates the elevated temperature-induced hypocotyl elongation (Koini et al., 2009, Stavang et al., 2009, Fiorucci et al., 2019, Chung et al., 2020). PIF4 also regulates hypocotyl elongation in diurnal conditions, stomatal development, chlorophyll degradation, freezing tolerance, and anthocyanin biosynthesis (Nozue et al., 2007, Casson et al., 2009, Lee & Thomashow, 2012, Nieto et al., 2015). PIF5 is also identified as a positive regulator for chlorophyll degradation and a negative regulator for anthocyanin biosynthesis (Sakuraba et al., 2014, Song et al., 2014, Liu et al., 2015, Zhang et al., 2015).

PIF2 (PIL1), PIF6, and PIF8 are the less-characterised PIF members. PIF8 has been recently shown to be important in phyA-mediated light responses, including seed germination and suppression of hypocotyl elongation (Oh et al., 2020). Unlike the general role of most PIFs as negative regulators of photomorphogenesis, PIF2 (PIL1) interacts with PIF1, PIF3, PIF4, and PIF5 and prevents the expression of their target genes, positively regulating de-etiolation (Luo et al., 2014). Similarly, PIF6 functions as a positive regulator, inhibiting hypocotyl elongation under continuous red light (Penfield et al., 2010).

### **Regulation of PIF abundance and activity**

PIFs interact with Pfr through short domains located towards their amino-terminus. They are known as APB (Active PhyB binding) domain for phyB-PIF interactions and APA (Active PhyA binding) domain for phyA-PIF interactions. All PIFs have the APB motif, whereas APA motif is only present in PIF1 and PIF3. PIF-Pfr interaction inactivates PIFs by regulating PIF protein availability through several mechanisms (Fig. 4a) (Legris et al., 2019). First, phyB-PIF interaction

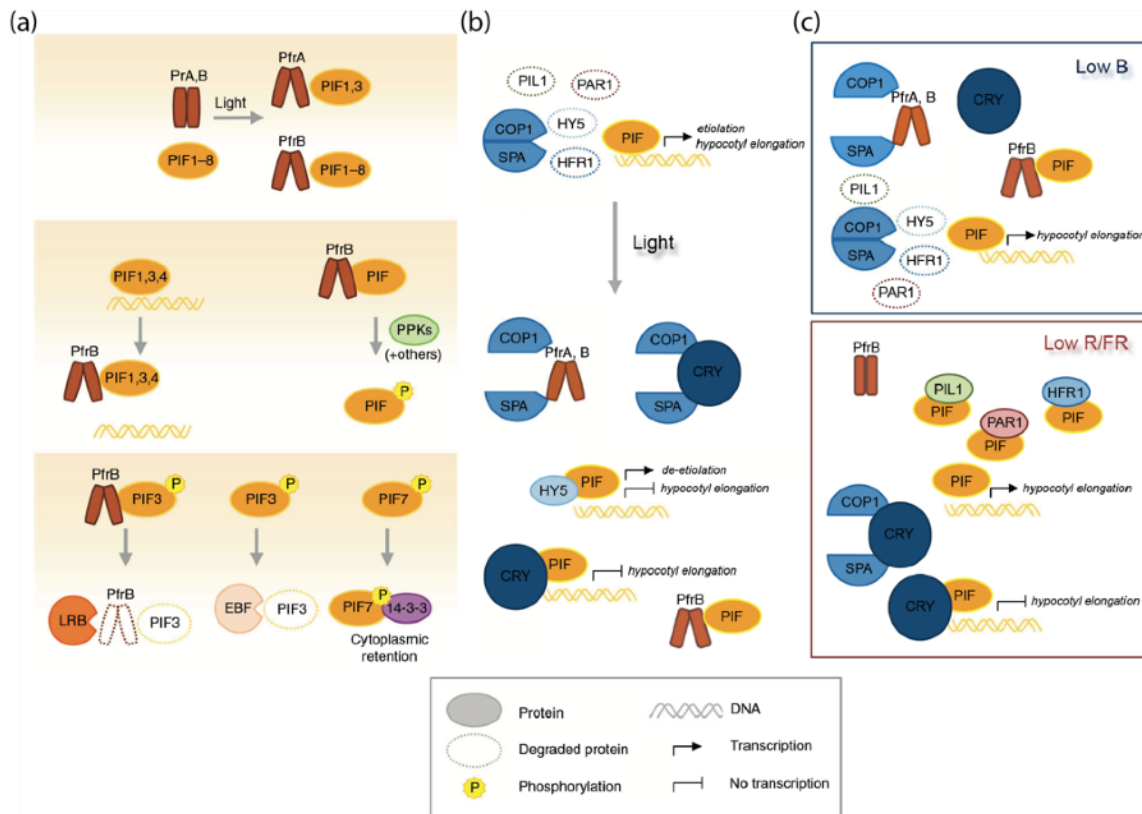


**Figure 4. Mechanisms regulating PIF abundance.**

(a) Phytochrome-mediated regulation of PIFs. PfrA interacts with PIF1 and PIF3 while PfrB interacts with PIF1–PIF8 (top). PfrB inhibits DNA binding of PIF1, 3 and 4 and interaction with Pfr leads to phosphorylation of PIFs (middle). Phosphorylated PIF3 is degraded by LRBs and EBFs with phyB co-degradation occurring in the LRB-mediated process (left, center), phosphorylated PIF7 interacts with 14-3-3 proteins and remains in the cytoplasm (right) (bottom). (b) Other factors regulating PIFs. COP1/SPA regulates abundance of PIF targets in dark (top), whereas light-activated cryptochromes and phytochromes bind COP1/SPA and inhibit its downstream functions (bottom). HY5 and cryptochromes inhibit PIF transcriptional activities (bottom). (c) Suggested models for Low B and Low R/FR responses. In low B, phytochromes are still active, whereas cryptochromes are inactive, which allows partial induction of PIF-mediated transcriptional responses (top). In low R/FR, cryptochromes are still active, whereas phytochromes are inactive, allowing PIF-mediated responses to a certain extent. Active cryptochromes also bind to COP1/SPA, inhibiting degradation of PIF negative regulators including HFR1, PAR1, and PIL1 (bottom) (Adapted and modified from Legris et al., 2019).

results in blocking DNA-binding capacity of PIF1 and PIF3 (Park et al., 2012, Qiu et al., 2017, Park et al., 2018). Second, the interaction leads to rapid phosphorylation of PIFs, followed by their ubiquitination and proteasome-mediated degradation, PIF7 being an exception (Legris et al., 2019). PIF7 phosphorylation is photo-reversible and is not followed by protein degradation, but rather results in interaction with 14-3-3 proteins and nuclear export (Fig. 4a) (Leivar & Monte, 2014, Huang et al., 2018).

Phytochromes contain a histidine kinase-related domain and were reported to have protein kinase activity (Yeh & Lagarias, 1998). Although several studies proposed that they might directly phosphorylate PIFs, additional research is needed to validate the importance of phytochromes as kinases for PIF phosphorylation (Shin et al., 2016, reviewed in Legris et al., 2019). Other PIF kinases from four different families were identified including CK2, BIN2, PPKs, and MPK6 (reviewed in Pham et al., 2018, Legris et al., 2019). Of particular interest are Photoregulatory Protein Kinases (PPK1-4; formerly called MUT9-Like Kinases (MLKs)), which redundantly bind and phosphorylate PIF3 in a red light induced manner (Ni et al., 2017). The quadruple *ppk* null mutant is not viable and PIF3 phosphorylation and subsequent degradation is not observed in knockdown *amiR-PPK1234* mutant, indicating the necessity of PPKs in the process. PhyB enhances interaction between PPK1 and PIF3 in a conformation independent manner and phosphorylated PIF3 is observed only in the presence of phyB and PPK1 together. Thus, the authors propose that phyB may be a pseudokinase enhancing PIF3 phosphorylation by PPKs (Ni et al., 2017). Taken together, phytochrome activation is clearly required for light-induced PIF phosphorylation, most likely by functioning upstream of other kinases reviewed in (reviewed in Pham et al., 2018, Legris et al., 2019). However, we still have a poor understanding how Pfr mediates phosphorylation and whether there is a global mechanism for phosphorylation of all PIFs.

Phosphorylation of several PIFs is followed by PIF ubiquitination by CULLIN (CUL) RING UBIQUITIN LIGASEs (CRLs) (reviewed in Pham et al., 2018, Legris et al., 2019). Five different families of substrate recognition components have been identified to mediate ubiquitination of different PIFs through three members of CRLs: CUL1, CUL3, and CUL4. PIF1 is ubiquitinated by CUL4<sup>COP1/SPA</sup> and CUL1<sup>CTG10</sup>; PIF3 by CUL3<sup>LRB1/2/3</sup> and CUL1<sup>EBF1/2</sup>; PIF4 by CUL3<sup>BOP1/2</sup>; and PIF5 by also CUL4<sup>COP1/SPA</sup> (reviewed in Pham et al., 2018, Legris et al., 2019). While light treatment is shown to be indispensable for all cases mentioned above, phosphorylation is not (reviewed in Pham et al., 2018, Legris et al., 2019)). Thus, it raises the question whether phytochromes are involved in PIF ubiquitination through other mechanisms than being required for PIF phosphorylation.

PhyB is shown to directly interact with PIF regulators HMR and PIL1, promoting their protein accumulation (Galvao et al., 2012, Luo et al., 2014). HMR is a transcriptional co-activator interacting with all PIFs and required for light-mediated degradation of PIF1 and PIF3, whereas promoting PIF4 accumulation in elevated temperatures (Chen et al., 2010, Qiu et al., 2015, Qiu et al., 2019). HMR is also required the transactivation of a set of PIF target genes, showing a dual role for HMR in regulation of PIF-mediated responses including PIF4-mediated elevated temperature response (Qiu et al., 2015, Qiu et al., 2019).

Cryptochromes are other important regulators of PIFs in blue light regulated responses (Keller et al., 2011, Keuskamp et al., 2011, Ma et al., 2016, Pedmale et al., 2016, Boccaccini et al., 2020). Cry1 interacts with PIF4 on DNA and represses its transcriptional activity in a blue light-dependent manner in elevated temperature (Ma et al., 2016). Furthermore, cry1 inhibits *PIF4* expression and PIF4 and PIF5 protein accumulation in a blue light-dependent manner (Boccaccini et al., 2020). Similarly, cry2-PIF4 and cry2-PIF5 complexes are detected on chromatin; however, in contrast to the previous study the authors argue that these interactions rather promote transcriptional activity of PIFs in

response to LB (Pedmale et al., 2016). However, the underlying mechanism for this regulation remains unclear.

Phytochromes, cryptochromes, and UVR8 also indirectly regulate PIF abundance through interacting with COP1/SPA complex (Fig. 4b, 4c). COP1 import into the nucleus is enhanced in elevated temperature and LRRF (Pacin et al., 2013, Park et al., 2017). COP1/SPA complex functions as E3 ligase for bHLH proteins that negatively regulate PIF abundance in shade and elevated temperature. These targets include HFR1, PIL1 (PIF2), PAR1, and PAR2 that are shade-induced bHLH proteins lacking the typical basic DNA-binding domain (reviewed in Hoecker, 2017). PIF4, PIF5, and PIF7 are involved in LRRF-induced expression of these bHLH proteins (Hornitschek et al., 2009, Hornitschek et al., 2012, Li et al., 2012). Hetero-dimers between several PIFs and HFR1 or PAR1 are detected, which inhibit transcriptional activity of PIFs in prolonged LRRF and elevated temperature (Hornitschek et al., 2009, Hao et al., 2012). HFR1 also acts downstream of cry1 to inhibit PIF4 and elevated temperature-induced hypocotyl elongation in blue light (Foreman et al., 2011). However, combination of LB with LRRF reduces the HFR1 protein levels, enhancing PIF activity likely through cry inactivation and indirectly through relieved inhibition of COP1 (Fig. 4c) (de Wit et al., 2016b). Similarly, HFR1 protein levels increase and inhibit PIF-dependent gene expression in response to UV-B in elevated temperature and LRRF, suggesting UVR8 enables the accumulation of PIF-negative regulators via sequestering COP1 (Hayes et al., 2017, Tavridou et al., 2020). Although we have limited information about the other bHLH negative regulators of PIFs, it has been shown that PIL1 interacts with PIF1, PIF3, PIF4 and PIF5, resulting in the inhibition of PIF-mediated transcription (Luo et al., 2014). The interaction between PAR2 and PIFs is not shown, yet the *par2* mutant analysis supports a similar mode of action for PAR2 as PAR1 (Roig-Villanova et al., 2007). Therefore, COP1/SPA complex is an important regulator for PIF activity and abundance.

HY5 and PIFs are key transcription factors that antagonistically modulate photomorphogenesis and skotomorphogenesis, respectively (Fig. 1). COP1/SPA complex positively regulating PIF4 abundance via control of HY5 is shown for elevated temperature responses (Delker et al., 2014, Gangappa & Kumar, 2017). HY5 inhibits PIF4 activity by competing with PIF4 for the same G-box binding elements and directly suppressing *PIF4* expression (Fig. 4b) (Gangappa & Kumar, 2017). Furthermore, HY5 negatively regulates *PIF4* expression in response to elevated temperatures, resulting in reduced PIF4 target gene expression (Delker et al., 2014, Gangappa & Kumar, 2017). It is also shown that sunflecks, the brief periods of exposure to unfiltered sunlight, induce HY5 downstream of phytochromes and UVR8, which inhibit shade-induced hypocotyl elongation (Sellaro et al., 2011, Moriconi et al., 2018). Thus, HY5 is another modulator of PIF activities in light downstream of photoreceptors.

PIFs also interact with DELLAs, a family of growth-suppressing proteins. DELLAs, are important signalling elements of the GA pathway and their abundance is negatively regulated by GA levels (Feng et al., 2008). DELLAs interact with PIF1, PIF3, PIF4, and PIF5 independent of light conditions and mediate their degradation via the proteasome system (Li et al., 2016). These interactions also result in blocking transcriptional activity of PIF3 and PIF4 (Feng et al., 2008, de Lucas et al., 2008). Expression of GA biosynthesis genes are induced in LRF and elevated temperatures, whereas GA levels increase 24h after LRF treatment (Stavang et al., 2009, Bou-Torrent et al., 2014). Consistently, levels of the DELLA proteins decrease in LRF and elevated temperature (Djakovic-Petrovic et al., 2007, Stavang et al., 2009, Blanco-Tourinan et al., 2020). Furthermore, COP1 physically interacts with DELLAs and promotes their degradation in LRF and elevated temperatures independent of GA-mediated pathway (Blanco-Tourinan et al., 2020). Thus, COP1 together with the increased levels of GA in LRF and elevated temperatures promote DELLA degradation, forming a positive feedback loop for PIFs. On the other hand, UV-B inhibits GA biosynthesis gene

expression downstream of UVR8, which partially contributes to UVR8-dependent inhibition of LRRF-induced hypocotyl elongation via stabilisation of DELLAs (Hayes et al., 2014). These studies indicate that GA modulates PIF activity and abundance via regulating DELLAs in varying light conditions.

Circadian clock components regulate PIF abundance and activity. As an important element of circadian clock of plants, the evening complex (EC) is composed of EARLY FLOWERING 3 (ELF3), ELF4, and LUX ARRHYTHMO (LUX) at the end of day. EC represses *PIF4* and *PIF5* expression in the early evening, restricting the expression of these genes to daytime in long-days (LDs) (Nusinow et al., 2011). Elevated temperatures attenuate the activity of EC by reducing ELF3 and LUX binding to their target promoters, leading to high *PIF4* expression (Mizuno et al., 2014, Box et al., 2015, Ezer et al., 2017). It has been also shown that ELF3 protein binds to PIF4 protein and prevents PIF4 from activating its transcriptional targets (Nieto et al., 2015). Furthermore, active phyB is considered to contribute to this regulation as it is not only interacts with ELF3, but also is needed for ELF3 protein accumulation of in the light (Nieto et al., 2015). Other clock components including GIGANTEA (GI), TIMING OF CAB EXPRESSION 1 (TOC1)/ PSEUDO-RESPONSE REGULATOR 1 (PRR1), repress *PIF4* and *PIF5* transcription, while TOC1, PRR5, PRR7, and PRR9 interact with several PIFs, inhibiting their transcriptional activity (Kidokoro et al., 2009, Soy et al., 2016, Zhu et al., 2016, Martin et al., 2018, Li et al., 2020, Zhang et al., 2020). Finally, it has been reported that PCH1 (PHOTOPERIODIC CONTROL OF HYPOCOTYL1) regulates phyB signalling by stabilising phyB-photobody formation (Huang et al., 2016). In tune with its hypocotyl growth, *pch1* mutants have both upregulated *PIF4* transcripts and proteins, suggesting PCH1 may modulate PIF4 levels in the evening (Huang et al., 2016). Thus, the diurnal regulation of PIF activity and abundance is under direct control of circadian clock components.

In summary, phytochromes and cryptochromes interact with PIFs and directly regulate their abundance and activity directly. In addition, together with UVR8, they inhibit PIF-abundance and activity via their downstream regulators, where COP1/SPA is a key complex. HFR1, PIL1, PAR1, HY5, and DELLAs are among these downstream regulators. Finally, circadian clock components are important for regulating daily oscillating PIF levels.

## **Shade and thermomorphogenesis regulate auxin pathway through PIF proteins**

PIF4, PIF5, and PIF7 are identified as major regulators for shade responses (Lorrain et al., 2008, Li et al., 2012), while PIF4, PIF7 and to a lesser extent PIF5 regulates the elevated temperature-induced hypocotyl elongation (Koini et al., 2009, Stavang et al., 2009, Fiorucci et al., 2019, Chung et al., 2020). Transcriptomic analyses of *pif4pif5* and *pif7* mutants show that PIF4, PIF5, and PIF7 control expression of a large number of growth-related genes (Hornitschek et al., 2012, Li et al., 2012, Chung et al., 2020). Furthermore, analysis of LRRFR-regulated genes and PIF5 binding sites reveals that about half of the genes upregulated in shade are direct PIF5 targets (Hornitschek et al., 2012, Kohnen et al., 2016). Moreover, the comparison of PIF4 and PIF5 binding sites shows that PIF4 and PIF5 share over 80% of their binding sites (Hornitschek et al., 2012, Kohnen et al., 2016). Similarly, PIF7 is able to bind to the same genes as PIF4 and PIF5 (Hornitschek et al., 2012, Li et al., 2012, Chung et al., 2020). These indicate that PIF4, PIF5, and PIF7 functions are partially redundant via their shared genomic targets.

Auxin levels and responses oscillate in line with the hypocotyl elongation rhythms (Covington & Harmer, 2007, Nozue et al., 2011). Auxin also plays a central and direct role in LRRFR- and elevated temperature-induced elongation responses. PIFs regulate auxin responses through several steps. In the next

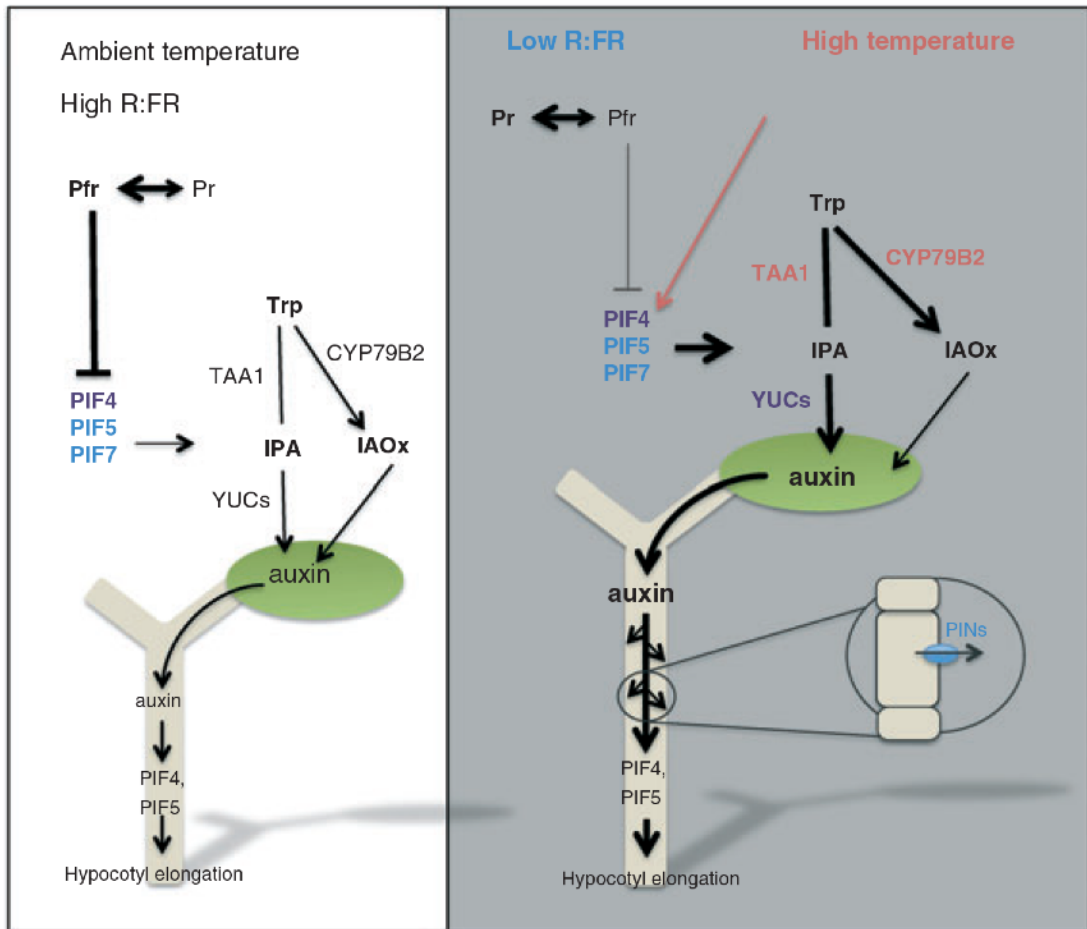


**Figure 5. LRFR- and elevated temperature-induced auxin signaling model in *Arabidopsis* seedlings.**

LRFR and elevated temperature induce auxin production downstream of PIFs through the TAA1-YUC pathway in the cotyledons. LRFR inactivates PhyB, allowing PIFs to bind to their targets, among which are the *YUCCA* auxin biosynthesis genes. In elevated temperature, PIF4 mediates auxin biosynthesis through the TAA1-YUC pathway and the CYP79B2 pathway. Auxin is transported from the cotyledons to the hypocotyl, where PIFs play a role in enhanced auxin sensitivity. PINs laterally distribute auxin, leading to enhanced hypocotyl elongation. Red color: regulation in elevated temperature, blue color: regulation in LRFR, purple color: regulation in both elevated temperature and LRFR (Adapted from de Wit et al., 2014).

paragraphs, I will describe in more detail how PIFs regulate auxin biosynthesis, transport and signalling.

## **Auxin Production**

Levels of indole acetic acid (IAA), a naturally occurring auxin, increase rapidly in response to LRFR and elevated temperature (Tao et al., 2008, Franklin et al., 2011, Hornitschek et al., 2012, Sun et al., 2012, Bou-Torrent et al., 2014, Hersch et al., 2014, Procko et al., 2014). The IAA biosynthesis pathway induced in response to LRFR is the indole-3-pyruvic acid (IPyA)-dependent pathway, in which YUCCAs (flavin-containing monooxygenase) are responsible for the rate-limiting step: conversion of IPyA to IAA (Fig. 5) (Zhao et al., 2001, Stepanova et al., 2008, Tao et al., 2008, Mashiguchi et al., 2011, Won et al., 2011). Expression of *YUC2*, *YUC5*, *YUC8*, and *YUC9* is rapidly induced specifically in cotyledons under LRFR (Nito et al., 2015, Kohnen et al., 2016). Similarly, *YUC8* and *YUC9* expression is strongly induced in cotyledons compared to hypocotyls in elevated temperature (Stavang et al., 2009). Furthermore, *TAA1* and *CYB79B2* expression is induced in elevated temperature, indicating another auxin biosynthesis pathway is involved (Fig. 5) (Franklin et al., 2011). Mutant analyses with these genes confirm their roles in LRFR and elevated temperature responses (Tao et al., 2008, Franklin et al., 2011, Li et al., 2012, Nozue et al., 2015, Kohnen et al., 2016). It is clearly established that PIF4, PIF5, and PIF7 bind to the promoters of *YUC8* and *YUC9*, indicating direct regulation of auxin biosynthesis by PIFs in LRFR and elevated temperature (Franklin et al., 2011, Hornitschek et al., 2012, Li et al., 2012, Fiorucci et al., 2019). Correspondingly, IAA concentration remains at basal levels in the *pif4pif5* and *pif7* mutant seedlings after low R/FR treatment (Hornitschek et al., 2012, Li et al., 2012). Similarly, PIF4 also binds to the promoters of *TAA1*, and *CYP79B2* in elevated temperature (Franklin et al., 2011). Furthermore, PIF4 promotes expression of *LONGIFOLIA 1 (LNG1)* and *LNG2* that likely promotes auxin pathway in elevated temperature (Hwang et al., 2017).

Unlike LRFR and elevated temperature, auxin biosynthesis is not transcriptionally induced in LB (Keuskamp et al., 2011, Pedmale et al., 2016). However, the loss of *TAA1* results in impaired hypocotyl elongation response in LB (Keuskamp et al., 2011, Pedmale et al., 2016), suggesting that auxin biosynthesis is still required in LB-induced hypocotyl elongation. These studies indicate that auxin production in the distal organ cotyledons via PIF activity is essential for hypocotyl elongation responses in response to shade, neighbour proximity and elevated temperature.

### **Auxin transport**

For both LRFR and elevated temperature, auxin produced in cotyledons is subsequently transported to hypocotyls where the elongation occurs (Gray et al., 1998, Stavang et al., 2009, Keuskamp et al., 2010, Procko et al., 2014, Kohnen et al., 2016, Bellstaedt et al., 2019). PIN auxin efflux carriers are responsible for auxin transport (Bennett, 2015). PIFs regulate expression of *PIN3*, *PIN4*, and *PIN7*, thereby contributing to the regulation of auxin transport in LRFR (Li et al., 2012, de Wit et al., 2015, Kohnen et al., 2016). The triple mutant *pin3pin4pin7* hypocotyl elongation is completely impaired in LRFR, indicating the importance of PIN transporters (Kohnen et al., 2016). *PIN3* promoter is identified as a direct target of PIF4 and PIF5 (Hornitschek et al., 2012). Furthermore, the expression of *D6PK* and *D6PKL1* coding for D6 PROTEIN KINASE that phosphorylates PINs for the activation, is upregulated and the loss of function mutant showed a reduced hypocotyl elongation in LRFR (Kohnen et al., 2016). Although there is no transcriptional regulation, the mutant analyses and the inhibition of auxin transport via drug treatment indicates that auxin transport is also indispensable in LB-induced hypocotyl elongation (Keuskamp et al., 2012, Pedmale et al., 2016). Therefore, PIFs are also key modulators of auxin transport which is required for elongation responses of the young seedlings.

### **Auxin response**

PIFs function in auxin responses by regulating expression of genes coding for auxin receptors and auxin repressor proteins (Aux/IAAs) and by co-regulating

expression of a subset of growth-related genes with auxin response factors (ARFs) (Hornitschek et al., 2012, Hersch et al., 2014, Oh et al., 2014, Kohnen et al., 2016). Hypocotyl elongation analyses of *pif4pif5* double and *pif457* triple mutants in response to exogenous auxin treatment indicate PIF involvement in auxin perception and signalling, as auxin treatment cannot completely rescue their impaired hypocotyl elongation response to shade (Nozue et al., 2011, Hornitschek et al., 2012, Hersch et al., 2014, Kohnen et al., 2016). TIR1/AFB proteins are auxin receptors, which form a complex with Aux/IAA repressor proteins in the presence of auxin, leading to proteasome-mediated degradation of Aux/IAAs (Hayashi, 2012). Since Aux/IAA proteins repress auxin-responsive gene expression by inhibiting ARF transcription factors, degradation of Aux/IAAs releases ARFs for auxin-induced gene expression (Hayashi, 2012). PIFs function at several levels in this pathway. First, PIF4 and PIF5 regulate expression of *AFB1*, a member of the TIR1/AFB family, specifically in the hypocotyls (Hersch et al., 2014, Kohnen et al., 2016). The mutants of these receptors or their chemical inhibition strongly reduce hypocotyl elongation in LRFR, LB, and elevated temperature (Gray et al., 1998, Keuskamp et al., 2010, Keuskamp et al., 2011). Second, PIF4, BZR1, and ARF6 share genomic targets including many genes with known functions in cell elongation and auxin response (Oh et al., 2014). In addition, PIF4 also binds ARF6 and *PIF4* over expression increases ARF6 DNA-binding to PIF4-ARF6 common targets (Oh et al., 2014). It is also shown that the loss-of-function mutants of ARF6, ARF7, and ARF8 are impaired in LRFR- and elevated temperature-induced hypocotyl elongation (Reed et al., 2018), indicating other ARFs are also required for the process. Third, two AUX/IAA protein-coding genes, *IAA19* and *IAA29*, are direct targets of ARF6, PIF4, and PIF5 and their expression is upregulated in response to shade (Hornitschek et al., 2009, Hornitschek et al., 2012, Li et al., 2012, Hersch et al., 2014, Oh et al., 2014). *IAA19* and *IAA29* expression is also inducible by exogenous auxin application (Tao et al., 2008, Li et al., 2012), indicating possible coordinated

function of both PIFs and auxin (through ARFs) for expression of these genes. Furthermore, it was recently shown that although auxin levels return to the basal levels after prolonged LRFR, PIF4 levels increase in the vascular tissues of the stem and elevates the expression of *IAA19* and *IAA29* (Pucciariello et al., 2018). Degradation of Aux/IAs specifically in the epidermis is particularly important for hypocotyl elongation in both elevated temperature and LRFR (Procko et al., 2016, Kim et al., 2020). It is shown that PIF4 activity is specifically required in the epidermis, including the induction of *IAA19* expression (Kim et al., 2020). Overall, PIFs are important regulators of auxin response both by regulating gene expression of auxin-signalling elements and through their coordinated function with ARFs for regulation of cell elongation.

### **Brassinosteroids**

Brassinosteroids (BRs) are plant steroid hormones that are indispensable for hypocotyl elongation in LB, LRFR, and elevated temperature (Stavang et al., 2009, Keller et al., 2011, Keuskamp et al., 2012, Bou-Torrent et al., 2014, Ibanez et al., 2018). BRs are synthesised downstream of sterol biosynthesis pathway, where campesterol is the progenitor (Clouse, 2011). BRs are mainly perceived by BRASSINOSTEROID-INSENSITIVE 1 (BRI1) located in plasma membrane (PM) (Wei 2016). Upon BR binding, BRI1 phosphorylates a downstream negative regulator BRI1 KINASE INHIBITOR 1 (BKI1) that dissociates from PM, allowing BRI1 to recruit its co-receptor BRI1-ASSOCIATED RECEPTOR KINASE 1 (BAK1) and get activated. The active BRI1 phosphorylates membrane-bound cytoplasmic kinases which activate BRI1-SUPPRESSOR 1 (BSU1), a PP1-type phosphatase. BSU1 dephosphorylates and inactivates a key negative regulator of BR signalling, BRASSINOSTEROID-INSENSITIVE 2 (BIN2), leading the transcriptional regulation of BR-responsive genes downstream of two transcription factors BRASSINAZOLE-RESISTANT 1 (BZR1) and BRI1-EMS-SUPPRESSOR 1 (BES1/BZR2). BRI1 expression is induced in LRFR (Roig-Villanova et al., 2006, Sorin et al., 2009). Furthermore, exogenous application of auxin and

LRFR promotes nuclear accumulation of BZR1 in the hypocotyl epidermis (Procko et al., 2016). BZR1 and PIF4 physically interact and co-regulate common target genes with the involvement of ARF6 (Oh et al., 2014). Interestingly, BR levels decrease in short periods of LRFR treatment, yet exogenously applied BR significantly enhances the hypocotyl elongation (Bou-Torrent et al., 2014). This suggests that BR-mediated hypocotyl elongation in LRFR is due to enhanced BR-signalling rather than the biosynthesis. BR signalling is also shown to be important for expression of LRFR-induced genes including auxin responsive genes (Kozuka et al., 2010, Cifuentes-Esquivel et al., 2013). In elevated temperature, BZR1 accumulates in the nucleus and induce PIF4 expression (Ibanez et al., 2018). PIF4 also interacts with BES1 and de-represses elevated temperature-induced gene expression including BR biosynthetic genes that are repressed by BES1 homodimers (Martinez et al., 2018). Finally, auxin transport is shown to be important for BR-induced responses in elevated temperature (Bellstaedt et al., 2019). Overall, BRs alone or together with PIFs and auxin regulate hypocotyl elongation in response to changing environmental cues.

## **Gibberellins**

Gibberellins (GAs) are diterpene phytohormones that derived from the isoprenoid biosynthetic pathway (Sun, 2008, Hernandez-Garcia et al., 2020). 2-oxoglutarate-dependent dioxygenases (2-OGD) namely GA20-oxidase (GA20ox), GA3ox, and GA13ox are the key enzymes for the production of bioactive GAs. On the other hand, another type of 2-OGD, GA2ox converts the active GAs to inactive forms via 2 $\beta$ -hydroxylation. The binding of bioactive GAs to the GA receptor, GIBBERELLIN INSENSITIVE DWARF1 (GID1) that is found in nucleus and the cytoplasm induces a conformational change of the receptor, enabling GID1 interaction with the DELLAs, the key transcriptional regulator of GA signalling (Hernandez-Garcia et al., 2020). Inhibition of GA biosynthesis and signalling impairs hypocotyl elongation in LRFR and elevated temperature (Djakovic-Petrovic et al., 2007, Stavang et al., 2009). LRFR, elevated

temperature, and exogenous auxin treatment modulate expression of several genes in the GA biosynthesis pathway including members of GA20OXs, GA3OXs, and GA2OXs (Djakovic-Petrovic et al., 2007, Stavang et al., 2009, Chapman et al., 2012). It is also shown that GA levels increase 24h after LRFR treatment (Bou-Torrent et al., 2014). As mentioned earlier, GAs are important for hypocotyl elongation responses mainly via proteasomal degradation of DELLA proteins that are negative regulators of PIFs (Djakovic-Petrovic et al., 2007, Feng et al., 2008, de Lucas et al., 2008, Stavang et al., 2009, Li et al., 2016).

## **Ethylene**

The rate limiting step of ethylene biosynthesis is the conversion of S-AdoMet to 1-AMINOCYCLOPROPANE-1-CARBOXYLATE (ACC) by ACC SYNTHASE (ACS) (Wang 2002). Several ACS genes are upregulated in LRFR or low light treated young seedlings and rosettes (Vandenbussche et al., 2003, Kohnen et al., 2016). Low light enhances ethylene production in Arabidopsis rosettes, whereas LRFR increases the ethylene in tobacco (Vandenbussche et al., 2003, Pierik et al., 2004). Gene ontology (GO) term analysis from LRFR-regulated genes indicates that response to ethylene is enriched among genes upregulated in cotyledons and downregulated in the hypocotyl (Kohnen et al., 2016). Ethylene insensitive mutants retain a full hypocotyl elongation response whereas the petiole elongation is impaired in LRFR, indicating organ-specific roles for ethylene in LRFR (Pierik et al., 2009, Das et al., 2016). However, exogenous application of ethylene induces hypocotyl elongation somewhat similar to LRFR treatment (Das et al., 2016). Transcriptome comparison of ethylene- and LRFR-treated seedlings indicates that both treatments upregulated genes related hormonal responses and cell growth (Das et al., 2016). Although the role of ethylene is less-characterised in hypocotyl elongation responses, these studies show that ethylene is another key hormone in the process.

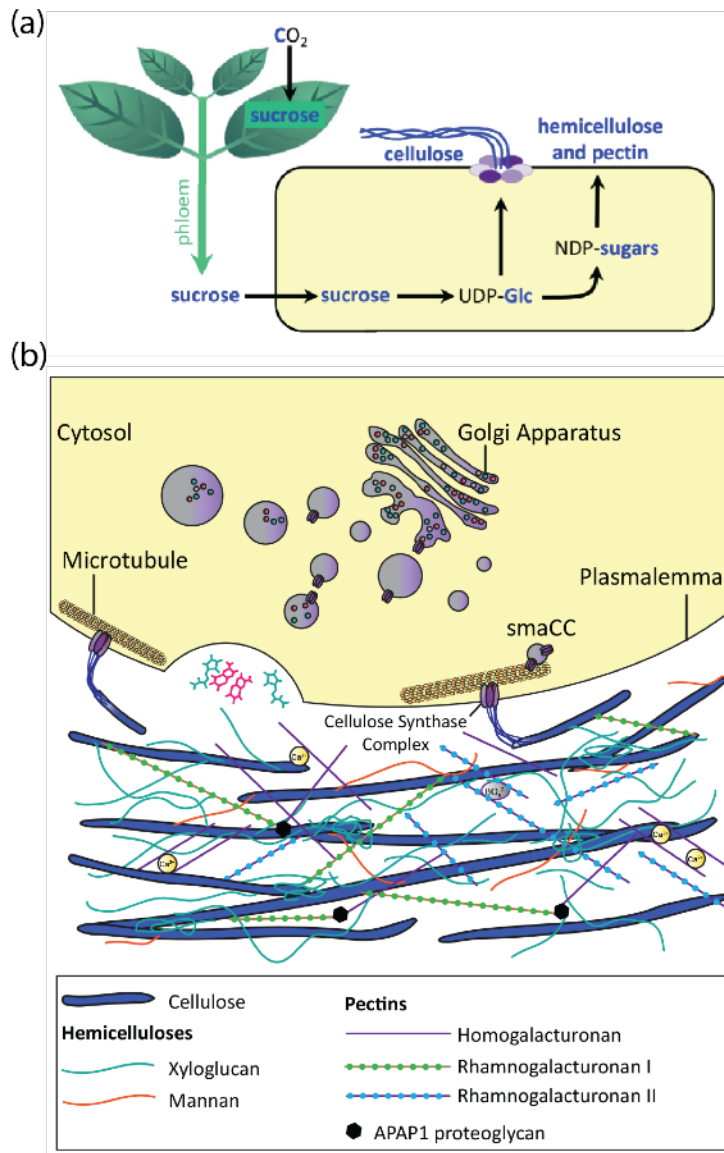


**Figure 6. The model for cell wall biosynthesis and structure.**

(a) The photosynthetically fixed CO<sub>2</sub> in source leaves is transported to the sink organ (hypocotyls) in the form of sucrose. Sucrose is first catabolised to UDP-Glc that is used for biosynthesis of cellulose or further converted to other forms of nucleotide-sugars that are the precursors of hemicelluloses and pectin. (b) Cell walls are composed of glucan-based cellulose microfibrils embedded in a highly hydrated matrix composed of pectins (homogalacturonan and rhamnogalacturonans), hemicelluloses (xyloglucan and mannan), structural proteins (e.g. extensins and arabinogalactan proteins) and proteoglycans. New cell wall material and cellulose synthase complexes (CSCs) are produced in Golgi and secreted to the extracellular space and PM by exocytosis, respectively (Adapted and modified from Verbancic et al., 2018).

## Regulation of cellular elongation

### Cell wall extension is the key for the cellular elongation

Hypocotyl growth occurs through cellular elongation rather than division (Gendreau et al., 1997). In the case of LRF and elevated temperature, it is shown that the epidermal cell elongation is the limiting factor for hypocotyl elongation (Procko et al., 2016, Kim et al., 2020). The dynamics of cell elongation are partially established using rapidly elongating pollen tubes, root hair cells, etiolated hypocotyls, and cells in root elongation zone (Hepler et al., 2013, Kutschera & Niklas, 2013, Ackerman-Lavert & Savaldi-Goldstein, 2020). As it determines the boundaries of a cell, cell elongation is directly dependent on the properties of the primary cell wall (CW). CW in Arabidopsis is composed of cellulose microfibrils (CMFs) embedded in a hydrated matrix of hemicelluloses (xyloglucan), pectins (homogalacturonan and rhamnogalacturonan), and structural proteins (e.g., extensins and arabinogalactan proteins) (Fig. 6b) (Verbancic et al., 2018). Cell elongation occurs via two distinct changes in CW: (i) biosynthesis and deposition of new CW components and (ii) increasing the flexibility of CW via loosening the CW matrix.

The building blocks for synthesis of cell wall polysaccharides are nucleotide sugars, e.g., uridine diphosphate (UDP) glucose (UDP-Glc). The ultimate source of C for the synthesis of UDP-Glc is the photosynthetically fixed CO<sub>2</sub> in source leaves. Usually, the rapid cellular elongation rather happens in sink tissues such as hypocotyls and roots whereas there is not much CW biosynthesis in the fully expanded source leaves. Therefore, in the source tissues, the most of the UDP-Glc is converted to sucrose, which is the only form of C-assimilates that can be exported to the sink organs via phloem (Verbancic et al., 2018) (Fig. 6a). Sucrose-H<sup>+</sup> symporters (SUT) can take up apoplastic sucrose directly into the cell. As a second pathway, sucrose is first hydrolysed to glucose and fructose by cell wall invertase (cwINV), which is followed by the import of the hexose sugars by sugar

transport proteins (STP). Sucrose is not only used as an energy source to drive events required for cellular elongation but also used as the C-source for biosynthesis of CW material. Sucrose is first catabolised to UDP-Glc by sucrose synthase (SUS) or invertase (INV) and UDP-Glc pyrophosphorylase (UGP) in the cytosol. UDP-Glc is later used for synthesis of cellulose or further converted to other forms of nucleotide-sugars that are the precursors of hemicelluloses and pectin (Fig. 6a) (reviewed in Verbancic et al., 2018).

The main components of CW, CMFs are synthesised by Cellulose Synthase A (CESA) complexes (CSCs) located at the plasma membrane (PM) (Fig. 6). The CESAs are assembled into CSCs either at the ER or at Golgi apparatus. After they assembled, CSCs are secreted to the PM via Golgi-driven vesicles. Hemicellulose and pectin polymers are made in Golgi and similarly secreted the PM by exocytosis (Verbancic et al., 2018) (Fig. 6b). The exocytosis of CSCs and other CW polymers also supply the new PM material required for the elongating cell (Steer & Steer, 1989, Hepler et al., 2013). However, it is evident that PM material delivered during the secretory process is more than the requirement of the elongating cell. Thus, the excess is retrieved through endocytosis (Steer & Steer, 1989, Hepler et al., 2013). The exocytosis and endocytosis processes are guided by cytoskeleton arrangements where actin filaments are the railways for the vesicles (Hepler et al., 2013, Wang et al., 2020). The cell elongation is a polarised process thus requires directional delivery of the CSCs and other CW materials. Cortical microtubules (CMTs) are rapidly oriented in a transverse direction, leading the anisotropic growth by orienting CSCs in elongating cells including shaded petiole cells (Paradez et al., 2006, Sasidharan et al., 2014) (Fig. 6b).

CW loosening occurs via acidification of CW space by activation of PM-H<sup>+</sup>ATPases (i.e., acid growth) and modification of CW polysaccharides to relax the matrix by CW remodelling enzymes such as EXPANSINs (EXPs), XYLOGLUCAN ENDOTRANSGLUCOSYLASE/HYDROLASEs (XTHs), PECTIN

METHYLESTERASEs (PME), EXTENSINs (EXT), and ARABINOGALACTAN PROTEINs (AGPs). The acidification is not only required to physically induce loosening of the matrix, but also provides an optimum range for activity of proteins functioning in CW loosening (Rayle & Cleland, 1992). On the contrary to H<sup>+</sup> ions increasing CW flexibility, Ca<sup>2+</sup> ions bind to de-esterified pectin acidic residues in the extracellular space, cross-linking them to stop CW expansion (Hepler et al., 2013). However, Ca<sup>2+</sup> gradient in cytosol regulates the direction of growth, presumably by controlling the location of vesicle secretion (Hepler et al., 2013). In addition, boron further contributes to interlinking the pectin network by crosslinking pectin polymers (Verbancic et al., 2018). These reports show the involvement of several regulatory elements during CW loosening.

### **PIFs and hormonal responses regulate cell elongation**

PIFs and downstream hormonal responses are shown to regulate several of the above-mentioned cell elongation pathways.

Auxin is a key hormone regulating cell elongation via several pathways. Increased auxin levels mediate cell elongation by osmoregulation and induction of cell wall modifications (Keller & Van Volkenburgh, 1996, lino et al., 2001, Teale et al., 2006). Studies on *Avena sativa* L. and *Phaseolus vulgaris* protoplasts indicate that IAA increases the conductance of the plasma membrane to K<sup>+</sup> and Cl<sup>-</sup>, resulting in swelling of protoplasts (Keller & Van Volkenburgh, 1996, lino et al., 2001). Moreover, auxin activates plasma membrane (PM) H<sup>+</sup>ATPases by promoting their phosphorylation (Takahashi et al., 2012, Spartz et al., 2014, Ren & Gray, 2015). PP2C-D phosphatases are responsible for dephosphorylation of PM-H<sup>+</sup>ATPases thereby inhibiting their activity. Increase in auxin levels trigger expression of *SMALL AUXIN UP-RNA (SAUR)* genes, several members of which interact with the PP2C-D phosphatases and inhibit dephosphorylation of plasma membrane H<sup>+</sup>ATPases (Spartz et al., 2014, Ren & Gray, 2015). Activation of PM-H<sup>+</sup>ATPases lowers the pH of the cell wall space, which is also observed in *Arabidopsis* petioles after green shade treatment (Rayle & Cleland, 1992,

Sasidharan et al., 2010). High auxin levels also directly regulate CW modification by inducing expression of genes coding for EXPs and XTHs, AGPs, EXTs, and class III peroxidases (Teale et al., 2006, Chapman et al., 2012). Furthermore, auxin is likely to contribute to anisotropic growth by regulating cytoskeletal elements. Auxin can rapidly lead transverse orientation of CMTs in both *Arabidopsis* root and hypocotyl epidermal cells (Vineyard et al., 2013, Chen et al., 2014b). A recent study shows that transverse orientation of CMTs in light-grown hypocotyls is dependent on the TIR1/ABF auxin co-receptors (True & Shaw, 2020). Moreover, auxin regulates actin filament orientation in *Oryza sativa* in order to mediate polar auxin transport required for gravitropic responses (Nick et al., 2009). Lastly, exogenous application of auxin induces a small and slow increase in  $Ca^{2+}$  in some of the treated cells (Ayling et al., 1994). Overall, auxin functions as a key phytohormone for modulation of CW organisation.

BR signalling also induces expression of various CW biosynthesis and remodelling genes in dark, LRF, and elevated temperature either alone or together with PIF4 and ARF6 (Stavang et al., 2009, Keller et al., 2011, Keuskamp et al., 2012, Bou-Torrent et al., 2014, Ibanez et al., 2018, Ackerman-Lavert & Savaldi-Goldstein, 2020). It is shown that BES1 can bind to promoters of several CESAs (Xie et al., 2011). Furthermore, BIN2 negatively regulates CSC activity by phosphorylating at least one component of CSC in the absence of BR (reviewed in Wang et al., 2020). BR biosynthesis and signalling mutants also show longitudinally oriented CMT arrays, which can reorient transversely upon exogenous BR treatment (Wang et al., 2012). Finally, BR contributes to CW loosening via phosphorylation and activation  $H^+$ -ATPases (reviewed in Ackerman-Lavert & Savaldi-Goldstein, 2020). Thus, BRs are another key hormones that is important for CW organisation.

GA is shown to affect cellulose synthesis in cotton, sorghum, and rice (reviewed in Wang et al., 2020). GA effects on CMT organisation and dynamics are also shown. GA deficient mutants and inhibition of GA biosynthesis caused

disordered CMTs in the root cortex of maize (Baluska & Barlow, 1993). Prefoldin complex that plays an important role in tubulin dimer assembly, interacts with DELLAs, which leads to CMT disorganisation (Locascio 2013). In the presence of GA, DELLAs are degraded and prefoldin complex remains functional to regulate tubulin folding (Locascio et al., 2013). These studies indicate that GA functions on cell elongation via several mechanisms.

As summarised in the previous section, PIFs induce expression of auxin related genes, interacts with ARF6, BZR1, and BES1 to regulate transcription in shade and elevated temperature. However, the impaired LRFR-hypocotyl elongation of *pif4pif5* and *pif4pif5pif7* mutants cannot be completely rescued by application of exogenous auxin (Nozue et al., 2011, Hornitschek et al., 2012, Kohnen et al., 2016). Moreover, transcriptomic comparison of LRFR-treated and auxin-treated seedlings reveals that only half of the shade-induced genes are induced by auxin treatment (Tao et al., 2008). Genes, of which expression are differentially regulated in response to LRFR but not to auxin, include members of cell wall remodelling gene families such as *EXPs*, *XTHs*, and *AGPs* (Chapman et al., 2012, Kohnen et al., 2016). Genome-wide transcriptomic analyses reveal that expression of several members of these three gene families is misregulated in LRFR- or LB-treated *pif4pif5* and *pif7* mutant seedlings (Hornitschek et al., 2012, Li et al., 2012, Pedmale et al., 2016). Furthermore, promoter regions of several *EXPs*, *XTHs* and *AGPs* are identified as direct targets PIF4 and PIF5 (Hornitschek et al., 2012, Oh et al., 2014). Altogether, several lines of evidences indicate that PIF4, PIF5, and PIF7 induce genes required for cell elongation also independent of auxin, by directly inducing expression of gene families responsible for cell wall remodelling.

In summary, PIFs regulate cell elongation distally in the major light and temperature sensing organs, cotyledons by inducing expression of auxin production and transport genes. Although the local PIF action in the elongating hypocotyls is less characterised, PIFs promote expression of genes required for

cell wall organisation and auxin responses. PIFs interact with auxin and BR related transcription factors to regulate transcription of many genes, yet they can also work partially independent of auxin and BRs.

## Aim of the study

The aim of my thesis is to investigate organ-specific PIF-mediated growth responses in order to increase our understanding of molecular mechanisms underlying hypocotyl elongation response in LRFR, LB, and elevated temperature.

It is well established that PIF4 mediates hypocotyl elongation responses in elevated temperature. Surprisingly, little is known about the contribution of other PIFs, especially PIF7 that is the major regulator of LRFR-induced hypocotyl elongation. In Chapter 1, considering the overlap between molecular pathways and signalling components regulating LRFR and elevated temperature responses, we investigated the role of PIF7 in elevated temperature in comparison to PIF4.

The perception LRFR leads to morphological changes in young seedlings where hypocotyls elongate and cotyledon growth is arrested. Cotyledons are the source organs where CO<sub>2</sub> fixation mainly occurs and supply necessary resources to the growing sink organs. While the rate of photosynthesis is not affected by LRFR in leaves, the photosynthetic capacity of tomato stems decreases to almost zero in LRFR. Biosynthesis of cell wall polysaccharides and other cellular components are thus expected to be driven by the C-fixed in cotyledons in LRFR. In Chapter 2, we investigated how the fixed carbon partitioned between cotyledons and hypocotyls of *Arabidopsis thaliana* and *Brassica rapa* seedlings in LRFR.

Unlike LRFR, the photosynthetically active radiation (PAR) decreases in LB, which is expected to reduce carbon fixation due to reduced photosynthesis. However, LB and LRFR induce elongation of hypocotyl to a similar extent, raising the question to what extent the molecular mechanisms providing the materials needed for cell elongation in LB and LRFR are similar or different. In Chapter 3, we studied organ-specific transcriptome responses in LB and LRFR in order to

better understand the similarities and differences between these two light conditions. Furthermore, although the mutants lacking PIFs or auxin biosynthesis genes are impaired in LB-induced hypocotyl elongation, their role in LB-regulated transcriptional changes remains largely elusive. Therefore, we also analysed organ-specific LB-transcriptome of *pif457* and *yuc2589* mutants that are completely impaired in LB-induced hypocotyl elongation.

The distal role of PIFs in LRFR-induced hypocotyl elongation via induction of auxin biosynthesis and transport is well established. However, what PIFs locally do in elongating hypocotyls remains largely unclear. The exocytosis-mediated secretion of cell wall material provides the new plasma membrane required for elongating cells. Transcriptome analysis shows that genes coding for enzymes functioning in biosynthesis of lipids including PM lipids are specifically induced in hypocotyls in LRFR. Therefore, in Chapter 3, we also studied the local roles of PIFs in LRFR with a focus on PM lipids. We investigated mutants impaired in biosynthesis of sterol, a major component of PM. Furthermore; we compared the organ-specific transcriptome responses of *pif457* and *yuc2589* mutants in order to establish auxin-dependent roles of PIFs in LRFR.

## **RESULTS**

**Chapter 1. PHYTOCHROME INTERACTING  
FACTOR 7 is important for early responses to  
elevated temperature in Arabidopsis  
seedlings**

## OVERVIEW

I collaborated with Dr. Anne-Sophie Fiorucci and Dr. Vinicius Costa Galvao on this project where we studied the role of PIF7 during elevated temperature-induced elongation responses in *Arabidopsis*, under the supervision of Prof. Christian Fankhauser. We published our results in the journal *New Phytologist* in 2019 (Fiorucci et al., 2019).

I was one of the three leading investigators together with Dr. Fiorucci and Dr. Galvao. I was involved in the project to design and perform the experiments which combined phenotyping, pharmacological and genetic approaches. I conducted and analysed the experiments for hypocotyl elongation (Fig. 1a, 1b, 2d, S2a, S2b, S2c), the detection of PIF7 protein levels (Fig. 4c, S6a, S6b), and gene expression analyses (RT-qPCR) of various genes (Fig 2a, 3b, 4b, S4). I analysed and interpreted data with the participation of the authors of the publication. Prof. Christian Fankhauser wrote the manuscript.

## Rapid report

# PHYTOCHROME INTERACTING FACTOR 7 is important for early responses to elevated temperature in *Arabidopsis* seedlings

Author for correspondence:  
Christian Fankhauser  
Tel: +41 21 692 3941  
Email: christian.fankhauser@unil.ch

Received: 16 July 2019  
Accepted: 5 November 2019

Anne-Sophie Fiorucci\* , Vinicius Costa Galvão\* , Yetkin Çaka Ince\* ,  
Alessandra Boccaccini , Anupama Goyal, Laure Allenbach Petrolati ,  
Martine Trevisan  and Christian Fankhauser 

Faculty of Biology and Medicine, Centre for Integrative Genomics, University of Lausanne, Génopode Building, Lausanne CH-1015, Switzerland

*New Phytologist* (2019)  
doi: 10.1111/nph.16316

**Key words:** *Arabidopsis thaliana*, auxin, PIF4, PIF7, thermomorphogenesis.

### Summary

- In response to elevated ambient temperature *Arabidopsis thaliana* seedlings display a thermomorphogenic response that includes elongation of hypocotyls and petioles. Phytochrome B and cryptochrome 1 are two photoreceptors also playing a role in thermomorphogenesis. Downstream of both environmental sensors PHYTOCHROME INTERACTING FACTOR 4 (PIF4) is essential to trigger this response at least in part through the production of the growth promoting hormone auxin.
- Using a genetic approach, we identified PHYTOCHROME INTERACTING FACTOR 7 (PIF7) as a novel player for thermomorphogenesis and compared the phenotypes of *pif7* and *pif4* mutants. We investigated the role of PIF7 during temperature-regulated gene expression and the regulation of PIF7 transcript and protein by temperature.
- Furthermore, *pif7* and *pif4* loss-of-function mutants were similarly unresponsive to increased temperature. This included hypocotyl elongation and induction of genes encoding auxin biosynthetic or signalling proteins. PIF7 bound to the promoters of auxin biosynthesis and signalling genes. In response to temperature elevation *PIF7* transcripts decreased while PIF7 protein levels increased rapidly.
- Our results reveal the importance of PIF7 for thermomorphogenesis and indicate that PIF7 and PIF4 likely depend on each other possibly by forming heterodimers. Elevated temperature rapidly enhances PIF7 protein accumulation, which may contribute to the thermomorphogenic response.

### Introduction

Ambient temperature influences plants in numerous ways. Their distribution, phenology, defence capacity, growth and development are altered by modest changes in average temperature (Quint *et al.*, 2016; Gangappa *et al.*, 2017; Lau *et al.*, 2018; Casal & Balasubramanian, 2019). In response to mild temperature elevation *Arabidopsis* displays a number of growth and developmental responses known as thermomorphogenesis, which include accelerated flowering, hypocotyl and petiole elongation, a reduction of the stomatal index and leaf hyponasty (Quint *et al.*, 2016; Casal & Balasubramanian, 2019). Some of these responses improve the cooling capacity of *Arabidopsis* rosettes, which is likely important

for plants to cope with increased temperature (Crawford *et al.*, 2012).

Thermomorphogenesis and photomorphogenesis are similar at different levels. This is particularly obvious when comparing shade and elevated temperature responses (Legris *et al.*, 2017). In both cases environmental sensing depends at least in part on the photoreceptors phytochrome B (phyB) and cryptochrome 1 (cry1) (Jung *et al.*, 2016; Legris *et al.*, 2016; Ma *et al.*, 2016; Pedmale *et al.*, 2016; Casal & Balasubramanian, 2019). Other signalling components including ELONGATED HYPOCOTYL 5 (HY5), CONSTITUTIVELY PHOTOMORPHOGENIC 1 (COP1) and DE-ETIOLATED 1 (DET1), which were initially identified for their role in light responses, also play an important role in thermomorphogenesis (Delker *et al.*, 2014; Gangappa & Kumar, 2017; Park *et al.*, 2017).

\*These authors contributed equally to this work (listed alphabetically).

PHYTOCHROME INTERACTING FACTOR 4 (PIF4) is an essential component for high temperature response under most tested conditions, while the role of PIF1, PIF3 and PIF5 is minor (Koini *et al.*, 2009; Stavang *et al.*, 2009; Nomoto *et al.*, 2012; Zhu *et al.*, 2016; Qiu *et al.*, 2019). PIF4 is inhibited by phyB and cry1 (Ma *et al.*, 2016; Qiu *et al.*, 2019), while PIF4 function depends on HEMERA that regulates both PIF4 abundance and its transactivating potential (Qiu *et al.*, 2019). A key role of PIF4 is to induce expression of auxin biosynthetic and signalling genes ultimately leading to hypocotyl elongation (Franklin *et al.*, 2011; Sun *et al.*, 2012; Raschke *et al.*, 2015). Hypocotyl elongation in response to shade and temperature elevation also depends on other phytohormones including gibberellic acid (GA) and brassinosteroids (BR) (Quint *et al.*, 2016; Legris *et al.*, 2017; Casal & Balasubramanian, 2019). BR acts in the hypocotyl while auxin biosynthesis mainly occurs in cotyledons before being transported to the hypocotyl to promote elongation (Stavang *et al.*, 2009; Oh *et al.*, 2012; Kohnen *et al.*, 2016; Procko *et al.*, 2016; Ibanez *et al.*, 2018; Martinez *et al.*, 2018; Bellstaedt *et al.*, 2019).

Given the overlap of signalling components regulating temperature and shade responses and the central role of PHYTOCHROME INTERACTING FACTOR 7 (PIF7) in the phyB-mediated neighbour proximity response, we decided to test whether PIF7 is required for elevated temperature-induced growth responses.

## Materials and Methods

### Plant material

*Arabidopsis thaliana* Columbia (Col-0) ecotype was used. The mutants *phyB-9* (Neff *et al.*, 1998), *cry1-304* (Mockler *et al.*, 1999), *yuc2yuc5yuc8yuc9* (Nozue *et al.*, 2015), *pif4-101*, *phyBpif4* (Lorrain *et al.*, 2008), *phyBpif7* (Galvao *et al.*, 2019), *phyB-9pif4-101pif5-3pif7-1* (Goyal *et al.*, 2016), *pif4-101pif5-3pif7-1* (de Wit *et al.*, 2015), *pif7-1* and *pif7-2* (Leivar *et al.*, 2008), were previously characterized. The transgenic PIF7-HA line (*pif7-2/pPIF7::PIF7-3HA-tPIF7*) was previously described (Galvao *et al.*, 2019). Furthermore, *cry1-304phyB-9*, *pif4-101pif7-2*, *cry1-304pif4-101pif5-3* and *cry1-304pif4-101pif5-3pif7-1*, *yuc2yuc5yuc8*, *yuc2yuc5yuc9*, *yuc2yuc8yuc9* and *yuc5yuc8yuc9* were generated by crosses and confirmed by genotyping using oligonucleotides listed in the Supporting Information Table S1. The *yuc* alleles are as in Nozue *et al.* (2015).

### Phenotypic characterization and growth conditions

Seed sterilization and stratification, plant growth and light conditions were described previously (de Wit *et al.*, 2015; Kohnen *et al.*, 2016). Long-day (LD) or short-day (SD) photoperiods correspond to 16 h light : 8 h dark or 8 h light : 16 h dark, respectively, with *c.* 120  $\mu\text{moles m}^{-2} \text{s}^{-1}$  of photosynthetically active radiation (PAR) in LD and SD. For hypocotyl elongation measurements, seeds were sown on sterile nylon meshes on the growth media. Seedlings were grown on vertical plates in an incubator (Model AR-22L; CLF Plant Climatics, Wertingen, Germany) for 4 d at 21°C. High temperature treatment (28°C)

started on day 5 at ZT2. For picloram (Sigma-Aldrich, Steinheim, Germany, P5575) treatment, nylon meshes were transferred on day 5 before the temperature shift to half strength MS medium with the indicated picloram concentration (0.1% dimethyl sulphoxide (DMSO) for Mock). Seedlings imaging and measurements were described previously (de Wit *et al.*, 2018). Petiole measurements were performed as described (de Wit *et al.*, 2015). Following 14 d in a LD growth room, plants were transferred to AR-22L incubators and acclimated for 1 d to constant 21°C (LD). The next morning (ZT3), temperature in one incubator was shifted to constant 28°C. Petiole length of leaf 3 was measured after 3 d of treatment.

### RNA isolation and quantitative RT-PCR

RNA isolation and reverse transcription quantitative polymerase chain reaction (RT-qPCR) reactions were performed as previously described (Kohnen *et al.*, 2016). Oligonucleotides are listed in Table S1.

### ChIP-qPCR

Briefly, 6-d-old PIF7-HA (Galvao *et al.*, 2019) seedlings grown in LD at 21°C were either kept at 21°C or shifted at ZT2 to 28°C for 2 h before harvesting in liquid nitrogen. Chromatin extraction was performed as described previously (Bourbousse *et al.*, 2018) except that samples were crosslinked only with formaldehyde. Immunoprecipitation was performed as described previously (Gendrel *et al.*, 2005) using an anti-HA antibody (Santa Cruz Biotechnology, Inc., Dallas, TX, USA; sc-7392 X). The qPCR was done in triplicates on input and immunoprecipitated DNA. Oligonucleotides are listed in Table S1.

### Western-blot analysis

Total protein extracts from PIF7-HA seedlings were obtained as previously described (Galvao *et al.*, 2019). For PIF4 Western-blot 20–25 seedlings were collected in liquid nitrogen and proteins extracted in 90  $\mu\text{l}$  extraction buffer (100 mM Tris-HCl pH 6.8, 5% SDS, 20% glycerol, 80  $\mu\text{M}$  MG132, 20 mM DTT, 1 $\times$  protease inhibitor cocktail (P9599; Sigma-Aldrich), 1 mM bromophenol-blue), boiled at 95°C for 5 min and centrifuged for 2 min. Protein samples were separated on 4–20% Mini-Protean TGX gels (Bio-Rad, Hercules, CA, USA) and blotted on nitrocellulose membrane (Bio-Rad) using Turbo transfer system (Bio-Rad). Membranes were blocked with 5% milk overnight at 4°C for  $\alpha$ PIF4, and 1 h at room temperature for  $\alpha$ HA, before probing with anti-HA coupled with horseradish peroxidase (HRP) (Roche, Mannheim, Germany; Cat. 12013819001), polyclonal H3 (1 : 2000; Abcam, Cambridge, UK; Cat. no.1791), polyclonal PIF4 (1 : 3000, Abiocode R2534-4) or DET3 (1 : 20 000) antibodies. HRP-conjugated anti-rabbit was used as secondary antibody. Chemiluminescence signal were obtained with Immobilon Western Chemiluminescent HRP Substrate (Millipore, Merck KGaA, Darmstadt, Germany) on an ImageQuant LAS 4000 mini (GE Healthcare, Buckinghamshire, UK). Relative intensities correspond to the average of HA/H3 of six biological replicates obtained with IMAGEJ (<https://imagej.nih.gov/ij/>).

## Yeast two-hybrid assay

*PIF7* and *PIF4* full length coding sequences were cloned into the pGBKT7 and pGADT7 vectors (Clontech, Mountain View, CA, USA). After co-transformation of yeast strain TATA (Hybrigenics, Paris, France) and selection of transformants, serial cell suspensions were spotted on synthetic drop-out medium lacking leucine and tryptophan (SD-LW) and plates were put at 30°C for 2 d. A  $\beta$ -galactosidase assay was performed directly on yeast spots as previously described (Duttweiler, 1996).

## Statistical analysis

We performed two-way analysis of variance (ANOVA) (aov) and computed Tukey's Honest Significance Differences (HSD) test (AGRICOLAE package) with default parameters using R software (<https://www.r-project.org/>).

## Results

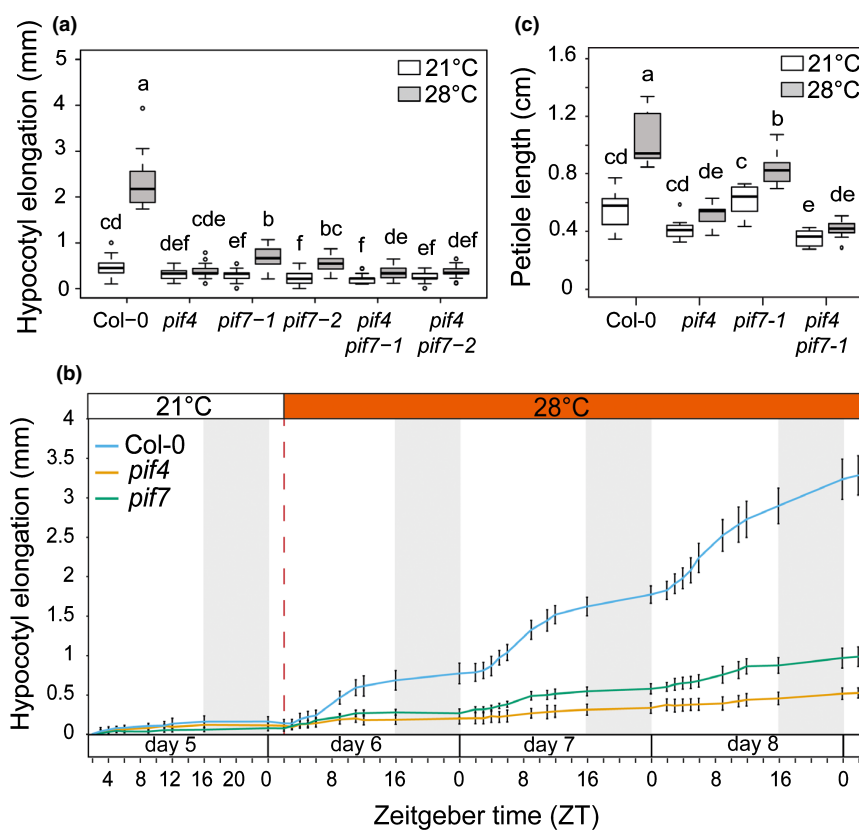
### The thermomorphogenic response depends on PIF7

We analysed the thermomorphogenic response in 4-d-old seedlings grown under LDs that were either kept at 21°C or transferred to 28°C for three additional days. We used this shift protocol to allow us to investigate the early response to increasing temperature. Consistent with previous reports (Koini *et al.*, 2009; Stavang *et al.*, 2009), wild-type Col-0 (WT) hypocotyl elongated robustly at

28°C while *pif4* was largely unresponsive (Fig. 1a). The phenotype of both tested *pif7* alleles was slightly less severe than *pif4* while *pif4pif7* was similar to *pif4* (Fig. 1a). We also analysed the thermomorphogenic hypocotyl elongation response in SDs and found that *pif7* like *pif4* was largely unresponsive to temperature elevation (Fig. S1). We conclude that PIF7 is required for elevated ambient temperature-induced hypocotyl elongation irrespective of day length and conducted all subsequent experiments in LDs because in nature higher temperatures are more common when days get long.

To determine whether the phenotype observed after 3 d reflects a similar defect in the growth pattern we followed growth kinetics of the WT, *pif4* and *pif7*. Elevated temperature enhanced growth during the day while growth at night was limited in both conditions (Fig. 1b) (Park *et al.*, 2017). Enhanced elongation triggered at 28°C during the first day of treatment depended on *PIF4* and *PIF7* (Fig. 1b). Consistent with the phenotype observed after 3 d, *pif7* grew slightly more than *pif4* during the next 2 d (Fig. 1b). We conclude that in response to temperature elevation growth during the day depends on PIF4 and PIF7. In constant light and LD, *PIF4* controls day growth downstream of *phyB* and *cry1* (Ma *et al.*, 2016; Qiu *et al.*, 2019). The importance of PIF7 in warm LD (Fig. 1a,b) prompted us to measure hypocotyl growth of *phyBpif* and *cry1pif* mutant combinations. Both *phyB* and *cry1* mutants showed robust temperature-induced elongation while the *phyBcry1* double mutant was unresponsive suggesting that both photoreceptors are crucial for temperature-controlled hypocotyl elongation (Fig. S2a). However, we note that *cry1phyB* double mutant had very long

**Fig. 1** Thermomorphogenic response requires both PIF4 and PIF7 for hypocotyl and petiole elongation in Arabidopsis. (a) Hypocotyl elongation of wild-type (Col-0) and *pif* mutants grown in long days (LDs) at 21°C for 4 d then either kept at 21°C or transferred to 28°C (at ZT2 on day 5) for three additional days. Elongation during the last 3 d is indicated. Different letters indicate significant difference (two-way ANOVA with Tukey's HSD test,  $P < 0.05$ ,  $n > 25$ ). (b) High-resolution growth analysis of Col-0, *pif4-101*, and *pif7-1* seedlings. Hypocotyl elongation from LD-grown seedlings (21°C) was measured from time-lapse images with indicated intervals starting from ZT0 on day 5. The red dashed line indicates start of 28°C treatment at ZT2 on day 6. The grey zone represents the dark period. Data represent means  $\pm$  2 SE;  $n > 8$ . (c) Petiole lengths (leaf 3) of Col-0 and *pif* mutants grown in LD at 21°C for 15 d then either kept at 21°C or transferred to 28°C for three additional days. Different letters indicate significant difference (two-way ANOVA with Tukey's HSD test,  $P < 0.05$ ,  $n = 10$ ). For (a) and (c) the horizontal bar represents the median, boxes extend from the 25<sup>th</sup> to the 75<sup>th</sup> percentile, while whiskers extend to 1.5 times the interquartile range of the lower and upper quartiles, respectively, outliers are indicated with circles.



hypocotyls at 21°C possibly limiting further elongation at 28°C. As observed previously (Qiu *et al.*, 2019), *pif4* partially suppressed *phyB* (Fig. S2a,b). However, *phyBpif7* had shorter hypocotyls than *phyBpif4*, both at 21°C and 28°C, highlighting the importance of PIF7 for *phyB* repressed hypocotyl elongation (Fig. S2a,b). The *phyB* phenotype was almost totally suppressed in *phyBpif4pif5pif7* (Fig. S2b). Consistent with the dominant function of PIF4 downstream of *cry1* (Ma *et al.*, 2016), *pif4pif5* was epistatic over *cry1* with no further suppression observed in *cry1pif4pif5pif7* (Fig. S2c). We conclude that PIF4 and PIF7 both promote hypocotyl elongation in response to increased temperature in LD, while their regulation by photoreceptors differs at least partially.

Later in development high temperature leads to petiole elongation (Koini *et al.*, 2009), which we analysed in young rosettes that were either maintained at 21°C or transferred for 3 d to 28°C. Elevated temperature-induced petiole elongation was most affected in *pif4*, but also impaired in *pif7* and the response of *pif4pif7* was very similar to *pif4* (Fig. 1c). Taken together our results indicate that PIF7 is almost as important as PIF4 for thermomorphogenic growth responses.

#### PIF7 controls temperature-induced expression of 'auxin' genes

PIF4 is essential to induce expression of *YUC* genes leading to higher auxin levels and growth (Sun *et al.*, 2012). Transfer to 28°C led to significantly increased expression of *YUC8* and *YUC9* (after 90 and 180 min) while *YUC2* induction was modest and not significant (Figs 2a, S3). PIF4 and PIF7 were required for temperature-induced expression of *YUC8* and the auxin signalling genes *IAA29* and *SAUR22* (Fig. 2a), demonstrating the requirement of both phytochrome-interacting factors (PIFs) for enhanced 'auxin gene' expression and growth (Figs 1, 2). To test whether PIF7 may directly control the expression of *YUC8* and *IAA29* we performed ChIP experiments using a full genomic PIF7-HA line (Galvao *et al.*, 2019). This experiment showed that after 2 h at 28°C PIF7 was bound to the promoter of *YUC8* and *IAA29* at a position where PIF4 binding was reported previously (Fig. 2b) (Hornitschek *et al.*, 2012; Sun *et al.*, 2012). To assess the functional importance of temperature-induced *YUC* expression we analysed hypocotyl elongation in a *yuc2yuc5yuc8yuc9* quadruple mutant and all possible triple mutants. This experiment confirmed the importance of *YUC8* and revealed a role for *YUC2* in thermomorphogenesis (Fig. 2c) (Sun *et al.*, 2012). In response

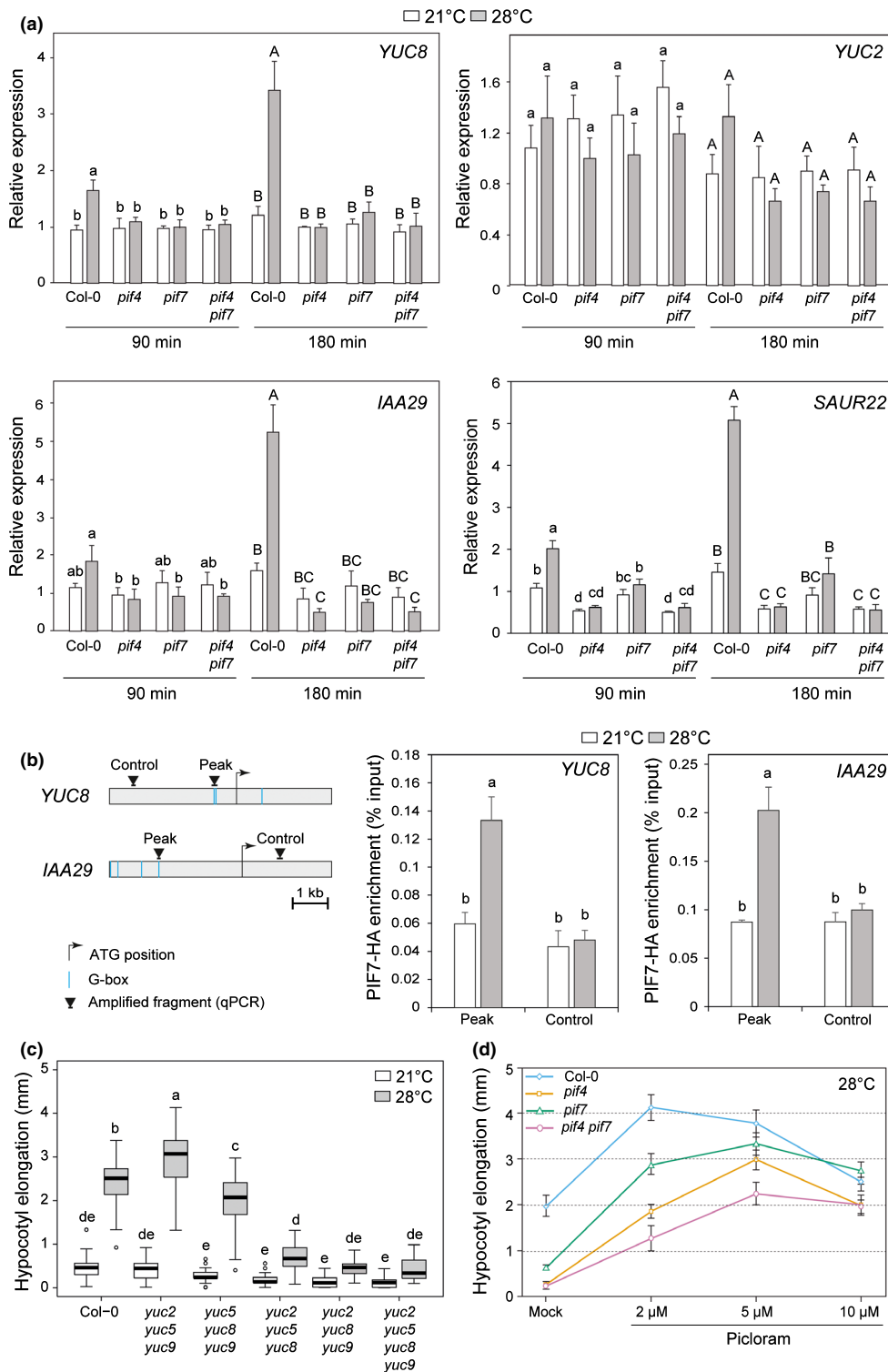
to a lower red to far-red (R : FR) ratio indicative of neighbouring plants PIF7 plays a particularly important role to enhance auxin production while PIF4 also regulates the response to auxin (Nozue *et al.*, 2011; Hornitschek *et al.*, 2012; Li *et al.*, 2012; Pucciariello *et al.*, 2018). We therefore compared the sensitivity of *pif4*, *pif7* and *pif4pif7* mutants to the synthetic auxin picloram in seedlings grown at 28°C (Fig. 2d). This experiment showed that although *pif7* had a very small response to 28°C (mock) it responded like the WT to 2 µM picloram, while *pif4* had a reduced response. At higher picloram concentrations *pif7* also responded less than the WT. We note that the lower picloram response of *pif4* compared to *pif7* correlates with the growth phenotypes of the mutants after prolonged elevated temperature treatments (Figs 1, 2d).

To investigate whether PIF4 and PIF7 regulate the same process required for temperature-induced hypocotyl elongation rather than different independently required steps, we analysed expression of hormone biosynthetic genes that were previously implicated in thermomorphogenesis (Stavang *et al.*, 2009). In our conditions expression of the BR biosynthetic gene *BRASSINOSTEROID-6-OXIDASE 2 (BR6ox2)* was induced by higher temperature in WT plants but not in *pif7* and *pif4* (Figs S3, S4). Temperature-induced expression of *CONSTITUTIVE PHOTOMORPHOGENIC DWARF (CPD)* depended more on PIF4 than PIF7 while higher expression of the gibberellic acid biosynthesis gene *GIBBERELLIN-3-OXIDASE 1 (GA3OX1)* was largely independent of PIF4 or PIF7 (Figs S3, S4). Similarly, strong induction of a small heat-shock gene (*HSP17.6B*) was unaffected in the tested *pif* mutants (Figs S3, S4). We therefore conclude that *pif4* and *pif7* show a similar temperature-regulated gene expression pattern with a particularly obvious effect on auxin biosynthesis and response genes (Figs 2, S3, S4).

#### PIF7 does not regulate PIF4 accumulation but both PIFs can interact with each other

The central importance of PIF4 for thermomorphogenesis prompted us to determine whether PIF7 is required for PIF4 accumulation. We compared *PIF4* mRNA levels in the WT and *pif7* at 21°C and 28°C and did not detect a major effect of PIF7 on *PIF4* expression (Fig. 3a,b). *PIF4* protein levels at 21°C and the slight increase observed after 3 h at 28°C were similar in the WT and *pif7* (Fig. 3c). Consistent with *phyB* promoting PIF4 degradation (de Lucas *et al.*, 2008), we detected high PIF4 levels

**Fig. 2** PIF4 and PIF7 regulate the auxin pathway during thermomorphogenesis in Arabidopsis. (a) Relative expression of auxin biosynthesis (*YUC2* and *YUC8*) and auxin response (*IAA29* and *SAUR22*) genes in 5-d-old Col-0 and *pif* mutants either kept at 21°C or transferred to 28°C at ZT2; samples at 21 and 28°C were harvested at the same ZT. Gene expression values were calculated as fold induction relative to a Col-0 sample at 21°C,  $t = 90$  min.  $n = 3$  (biological) with three technical replicas for each RNA sample. Data are means,  $\pm 2$  SE. Different letters indicate significant differences within timepoints ( $P < 0.05$ ). (b) PIF7-HA binding to the promoter of *YUC8* and *IAA29* evaluated by ChIP-qPCR in 6-d-old seedlings either kept at 21°C or transferred for 2 h to 28°C at ZT2. Input and immunoprecipitated DNA were quantified by qPCR using primers shown on the schematic representation of the genes with 'Peak' indicating where PIF4 binding was identified before (left). PIF7-HA enrichment is presented as IP/Input and error bars show standard deviation from three technical replicas. Different letters indicate significant differences ( $P < 0.05$ ). Data from one representative experiment are shown. (c) Hypocotyl length of wild-type (Col-0) and *yuc* mutants grown in long day (LD) at 21°C for 4 d then kept at 21°C or transferred to 28°C for three additional days. Growth during the last 3 d is indicated. The horizontal bar represents the median, boxes extend from the 25<sup>th</sup> to the 75<sup>th</sup> percentile, while whiskers extend to 1.5 times the interquartile range of the lower and upper quartiles, respectively, outliers are indicated with circles. Different letters indicate significant difference (two-way ANOVA with Tukey's HSD test,  $P < 0.05$   $n > 25$ ). (d) Hypocotyl elongation at 28°C of Col-0 and *pif* mutants in response to indicated concentrations of exogenously applied synthetic auxin, picloram. Seedlings were grown and measured as indicated in (a) picloram was applied at the time of transfer to 28°C. Data represent means  $\pm 2$  SE;  $n > 25$ .



in *phyB* and *phyBpif7* at 21°C and PIF4 levels increased at 28°C independently of PIF7 (Fig. 3c). Alternatively, PIF4 and PIF7 might be both required for thermomorphogenesis because they work as a heterodimer to regulate gene expression (Fig. 2). We used the yeast two-hybrid assay to determine whether both proteins can

interact and found that PIF4 and PIF7 form homodimers and heterodimers in yeast (Fig. S5). We conclude that the strong thermomorphogenic phenotype of *pif7* cannot be explained by lower PIF4 protein levels but may be due to PIF4/PIF7 heterodimer-mediated gene expression (Figs 2, S5).

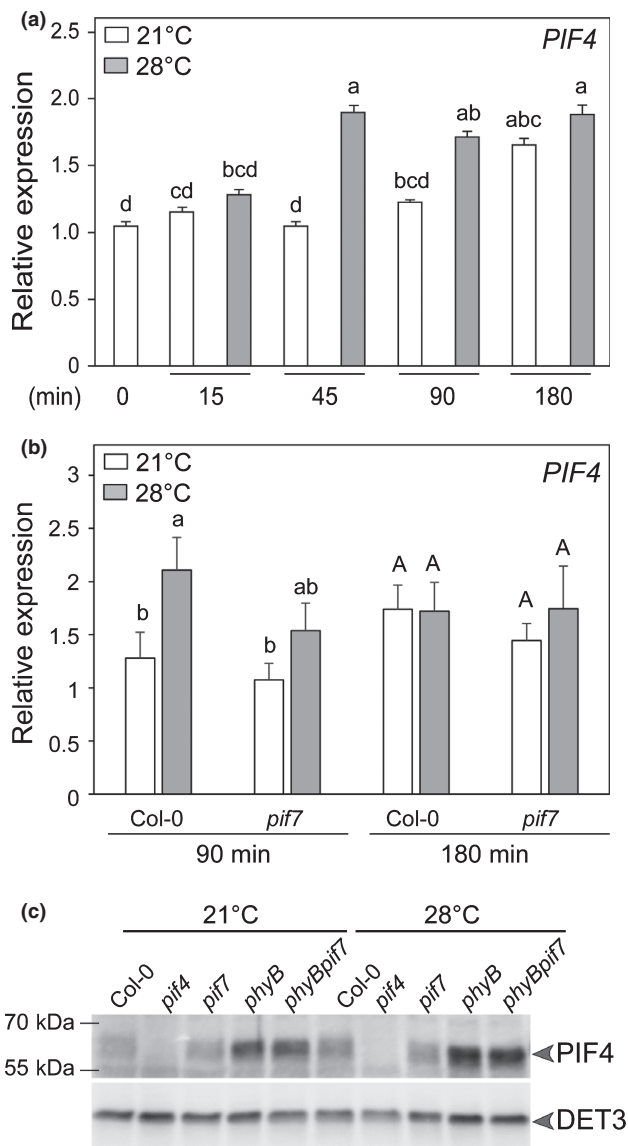


**Fig. 3** Regulation of *PIF4* mRNA and protein levels in thermomorphogenesis in Arabidopsis. (a) Relative expression of *PIF4* in 5-d-old Col-0 and (b) in Col-0 and *pif7-1* mutants. Seedlings were grown as in Fig. 2(a). Gene expression values were calculated as fold induction relative to a Col-0 sample at 21°C,  $t = 0$  (a) and  $t = 90$  min (b).  $n = 3$  (biological) with three technical replicas for each RNA sample. Data are means,  $\pm 2$  SE. Different letters indicate significant differences ( $P < 0.05$ ). (c) *PIF4* protein levels in the indicated genotypes detected with anti-*PIF4* antibody from total protein extracts after 3 h of 21°C and 28°C treatment in 5-d-old long day-grown seedlings treated at ZT2. DET3 was used as a loading control.

### PIF7 protein levels increase rapidly upon transfer to 28°C

The requirement of *PIF7* for rapid temperature-induced changes in gene expression and hypocotyl elongation (Figs 1, 2) suggested that *PIF7* function and/or accumulation might be temperature-regulated. Upon transfer to 28°C *PIF7* transcript levels declined in the WT while in *pif4* we observed a similar but not significant reduction (Fig. 4a,b). To analyse *PIF7* protein we used a *PIF7*-HA

line (Galvao *et al.*, 2019) and found that in contrast to *PIF7* RNA, *PIF7* protein levels increased significantly 90 min after the transfer to 28°C (Fig. 4c). As observed previously *PIF7* was present as two major isoforms (Li *et al.*, 2012) (Fig. 4c). Transfer to 28°C specifically led to increased abundance of the faster migrating isoform (Figs 4c, S6). We propose that temperature-induced *PIF7* levels may contribute to enhanced *PIF7* activity required for rapid thermomorphogenic responses.

### Discussion

*PIF4* was believed to have a uniquely important function in thermomorphogenesis (Koini *et al.*, 2009; Sun *et al.*, 2012; Ma *et al.*, 2016; Casal & Balasubramanian, 2019; Qiu *et al.*, 2019). Our work shows that in seedlings the role of *PIF7* is almost as important as *PIF4* (Figs 1, 2, S1, S2). However, upon prolonged growth at 28°C we observed a slightly greater growth response in *pif7* than *pif4* (Fig. 1b,c). In addition, we found that at 28°C *pif4* responds less to picloram than *pif7* (Fig. 2c). A greater role of *PIF4* than *PIF7* in controlling auxin responsiveness may explain the small phenotypic difference between both *pif* mutants. Our data on thermomorphogenesis reveals interesting similarities and differences with the shade avoidance response. A reduction of the R : FR ratio indicative of neighbour proximity leads to auxin synthesis that primarily depends on *PIF7* (Li *et al.*, 2012). Our data suggests that during thermomorphogenesis *PIF4* and *PIF7* are similarly important to promote auxin biosynthesis (Fig. 2a). *PIF4* and *PIF5* rather than *PIF7* have been implicated in the control of auxin sensitivity (Nozue *et al.*, 2011; Hornitschek *et al.*, 2012; Li *et al.*, 2012; Hersch *et al.*, 2014; Pucciariello *et al.*, 2018). We find that during thermomorphogenesis *PIF4* also plays a more important function than *PIF7* to promote auxin responsiveness (Fig. 2d). Finally, our data on temperature-induced growth (Figs 1, 2) is consistent with a model emerging from the study of the low R : FR response with an early phase depending on auxin production (Tao *et al.*, 2008; Li *et al.*, 2012) and a prolonged response requiring *PIF4*-controlled auxin sensitivity (Pucciariello *et al.*, 2018).

Several possibilities can explain the requirement of *PIF4* and *PIF7* for thermomorphogenesis. Each of them might control different essential steps for elevated temperature-induced growth. Given the similar gene expression profile of *pif4* and *pif7*, this is an unlikely explanation (Figs 2, S4). However, more research is required to test this hypothesis on a larger scale and with better spatial resolution (e.g. hypocotyls vs cotyledons). Given that both single mutants and the *pif4pif7* double mutant have similar phenotypes (Figs 1, 2, S1), the function of these *PIFs* might depend on each other. We showed that *PIF7* is not required for normal accumulation of *PIF4* transcript or *PIF4* protein and *PIF7* mRNA expression is largely unaffected in *pif4* (Figs 3, 4). As bHLH transcription factors bind DNA as dimers, an attractive hypothesis is that a *PIF4/PIF7* heterodimer regulates expression of target genes such as *YUC8* or *IAA29* (Fig. 2) (Hornitschek *et al.*, 2012; Li *et al.*, 2012; Sun *et al.*, 2012). Consistent with this hypothesis, *PIF4* and *PIF7* interact with each other when co-expressed in mesophyll protoplasts (Kidokoro *et al.*, 2009) and in the yeast two-hybrid assay (Fig. S5). Collectively, these findings support the *PIF4/PIF7*

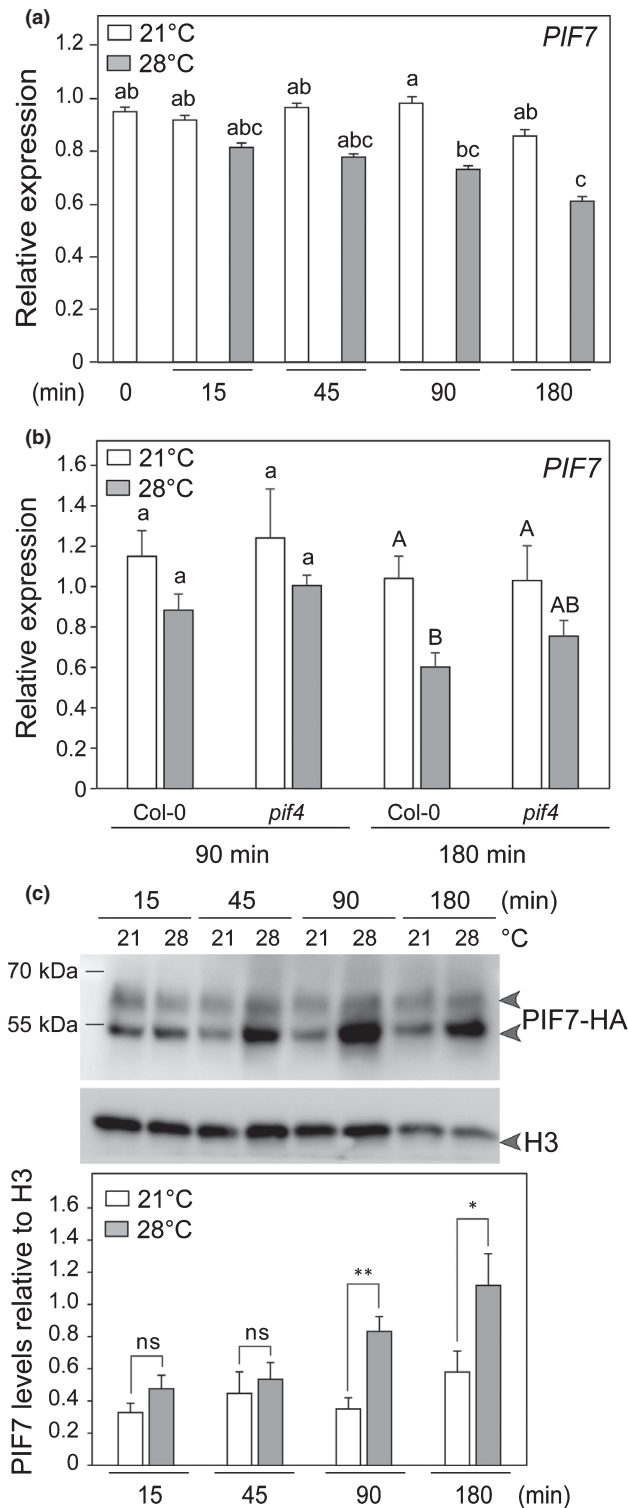


**Fig. 4** Regulation of PIF7 mRNA and protein levels in thermomorphogenesis in Arabidopsis. (a) Relative expression of *PIF7* in 5-d-old Col-0 and (b) in Col-0 and *pif4* mutant. Seedlings were grown as in Fig. 2(a). Gene expression values were calculated as fold induction relative to a Col-0 sample at 21°C,  $t = 0$  (a) and  $t = 90$  min (b).  $n = 3$  (biological) with three technical replicates for each RNA sample. Data are means,  $\pm 2$  SE. Different letters indicate significant differences ( $P < 0.05$ ). (c) PIF7-HA protein levels detected with an anti-HA antibody from total protein extract after indicated time points at 21°C and 28°C in 5-d-old long day-grown seedlings treated at ZT2. The HA signal was quantified and normalized to H3 signal ( $n = 6$ ). Data are means,  $\pm$  SE. Asterisks indicate significant ( $P$  values) between 28°C and 21°C samples at a given timepoint (Student's  $t$ -test: \*  $< 0.05$ ; \*\*  $< 0.01$ ), ns, nonsignificant.

effects of PIF4 and PIF7 have also been observed during etiolation and shade avoidance (Leivar *et al.*, 2008; de Wit *et al.*, 2016). Similarly, PIF4 and PIF7 act independently of each other to suppress cold tolerance during long days (Lee & Thomashow, 2012). We conclude that additional research is required to understand to what extent PIF4 and PIF7 activity depend on each other and how this dependency may be regulated by development or the environment.

Temperature elevation regulates *PIF7* transcript and protein levels in opposite ways with a reduction of transcript but more PIF7 protein (Fig. 4). Reducing the R : FR ratio also leads to lower *PIF7* transcripts, while PIF7 phosphorylation changes, which regulates PIF7 accumulation in the nucleus (Li *et al.*, 2012; Huang *et al.*, 2018). Photoperiod also regulates PIF7 protein and *PIF7* mRNA with higher levels of *PIF7* transcript and PIF7 protein in LD (Lee & Thomashow, 2012). In response to increasing ambient temperature PIF7 protein levels, particularly its faster isoform increased rapidly (Figs 4c, S6). We propose that the temperature-enhanced PIF7 protein levels may contribute to the thermomorphogenic response. It will be interesting to decipher the mechanisms underlying this change in PIF7 accumulation and if/how this regulation contributes to enhanced PIF7 function at elevated temperature.

### Acknowledgements

The authors thank Mieke de Wit for the initial observation that *pif7* mutants are unresponsive to elevated temperature, Martina Legris for comments on the manuscript, Philip A. Wigge (University of Potsdam) for sharing unpublished results and the Genomic Technologies Facility (GTF) for assistance with RT-qPCR assays. Work in the Fankhauser laboratory is funded by the University of Lausanne and grants from the Swiss National Science Foundation (no. 310030B\_179558 and CRSII3\_154438). VCG was supported by an EMBO Long Term fellowship (ALTF 293-2013).

### Author contributions

Conceptualization, ASF, VCG, YCI and CF; investigation, ASF, VCG, YCI and AB; resources, AG, MT and LAP; funding acquisition, CF; writing, CF; supervision, CF. ASF, VCG and YCI contributed equally to this work.

heterodimer hypothesis during thermomorphogenesis. However, in the *phyB* mutant background *pif* mutants act additively with almost full *phyB* suppression in *phyBpif4pif5pif7* indicating that the different PIFs can act independently (Fig. S2b). Additive

## ORCID

- Laure Allenbach Petrolati  <https://orcid.org/0000-0002-9074-5350>
- Alessandra Boccaccini  <https://orcid.org/0000-0001-8698-4722>
- Christian Fankhauser  <https://orcid.org/0000-0003-4719-5901>
- Anne-Sophie Fiorucci  <https://orcid.org/0000-0002-3254-5967>
- Vinicius Costa Galvão  <https://orcid.org/0000-0002-0973-222X>
- Yetkin Çaka Ince  <https://orcid.org/0000-0002-4395-8599>
- Martine Trevisan  <https://orcid.org/0000-0002-6610-6954>

## References

- Bellstaedt J, Trenner J, Lippmann R, Poeschl Y, Zhang X, Friml J, Quint M, Delker C. 2019. A mobile auxin signal connects temperature sensing in cotyledons with growth responses in hypocotyls. *Plant Physiology* **180**: 757–766.
- Bourbousse C, Vegesna N, Law JA. 2018. SOG1 activator and MYB3R repressors regulate a complex DNA damage network in Arabidopsis. *Proceedings of the National Academy of Sciences, USA* **115**: E12453–E12462.
- Casal JJ, Balasubramanian S. 2019. Thermomorphogenesis. *Annual Review of Plant Biology* **70**: 321–346.
- Crawford AJ, McLachlan DH, Hetherington AM, Franklin KA. 2012. High temperature exposure increases plant cooling capacity. *Current Biology* **22**: R396–397.
- de Lucas M, Daviere JM, Rodriguez-Falcon M, Pontin M, Iglesias-Pedraz JM, Lorrain S, Fankhauser C, Blazquez MA, Titarenko E, Prat S. 2008. A molecular framework for light and gibberellin control of cell elongation. *Nature* **451**: 480–484.
- de Wit M, George GM, Ince YC, Dankwa-Egli B, Hersch M, Zeeman SC, Fankhauser C. 2018. Changes in resource partitioning between and within organs support growth adjustment to neighbor proximity in Brassicaceae seedlings. *Proceedings of the National Academy of Sciences, USA* **115**: E9953–E9961.
- de Wit M, Keuskamp DH, Bongers FJ, Hornitschek P, Gommers CMM, Reinen E, Martinez-Ceron C, Fankhauser C, Pierik R. 2016. Integration of phytochrome and cryptochrome signals determines plant growth during competition for light. *Current Biology* **26**: 3320–3326.
- de Wit M, Ljung K, Fankhauser C. 2015. Contrasting growth responses in lamina and petiole during neighbor detection depend on differential auxin responsiveness rather than different auxin levels. *New Phytologist* **208**: 198–209.
- Delker C, Sonntag L, James GV, Janitza P, Ibanez C, Ziermann H, Peterson T, Denk K, Mull S, Ziegler J *et al.* 2014. The DET1-COP1-HY5 pathway constitutes a multipurpose signaling module regulating plant photomorphogenesis and thermomorphogenesis. *Cell Reports* **9**: 1983–1989.
- Duttweiler HM. 1996. A highly sensitive and non-lethal beta-galactosidase plate assay for yeast. *Trends in Genetics* **12**: 340–341.
- Franklin KA, Lee SH, Patel D, Kumar SV, Spartz AK, Gu C, Ye S, Yu P, Breen G, Cohen JD *et al.* 2011. Phytochrome-interacting factor 4 (PIF4) regulates auxin biosynthesis at high temperature. *Proceedings of the National Academy of Sciences, USA* **108**: 20231–20235.
- Galvao VC, Fiorucci AS, Trevisan M, Franco-Zorrilla JM, Goyal A, Schmid-Siegert E, Solano R, Fankhauser C. 2019. PIF transcription factors link a neighbor threat cue to accelerated reproduction in Arabidopsis. *Nature Communications* **10**: 4005.
- Gangappa SN, Berriri S, Kumar SV. 2017. PIF4 coordinates thermosensory growth and immunity in Arabidopsis. *Current Biology* **27**: 243–249.
- Gangappa SN, Kumar SV. 2017. DET1 and HY5 control PIF4-mediated thermosensory elongation growth through distinct mechanisms. *Cell Reports* **18**: 344–351.
- Gendrel AV, Lippman Z, Martienssen R, Colot V. 2005. Profiling histone modification patterns in plants using genomic tiling microarrays. *Nature Methods* **2**: 213–218.
- Goyal A, Karayekov E, Galvao VC, Ren H, Casal JJ, Fankhauser C. 2016. Shade promotes phototropism through phytochrome B-controlled auxin production. *Current Biology* **26**: 3280–3287.
- Hersch M, Lorrain S, de Wit M, Trevisan M, Ljung K, Bergmann S, Fankhauser C. 2014. Light intensity modulates the regulatory network of the shade avoidance response in Arabidopsis. *Proceedings of the National Academy of Sciences, USA* **111**: 6515–6520.
- Hornitschek P, Kohnen MV, Lorrain S, Rougemont J, Ljung K, Lopez-Vidriero I, Franco-Zorrilla JM, Solano R, Trevisan M, Pradervand S *et al.* 2012. Phytochrome interacting factors 4 and 5 control seedling growth in changing light conditions by directly controlling auxin signaling. *The Plant Journal* **71**: 699–711.
- Huang X, Zhang Q, Jiang Y, Yang C, Wang Q, Li L. 2018. Shade-induced nuclear localization of PIF7 is regulated by phosphorylation and 14-3-3 proteins in Arabidopsis. *eLife* **7**: pii: e31636.
- Ibanez C, Delker C, Martinez C, Burstenbinder K, Janitza P, Lippmann R, Ludwig W, Sun H, James GV, Klecker M *et al.* 2018. Brassinosteroids dominate hormonal regulation of plant thermomorphogenesis via BZR1. *Current Biology* **28**: 303–310.e3.
- Jung JH, Domijan M, Klose C, Biswas S, Ezer D, Gao M, Khattak AK, Box MS, Charoensawan V, Cortijo S *et al.* 2016. Phytochromes function as thermosensors in Arabidopsis. *Science* **354**: 886–889.
- Kidokoro S, Maruyama K, Nakashima K, Imura Y, Narusaka Y, Shinwari ZK, Osakabe Y, Fujita Y, Mizoi J, Shinozaki K *et al.* 2009. The phytochrome-interacting factor PIF7 negatively regulates DREB1 expression under circadian control in Arabidopsis. *Plant Physiology* **151**: 2046–2057.
- Kohnen MV, Schmid-Siegert E, Trevisan M, Petrolati LA, Senecal F, Muller-Moule P, Maloof J, Xenarios I, Fankhauser C. 2016. Neighbor detection induces organ-specific transcriptomes, revealing patterns underlying hypocotyl-specific growth. *Plant Cell* **28**: 2889–2904.
- Koini MA, Alvey L, Allen T, Tilley CA, Harberd NP, Whitelam GC, Franklin KA. 2009. High temperature-mediated adaptations in plant architecture require the bHLH transcription factor PIF4. *Current Biology* **19**: 408–413.
- Lau OS, Song Z, Zhou Z, Davies KA, Chang J, Yang X, Wang S, Lucyshyn D, Tay IHZ, Wigge PA *et al.* 2018. Direct control of SPEECHLESS by PIF4 in the high-temperature response of stomatal development. *Current Biology* **28**: 1273–1280.e3.
- Lee CM, Thomashow MF. 2012. Photoperiodic regulation of the C-repeat binding factor (CBF) cold acclimation pathway and freezing tolerance in *Arabidopsis thaliana*. *Proceedings of the National Academy of Sciences, USA* **109**: 15054–15059.
- Legris M, Klose C, Burgie ES, Rojas CC, Neme M, Hiltbrunner A, Wigge PA, Schafer E, Vierstra RD, Casal JJ. 2016. Phytochrome B integrates light and temperature signals in Arabidopsis. *Science* **354**: 897–900.
- Legris M, Nieto C, Sellaro R, Prat S, Casal JJ. 2017. Perception and signalling of light and temperature cues in plants. *The Plant Journal* **90**: 683–697.
- Leivar P, Monte E, Al-Sady B, Carle C, Storer A, Alonso JM, Ecker JR, Quail PH. 2008. The Arabidopsis phytochrome-interacting factor PIF7, together with PIF3 and PIF4, regulates responses to prolonged red light by modulating phyB levels. *Plant Cell* **20**: 337–352.
- Li L, Ljung K, Breton G, Schmitz RJ, Pruneda-Paz J, Cowing-Zitron C, Cole BJ, Ivans LJ, Pedmale UV, Jung HS *et al.* 2012. Linking photoreceptor excitation to changes in plant architecture. *Genes & Development* **26**: 785–790.
- Lorrain S, Allen T, Duek PD, Whitelam GC, Fankhauser C. 2008. Phytochrome-mediated inhibition of shade avoidance involves degradation of growth-promoting bHLH transcription factors. *The Plant Journal* **53**: 312–323.
- Ma D, Li X, Guo Y, Chu J, Fang S, Yan C, Noel JP, Liu H. 2016. Cryptochrome 1 interacts with PIF4 to regulate high temperature-mediated hypocotyl elongation in response to blue light. *Proceedings of the National Academy of Sciences, USA* **113**: 224–229.
- Martinez C, Espinosa-Ruiz A, de Lucas M, Bernardo-Garcia S, Franco-Zorrilla JM, Prat S. 2018. PIF4-induced BR synthesis is critical to diurnal and thermomorphogenic growth. *EMBO Journal* **37**: pii: e99552.
- Mockler TC, Guo H, Yang H, Duong H, Lin C. 1999. Antagonistic actions of Arabidopsis cryptochromes and phytochrome B in the regulation of floral induction. *Development* **126**: 2073–2082.
- Neff MM, Neff JD, Chory J, Pepper AE. 1998. dCAPS, a simple technique for the genetic analysis of single nucleotide polymorphisms: experimental applications in *Arabidopsis thaliana* genetics. *The Plant Journal* **14**: 387–392.

- Nomoto Y, Kubozono S, Miyachi M, Yamashino T, Nakamichi N, Mizuno T. 2012. A circadian clock- and PIF4-mediated double coincidence mechanism is implicated in the thermosensitive photoperiodic control of plant architectures in *Arabidopsis thaliana*. *Plant and Cell Physiology* 53: 1965–1973.
- Nozue K, Harmer SL, Maloof JN. 2011. Genomic analysis of circadian clock-, light-, and growth-correlated genes reveals PHYTOCHROME-INTERACTING FACTOR5 as a modulator of auxin signaling in *Arabidopsis*. *Plant Physiology* 156: 357–372.
- Nozue K, Tat AV, Kumar Devisetty U, Robinson M, Mumbach MR, Ichihashi Y, Lekkala S, Maloof JN. 2015. Shade avoidance components and pathways in adult plants revealed by phenotypic profiling. *PLoS Genetics* 11: e1004953.
- Oh E, Zhu JY, Wang ZY. 2012. Interaction between BZR1 and PIF4 integrates brassinosteroid and environmental responses. *Nature Cell Biology* 14: 802–809.
- Park YJ, Lee HJ, Ha JH, Kim JY, Park CM. 2017. COP1 conveys warm temperature information to hypocotyl thermomorphogenesis. *New Phytologist* 215: 269–280.
- Pedmale UV, Huang SC, Zander M, Cole BJ, Hetzel J, Ljung K, Reis PAB, Sridevi P, Nito K, Nery JR *et al.* 2016. Cryptochromes interact directly with PIFs to control plant growth in limiting blue light. *Cell* 164: 233–245.
- Procko C, Burko Y, Jaillais Y, Ljung K, Long JA, Chory J. 2016. The epidermis coordinates auxin-induced stem growth in response to shade. *Genes & Development* 30: 1529–1541.
- Pucciariello O, Legris M, Costigliolo Rojas C, Iglesias MJ, Hernando CE, Dezar C, Vazquez M, Yanovsky MJ, Finlayson SA, Prat S *et al.* 2018. Rewiring of auxin signaling under persistent shade. *Proceedings of the National Academy of Sciences, USA* 115: 5612–5617.
- Qiu Y, Li M, Kim RJ, Moore CM, Chen M. 2019. Daytime temperature is sensed by phytochrome B in *Arabidopsis* through a transcriptional activator HEMERA. *Nature Communications* 10: 140.
- Quint M, Delker C, Franklin KA, Wigge PA, Halliday KJ, van Zanten M. 2016. Molecular and genetic control of plant thermomorphogenesis. *Nature Plants* 2: 15190.
- Raschke A, Ibanez C, Ullrich KK, Anwer MU, Becker S, Glockner A, Trenner J, Denk K, Saal B, Sun X *et al.* 2015. Natural variants of ELF3 affect thermomorphogenesis by transcriptionally modulating PIF4-dependent auxin response genes. *BMC Plant Biology* 15: 197.
- Stavang JA, Gallego-Bartolome J, Gomez MD, Yoshida S, Asami T, Olsen JE, Garcia-Martinez JL, Alabadi D, Blazquez MA. 2009. Hormonal regulation of temperature-induced growth in *Arabidopsis*. *The Plant Journal* 60: 589–601.
- Sun J, Qi L, Li Y, Chu J, Li C. 2012. PIF4-mediated activation of YUCCA8 expression integrates temperature into the auxin pathway in regulating *Arabidopsis* hypocotyl growth. *PLoS Genetics* 8: e1002594.
- Tao Y, Ferrer JL, Ljung K, Pojer F, Hong F, Long JA, Li L, Moreno JE, Bowman ME, Ivans LJ *et al.* 2008. Rapid synthesis of auxin via a new tryptophan-dependent pathway is required for shade avoidance in plants. *Cell* 133: 164–176.
- Zhu JY, Oh E, Wang T, Wang ZY. 2016. TOC1-PIF4 interaction mediates the circadian gating of thermoresponsive growth in *Arabidopsis*. *Nature Communications* 7: 13692.

## Supporting Information

Additional Supporting Information may be found online in the Supporting Information section at the end of the article.

**Fig. S1** Thermomorphogenic response requires both PIF4 and PIF7 for hypocotyl elongation in short day (SD).

**Fig. S2** PIF4 and PIF7 regulate thermomorphogenic hypocotyl elongation downstream of phyB and cry1.

**Fig. S3** Relative expression of genes that were previously implicated in thermomorphogenesis.

**Fig. S4** Relative expression of temperature-induced genes in Col-0 and pif mutants.

**Fig. S5** PIF7 and PIF4 form homodimers and heterodimers in yeast.

**Fig. S6** Regulation of the levels of both PIF7 isoforms in thermomorphogenesis.

**Table S1** List of oligonucleotides used in this study.

Please note: Wiley Blackwell are not responsible for the content or functionality of any Supporting Information supplied by the authors. Any queries (other than missing material) should be directed to the *New Phytologist* Central Office.

### **New Phytologist Supporting Information**

Article title: **PHYTOCHROME INTERACTING FACTOR 7 is important for early responses to elevated temperature in Arabidopsis seedlings.**

Authors: Anne Sophie Fiorucci, Vinicius Costa Galvão, Yetkin Çaka Ince, Alessandra Boccaccini, Anupama Goyal, Laure Allenbach Petrolati, Martine Trevisan and Christian Fankhauser

Article acceptance date: 5 November 2019

The following Supporting Information is available for this article:

**Fig. S1** Thermomorphogenic response requires both PIF4 and PIF7 for hypocotyl elongation in short-day (SD).

**Fig. S2** PIF4 and PIF7 regulate thermomorphogenic hypocotyl elongation downstream of phyB and cry1.

**Fig. S3** Relative expression of genes that were previously implicated in thermomorphogenesis.

**Fig. S4** Relative expression of temperature-induced genes in Col-0 and *pif* mutants.

**Fig. S5** PIF7 and PIF4 form homo- and hetero-dimers in yeast.

**Fig. S6** Regulation of the levels of both PIF7 isoforms in thermomorphogenesis.

**Table S1** List of oligonucleotides used in this study.

**Fig. S1.** Thermomorphogenic response requires both PIF4 and PIF7 for hypocotyl elongation in short-day (SD). Hypocotyl elongation of wild-type (Col-0) and *pif* mutants grown in SD (8h light, 16 hour dark) at 21°C for 4 days then either kept at 21°C or transferred to 28°C (at ZT2 on day 5) for five additional days. Elongation during the last 5 days is indicated. Different letters indicate significant difference (two-way ANOVA with Tukey's HSD test,  $P < 0.05$ ,  $n > 25$ ).

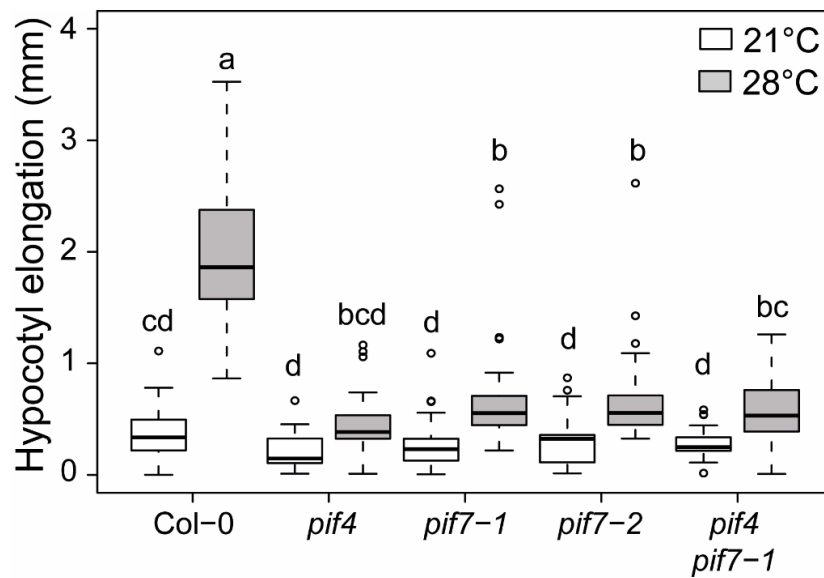


**Fig. S2** PIF4 and PIF7 regulate thermomorphogenic hypocotyl elongation downstream of phyB and cry1. (a-c) Hypocotyl elongation of indicated genotypes grown in LD at 21°C for 4 days then either kept at 21°C or transferred to 28°C for three additional days. Elongation during the last 3 days is indicated. Different letters indicate significant difference (two-way ANOVA with Tukey's HSD test,  $P < 0.05$ ,  $n > 25$ ).

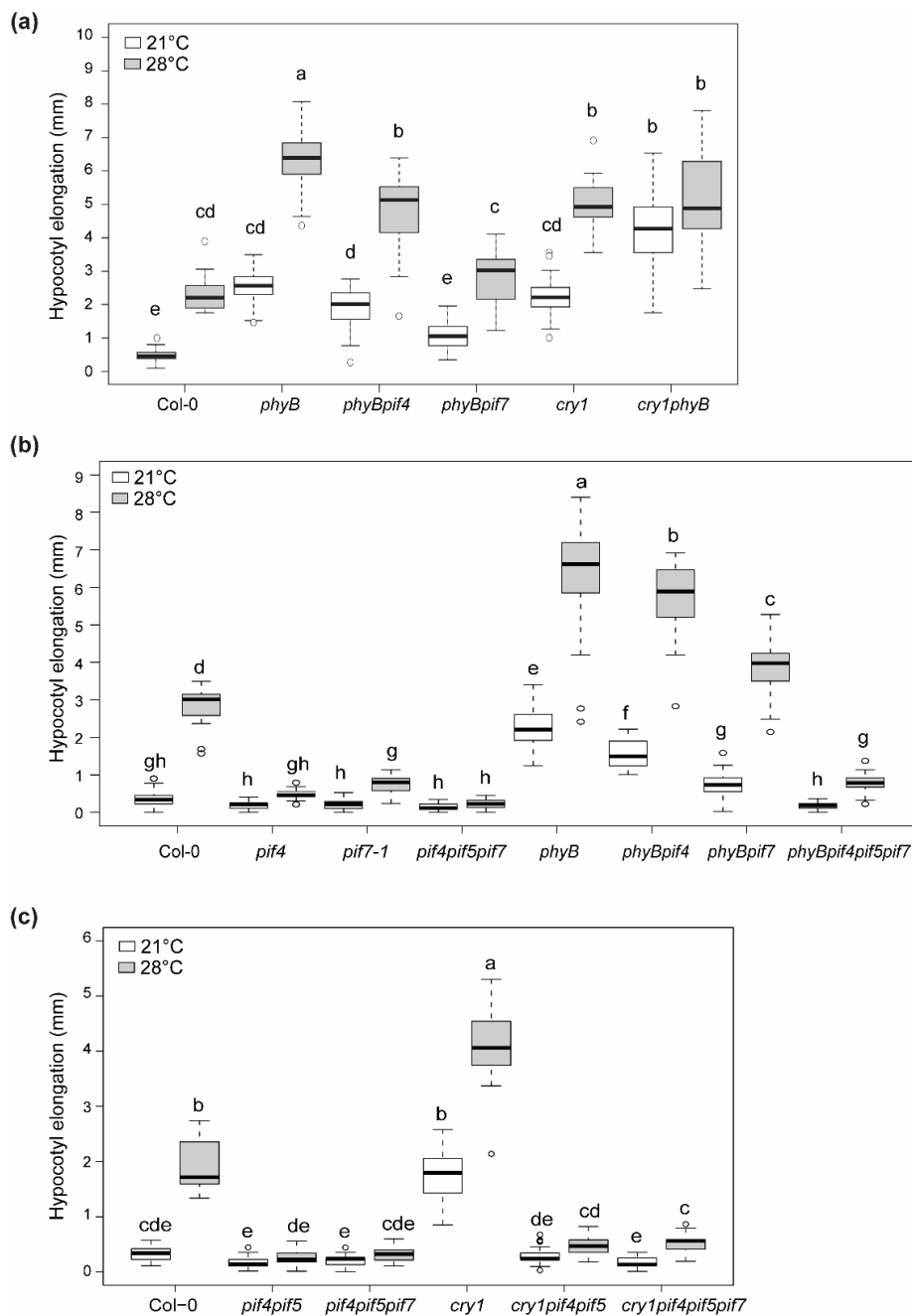


**Fig. S3** Relative expression of genes that were previously implicated in thermomorphogenesis. Seedlings were grown as indicated in Fig. 2a. Gene expression values were calculated as fold induction relative to a Col-0 sample at 21°C, t = 0. n = 3 (biological) with 3 technical replicas for each RNA sample. Data are mean, error bar indicates 2XSE. Different letters indicate significant difference (two-way ANOVA with Tukey's HSD test,  $P < 0.05$ ).

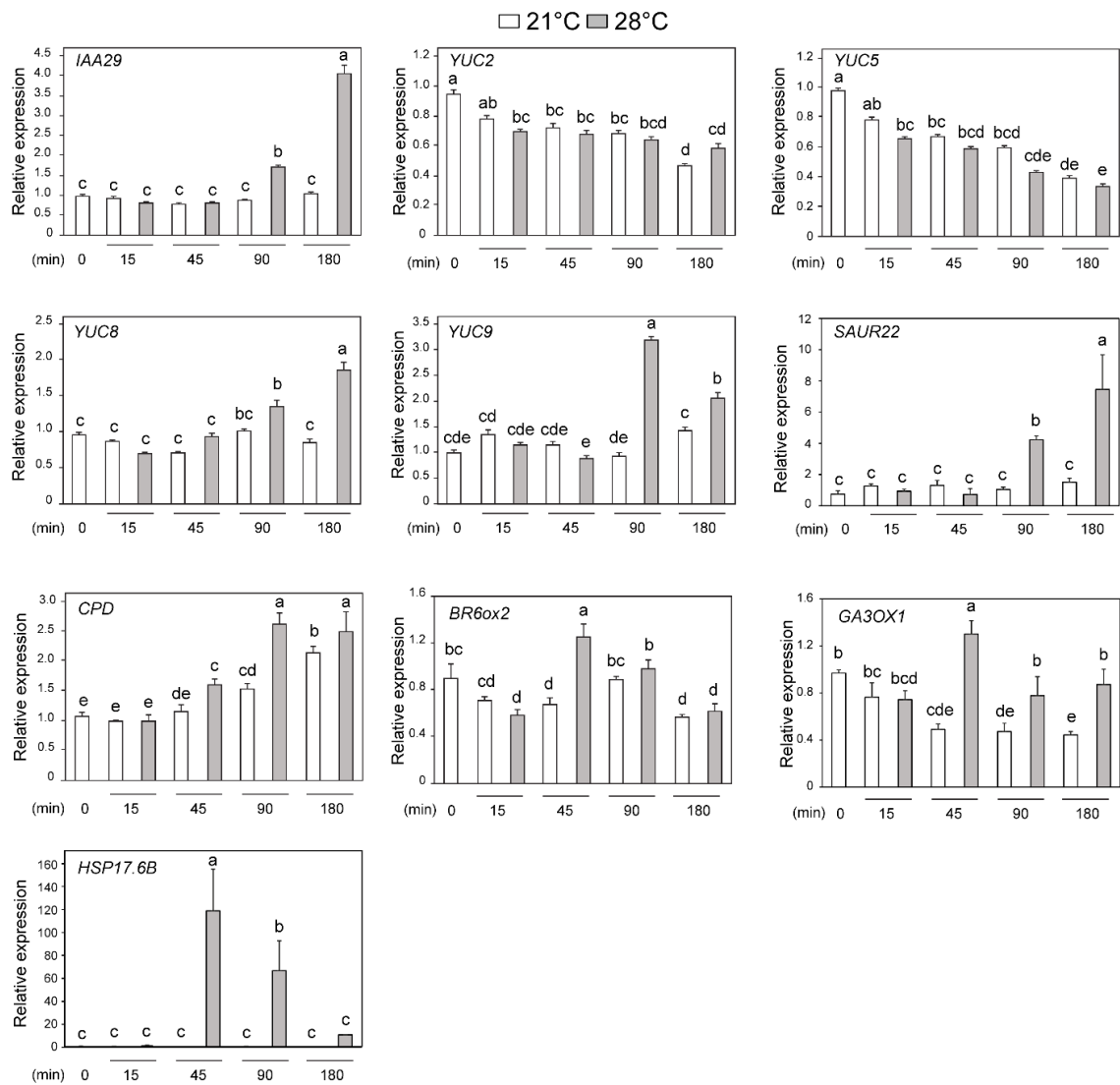


**Fig. S4** Relative expression of temperature-induced genes in Col-0 and *pif* mutants. Seedlings were grown as indicated in Fig. 2a. Gene expression values were calculated as fold induction relative to a Col-0 sample at 21°C, t = 90 min. n = 3 (biological) with 3 technical replicas for each RNA sample. Data are mean, error bar indicates 2XSE. Different letters indicate significant differences within timepoints (p<0.05).

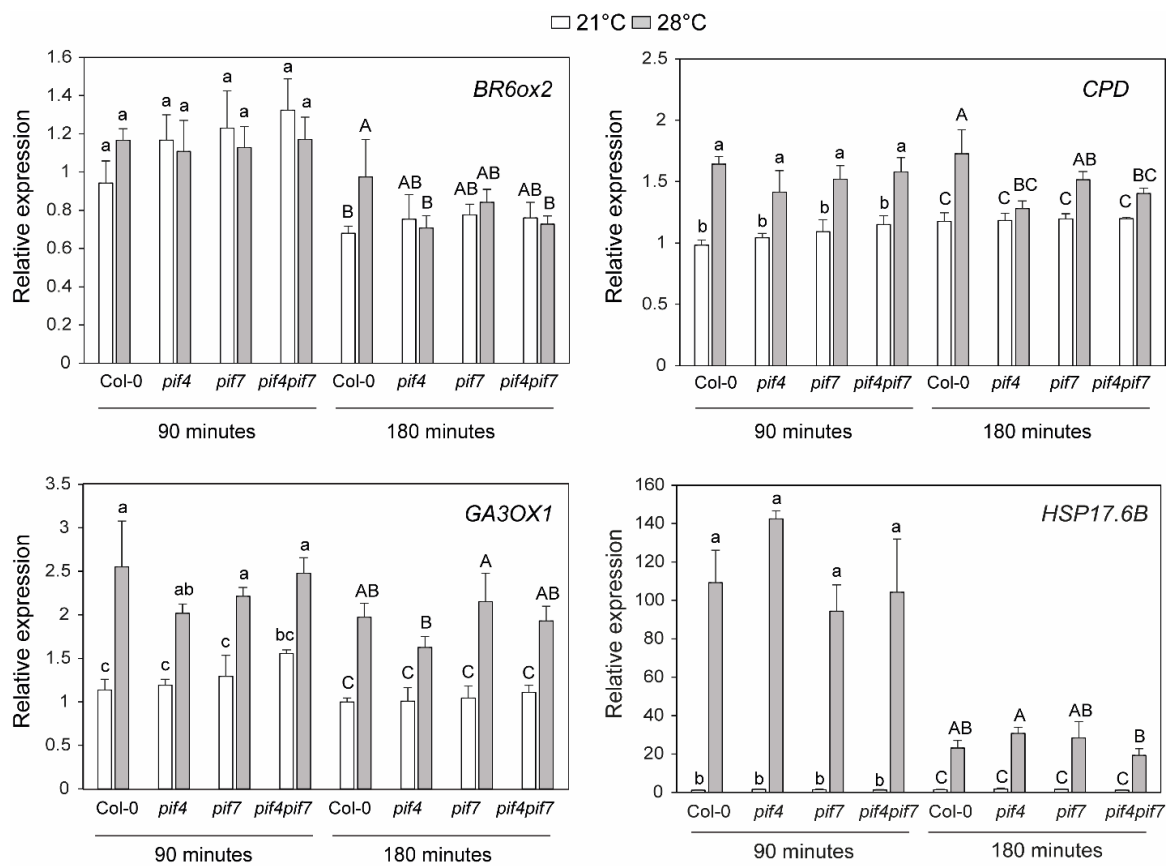


**Fig. S5** PIF7 and PIF4 form homo- and hetero-dimers in yeast. Yeast two-hybrid  $\beta$ -galactosidase assay testing the interactions between full-length PIF7 and PIF4 fused to either GAL4 binding domain (BD-) or GAL4 activation domain (AD-). Yeast co-transformed with the indicated vectors were spotted on SD-LW medium (10x serial dilutions from OD0.1 to OD0.001) and grown for two days at 30°C before an X-gal-containing agarose overlay. Plates were kept at 37°C in darkness and pictures were taken after 5h (all combinations with BD-PIF4) and 22h (all the others). Empty pGBKT7 and pGADT7 vectors are used as negative controls.

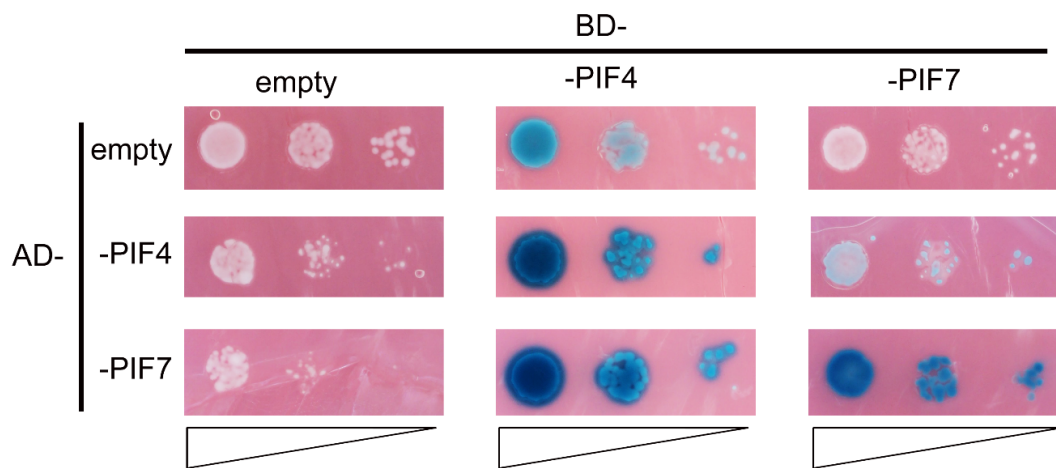


**Fig. S6** Regulation of the levels of both PIF7 isoforms in thermomorphogenesis. (a) Slow-migrating and (b) fast-migrating isoforms of PIF7-HA protein detected with anti-HA antibody from total protein extracts after the indicated time points at 21°C and 28°C in 5-days-old LD-grown PIF7-HA seedlings treated at ZT2. The HA signal was quantified and normalized to H3 signal (n = 6). Data are mean, error bar indicates SE. Asterisks indicate significant difference (*p* values) between 28°C and 21°C samples at a given timepoint (Student's t-test, \* < 0.05, \*\* < 0.01), n.s. non significant.

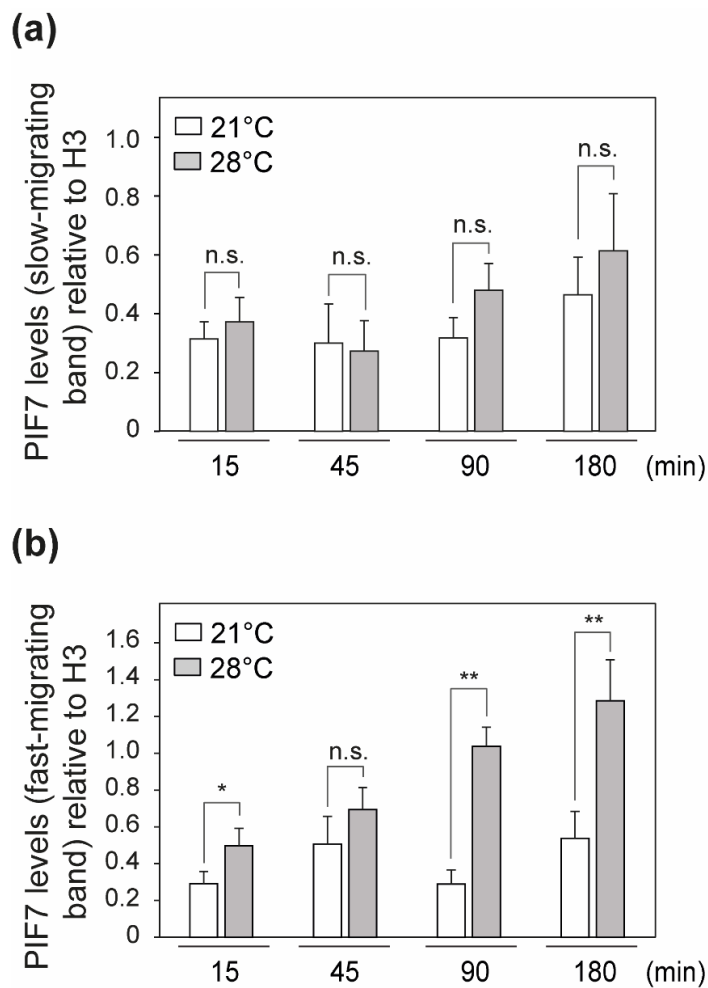


**Table S1** List of oligonucleotides used in this study.

Oligos used for genotyping			
Allele	Collection	Oligonucleotide	Sequence
<i>phyB-9</i>	Point mutation	PB9	GTGTCTGCGTTCTCAAACG
		B9dCAPS	GTGGAAGAAGCTCGACCAGGCTTTG
<i>cry1-304</i>	Deletion	CF586	GGTAGGGTTTCTAGGTGGTGGCTC
		CF587	GGTGAAGAAGAGGAGACTCAGGG
<i>yuc2-1</i>	SALK_030199	oJM1845	TTCTTGCATTTTCTCGCTCTACG
		MT440	AACCCGTGGCGAGTATAATG
<i>yuc5-3</i>	GT6160	oJM1203	CGGACTCTAATCAAAGTCCC
		oJM1204	GGAGATTTCAAACCTAGATTTG
<i>yuc8-1</i>	CS110939	oJM1206	CATCCTCTCCACGTGGCTTCC
		oJM1207	GAAGTACGCTTCGTGGGTAC
<i>yuc9-1</i>	SAIL_871G01	oJM1199	GCTCGGTAAGCAAAAACAAAAGT
		oJM1200	GAAGGAAATGCCCAATGAGAC
<i>pif4-101</i>	SAIL_114_G06	SL-43	CAGACGGTTGATCATCTG
		oVCG-61	TAGCATCTGAATTTCATAACCAATCTCGATACAC
<i>pif5-3 (pil6-1)</i>	SALK_087012	SL-46	TCGCTCACTCGTTACTTAC
		oVCG-56	ATTTTGCCGATTTGCGAAC
<i>pif7-1</i>	CS68809	SL-195	GTGGCAAGTTGGCTCTTAGG
		SL-169	TGATAGTGACCTTAGCGACTTTTGAACGC
<i>pif7-2</i>	SAIL_622_G02	oASF-27	GGAGAGCCATAGAGTTGG
		oVCG-61	TAGCATCTGAATTTCATAACCAATCTCGATACAC

Oligos used for RT-qPCR			
Target	Primer Efficiency	Oligonucleotide	Sequence
UBC	1.94	UBC-F	CAGTCTGTGTAGAGCTATCATAGCAT
		UBC-R	AGAAGATTCCTGAGTCGCAGTT
YSL8	2.00	YSL8-F	TCATTCGTTTCGGCCATGA
		YSL8-R	CTCAGCAACAGACGCAAGCA
PIF4	2.02	oVCG-246	TACCTCGATTTCCGTTATGGATC
		oVCG-247	GTTGTTGACTTTGCTGTCCCGC
	1.78	SL63	TTCTCCTCCCACTTCTTCTC
		SL64	AGGTTCAGGACTGGACTTAG
PIF7	2.01	oVCG-588	GAGCAGCTCGTAGGTACATG
		oVCG-589	GTTGTTGTTGCACGGTCTG
YUC2	1.94	MT-437	AACTCCGGGATGGAAGTTTG
		MT-438	CCCGAAAGTCGATATACCTAGC
YUC5	1.9	MT-459	TGGAGCTAGTAGACGGTCAG
		MT-460	GAAACGGCGATTTCCGGGAAC
YUC8	2.0	MT-271	GGCGGCTGTCTCCATGAAC

		PH-171	GATGAACTGACGCTTCGTCG
YUC9	2.0	MT-297	GCTAACCACAATGCAATTAC
		MT-298	CATCACTGAGATTCCAAATG
IAA29	1.94	MT-157	CTTCCAAGGGAAAGAGGGTGA
		MT-158	TTCCGCAAAGATCTTCATGTAAC
BR6ox2	2.05	oVCG-740	GTGAGCGGTTTCGTACAGGTC
		oVCG-741	GGTAACGATCTTGATTCCGG
CPD	2.06	oVCG-726	GCACTTTCAACCCTTGAGAGA
		oVCG-727	CAGAGAGTGCAACCCTAGCC
HSP17.6B	2.21	YI578	CAGGTTAAGGCTGCGATGGA
		YI579	AGCCTTAGGCACCGTAACAG
GA3OX1	1.88	YI622	TACCGACTCCACCCTCTAA
		YI623	GACCCAACCAAGATCATCGC
SAUR22	1.99	MT515	GTATGAGAGTGGCACTAAG
		MT516	GCTCTGGTGAGAAGTCTAC

#### Oligos used for ChIP-qPCR

Target	Primer Efficiency	Oligonucleotide	Sequence
IAA29 peak (G-box)	1.86	MK54	ACATTACGCCACGAGTAG
		MK55	GATCAACCAAGCAGAAGAG
IAA29 control	1.92	MK60	GGGATGTTACATGGAAGTAAG
		MK61	ATGAACAGATTCGCAAAG
YUC8 peak (G-box)	1.97	oASF213	GGAATGGGTTTGATGTGGAA
		oASF214	GATTCITTTGTGGACCAACG
YUC8 control	2.03	MK34	AGCTGGCCTATGAAATAAC
		MK35	AGTGGACGATCAATTCTC

#### Oligos used for cloning (Two-hybrid vectors)

Plasmid	Strategy	Oligonucleotide	Sequence
pAD-PIF7 (pVG20)	Digestion of amplified fragment and pGADT7 with EcoRI and BamHI followed by T4 ligation.	oVCG-193 (EcoRI)	TGAATCCAaTCGAATTATGGAGTTAAAGAG
		oVCG-194 (BamHI)	CGATGGATCCCCTAATCTCTTTTCTCATGA
pAD-PIF4 (pVG22)	Blunt T4 ligation of amplified fragment into SmaI digested pGADT7	33265	GAACACCAAGTTGGAGT
		33183	CTAGTGGTCCAAACGAGAAC
pBD-PIF7 (pASF13)	InFusion cloning between NcoI-linearized	oASF205	AGGACCTGCATATGGCCATGTCGAATTATGGAGTTAAAGAGCTCACA
		oASF206	CCGGGAATTCGGCCTCCATGCTAATCTCTTTTCTCATGATTCGAAGAAGTTGAAG
pBD-PIF4 (pASF14)	pGBKT7 and PCR amplified PIF7/PIF4.	oASF207	AGGACCTGCATATGGCCATGGAACACCAAGTTGGAGTTTTG
		oASF208	CCGGGAATTCGGCCTCCATGCTAGTGGTCCAAACGAGAACC

**Chapter 2. Changes in resource partitioning  
between and within organs support growth  
adjustment to neighbour proximity in  
*Brassicaceae* seedlings**

## OVERVIEW

During the second year of my thesis studies, I contributed a collaborative project between Prof. Christian Fankhauser lab and Prof. Samuel C. Zeeman lab in which Dr. Mieke de Wit and Dr. Gavin George were the leading investigators. In this study, we investigated how photosynthetically fixed CO<sub>2</sub> is partitioned between cotyledons and hypocotyls during shade avoidance using *Arabidopsis thaliana* and *Brassica rapa* seedlings. This study resulted in a publication in the journal of Proceedings of the National Academy of Sciences (PNAS, USA) (de Wit et al., 2018). My involvement in the project included high-resolution growth analysis of *Arabidopsis* seedlings (Fig. 4c), hypocotyl elongation analysis of *Arabidopsis* starch mutants (Fig. 5a, S4e), iodine staining and microscopy of starch mutants (Fig. 5b-h, S4f-g), genotyping and phenotyping of *pgm1pif7* double mutants (Fig. 5j). Finally, I analysed and interpreted data in collaboration with the authors of the publication.



# Changes in resource partitioning between and within organs support growth adjustment to neighbor proximity in *Brassicaceae* seedlings

Mieke de Wit<sup>a,1,2</sup>, Gavin M. George<sup>b,1</sup>, Yetkin Çaka Ince<sup>a</sup>, Barbara Dankwa-Egli<sup>b,3</sup>, Micha Hersch<sup>c,d</sup>, Samuel C. Zeeman<sup>b</sup>, and Christian Fankhauser<sup>a,4</sup>

<sup>a</sup>Center for Integrative Genomics, Faculty of Biology and Medicine, University of Lausanne, CH-1015 Lausanne, Switzerland; <sup>b</sup>Plant Biochemistry, Institute of Molecular Plant Biology, ETH Zurich, 8092 Zurich, Switzerland; <sup>c</sup>Department of Computational Biology, University of Lausanne, CH-1015 Lausanne, Switzerland; and <sup>d</sup>Swiss Institute of Bioinformatics, CH-1015 Lausanne, Switzerland

Edited by Winslow R. Briggs, Carnegie Institution for Science, Stanford, CA, and approved September 4, 2018 (received for review April 9, 2018)

In shade-intolerant plants, the perception of proximate neighbors rapidly induces architectural changes resulting in elongated stems and reduced leaf size. Sensing and signaling steps triggering this modified growth program have been identified. However, the underlying changes in resource allocation that fuel stem growth remain poorly understood. Through <sup>14</sup>CO<sub>2</sub> pulse labeling of *Brassica rapa* seedlings, we show that perception of the neighbor detection signal, low ratio of red to far-red light (R:FR), leads to increased carbon allocation from the major site of photosynthesis (cotyledons) to the elongating hypocotyl. While carbon fixation and metabolite levels remain similar in low R:FR, partitioning to all downstream carbon pools within the hypocotyl is increased. Genetic analyses using *Arabidopsis thaliana* mutants indicate that low-R:FR-induced hypocotyl elongation requires sucrose transport from the cotyledons and is regulated by a PIF7-dependent metabolic response. Moreover, our data suggest that starch metabolism in the hypocotyl has a growth-regulatory function. The results reveal a key mechanism by which metabolic adjustments can support rapid growth adaptation to a changing environment.

neighbor proximity detection | resource partitioning | starch | PIF7 | phytochrome B

To withstand environmental challenges, plants have a remarkably plastic phenotype, allowing them to optimize their architecture for the prevailing circumstances. Shade-intolerant plants compete for light with their neighbors, typically by accelerating growth of stem-like structures to bring their leaves toward the light in the so-called shade avoidance response (1). This enhanced stem elongation is reflected in increased biomass accumulation in stems, while growth of leaves, roots, and seeds is often reduced (2–6).

The presence of neighboring plants is perceived by the phytochrome (phy) photoreceptors, which detect a drop in the ratio of red to far-red light (R:FR) due to increased levels of FR reflected off green plant tissue (7). Given that FR light does not contribute to photosynthetically active radiation (PAR), a low-R:FR environment can be established through FR supplementation without affecting PAR. Similarly, a shade avoidance response can be induced by end-of-day exposure to FR (EOD-FR), which inactivates phy, relieving repression of the PHYTOCHROME INTERACTING FACTORS (PIFs) 4, 5, and 7 (8, 9). The PIFs subsequently activate an array of targets, including genes related to processes of auxin biosynthesis, transport, signaling, and cell wall biogenesis and modification (9, 10). While there appears to be a core set of shade avoidance genes (11), expression patterns become increasingly organ specific over time in *Arabidopsis* seedlings, which likely reflects the different growth responses of hypocotyl (embryonic stem) and cotyledons (embryonic leaves) (12).

Surprisingly little is known about metabolic changes involved in the shade avoidance response. Considering the major investment in stem growth, there must be considerable changes in resource partitioning while under the threat of light limitation. Photosynthates are transported through the phloem in the form of sucrose from high production sites (source) to organs in carbon deficit (sink) (13, 14). This was addressed in experiments in which radiolabeled carbon in the form of <sup>14</sup>C-urea was brushed onto the first pair of leaves of stem-forming plants. Such a treatment leads to release of <sup>14</sup>CO<sub>2</sub>, through urea uptake and endogenous enzymatic hydrolysis, which can be taken up by the plant during photosynthesis. More <sup>14</sup>C was recovered in internodes from sunflower plants (*Helianthus annuus*) that had been treated with 3 d of low R:FR compared with internodes from plants in high R:FR (15). In a similar experiment using <sup>14</sup>C urea, 24 h of low-R:FR treatment led to enhanced allocation of <sup>14</sup>C to the first internode of *Sinapis alba*, whereas a lower proportion of <sup>14</sup>C remained in the leaves of the plant (16). As the total amount

## Significance

In dense communities, plants compete for light and sense potentially threatening neighbors prior to actual shading. In response to neighbor proximity cues, shade-intolerant plants selectively elongate stem-like structures, thereby enhancing access to unfiltered sunlight. Although key steps in plant proximity sensing and signaling have been identified, we know little about the metabolic adaptations underlying enhanced stem growth. Here, we show that, following the detection of neighbor proximity cues, seedlings allocate more carbon fixed in the cotyledons to the faster elongating hypocotyl. Moreover, we show that sucrose transport and a transcription factor responding to light and metabolic cues control hypocotyl elongation. Collectively, our work provides important insights into the metabolic changes underlying organ-specific growth adaptations to an environmental stress signal.

Author contributions: M.d.W., G.M.G., M.H., S.C.Z., and C.F. designed research; M.d.W., G.M.G., Y.Ç.I., B.D.-E., and M.H. performed research; M.d.W., G.M.G., Y.Ç.I., B.D.-E., M.H., S.C.Z., and C.F. analyzed data; and M.d.W., G.M.G., and C.F. wrote the paper.

The authors declare no conflict of interest.

This article is a PNAS Direct Submission.

This open access article is distributed under Creative Commons Attribution-NonCommercial-NoDerivatives License 4.0 (CC BY-NC-ND).

<sup>1</sup>M.d.W. and G.M.G. contributed equally to this work.

<sup>2</sup>Present address: Research and Innovation, Natural Environment Research Council, SN2 1EU Swindon, United Kingdom.

<sup>3</sup>Present address: Schweizerische Studienstiftung, CH-8032 Zurich, Switzerland.

<sup>4</sup>To whom correspondence should be addressed. Email: christian.fankhauser@unil.ch.

This article contains supporting information online at [www.pnas.org/lookup/suppl/doi:10.1073/pnas.1806084115/-DCSupplemental](http://www.pnas.org/lookup/suppl/doi:10.1073/pnas.1806084115/-DCSupplemental).

Published online October 1, 2018.

of recovered radiolabeled carbon was similar in plants from both light treatments, a larger fraction of the total amount of assimilated  $^{14}\text{C}$  was partitioned toward the elongating internodes of shade-avoiding plants. While this leaf-targeted labeling suggests increased transport from leaves to stem in shade-avoiding plants,  $\text{C}$  uptake is not controlled in this method and the  $^{14}\text{CO}_2$  that is released from urea application is also available for fixation in other organs (17).

Steady-state measurements of soluble sugars and starch have produced varied results. Activity of sucrose phosphate synthase, a sucrose biosynthesis enzyme, was increased in leaves of low-R:FR-treated plants (18, 19). Low-R:FR and EOD-FR treatments were shown to increase the amounts of reducing sugars (i.e., glucose and fructose, products of sucrose hydrolysis) in leaves, internodes, and petioles of tobacco (*Nicotiana tabacum*), watermelon (*Citrullus lanatus*), mustard (*Sinapis alba*), and sunflower (*Helianthus annuus*) (15, 16, 20, 21). However, no changes in sucrose levels were found in leaves and petioles of radish plants (*Raphanus sativus*) after long-term low-R:FR treatment (18). Interpretation of steady-state measurements of soluble sugars are complicated by the fact that increased production could increase their concentration, while increased demand in the form of growth would have the opposite effect. Carbohydrates can also be stored in insoluble starch. In leaves, starch is accumulated during the day and degraded at night to provide soluble sugars for metabolism (22). The role of starch in stems is less well defined. Similarly to soluble sugars, the effect of low R:FR on starch accumulation is also apparently variable. Starch granules were found to be smaller and less abundant in chloroplasts of EOD-FR-treated tobacco leaves (*Nicotiana tabacum*) (20) and decreased starch levels were reported in radish (18) after phytochrome inactivation; however, starch was reported to be increased in mustard (16). In accordance with the latter, the constitutive shade-avoiding *phyA phyB phyD phyE Arabidopsis* mutant accumulates more starch per shoot fresh weight during the day, which correlates with reduced daytime shoot growth (23). In contrast, the *phyA phyB* mutant, which showed photosynthesis and fresh weight similar to the wild-type *Ler*, was found to accumulate less starch toward the end of the day (24). Interestingly, transcriptomic analyses of the shade avoidance response indicate down-regulation of genes involved in starch metabolism (11, 25).

Photosynthesis-related genes are also down-regulated by the perception of shade signals (25–27). Chlorophyll content per unit leaf area was reduced in EOD-FR-treated tobacco leaves, with chloroplasts containing smaller but more grana (20, 28). Nevertheless, leaf photosynthesis was unaffected by low R:FR and EOD-FR, as net  $\text{CO}_2$  uptake and total leaf carbohydrates were similar in control and treated plants (18, 28, 29). In contrast, photosynthetic capacity of tomato stems (*Solanum lycopersicum*), which was about one-third of leaf photosynthetic capacity, was rapidly reduced to almost zero in low R:FR (29). This corresponded to reduced dark respiration and chlorophyll content of the stem (29), suggesting that the photosynthetic apparatus is repressed upon low R:FR perception in this organ. These reports all point toward major metabolic adjustments accompanying elongation growth in low R:FR, although the inconsistencies between studies leave major questions unanswered.

The shade avoidance signaling pathway is extensively studied in plant seedlings. Here, we investigated carbon partitioning during shade avoidance in *Arabidopsis thaliana* and *Brassica rapa* seedlings, analyzing allocation both between organs and between carbon pools within organs. We provide insight into how resources are reallocated to adapt growth patterns to shade conditions.

## Results

**Low-R:FR Treatment Increases Carbon Allocation from Cotyledons to Hypocotyl.** Although *Arabidopsis* hypocotyls may assimilate some carbon locally, the substantial growth that takes place in low-R:FR-treated hypocotyls is expected to require resources from the cotyledons. This, in turn, is likely to impact on cotyledon growth, which is reduced in low R:FR (*SI Appendix*, Fig. S1 A and B). Using a previously published RNA-seq dataset from 5-d-old *Arabidopsis* seedlings (12), we looked for gene expression patterns related to carbon metabolism that might support a change in resource allocation in low R:FR. After 3 h of low R:FR, expression of several carbon metabolic pathways (photosynthesis, Calvin cycle, sucrose biosynthesis, starch biosynthesis and degradation) was significantly down-regulated in the hypocotyl but remained at a similar level in cotyledons (*SI Appendix*, Fig. S1C; see *Dataset S1* for gene lists). This organ-specific expression pattern suggests that carbon assimilation and storage might be reduced locally in the hypocotyl in response to low R:FR. The elongating hypocotyl may thus increase in sink strength not only because of its rapid growth but also because of reduced production of local photosynthate.

To study resource allocation during the shade avoidance response directly, we performed radioisotope-labeling experiments to quantitatively study carbon allocation into different organs. The small size of *Arabidopsis* seedlings being an impediment; we used *Brassica rapa* seedlings, which show a shade avoidance response similar to *Arabidopsis* (30, 31). This includes increased hypocotyl elongation and reduced cotyledon expansion (*SI Appendix*, Fig. S2 A and B), reflected in altered biomass accumulation in both organs (*SI Appendix*, Fig. S2C). Accelerated

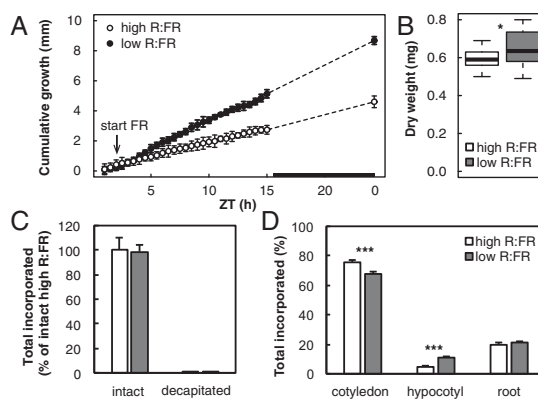


**Fig. 1.** Resource partitioning between *Brassica rapa* seedling organs after 9 h of light treatment. Five-day-old *B. rapa* seedlings grown in long days were subjected to high or low R:FR at ZT2. (A) Hypocotyl growth was measured from time-lapse images with 30-min intervals. The black bar in the x axis represents the dark period. Data represent means  $\pm$  2 SE;  $n = 9$ . (B) Hypocotyl biomass after 9 h of light treatment. Data are represented as standard boxplots representing median and interquartile (IQR) range between the 25th and 75th percentiles. Whiskers extend to 1.5-fold the IQR;  $n = 20$ . (C) Incorporation of radiolabeled C in intact seedlings or seedlings from which cotyledons had been removed (decapitated), harvested immediately after a 10-min pulse of  $^{14}\text{CO}_2$  following 9 h of light treatment. Values are expressed as the percentage of label recovered in each sample compared with the average total label of high-R:FR-treated intact plants. Data represent means  $\pm$  2 SE;  $n = 4$ . (D)  $^{14}\text{C}$  incorporation in cotyledon, hypocotyl, and root tissue after a 1-h chase. Values are expressed as a percentage of total label recovered in each organ. Data represent means  $\pm$  2 SE;  $n = 4$ . Asterisks indicate significant difference. Significance codes: \* $0.05 > P > 0.01$ , \*\* $0.01 > P > 0.001$ , \*\*\* $P < 0.001$ .

hypocotyl growth was observed after ~2 h of low-R:FR treatment (Fig. 1A), similar to what was previously reported in *Arabidopsis* (12, 32). We treated *Brassica* seedlings with a 10-min <sup>14</sup>CO<sub>2</sub> pulse after 9 h of low-R:FR treatment, when clear differences in hypocotyl length and a small but significant increase in hypocotyl dry weight could be detected (Fig. 1B). Using such an early time point allowed to focus on early events and minimizes the impact of increased size of the organ on C partitioning.

Total assimilation of CO<sub>2</sub> in low-R:FR-treated plants was unchanged compared with high-R:FR-treated plants (Fig. 1C), which indicates that the total amount of carbon available was similar for seedlings in both high and low R:FR. This allowed us to compare carbon fractions of the different light treatments as a percentage of the total amount of label found in a sample. Some carbon was expected to be fixed locally by the hypocotyl, which may influence the calculated partitioning between organs. To calculate this fraction, we provided a <sup>14</sup>CO<sub>2</sub> pulse to seedlings from which the cotyledons were removed immediately before labeling. These “decapitated” hypocotyls were harvested immediately to prevent loss of label through respiration. Compared with intact seedlings, less than 0.5% of the total <sup>14</sup>C was assimilated in decapitated hypocotyls (Fig. 1C), showing that the vast majority of CO<sub>2</sub> taken up by the plant is assimilated in the cotyledons. After a 1-h chase, more than 75% of the total assimilated <sup>14</sup>C was retained in the cotyledons in high R:FR (Fig. 1D). Of the 25% allocated to the other organs, 5% was taken up by the hypocotyl and 20% by the roots. Compared with high R:FR, 7% less <sup>14</sup>C was found in the cotyledons of low-R:FR-treated seedlings, while <sup>14</sup>C in the hypocotyl was increased by the same amount (Fig. 1D). As this increase in hypocotyl <sup>14</sup>C is much larger than the contribution of local assimilation (Fig. 1C), and because total <sup>14</sup>C allocated to the roots was unaffected, we conclude that increased <sup>14</sup>C in the hypocotyl of low-R:FR-treated seedlings is the direct result of carbon reallocation from the cotyledon.

**Carbon Partitioning Within Organs Corresponds With Their Growth Response to Low R:FR.** The cotyledon, hypocotyl, and root samples were further fractionated to determine partitioning into different pools of carbon within each organ. Initial fractionation separated into ethanol-soluble, water-soluble, or insoluble components. These three primary fractions in the cotyledons, hypocotyl, and root together contained the entire assimilated label, from which each fraction was calculated as a percentage (Fig. 2). The ethanol-soluble fraction contains predominantly lipids and waxes. The water-soluble fraction was further separated into an acidic fraction (containing mostly phosphorylated sugars and organic acids), a basic fraction (mostly amino acids), and neutral components (mostly neutral sugars). From the insoluble fraction, starch was measured and the remaining label represents assimilated carbon in cell walls and the remaining proteins (Fig. 2D).

In cotyledons of low-R:FR-treated seedlings, a lower percentage of <sup>14</sup>C was committed to starch as well as to protein and cell walls (Fig. 2A), which corresponds to the reduced growth of this organ in low R:FR (SI Appendix, Fig. S2B). There were trends toward less <sup>14</sup>C recovery in the rapidly turned-over pool of soluble sugars ( $P = 0.050$ ) and more partitioning into the acidic fraction ( $P = 0.060$ ). These changes are likely due to an increased flux toward sucrose, via sugar phosphates, and faster export of sucrose toward sink organs. In the root, small changes in partitioning were observed, suggesting slightly more commitment to growth after 9 h of low R:FR (Fig. 2C).

Strikingly, in low-R:FR-treated plants, increased partitioning to the hypocotyl (Fig. 1C) was reflected in all of the downstream carbon pools of this organ (Fig. 2B). Only a small proportion of <sup>14</sup>C was partitioned into starch; however, this was increased more than fourfold from 0.13 to 0.6% in low R:FR. The neutral fraction increased more than twofold, which is an expected result

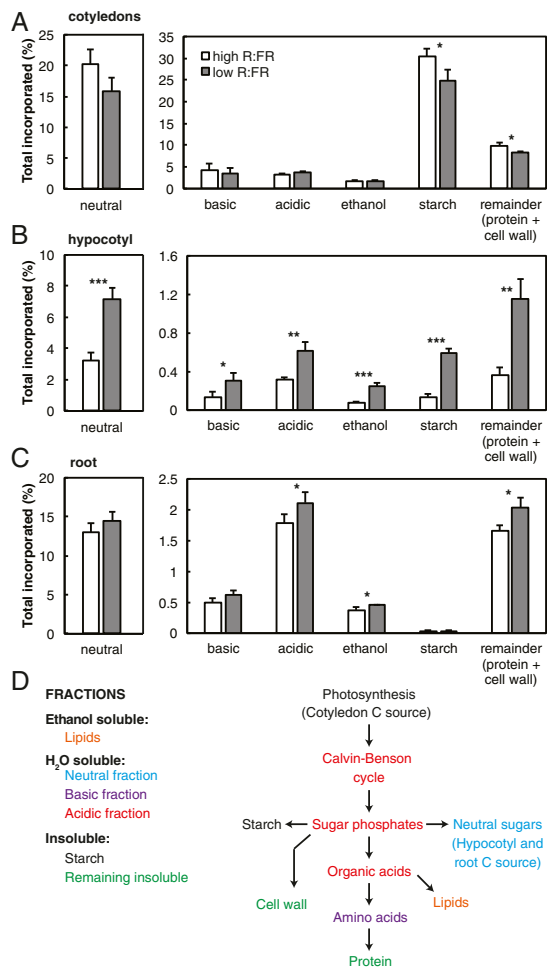


**Fig. 2.** Carbon partitioning within organs after 9 h of low R:FR. Cotyledon (A), hypocotyl (B), and root (C) samples of 5-d-old seedlings grown in long days, harvested after a 1-h chase following exposure to a 10-min pulse of <sup>14</sup>CO<sub>2</sub>, 9 h after start of light treatment. Samples were processed into primary fractions of ethanol-soluble, H<sub>2</sub>O-soluble, and insoluble components. The water-soluble fraction was further fractionated into basic, acidic, and neutral fractions and the insoluble fraction into starch and a remaining fraction containing proteins and cell walls (D). Data represent means ± 2 SE;  $n = 4$ . Asterisks indicate significant difference. Significance codes: \* $0.05 > P > 0.01$ , \*\* $0.01 > P > 0.001$ , and \*\*\* $P < 0.001$ .

of increased sucrose transport from the cotyledons. The increased allocation to the ethanol-soluble fraction (lipids and cell membranes) and the protein and cell wall-insoluble fraction indicates an increased investment into growth components, corresponding with low-R:FR-induced hypocotyl elongation and biomass accumulation (Fig. 1C and SI Appendix, Fig. S2 A and C).

**Metabolite Levels Are Stable During the First 24 h of Low-R:FR Treatment.** To test whether the observed changes in <sup>14</sup>C allocation lead to changes in metabolite levels, we determined sugar concentrations in hypocotyls and cotyledons during the first 24 h

of neighbor detection. Overall, low-R:FR treatment induced little to no significant changes in metabolite levels in both organs (Fig. 3 and *SI Appendix*, Fig. S3). As  $^{14}\text{C}$  partitioning increased more than threefold in the ethanol-soluble and -insoluble hypocotyl fractions (Fig. 2 *A* and *B*), it is likely that transported sugars are rapidly utilized to produce the components of growth, cell membranes, cell walls, and proteins and hence do not accumulate. Starch levels in cotyledons showed a typical accumulation during the day and depletion during the night (*SI Appendix*, Fig. S3). Interestingly, the increased partitioning toward starch in the hypocotyl did not result in measurably more starch accumulation (Fig. 3*D*). This may be due to simultaneous starch degradation (i.e., turnover), but we were unable to verify this as maltose, a key intermediate of starch degradation, was below the limit of detection in our analysis. Taken together, increased  $^{14}\text{C}$  partitioning toward hypocotyls combined with relatively stable metabolite levels suggests that low R:FR leads to a rapid turnover of metabolites and an increased flux through the measured carbon pools to the end products of growth.

#### Shade-Induced Hypocotyl Elongation Requires Sucrose Transport.

Our partitioning data strongly suggest an increased flow of sucrose from the cotyledons to the hypocotyl in low-R:FR-treated seedlings (Figs. 1*D* and 2). To test whether phloem transport plays a role in the hypocotyl elongation response to low R:FR, we measured hypocotyl lengths of two *Arabidopsis* sucrose transporter mutants. Despite their deficiency in apoplastic phloem loading, 5-d-old *suc2* and *sweet11 sweet12* seedlings showed hypocotyl growth comparable to that of the wild-type Columbia-0 (Col-0) in high R:FR (Fig. 4 *A* and *B*). At this early developmental stage, carbon is derived from seed-lipid catabolism and gluconeogenesis rather than from photosynthesis (33). After these initial 5 d of growth, the *suc2* mutant showed somewhat reduced hypocotyl growth after 3 additional days of high R:FR (Fig. 4*A*), while the *sweet11 sweet12* mutant had a wild-type phenotype. Both mutants had an impaired elongation response compared with the wild type after 3 d of low R:FR with a particularly strong defect in *suc2* (Fig. 4 *A* and *B*). This im-

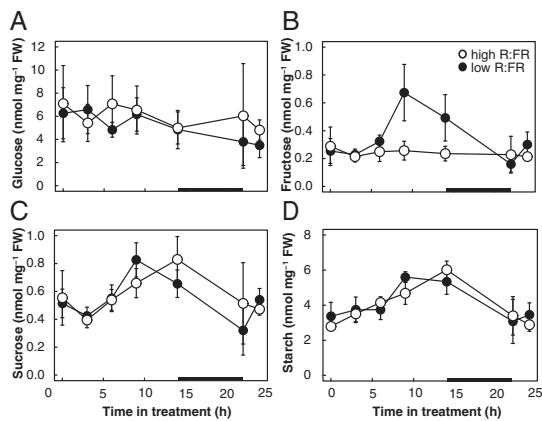


**Fig. 3.** Metabolite levels in *Brassica rapa* hypocotyls during the first 24 h of the shade avoidance response. Five-day-old *B. rapa* seedlings were grown in long days and subjected to high or low R:FR at ZT2 ( $t = 0$ ). Hypocotyls were analyzed for glucose (*A*), fructose (*B*), sucrose (*C*), and starch (*D*) levels at the indicated time points after the start of low R:FR, including just before dark and immediately after dawn. The black bar in the x axis represents the dark period. Data represent means  $\pm$  2 SE;  $n = 4$  replicates of four pooled seedlings. Corresponding cotyledon data are shown in *SI Appendix*, Fig. S3.

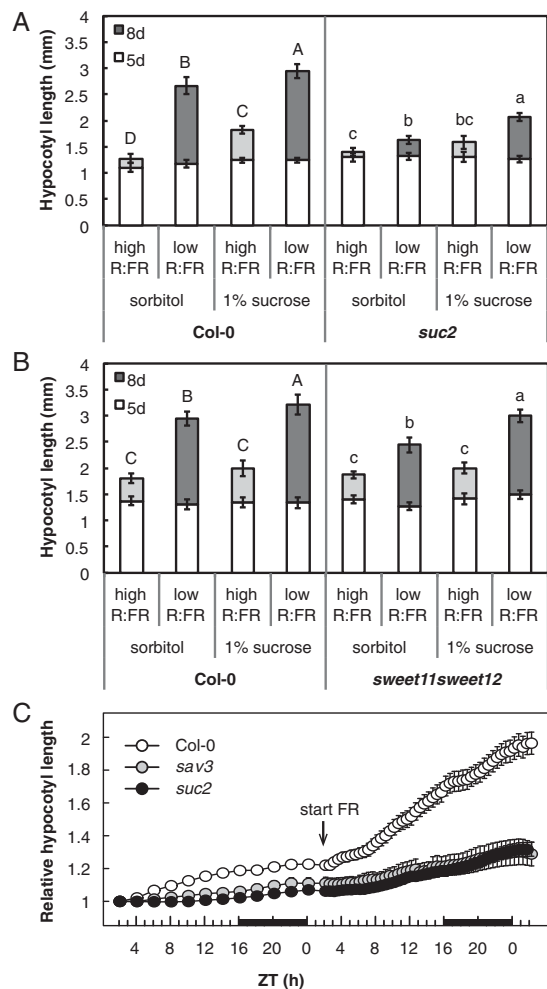


**Fig. 4.** Shade-induced hypocotyl growth requires sugar transport. Hypocotyl length of sucrose transport mutants *suc2* (*A*) and *sweet11 sweet12* (*B*), grown in long days. Length was measured after 5 d of growth in high R:FR and a subsequent 3 d in high (light gray) or low R:FR (dark gray). Seedlings were transferred to medium supplemented with 1% sucrose or the molar equivalent in sorbitol after 5 d. Data represent means  $\pm$  2 SE;  $n > 20$ . Different letters indicate significant difference after 8 d. Statistics (two-way ANOVA,  $P < 0.05$ ) were split per genotype due to significant interaction effects. (*C*) High-resolution growth analysis of Col-0, *suc2*, and *sav3* seedlings around the start of low-R:FR treatment. Hypocotyl length from long-day grown seedlings was measured from time-lapse images with 2-h intervals starting from ZT2 after 4 d of growth. The next day, images were taken at 30-min intervals after the start of low-R:FR treatment at ZT2. Relative hypocotyl length was calculated by dividing hypocotyl length at each time point by its length at the start of measurements. The black bar in the x axis represents the dark period. Data represent means  $\pm$  2 SE;  $n > 30$ .

paired response was apparent from the start of the treatment. While Col-0 showed a steady increase in absolute hypocotyl growth  $\sim$ 2 h after the start of low-R:FR treatment, this was delayed and much reduced in *suc2*, similar to *sav3*, a mutant that is defective in auxin production (Fig. 4*C*) (34). Adding 1% sucrose to the medium after 5 d of growth increased hypocotyl

length in Col-0 particularly in low R:FR and (partially) rescued the low-R:FR hypocotyl response of the sucrose transport mutants (Fig. 4 *A* and *B*). These results suggest that the sucrose transport mutants have a shortage of carbon supply to fuel-enhanced hypocotyl growth after the first 5 d of growth, and confirm that low-R:FR-induced hypocotyl elongation indeed requires rapid source to sink transport of photoassimilates through the phloem.

To test whether perturbed sugar metabolism affects seedling growth, we measured hypocotyl lengths of the *pgi1*, *pgm1*, and *adg2* *Arabidopsis* mutants, which are deficient in three subsequent steps of starch biosynthesis, impairing the pathway to varying degrees (SI Appendix, Fig. S4). Of these mutants, *pgm1* is known to have increased daytime sucrose levels and increased shoot to root transport in adult plants (35, 36). Starch levels in cotyledons of 8-d-old *pgm1* seedlings were reduced to almost zero, while soluble sugars were increased more than twofold (SI Appendix, Fig. S4). *pgi1* cotyledons had intermediate sugar concentrations, with strongly reduced (64%) starch levels and slightly increased soluble sugar content (SI Appendix, Fig. S4). Starch levels in *adg2* cotyledons were reduced by only 24%, which may be explained by partial compensation of the structural role conferred by ADG2 by another large subunit (likely APL3) in leaves (37, 38). Soluble sugar levels in *adg2* cotyledons were comparable to those of the wild-type Col-0 (SI Appendix, Fig. S4). Interestingly, the sugar concentrations in these mutants did not correspond to their hypocotyl phenotypes. *pgm1* (low-starch, high-soluble sugars) and *adg2* (moderately reduced starch, wild-type soluble sugar levels) had longer hypocotyls than Col-0 in both high and low R:FR, while *pgi1* (reduced starch, increased soluble sugars) had a wild-type phenotype in high R:FR but an impaired low-R:FR response (Fig. 5*A*). These results indicate that hypocotyl growth is indeed affected by perturbed starch biosynthesis, but that this cannot be directly linked to altered total sugar levels in the cotyledons.

Alternatively, the difference between the elongated mutants (*pgm1* and *adg2*) versus the shorter wild type and *pgi1* may be related to the capacity to store starch in the hypocotyl. In heterotrophic tissues such as the hypocotyl, the early step in starch biosynthesis catalyzed by phosphoglucose isomerase (PGI) can be bypassed through the import of glucose 6-phosphate into the plastid, allowing the production of starch in such tissues of the *pgi1* mutant (39). Indeed, the *pgm1* and *adg2* seedlings overall showed no and little starch with iodine staining, respectively, while *pgi1* seedlings accumulated starch in the hypocotyl similarly to the wild type (Fig. 5 *B–E*). Consequently, the hypocotyl phenotypes of the starch mutants appear to correspond with their capacity to produce starch in the hypocotyl irrespective of starch and sugar levels in the cotyledons. Failure to partition carbon into hypocotyl starch may thus lead to elongated hypocotyls even in unshaded conditions, as in *pgm1* and *adg2*. This correlation was extended by the analysis of *adg1*, which like *pgm1* has low starch in all tissues. *adg1* seedlings showed no starch accumulation in hypocotyls and had elongated hypocotyls in high R:FR (SI Appendix, Fig. S4). All starch mutants, however, maintained a hypocotyl elongation response to low R:FR, likely fueled by resources from the cotyledons. Failure to mobilize starch in the hypocotyl may also inhibit its growth. We therefore tested the starch degradation mutant *sex1*, which is prevented from completely degrading starch during the night in both the leaves and in the hypocotyl (40). Indeed, *sex1* hypocotyls were shorter than wild type in high R:FR and had a reduced response to low R:FR (Fig. 5*F*; two-way ANOVA genotype by light treatment interaction,  $P = 0.00015$ ), which correlated with high starch accumulation in the morning (Fig. 5 *G* and *H*).

**PIF7 Is Required for Sucrose-Induced Hypocotyl Elongation.** The elongated hypocotyls of *pgm1*, *adg1*, and *adg2* suggest that sugars

in the hypocotyl are directed to growth processes if they are not partitioned into the local starch pool. As PIFs have been identified as central integrators of growth (41), we asked whether the PIFs that are required for shade avoidance are involved in this process. Hypocotyl elongation induced by exogenously applied sucrose was previously shown to be impaired in the *pif1 pif3 pif4 pif5* mutant (42–44), and we now investigated the role of PIF7, a central signaling component of the shade avoidance response (9). Sucrose added to the medium did not induce hypocotyl elongation in the *pif7* mutant in high R:FR (Fig. 5*I*), suggesting that PIF7 is indeed important for the regulation of hypocotyl elongation in response to sugar. There was a small elongation response to added sucrose in low R:FR (Fig. 5*I*), which may be due to the action of PIF4 and PIF5 that also promote shade-induced growth (8). Indeed, sucrose responsiveness was abolished in the *pif4 pif5 pif7* mutant, both in high and low R:FR (Fig. 5*I*). A role for PIF7 in the conversion of hypocotyl sugars to growth was further confirmed in the *pgm1 pif7* double mutant. Sugar levels in *pgm1 pif7* were comparable to *pgm1*, with increased soluble sugar concentrations and very low starch levels in both cotyledons and hypocotyl (SI Appendix, Fig. S5). Strikingly, while *pgm1* was epistatic over *pif7* with respect to sugar concentrations, *pif7* was epistatic over *pgm1* with respect to hypocotyl growth. Similar to *pif7*, *pgm1 pif7* showed very little growth between days 5 and 8 in high R:FR (Fig. 5*J*). While the double mutant was slightly longer than *pif7* in low R:FR, it was much shorter than *pgm1* in this condition (Fig. 5*J*). Thus, the *pgm1* sugar phenotype is not converted into elongated hypocotyls in a PIF7-deficient background, underlining the importance of PIFs as central regulators of growth in response to both environmental and metabolic signals.

## Discussion

The shade avoidance response of elongating stems and reduced leaf growth has often been ascribed to altered resource allocation, but direct evidence for this hypothesis is limited. In previous reports, more radiolabeled carbon from  $^{14}\text{C}$ -urea applied to leaves was found to accumulate in internodes of shade-treated plants than in control plants (15, 16). In our experiments,  $^{14}\text{C}$  was taken up as  $^{14}\text{CO}_2$  during photosynthesis, allowing for a defined duration of pulse and chase to study both carbon fixation and its subsequent allocation. Since total  $^{14}\text{C}$  assimilation was not affected in low-R:FR-treated *B. rapa* seedlings and hypocotyl photosynthesis contributed only marginally to  $^{14}\text{C}$  uptake (Fig. 1*C*), our experiments demonstrate specific resource reallocation from cotyledons to the hypocotyl in shade-avoiding seedlings. Our data indicate that increased allocation to the hypocotyl takes place in the form of sucrose channeled through the phloem (Figs. 2 and 4 *A* and *B*). Consistent with this hypothesis, the *Arabidopsis* mutants in apoplastic phloem loading *suc2* and *sweet11 sweet12* indicate that a downward flux of sucrose is required for low-R:FR-induced hypocotyl elongation (Fig. 4). Interestingly, reduced expression of the sucrose transporter SUT4 in potato *StSUT4-RNAi* plants was previously shown to compromise internode elongation in response to shade, highlighting the importance of this mechanism in several plant species (45). Our kinetic analysis of low-R:FR-induced growth indicates that, similar to indole-3-acetic acid production, sucrose transport is required for rapid shade-induced hypocotyl elongation (Fig. 4*C*) (34).

Overall, the partitioning changes in carbon pools within organs correspond well with their growth response in low R:FR. The increased partitioning toward the hypocotyl in low R:FR did not lead to accumulation of sugars (Fig. 3), which indicates that the flux through the different carbon pools is higher in low R:FR. The increased amount of carbon that reaches the hypocotyl thus appears to be efficiently turned over into growth products, correlating with a hypocotyl-specific increase in gene expression

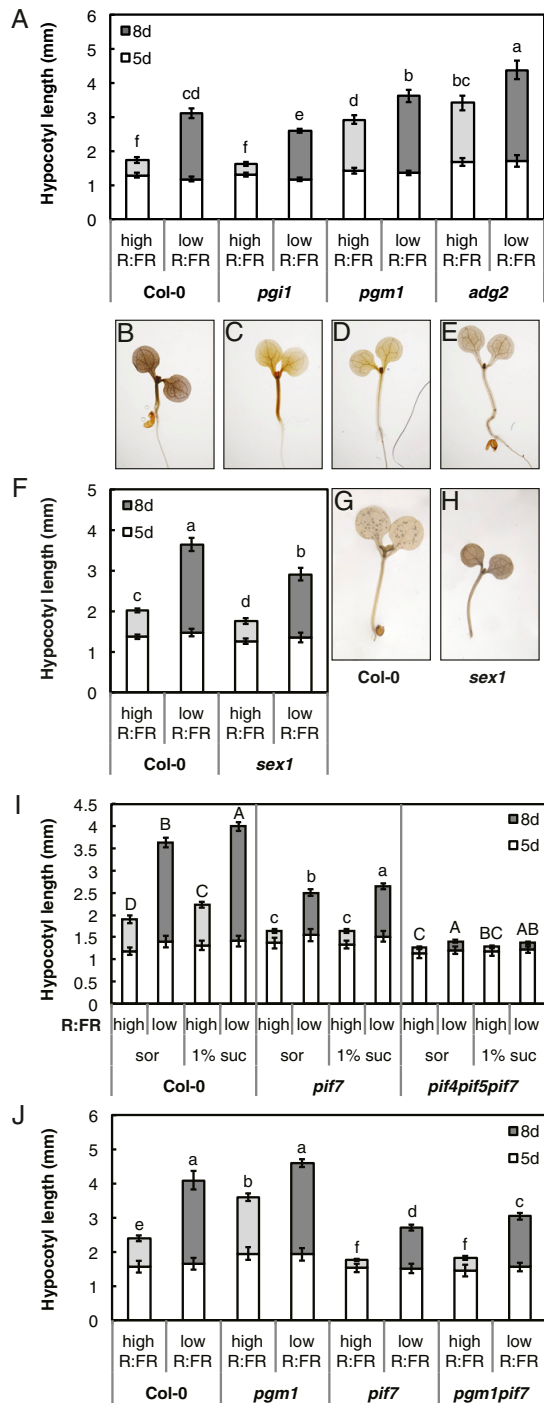


**Fig. 5.** Shade-regulated hypocotyl growth control involves starch metabolism and PIF7. Hypocotyl length of starch (A and F) and shade avoidance mutants (I and J) grown in long days after 5 d of growth in high R:FR and

related to protein, cell wall, and lipid biosynthesis found previously in low-R:FR-treated *Arabidopsis* seedlings (12).

Increasing sugar levels in the medium leads to modest hypocotyl elongation in the wild type (Figs. 4 A and B and 5 I and J). However, the characterization of starch synthesis and degradation mutants suggests that the capacity to store carbon as starch in the hypocotyl may play a role in the conversion of a metabolic signal into growth (Fig. 5). Carbon allocation to hypocotyl starch is increased in low-R:FR-treated seedlings (Fig. 2A). This starch is predominantly produced from carbon supplied by the cotyledons as the percentage of  $^{14}\text{C}$  partitioned to hypocotyl starch in low R:FR exceeds the amount contributed by hypocotyl photosynthesis (Figs. 1C and 2B). Furthermore, starch in the *pgi1* mutant cannot be produced from local photosynthate as this reaction links the Calvin cycle to starch production in the chloroplast. Therefore, accumulation of hypocotyl starch in this mutant confirms local starch production from imported carbon (Fig. 4). While partitioning to starch increased in low R:FR, starch levels remained largely unchanged (Fig. 3 and SI Appendix, Fig. S3). The unaffected starch accumulation in low-R:FR-treated hypocotyls may indicate that starch is being degraded in the light, a phenomenon recently shown to occur at dusk in *Arabidopsis* leaves (46). While the function of starch as carbon supply for growth and metabolism during the night is well known in leaves, its role in the hypocotyl is not well understood. The diel pattern of starch turnover in *B. rapa* cotyledons was similar to that described for *Arabidopsis* (22) (SI Appendix, Fig. S3). Starch turnover in the hypocotyl appeared to be much lower than in the cotyledon. Moreover, a significant proportion was retained at the end of the night, which suggests that the storage of carbohydrates into starch is not vital for the support of hypocotyl growth and metabolism at night (Fig. 3). This is supported by the elongated hypocotyl phenotype of the *Arabidopsis adg1*, *adg2*, and *pgm1* mutants, which display more hypocotyl growth despite accumulating little to no starch in this organ (Fig. 5 and SI Appendix, Fig. S4). On the other hand, *pgi1*, a starch biosynthesis mutant accumulating starch in the hypocotyl, does not have an elongated hypocotyl (Fig. 4 C and E). Finally, in *sex1*, a starch excess mutant with impaired starch degradation, hypocotyl elongation is reduced particularly in low R:FR (Fig. 5F). Together, these results suggest that carbon partitioning into hypocotyl starch may act as a growth-buffering mechanism for fluctuating carbon supply from the cotyledons rather than as a major carbohydrate store.

Hypocotyl elongation depends on PIF7, whether it is induced by low R:FR, by exogenous sucrose or by endogenous metabolic signals (Fig. 5 I and J). PIF7 is known to be an important regulator of shade-induced growth, where it is required for increased auxin levels and responsiveness leading to hypocotyl and petiole elongation (9, 12, 31, 47). Interestingly, sucrose addition to the medium induces a response similar to low R:FR, with increased auxin biosynthesis and enhanced auxin sensitivity (43, 44). The impaired sucrose response in *pif7* hypocotyls may thus result from a deficient auxin response. Furthermore, sucrose may directly promote PIF action through enhanced protein levels and increased promoter binding (43, 48). Hence, PIF7 may also

subsequent 3 d in high (light gray) or low (dark gray) R:FR. Seedlings in I were transferred to medium supplemented with 1% sucrose or the molar equivalent in sorbitol after 5 d. Data represent means  $\pm$  2 SE;  $n > 20$ . Different letters indicate significant difference after 8 d. Statistics in I (two-way ANOVA,  $P < 0.05$ ) were split per genotype due to significant interaction effects. (B–E) Iodine staining of starch biosynthesis mutants. Representative picture of Col-0 (B), *pgi1* (C), *pgm1* (D), and *adg2* (E) seedlings after 7 d in high R:FR harvested at ZT12. (G and H) Representative picture at ZT2 of iodine-stained Col-0 (G) and *sex1* (H) seedlings after 5 d of growth in high R:FR and 2 subsequent days in low R:FR.

regulate sugar delivery to the hypocotyl or act locally in the hypocotyl to enable growth enhancement triggered by an increase in sugar availability. While the exact mechanisms orchestrating the channeling of assimilated carbon into hypocotyl growth remain to be identified, it is clear that PIF7 plays a central role in shade and sugar metabolism-regulated growth (Fig. 4 H and I).

In conclusion, we show substantial resource reallocation and metabolic changes during the shade avoidance response. Our results suggest a model in which low-R:FR-induced hypocotyl elongation requires sucrose transported from the cotyledon and is controlled by regulation (PIF7) and local metabolic buffering (starch). Coordination of carbon partitioning, flux, and metabolite homeostasis appears to be a mechanism to precisely control growth in a situation in which carbon fixation is likely to become limited.

### Materials and Methods

**Plant Material and Growth Measurements.** All *Arabidopsis* plants were in the Col-0 background. We used the following mutants: *pif4 pif5 pif7* (47), *suc2-4* (49), *sweet11 sweet12* (50), *pgi1-1* (39), *adg1-1* (51), *adg2-1* (37), *pgm1-1* (52), *sex1-3* (53), and *sav3-2* (34). The *pgm1 pif7* double mutant was obtained by crossing *pgm1-1* with *pif7-1*. *Arabidopsis* seeds were surface sterilized and placed on top of a nylon mesh on 1/2 Murashige and Skoog (MS) medium (pH 5.7) containing 1.6% (m/vol) agar in square plates. After 3 d of stratification, the square plates were put upright in a Percival incubator at 20 °C in long days with a 16-h light period at 130  $\mu\text{mol}\cdot\text{m}^{-2}\cdot\text{s}^{-1}$  and a R:FR of 1.2 (measured with OceanOptics USB2000+ spectrometer). After 5 d of growth, plates were either kept in this condition, or transferred at Zeitgeber time 2 (ZT2) to a cabinet supplemented with FR LEDs to reach R:FR 0.2 with otherwise identical conditions. For sucrose treatments, the mesh containing the 5-d-old seedlings was transferred to a plate with fresh medium supplemented with 1% sucrose or the molar equivalent in sorbitol as an osmotic control. Hypocotyl length was measured from pictures after 5 and 8 d of growth with a customized MATLAB script developed in the C.F. laboratory. Time-lapse imaging was conducted as described in ref. 12, with the following differences: high-R:FR-grown seedlings were imaged at 2-h intervals from the fourth to the fifth day of growth. After transfer to low R:FR on ZT2 on the fifth day, images were taken every 30 min. Hypocotyl length was measured using an improved semiautomated MATLAB script. Relative hypocotyl length was calculated as hypocotyl length at each time point divided by hypocotyl length of the same seedling at the beginning of measurements on the fifth day.

For *Brassica rapa* experiments, the strain R-o-18 was used. For growth and metabolite measurements, *B. rapa* seeds were surface-sterilized and placed in square plates filled up to 3 cm with 1/2 MS medium containing 1.6% (m/vol) agar (pH 5.7), allowing the seedlings to grow vertically in the space not containing medium. After 2 d of stratification, a similar protocol as for *Arabidopsis* was followed, with plates divided over high and low R:FR after 5 d of initial growth in high R:FR. Hypocotyl length and cotyledon area were measured with customized MATLAB scripts for *B. rapa*. For growth kinetics, nine seedlings per treatment were photographed every 30 min during the light period using the time-lapse setup described in ref. 12. Cumulative growth was calculated as the sum of length increase between time points, averaging three consecutive time points in a sliding window to smooth the data for visualization. For biomass measurements, cotyledons and hypocotyls were dissected and dried separately at 60 °C for at least 48 h.

For labeling experiments, *B. rapa* seedlings were grown in enclosed, transparent plastic containers (Phytatray II; Sigma-Aldrich; length by width by height, 11.4 × 8.6 × 10.2 cm). Eight sterilized seeds per box were lightly pressed into a layer of 100 mL of 1/2 MS 0.8% (m/vol) agar (pH 5.7). The seeds were stratified for 2 d before transfer to a Percival growth cabinet. During germination and growth, the plants were supplied with 16-h photoperiod with 150  $\mu\text{mol}\cdot\text{m}^{-2}\cdot\text{s}^{-1}$  light intensity. After 5 d of growth, plants were split into two isolated compartments in the growth cabinet, one receiving high R:FR and the other supplemented with FR LEDs to reach low R:FR of 0.1. The plants were allowed to grow for a further 9 h or 3 d before labeling.

**Metabolic Pathway Enrichment.** To test whether low R:FR induced a coherent up- or down-regulation of genes involved in pathways associated with resource partitioning and allocation, we used the organ-specific transcriptomics dataset described in ref. 12. We considered the pathways related to photosynthetic activity and starch metabolism from the Plant Metabolic

Network database (AraCyc, version 15.0; ref. 54). For each pathway and condition, we assigned a score to the pathway computed as  $-\sum_i \log(p_i) \text{sign}(f_i)$ , where  $p_i$  is the  $P$  value of differential expression between the low-R:FR and high-R:FR condition for gene  $i$  in the pathway and  $f_i$  is the corresponding log fold change. From the expressed protein-coding genes, we then randomly selected half a million sets of the same size and computed their score to assess the empirical  $P$  value associated with the selected pathway. A Bonferroni correction for multiple pathway testing was applied to identify down- and up-regulated pathways.

**Analysis of Carbon Partitioning by  $^{14}\text{C}$  Labeling.** Labeling of photosynthetic products in *B. rapa* seedlings was performed using  $^{14}\text{C}$  as previously described (55), with several modifications. Immediately before the experiment, phytatrays containing the seedlings were opened and transferred to a custom-built, sealed, transparent chamber, lit with fluorescent lighting (150  $\mu\text{mol}\cdot\text{m}^{-2}\cdot\text{s}^{-1}$ ).  $^{14}\text{C}$  was released through the addition of lactic acid to  $\text{NaH}^{14}\text{CO}_3$  (Hartmann Analytic). After 10 min, labeling was stopped by opening the chamber in a fume hood to clear the  $^{14}\text{C}$ . Phytatrays were closed again for the 1-h chase before harvest during which time plants were allowed to metabolize the assimilated carbon. Cotyledons, hypocotyls, or roots from three seedlings were pooled per replicate, and weighed before being submerged in 2 mL of preheated 80% (vol/vol) ethanol for 20 min at 80 °C. The samples were homogenized in a all-glass homogenizer and the soluble and insoluble fractions separated by centrifugation [2,400 ×  $g$ , 12 min, room temperature (RT)]. Sequential extractions of the remaining pellet were performed with 1 mL of 50%, 20%, 0%, and then 80% (vol/vol) ethanol. The pellet was suspended in 1 mL of  $\text{H}_2\text{O}$ , yielding the insoluble fraction from which relative partitioning into starch and protein with cell wall could be determined as described by ref. 56. The soluble fractions were pooled concentrated under vacuum. A water-soluble subfraction was collected by dissolving the near-dry exsiccate in 2 mL of dd $\text{H}_2\text{O}$  collected after centrifugation (2,400 ×  $g$ , 1 min) while the remainder was dissolved in 2 mL of 98% (vol/vol) ethanol, yielding the wax and lipid fraction. Basic, acidic, and neutral fractions were separated from the water-soluble fraction by ion-exchange chromatography as described by ref. 57. Incorporation of  $^{14}\text{C}$  into each fraction was measured by liquid scintillation counting by a Tricarb 2100 (Toplab).

**Iodine Staining.** Seedlings were harvested at the end of the light period after 7 d of growth and heated in 80% (vol/vol) ethanol. When cleared of chlorophyll, seedlings were stained in Lugol solution ( $\text{I}_2/\text{KI}$ ; Sigma-Aldrich) for 5 min. Samples were subsequently rinsed in tap water for 2 min and immediately mounted under the stereomicroscope (Nikon SMZ1500 with associated Nikon D7000 camera) for imaging.

**Sugar Measurements.** Soluble sugars were extracted as described in ref. 58 with minor modifications. Aliquots of 50–80 mg fresh weight (FW) were extracted in ice-cold  $\text{CHCl}_3/\text{CH}_3\text{OH}$  (3:7, vol/vol), in a ratio of 710  $\mu\text{L}$  of  $\text{CHCl}_3/\text{CH}_3\text{OH}$  (3:7, vol/vol) per 50 mg FW. As an internal standard,  $\text{CHCl}_3/\text{CH}_3\text{OH}$  (3:7, vol/vol) was spiked with cellobiose (1 nmol of cellobiose/mg plant FW). After warming to  $-20$  °C with vigorous shaking and incubation for 2 h at  $-20$  °C with occasional vortexing, 710  $\mu\text{L}$  of water/50 mg FW was added and samples were warmed to 4 °C with repeated shaking. Separation of the upper aqueous- $\text{CH}_3\text{OH}$  phase from the lower  $\text{CHCl}_3$  phase was achieved by centrifugation at 15,000 ×  $g$  for 5 min at 4 °C. The aqueous- $\text{CH}_3\text{OH}$  phase was collected, evaporated to dryness at 30 °C, and redissolved in 500  $\mu\text{L}$  of water.

To also extract the insoluble components (including starch) contained in the lower  $\text{CHCl}_3$  phase, the protocol described in ref. 58 was adapted as follows. The  $\text{CHCl}_3$  phase was washed with 1 mL of 70% ethanol (9% vol/vol) by thorough vortexing. After centrifugation at 20,000 ×  $g$  for 5 min at RT, ethanol was removed. The pellet was dried at 20 °C for 15 min and resuspended in 500  $\mu\text{L}$  of water. Starch was digested as described in ref. 59. After the starch digest, samples were spiked with cellobiose (1.0 nmol of cellobiose/mg plant FW) as an internal standard. All samples were passed through sequential ion exchange columns (Dowex), and the eluted soluble sugars were quantified using high-performance anion-exchange chromatography with pulsed amperometric detection as described previously (59). For extraction of sugars from *Arabidopsis* seedlings, five 8-d-old cotyledons were harvested 8 h into the photoperiod and pooled per replicate. Soluble sugars were extracted through the sequential addition of 2 × 250  $\mu\text{L}$  of 80% (vol/vol) ethanol and a final extraction with 50% (vol/vol) ethanol. Each extraction was performed for 30 min at 80 °C with orbital shaking at 600 rpm. The sequential ethanolic extracts were pooled and dried under vacuum. Starch, remaining in the plantlets, was solubilized in 400  $\mu\text{L}$  of 0.2 M KOH at 95 °C for 1 h. Once

cooled to 20 °C, the solution was neutralized with 70 µL of 1 M acetic acid. Starch and soluble sugars were measured spectrophotometrically using enzyme-linked assays as described in refs. 60 and 61.

**ACKNOWLEDGMENTS.** We thank Gail Taylor for hosting M.d.W. at the University of Southampton during manuscript preparation. G.M.G., B.D.-E., and S.C.Z. gratefully acknowledge Michaela Fischer-Stettler for her contribution to the maintenance and management of the isotope laboratory. We are grateful to Norbert Sauer for kindly providing *suc2-4* seeds, to Wolf Frommer for *sweet11* *sweet12* seeds, and to Lars Østergaard for *B. rapa* seeds. We thank Bjorn Robroek from the Ecological Systems Laboratory at

the École Polytechnique Fédérale de Lausanne for help with dry weight measurements and Prashant Saxena (Indian Institute of Technology) and Kutalmis Gokalp Ince (Middle East Technical University) for developing the MATLAB script for hypocotyl length measurements. Research in the C.F. laboratory was funded by the Swiss National Science Foundation (Grants 31003A\_160326 and 310030B\_179558), SystemsX.ch (PlantMechanix 51RT-0\_145716), and the University of Lausanne. G.M.G., B.D.-E., and S.C.Z. gratefully acknowledge funding from ETH Zürich, the Zürich–Basel Plant Science Centre Plant Fellows Programme (Marie Skłodowska-Curie Action Grant GA-2010-267243), and SystemsX.ch (PlantMechanix 51RT-0\_145716).

1. Casal JJ (2013) Photoreceptor signaling networks in plant responses to shade. *Annu Rev Plant Biol* 64:403–427.
2. Morelli G, Ruberti I (2002) Light and shade in the photocontrol of *Arabidopsis* growth. *Trends Plant Sci* 7:399–404.
3. Kebrom TH, Bruntell TP (2007) The molecular analysis of the shade avoidance syndrome in the grasses has begun. *J Exp Bot* 58:3079–3089.
4. Franklin KA (2008) Shade avoidance. *New Phytol* 179:930–944.
5. Finlayson SA, Krishnareddy SR, Kebrom TH, Casal JJ (2010) Phytochrome regulation of branching in *Arabidopsis*. *Plant Physiol* 152:1914–1927.
6. Poorter H, et al. (2015) How does biomass distribution change with size and differ among species? An analysis for 1200 plant species from five continents. *New Phytol* 208:736–749.
7. Wang H, Wang H (2015) Phytochrome signaling: Time to tighten up the loose ends. *Mol Plant* 8:540–551.
8. Lorrain S, Allen T, Duek PD, Whitelam GC, Fankhauser C (2008) Phytochrome-mediated inhibition of shade avoidance involves degradation of growth-promoting bHLH transcription factors. *Plant J* 53:312–323.
9. Li L, et al. (2012) Linking photoreceptor excitation to changes in plant architecture. *Genes Dev* 26:785–790.
10. Hornitschek P, et al. (2012) Phytochrome interacting factors 4 and 5 control seedling growth in changing light conditions by directly controlling auxin signaling. *Plant J* 71:699–711.
11. Sellaro R, Pacin M, Casal JJ (2017) Meta-analysis of the transcriptome reveals a core set of shade-avoidance genes in *Arabidopsis*. *Photochem Photobiol* 93:692–702.
12. Köhnen MV, et al. (2016) Neighbor detection induces organ-specific transcriptomes, revealing patterns underlying hypocotyl-specific growth. *Plant Cell* 28:2889–2904.
13. Ruan YL (2014) Sucrose metabolism: Gateway to diverse carbon use and sugar signaling. *Annu Rev Plant Biol* 65:33–67.
14. Yu SM, Lo SF, Ho TD (2015) Source-sink communication: Regulated by hormone, nutrient, and stress cross-signaling. *Trends Plant Sci* 20:844–857.
15. Mazzella MA, Zanon MI, Fernie AR, Casal JJ (2008) Metabolic responses to red/far-red ratio and ontogeny show poor correlation with the growth rate of sunflower stems. *J Exp Bot* 59:2469–2477.
16. Casal JJ, Sanchez RA, Paganelliab AR, Izaguirre M (1995) Phytochrome effects on stem carbon gain in light-grown mustard seedlings are not simply the result of stem extension-growth responses. *Physiol Plant* 94:187–196.
17. Clifford PE, Marshall C, Sagar GR (1973) Examination of value of C-14-urea as a source of Co-14 for studies of assimilate distribution. *Ann Bot (Lond)* 37:37–44.
18. Keiller D, Smith H (1989) Control of carbon partitioning by light quality mediated by phytochrome. *Plant Sci* 63:25–29.
19. Yanovsky MJ, Casal JJ, Salerno GL, Sanchez RA (1995) Are phytochrome-mediated effects on leaf growth, carbon partitioning and extractable sucrose-phosphate synthase activity the mere consequence of stem-growth responses in light-grown mustard. *J Exp Bot* 46:753–757.
20. Kasperbauer MJ, Hamilton JL (1984) Chloroplast structure and starch grain accumulation in leaves that received different red and far-red levels during development. *Plant Physiol* 74:967–970.
21. Ranwala NKD, Decoteau DR, Ranwala AP, Miller WB (2002) Changes in soluble carbohydrates during phytochrome-regulated petiole elongation in watermelon seedlings. *Plant Growth Regul* 38:157–163.
22. Stitt M, Zeeman SC (2012) Starch turnover: Pathways, regulation and role in growth. *Curr Opin Plant Biol* 15:282–292.
23. Yang D, Seaton DD, Krahmer J, Halliday KJ (2016) Photoreceptor effects on plant biomass, resource allocation, and metabolic state. *Proc Natl Acad Sci USA* 113:7667–7672.
24. Han X, et al. (2017) Phytochrome A and B regulate primary metabolism in *Arabidopsis* leaves in response to light. *Front Plant Sci* 8:1394.
25. Pacin M, Semmoloni M, Legris M, Finlayson SA, Casal JJ (2016) Convergence of constitutive photomorphogenesis 1 and phytochrome interacting factor signalling during shade avoidance. *New Phytol* 211:967–979.
26. Devlin PF, Yanovsky MJ, Kay SA (2003) A genomic analysis of the shade avoidance response in *Arabidopsis*. *Plant Physiol* 133:1617–1629.
27. Das D, St Onge KR, Voesenek LA, Pierik R, Sasidharan R (2016) Ethylene- and shade-induced hypocotyl elongation share transcriptome patterns and functional regulators. *Plant Physiol* 172:718–733.
28. Kasperbauer MJ, Peaslee DE (1973) Morphology and photosynthetic efficiency of tobacco leaves that received end-of-day red and far red light during development. *Plant Physiol* 52:440–442.
29. Cagnola JI, Ploschuk E, Benec-Arnold T, Finlayson SA, Casal JJ (2012) Stem transcriptome reveals mechanisms to reduce the energetic cost of shade-avoidance responses in tomato. *Plant Physiol* 160:1110–1119.
30. Robson P, Whitelam GC, Smith H (1993) Selected components of the shade-avoidance syndrome are displayed in a normal manner in mutants of *Arabidopsis thaliana* and *Brassica rapa* deficient in phytochrome B. *Plant Physiol* 102:1179–1184.
31. Procko C, Crenshaw CM, Ljung K, Noel JP, Chory J (2014) Cotyledon-generated auxin is required for shade-induced hypocotyl growth in *Brassica rapa*. *Plant Physiol* 165:1285–1301.
32. Cole B, Kay SA, Chory J (2011) Automated analysis of hypocotyl growth dynamics during shade avoidance in *Arabidopsis*. *Plant J* 65:991–1000.
33. Eastmond PJ (2006) SUGAR-DEPENDENT1 encodes a patatin domain triacylglycerol lipase that initiates storage oil breakdown in germinating *Arabidopsis* seeds. *Plant Cell* 18:665–675.
34. Tao Y, et al. (2008) Rapid synthesis of auxin via a new tryptophan-dependent pathway is required for shade avoidance in plants. *Cell* 133:164–176.
35. Brauner K, Hörmiller I, Nägele T, Heyer AG (2014) Exaggerated root respiration accounts for growth retardation in a starchless mutant of *Arabidopsis thaliana*. *Plant J* 79:82–91.
36. Kölling K, Thalmann M, Müller A, Jenny C, Zeeman SC (2015) Carbon partitioning in *Arabidopsis thaliana* is a dynamic process controlled by the plants metabolic status and its circadian clock. *Plant Cell Environ* 38:1965–1979.
37. Lin TP, Caspar T, Somerville C, Preiss J (1988) Isolation and characterization of a starchless mutant of *Arabidopsis thaliana* (L.) heynl lacking ADP-glucose pyrophosphorylase activity. *Plant Physiol* 86:1131–1135.
38. Fritzius T, Aeschbacher R, Wiemken A, Winkler A (2001) Induction of Apl3 expression by trehalose complements the starch-deficient *Arabidopsis* mutant *adg2-1* lacking Apl1, the large subunit of ADP-glucose pyrophosphorylase. *Plant Physiol* 126:883–889.
39. Yu TS, Lue WL, Wang SM, Chen J (2000) Mutation of *Arabidopsis* plastid phosphoglucose isomerase affects leaf starch synthesis and floral initiation. *Plant Physiol* 123:319–326.
40. Vitha S, Yang M, Sack FD, Kiss JZ (2007) Gravitropism in the starch excess mutant of *Arabidopsis thaliana*. *Am J Bot* 94:590–598.
41. Leivar P, Monte E (2014) PIFs: Systems integrators in plant development. *Plant Cell* 26:56–78.
42. Stewart JL, Maloof JN, Nemhauser JL (2011) PIF genes mediate the effect of sucrose on seedling growth dynamics. *PLoS One* 6:e19894.
43. Lilley JL, Gee CW, Sairanen I, Ljung K, Nemhauser JL (2012) An endogenous carbon-sensing pathway triggers increased auxin flux and hypocotyl elongation. *Plant Physiol* 160:2261–2270.
44. Sairanen I, et al. (2012) Soluble carbohydrates regulate auxin biosynthesis via PIF proteins in *Arabidopsis*. *Plant Cell* 24:4907–4916.
45. Chincinska IA, et al. (2008) Sucrose transporter S5UT4 from potato affects flowering, tuberization, and shade avoidance response. *Plant Physiol* 146:515–528.
46. Fernandez O, et al. (2017) Leaf starch turnover occurs in long days and in falling light at the end of the day. *Plant Physiol* 174:2199–2212.
47. de Wit M, Ljung K, Fankhauser C (2015) Contrasting growth responses in lamina and petiole during neighbor detection depend on differential auxin responsiveness rather than different auxin levels. *New Phytol* 208:198–209.
48. Shor E, Paik I, Kangisser S, Green R, Huq E (2017) Phytochrome interacting factors mediate metabolic control of the circadian system in *Arabidopsis*. *New Phytol* 215:217–228.
49. Srivastava AC, Ganesan S, Ismail IO, Ayre BG (2008) Functional characterization of the *Arabidopsis* AtSUC2 Sucrose/H+ symporter by tissue-specific complementation reveals an essential role in phloem loading but not in long-distance transport. *Plant Physiol* 148:200–211.
50. Chen LQ, et al. (2012) Sucrose efflux mediated by SWEET proteins as a key step for phloem transport. *Science* 335:207–211.
51. Wang SM, et al. (1998) Characterization of ADG1, an *Arabidopsis* locus encoding for ADPG pyrophosphorylase small subunit, demonstrates that the presence of the small subunit is required for large subunit stability. *Plant J* 13:63–70.
52. Caspar T, Huber SC, Somerville C (1985) Alterations in growth, photosynthesis, and respiration in a starchless mutant of *Arabidopsis thaliana* (L.) deficient in chloroplast phosphoglucomutase activity. *Plant Physiol* 79:11–17.
53. Yu TS, et al. (2001) The *Arabidopsis* *sex1* mutant is defective in the R1 protein, a general regulator of starch degradation in plants, and not in the chloroplast hexose transporter. *Plant Cell* 13:1907–1918.
54. Mueller LA, Zhang P, Rhee SY (2003) AraCyc: A biochemical pathway database for *Arabidopsis*. *Plant Physiol* 132:453–460.
55. Kölling K, Müller A, Flüttsch P, Zeeman SC (2013) A device for single leaf labelling with  $^{14}C$  isotopes to study carbon allocation and partitioning in *Arabidopsis thaliana*. *Plant Methods* 9:45.

56. Zeeman SC, Ap Rees T (1999) Changes in carbohydrate metabolism and assimilate export in starch-excess mutants of *Arabidopsis*. *Plant Cell Environ* 22:1445–1453.
57. Quick P, Siegl G, Neuhaus E, Feil R, Stitt M (1989) Short-term water stress leads to a stimulation of sucrose synthesis by activating sucrose-phosphate synthase. *Planta* 177: 535–546.
58. Arrivault S, et al. (2009) Use of reverse-phase liquid chromatography, linked to tandem mass spectrometry, to profile the Calvin cycle and other metabolic intermediates in *Arabidopsis* rosettes at different carbon dioxide concentrations. *Plant J* 59:826–839.
59. Egli B, Kölling K, Köhler C, Zeeman SC, Streb S (2010) Loss of cytosolic phosphoglucomutase compromises gametophyte development in *Arabidopsis*. *Plant Physiol* 154: 1659–1671.
60. Müller-Röber B, Sonnewald U, Willmitzer L (1992) Inhibition of the ADP-glucose pyrophosphorylase in transgenic potatoes leads to sugar-storing tubers and influences tuber formation and expression of tuber storage protein genes. *EMBO J* 11:1229–1238.
61. Hostettler C, et al. (2011) Analysis of starch metabolism in chloroplasts. *Methods Mol Biol* 775:387–410.

## Supplementary Information for

Changes in resource partitioning between and within organs support growth adaptation to neighbour proximity in *Brassicaceae* seedlings

Mieke de Wit, Gavin M. George, Yetkin Çaka Ince, Barbara Dankwa-Egli, Micha Hersch, Samuel C. Zeeman, Christian Fankhauser

Corresponding author: Christian Fankhauser  
Email: [christian.fankhauser@unil.ch](mailto:christian.fankhauser@unil.ch)

### **This PDF file includes:**

Figs. S1 to S5

### **Other supplementary materials for this manuscript include the following:**

Dataset S1

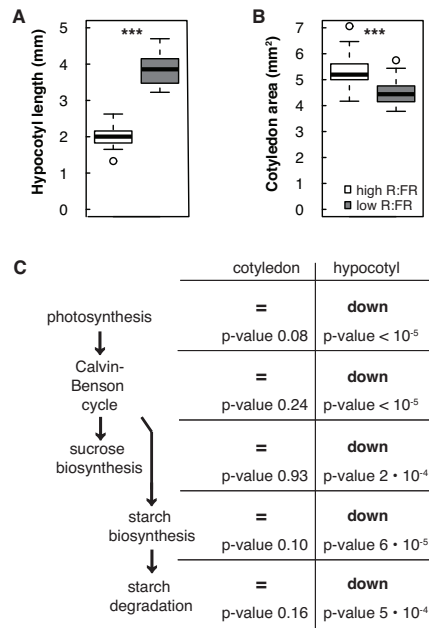


**Fig. S1. Shade avoidance response in *Arabidopsis thaliana* seedlings.** Hypocotyl length (A) and cotyledon area (B) in high and low R:FR. Col-0 seedlings were grown on horizontal plates in high R:FR for the first 3 d and subsequently divided over high and low R:FR for another 4 d of growth. Data are represented as standard boxplot representing median and interquartile (IQR) range between the 25th and 75th percentiles. Whiskers extend to 1.5-fold the IQR, dots represent data points outside 1.5-fold IQR. Hypocotyls and cotyledons were dissected and scanned for measurements after 7 d of growth. Asterisks indicate significant difference, n = 30. Significance codes: ‘\*’ 0.05 > p > 0.01, ‘\*\*’ 0.01 > p > 0.001, ‘\*\*\*’ p < 0.001. (C) Metabolic pathway enrichment analysis on genes differentially regulated in cotyledons and hypocotyls of 5-d-old *Arabidopsis* seedlings after 3 h of low R:FR, using the PlantCyc tool. =, no significant enrichment; down, pathway significantly downregulated.

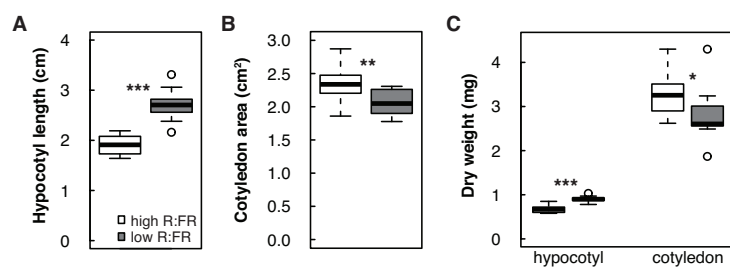


**Fig. S2. Shade avoidance response in *Brassica rapa* seedlings.** Five-day old *B. rapa* seedlings were divided over high or low R:FR treatment for another 2 d of growth. Hypocotyls and cotyledons were dissected after 2 d of treatment, and hypocotyl length (A), cotyledon area (B) and biomass (C) were subsequently determined. Data are represented as standard boxplot representing median and interquartile (IQR) range between the 25th and 75th percentiles. Whiskers extend to 1.5-fold the IQR, dots represent data points outside 1.5-fold IQR. n=30. Significance codes: ‘\*’  $0.05 > p > 0.01$ , ‘\*\*’  $0.01 > p > 0.001$ , ‘\*\*\*’  $p < 0.001$ .

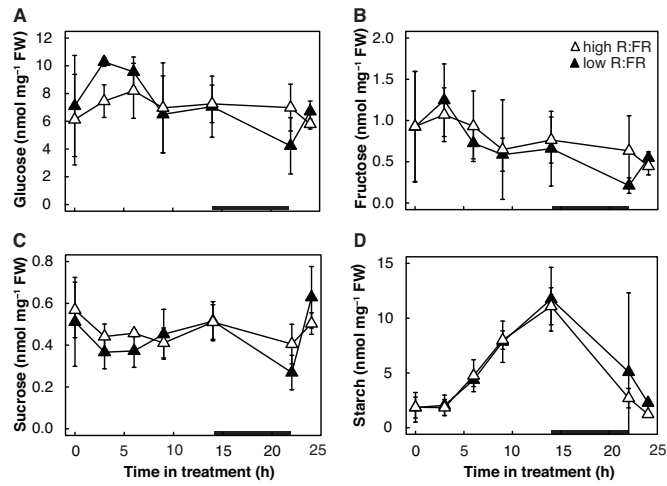


**Fig. S3. Metabolite levels in *Brassica rapa* cotyledons during the first 24 h of the shade avoidance response.** Five-day-old *B. rapa* seedlings were subjected to high or low R:FR at ZT2 ( $t = 0$ ). Cotyledons were analysed for glucose (A), fructose (B), sucrose (C) and starch (D) levels at the indicated time points after the start of low R:FR, including just before dark and immediately after dawn. Black bar in the x-axis represents the dark period. Data represent means  $\pm 2\text{SE}$ ,  $n = 4$  replicates of four pooled seedlings. Corresponding hypocotyl data is shown in Fig. 3.

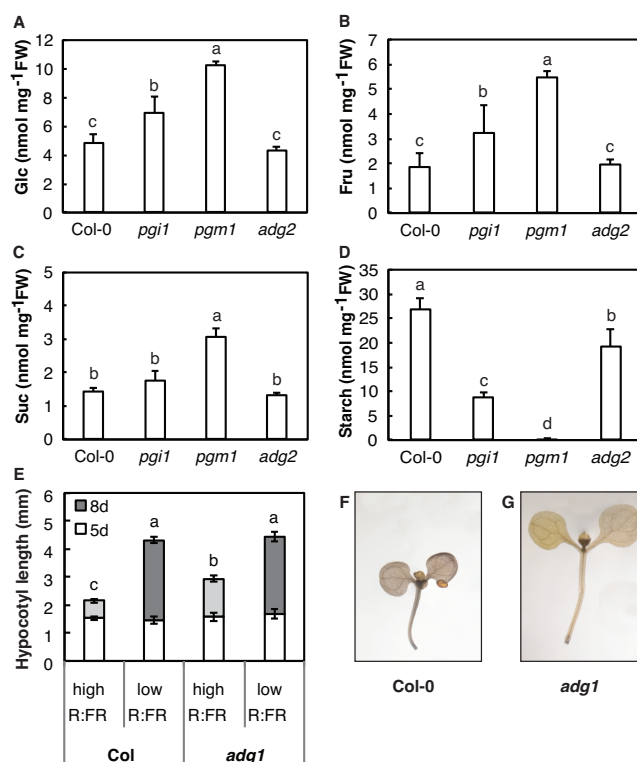


**Fig. S4. Metabolite levels in Arabidopsis starch mutant cotyledons.** Cotyledons from 8-d-old Arabidopsis seedlings were collected at midday and analysed for glucose (A), fructose (B), sucrose (C) and starch (D) levels. Data represent means  $\pm$  2SE,  $n = 4$  replicates of 5 pooled seedlings. Letters indicate significant differences ( $p < 0.05$ ). The *pgi1-1* mutant lacks the plastidial isoform of phosphoglucose isomerase, which interconverts fructose 6-phosphate and glucose 6-phosphate. The *pgm1-1* mutant lacks the plastidial isoform of phosphoglucomutase which interconverts glucose 6-phosphate and glucose 1-phosphate. The *adg2-1* mutant lacks the large, non-catalytic subunit of ADPglucose pyrophosphorylase, which interconverts ATP and glucose 1-phosphate with ADPglucose and inorganic pyrophosphate. (E) Hypocotyl length of the starch mutant *adg1-1* and wild type (Col) grown in long days after 5 d of growth in high R:FR and a subsequent 3 d in high (light grey) or low (dark grey) R:FR. Data represent means  $\pm$  2SE,  $n > 20$ , Two-Way ANOVA,  $p < 0.05$ . Starch staining of representative seedlings of Col-0 (F), *adg1-1* (G) seedlings after 7 d in high R:FR harvested at ZT12.

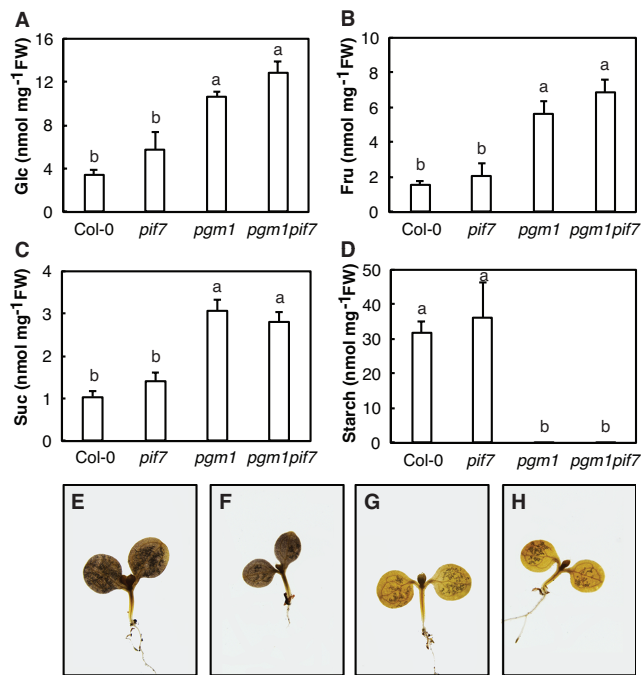


**Fig. S5. Metabolite levels in Arabidopsis *pif7* mutant cotyledons.** Cotyledons from 8-d-old Arabidopsis seedlings were collected at midday and analysed for glucose (A), fructose (B), sucrose (C) and starch (D) levels. Representative picture of iodine-stained Col-0 (E), *pif7* (F), *pgm1-1* (G) and *pgmpif7* (H) seedlings after 7 d in high R:FR harvested in the middle of the photoperiod. Data represent means  $\pm$  2SE, n = 4 replicates of 5 pooled seedlings. Letters indicate significant differences ( $p < 0.05$ ).

**Additional data (separate file)**

**Dataset S1:** Differential gene expression in the hypocotyl between white light and white light with additional far-red (FR) light for genes involved in carbon metabolism pathways.

[Download Dataset\\_S01](#)

# **Chapter 3. Distinct mechanisms underlying hypocotyl growth promotion in response to neighbour proximity and vegetative shade**

## OVERVIEW

I was the leading investigator in the last chapter of my thesis where we studied the mechanisms underlying hypocotyl growth promotion in response to neighbour proximity and vegetative shade. I designed the project together with Prof. Fankhauser and conducted all of the experiments with the exceptions: Mieke de Wit isolated RNAs used in expression analysis (Fig. 3b and S2), Anne-Sophie Fiorucci isolated and helped isolation of ChIP-DNA (Fig. S3a and S3b), Vinicius Costa Galvao isolated ChIP-DNA and did the ChIP-qPCR for *HFR1* (Fig. 3c, S3c, S3d), Anupama Goyal, Vinicius Costa Galvao, and Martine Trevisan generated the *yuc2589* mutant, Martine Trevisan isolated RNAs used in RNA-seq, Genomic Technologies Facility (GTF, UNIL) did the RNA-seq and initial data analysis, Prof. Sebastien Mongrand's lab (University of Bordeaux, France) did the sterol measurements, Prof. Julijana Ivanisevic's lab (Metabolomics Unit, UNIL) did the lipidomics analysis, Prof. Christian Hardtke (DBMV, UNIL) kindly provided *cvp2cvl1* seeds, Prof. Richard Vierstra (Washington University in St. Louis, USA) kindly provided *35S::ATG8-GFP* seeds in the *atg7* mutant background. I analysed and interpreted the data with the participation of people who conducted the experiments and my supervisor Prof. Christian Fankhauser. I wrote the chapter in the paper format in agreement with previous chapters under supervision of Prof. Christian Fankhauser.

## ABSTRACT

Vegetational shade and neighbour proximity both promote hypocotyl elongation. This growth response depends on allocation of additional resources including fixed CO<sub>2</sub>. However, in neighbour proximity (low red to far-red ratio, LRFR) CO<sub>2</sub> fixation remains constant while in true shade (mimicked in the lab with low blue light, LB) carbon fixation is reduced. Our transcriptome analyses indicate that while both light conditions converged at the transcriptional activation of known elongation mechanisms, LB and LRFR promoted catabolic and anabolic processes, respectively. Biochemical and cell biological assays showed that LB but not LRFR also induced autophagy post-transcriptionally. The distal roles of PIFs on induction of auxin biosynthesis in cotyledons is well-established in LRFR, yet their local roles in elongating hypocotyls remain largely unknown. PM elongation is an important step for cell elongation. In LRFR, we identified new local roles for PIFs that induced genes required in biosynthesis of sterols, a major component of PM. LRFR also promoted the accumulation of PM lipids in *B. rapa* hypocotyls. Hypocotyls elongated less in LRFR upon inhibition of sterol biosynthesis pharmacologically or genetically as in *smt2-1*. In contrast, LB-induced hypocotyl elongation was not impaired by these treatments. Interestingly, the *atg7* autophagy mutant showed the converse phenotype, with a stronger hypocotyl growth defect in LB than LRFR. Finally, *smt2atg7* hypocotyl elongation was completely impaired in all conditions. Overall, our results indicate that the biosynthesis in LRFR and recycling in LB are two complementary mechanisms that enable elongation in vegetative shade.

## INTRODUCTION

Plant leaves absorb blue (B) and red light (R) and transmit and reflect far-red (FR) light. Therefore, vegetative shade decreases the intensity of B and R light, thus the level of photosynthetically active radiation (PAR) (400-700 nm) reaching to plant photosynthetic organs (Casal, 2013). However, whether or not they are shaded, plants are exposed to an increased intensity of FR leading to low R/FR (LRFR) in the presence of neighbours. Laboratory model systems often use LRFR and low B (LB) to mimic neighbour proximity and vegetative shade, respectively, two conditions that similarly induce hypocotyl elongation in *Arabidopsis* seedlings (Pedmale et al., 2016). PIFs are key transcription factors regulating LB and LRFR-induced hypocotyl elongation (Lorrain et al., 2008, Li et al., 2012, Pedmale et al., 2016).

Upon perception of LRFR, PIF4, PIF5, and PIF7 promote auxin production in distal organ cotyledons through induction of *YUCCAs* (Li et al., 2012, Nito et al., 2015, Kohnen et al., 2016). Later, auxin is transported from cotyledons to hypocotyl to induce hypocotyl elongation, a process that also requires PIFs (Keuskamp et al., 2010, Procko et al., 2014, Kohnen et al., 2016). However, transcriptome comparison of LRFR- and auxin-treated seedlings reveals that only half of the shade-induced genes are induced by auxin treatment (Tao et al., 2008). PIFs also function in auxin perception and signalling by regulating expression of genes coding for auxin receptors and auxin repressor proteins (Aux/IAAs) and by co-regulating expression of a subset of growth-related genes with auxin response factors (ARFs) (Nozue et al., 2011, Hornitschek et al., 2012, Hersch et al., 2014, Oh et al., 2014, Kohnen et al., 2016). ARF6 and brassinosteroid (BR) - signalling factor BZR1 physically interact with PIF4 and three of them synergistically regulate target genes (Oh et al., 2014). BR biosynthesis and signalling are required for petiole and hypocotyl elongation in LRFR (Kozuka et al., 2010, Cifuentes-Esquivel et al., 2013). Organ-specific LRFR

transcriptome of *Arabidopsis* seedlings shows distinct expression patterns in cotyledons and hypocotyls, suggesting that the molecular mechanisms behind the local and distal regulation of LRF-induced hypocotyl elongation are different (Kohnen et al., 2016). Comparison of PIF targets and organ-specific LRF transcriptome suggests that PIFs locally induce the expression of several genes coding for key enzymes in different molecular mechanisms that lead to elongation of hypocotyls (Hornitschek et al., 2012, Oh et al., 2014, Kohnen et al., 2016). In addition to auxin transport and response, other hormone responses and cell wall organisation are among the suggested PIF-dependent mechanisms in hypocotyls (Hornitschek et al., 2012, Li et al., 2012, Oh et al., 2014, Kohnen et al., 2016). Although local functions of PIFs in hypocotyls emerge as a possible novel mechanism for LRF-induced hypocotyl elongation, we still lack direct evidence for mechanisms by which PIFs promote growth in the hypocotyl.

Molecular mechanisms in LB-induced hypocotyl elongation are less known compared to LRF. PIF4 is a key transcription factor in LB-induced hypocotyl elongation with minor contributions of PIF5 and PIF7 (Pedmale et al., 2016). CRY1 interacts with PIF4 on DNA and represses its transcriptional activity in a blue light-dependent manner (Ma et al., 2016). Similarly, CRY2-PIF4 and CRY2-PIF5 complexes are detected on chromatin; however, in contrast to the previous study the authors argue that these interactions rather promote transcriptional activity of PIFs in response to low B light (Pedmale et al., 2016). However, it is not clear which molecular pathways the CRY2-PIF complexes promote. Unlike LRF, the transcriptome data from whole seedlings indicates that auxin and brassinosteroid (BR) responses are not regulated in LB (Pedmale et al., 2016). However, LB-induced hypocotyl elongation of the mutants that are impaired either in auxin biosynthesis, transport and signalling or in BR biosynthesis is reduced (Keuskamp et al., 2011, Pedmale et al., 2016). Similar to LRF, cell wall organisation is transcriptionally induced in LB downstream of PIFs, auxin and BR (Keuskamp et al., 2011, Kohnen et al., 2016, Pedmale et al., 2016). Thus, studies

suggest that several growth-related pathways are similarly required and/or activated in LB and LRFR. However, it is still largely unclear what the differences are in the molecular mechanisms driving hypocotyl elongation in LB and LRFR.

Plasma membrane (PM) extension is an important step for cell elongation that remains under-examined in the vegetative shade-induced hypocotyl elongation. PM, together with the cell wall, defines the boundaries of a cell and needs to extend with the elongating cell. Cell wall is composed of cellulose microfibrils (CMFs) embedded in a matrix of pectins, hemicelluloses, structural proteins, and proteoglycans (Verbancic et al., 2018). Cell wall extension occurs via two mechanisms. First mechanism is the relaxation of the matrix, e.g., by breaking the link between hemicellulose xyloglucans and CMFs, which loosens the wall and allows the cell to inflate like a balloon with the increasing turgor pressure. Second, the new cell wall material including CMFs, structural proteins as well as the wall-loosening proteins are deposited. On the contrary, PM is flexible only to a limited extent. Depending on the lipid species, acyl chain unsaturation, temperature, pressure and several other parameters, lipid organisation of PM bilayer can transit between liquid ordered (Lo) and disordered (Ld) phases where the lipids are tightly or loosely packed, respectively (Mamode Cassim et al., 2019). Yet, PM is fairly rigid with a little expanding and contracting ability and can burst if a cell takes too much water, unlike the cell wall. Furthermore, PM curvature is low, which creates a more impermeable membrane and limits the PM extension ability (Boutté & Jaillais, 2020). Therefore, PM needs to grow with the deposition of new lipid material as the cell elongates. According to the model that explains the growth of rapidly elongating plant cells, e.g., pollen tubes and root hair cells, Golgi-derived secretory vesicles fuse with the apical PM, supplying the requirements for extension of growth of the PM during the delivery of the new cell wall material (Steer & Steer, 1989). Normally, such a process delivers the new membrane material more than the requirements for PM elongation, thus the excess membrane material is transported back via

endocytosis for recycling (Hepler et al., 2013). We previously reported that *Brassica rapa* seedlings allocate more cotyledon-fixed carbon to the elongating hypocotyl in LRFR (de Wit et al., 2018). Interestingly, the incorporation of labelled carbon to the ethanol-soluble fraction of hypocotyls that contains lipids and waxes together with all other fractions is increased in LRFR (de Wit et al., 2018). Furthermore, the composition saturated and unsaturated fatty acids (FA) changes in LRFR in a phyB and PIF-dependent manner via regulation of *FATTY ACID DESATURASE (FAD)* expression (Arico et al., 2019). Organ-specific LRFR transcriptome indicates that LRFR induces gene expression for biosynthesis of sterols in elongating hypocotyls (Kohnen et al., 2016). Sterols, together with glycerolphospholipids, and sphingolipids, compose the PM (Mamode Cassim et al., 2019). Plants possess a vast array of sterols and the most abundant sterols in *Arabidopsis* seedlings are sitosterol (64%), campesterol (11%), and stigmasterol (6%) (Valitova et al., 2016). Sterols regulate fluidity, permeability, and regional identity of the membranes. They bind to fatty acid chains and stabilise them, decreasing the PM permeability and fluidity (Valitova et al., 2016). Unlike sitosterol, campesterol, and cholesterol; stigmasterol increases the membrane disorder, thus the fluidity (Grosjean et al., 2015). In addition to their functions as the structural components of the PM, sterols are directly involved in regulation of plant growth and development. They are precursors of brassinosteroids (BR) that are also important hormones for shade-induced hypocotyl elongation (Keuskamp et al., 2011, Bou-Torrent et al., 2014, Valitova et al., 2016). Furthermore, together with sphingolipids, sterols are enriched in lipid microdomains in PM that serves as anchoring platforms for signalling and transport proteins (Yu et al., 2020). PIN auxin transport proteins co-localise with such microdomains (Lofke et al., 2013). Moreover, all sterol biosynthesis mutants upstream of 24-ethyl/24-methyl sterols showed defects in polar localisation of PINs with an altered distribution of auxin in *Arabidopsis* (Boutté & Jaillais, 2020). Cellulose synthase complexes (CSCs) are also considered to be co-localised with

the PM microdomains, as sphingolipid biosynthesis mutants show a decrease in cellulose biosynthesis (Turner & Kumar, 2018). Finally, a sitosterol derivative, sitosterol- $\beta$ -glucoside, serves as a primer for glucan polymerisation initiated by CesaA glucosyltransferase, directly contributing to cell wall extension (Valitova et al., 2016). The major structural and functional roles in PM make sterols likely important in vegetative shade-induced hypocotyl elongation.

PAR reaching to photosynthetic organs remains the same in LRFr but it decreases in LB. Production of new material that is required for cell elongation is dependent on carbon fixation rate by photosynthesis, thus the level of PAR. We previously showed that LRFr does not significantly decrease carbon fixation in *B. rapa* seedlings (de Wit et al., 2018). However, low light conditions decrease carbon fixation via reduction of Rubisco activity (Perchorowicz et al., 1981). Thus, it is expected that carbon fixation would decrease when the blue light is completely depleted as in LB, limiting to carbon resource availability to a certain extent. Carbon starvation induces autophagy that recycles the unused cellular material (Li & Vierstra, 2012, Wang et al., 2018a). There are three distinct autophagic routes that have been identified in plants: micro-, macro-, and mega-autophagy (Chen et al., 2019). Micro- and macro-autophagy are relatively well described in plants. Microautophagy occurs via the invagination of the tonoplast to trap cytoplasmic material creating autophagic bodies within the vacuole (Chen et al., 2019). In contrast, macroautophagy sequester cytosolic components in double-membrane vesicles called autophagosomes that fuse with the tonoplast to release their cargo into the vacuolar lumen. The released bodies are also called as autophagic bodies (Chen et al., 2019). The products that are degraded by vacuolar hydrolases are then exported back to cytosol to be reused. Macroautophagy employs Autophagy-related (ATG) protein-mediated autophagic system where ATG8 proteins play a central role and often used as an indicator of autophagic activity (Li & Vierstra, 2012). Formation of autophagosomes requires ATG8 anchorage to the pre-autophagosome

membrane (Chen et al., 2019). Furthermore, ATG8 promotes autophagosome membrane fusion with the tonoplast (Li & Vierstra, 2012). ATG8 anchorage requires the lipidation by phosphatidylethanolamine (PE), which is catalysed by ATG3, ATG4, ATG5, ATG7, ATG10, and ATG12 via consecutive steps (Li & Vierstra, 2012). There are also several forms of selective autophagy in plants, including selective degradation of cellular components, e.g., chloroplasts (chlorophagy) and lipids (lipophagy) (Chen et al., 2019). Lipophagy is connected to the lipid metabolism and storage in diverse model systems (Jaishy & Abel, 2016, Shatz et al., 2016, Elander et al., 2018). In addition to their structural roles in PM, lipids are used as substrates for energy production via  $\beta$ -oxidation of FA in mammals (Shatz et al., 2016), yeast (Kohlwein, 2010), and Arabidopsis (Fan et al., 2019) under nutrient starvation. Lipophagy in Arabidopsis requires the core components of macroautophagy, disruption of which reduces the membrane lipid turnover as well as the energy production (Fan et al., 2019). The fact that LB and LRFR differs in availability of the fixed carbon resources due to the different levels of photosynthesis rates suggest that the resource availability may have an impact on how the materials needed for cell elongation are obtained in these two conditions.

In summary, PIFs are key transcription factors regulating LB and LRFR-induced hypocotyl elongation. In distal organ cotyledons, they induce biosynthesis of auxin that is transported to hypocotyls and induce elongation in LRFR (Keuskamp et al., 2010, Li et al., 2012, Nito et al., 2015, Kohnen et al., 2016). However, what PIFs do in hypocotyls in addition to auxin response remains unclear (Fig. 1). Furthermore, we still have a poor understanding on functions of PIFs on LB-induced hypocotyl elongation. LRFR- and LB-induced hypocotyl elongation similarly requires auxin and BR biosynthesis and signalling and both light conditions promotes cell wall organisation transcriptionally (Keuskamp et al., 2011, Kohnen et al., 2016, Pedmale et al., 2016). PM elongation is another

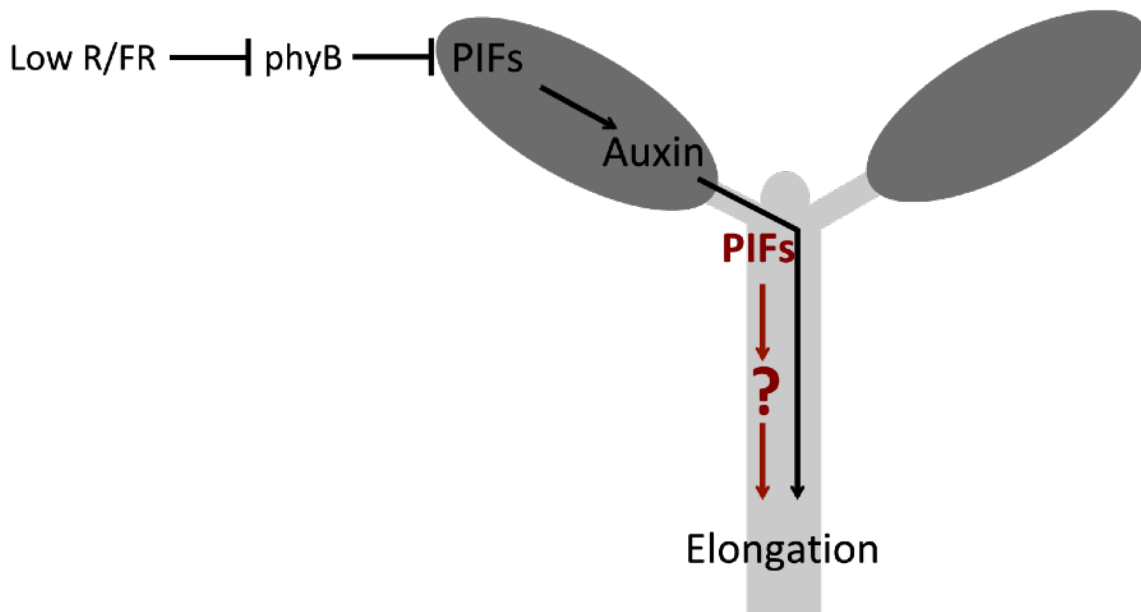


**Figure 1. The current model for PIF-mediated hypocotyl elongation in LRFR.**

Although the role of PIFs in auxin production in distal organ cotyledons is well documented, what PIFs do locally in hypocotyls remains to be investigated in LRFR-induced hypocotyl elongation.

important step for cell elongation (Steer & Steer, 1989, Hepler et al., 2013). Although previous studies indicate that LRFR induces biosynthesis of several PM components transcriptionally in hypocotyls and allocation of cotyledon-fixed carbon to the elongating hypocotyl (Kohnen et al., 2016, de Wit et al., 2018), the significance of PM elongation remains under-examined in shade-induced hypocotyl elongation. Lastly, the fixed carbon resources available for LB and LRFR are expected to differ as the light available for photosynthesis differs in two conditions. However, to what extent the molecular mechanisms providing the materials needed for cell elongation in LB and LRFR are similar or different also remains to be examined.

To characterise local and distal functions of PIFs in shade-induced hypocotyl elongation, we compared the transcriptome of the *pif457* mutant and Col-0 in dissected hypocotyls and cotyledons in LRFR. Furthermore, we included the *yuc2589* mutant in the expression analysis, which allowed us to differentiate PIF-

and auxin-mediated molecular pathways that are induced transcriptionally in LRFR. As previous reports indicated that lipid biosynthesis and in particular sterol biosynthesis genes are induced by LRFR in hypocotyls (Kohnen et al., 2016), we hypothesised that this could be a mechanism by which PIFs promote hypocotyl elongation locally. Therefore, we characterised an *Arabidopsis* sitosterol biosynthesis mutant, *smt2* in LRFR. More globally, we analysed the impact of LRFR on sterol and total lipid composition of *B. rapa* hypocotyls. We also examined the organ-specific transcriptome responses of *Arabidopsis* cotyledons and hypocotyls in two major components of vegetative shade, LB and LRFR and how PIFs and auxin contribute to these responses. Finally, we hypothesised that the availability of fixed carbon resources may regulate how the materials needed for cell elongation are obtained in LB and LRFR. Therefore, we focused on how anabolic and catabolic pathways contribute to LRFR- and LB-induced hypocotyl elongation with a focus on obtaining the required lipid material.

## RESULTS

### LRFR-induced hypocotyl elongation requires PIFs for more than induction of auxin biosynthesis in cotyledons

Previous reports indicate that exogenous application of synthetic auxin picloram cannot completely rescue impaired hypocotyl elongation of *pif457* in LRFR (Kohnen et al., 2016), suggesting that PIFs are required for more than auxin biosynthesis in LRFR-induced hypocotyls elongation. Considering that seedlings may process internally produced and exogenously applied auxin differently, we used a cotyledon specific, chemically inducible *FRO6::XVE::YUC3* line (*YUC3i*) (Chen et al., 2014a) in Col-0 and *pif457* backgrounds to understand to which extent PIF-induced elongation is mediated by YUCCA-dependent auxin production in cotyledons. Auxin production takes place in the cotyledons of the *YUC3i* line upon estradiol application (Chen et al., 2014a), mimicking the LRFR-induced auxin production (Fig. 2, left). *YUC3i* seedlings in Col-0 and *pif457* background were grown in WL for four days and then either kept in WL or transferred to LRFR for three days with or without the inducer, 10  $\mu$ M estradiol. Estradiol promoted *YUC3i* hypocotyl elongation more compared to *YUC3i pif457* in both WL and LRFR (Fig. 2, right). This result not only confirms the previous reports (Kohnen et al., 2016), but also further shows that cotyledon-sourced auxin is not enough to induce full hypocotyl elongation in LRFR when PIF4, PIF5, and PIF7 are absent. Therefore, we conclude that PIF4, PIF5, and PIF7 are required for normal hypocotyl elongation triggered by higher auxin levels.

### PIFs induce *SMT2* and *SMT3* expression in LRFR

In chapter 2, we showed that *Brassica rapa* seedlings allocate more cotyledon-fixed carbon to the elongating hypocotyl in LRFR (de Wit et al., 2018). Interestingly, the carbon fraction that contains lipids and waxes together with all other fractions in hypocotyls is increased in LRFR (de Wit et al., 2018).

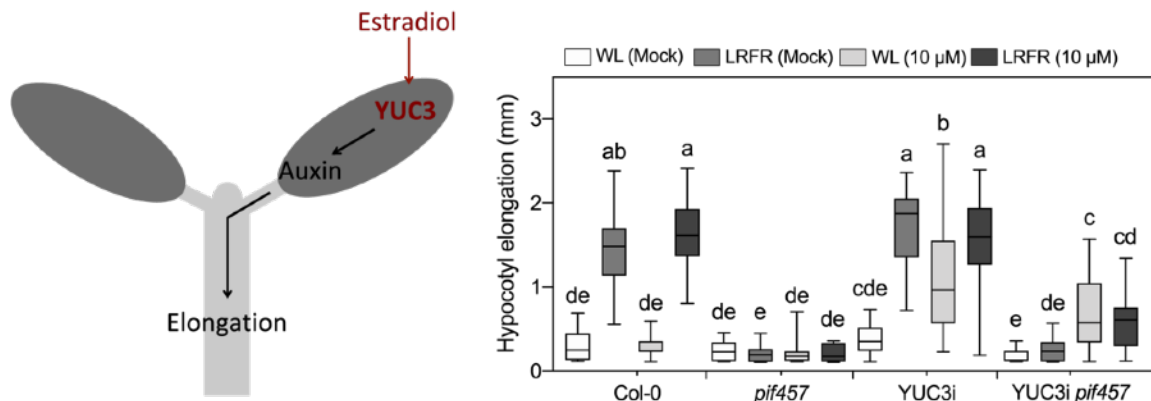


**Figure 2. PIFs are required for more than induction of auxin biosynthesis in cotyledons during LRFR-induced hypocotyl elongation.**

Hypocotyl elongation of indicated genotypes grown in long days (LDs) at WL for 4 d then either kept at WL or transferred to LRFR (at ZT2 on day 5) for three additional days with or without estradiol. Elongation during the last 3 d is indicated. Different letters indicate significant difference (two-way ANOVA with Tukey's HSD test,  $P < 0.05$ ,  $n > 30$ ).

As hypocotyl elongation occurs by cell elongation rather than cell division (Gendreau et al., 1997), we hypothesised that the deposition of newly synthesised lipid material in PM may be required for LRFR-induced hypocotyl elongation as observed in elongating pollen tubes and root hairs (Steer & Steer, 1989, Hepler et al., 2013). Previous transcriptome data indicate that LRFR induces gene expression for biosynthesis of sterols, one of the major components of PM (Kohnen et al., 2016). 51.5% of all annotated genes in sterol biosynthetic process GO term (17/33) are significantly upregulated in response to 3h of LRFR specifically in hypocotyls (Fig. S1, left panel) (data from Kohnen et al., 2016). In addition, 58.8% of the upregulated genes (10/17) are putative PIF4 targets and 29.4% (5/17) are also putative PIF5 targets (Fig. S1, right panel) (data from Hornitschek et al., 2012, Oh et al., 2014). Thus, we hypothesised that PIFs may locally contribute to PM extension in LRFR by modulating sterol biosynthesis in the hypocotyl. Sterols are indispensable constituents of PM and the mutants impaired in sterol biosynthesis are often embryo lethal or show serious growth defects (Valitova et al., 2016). Furthermore,

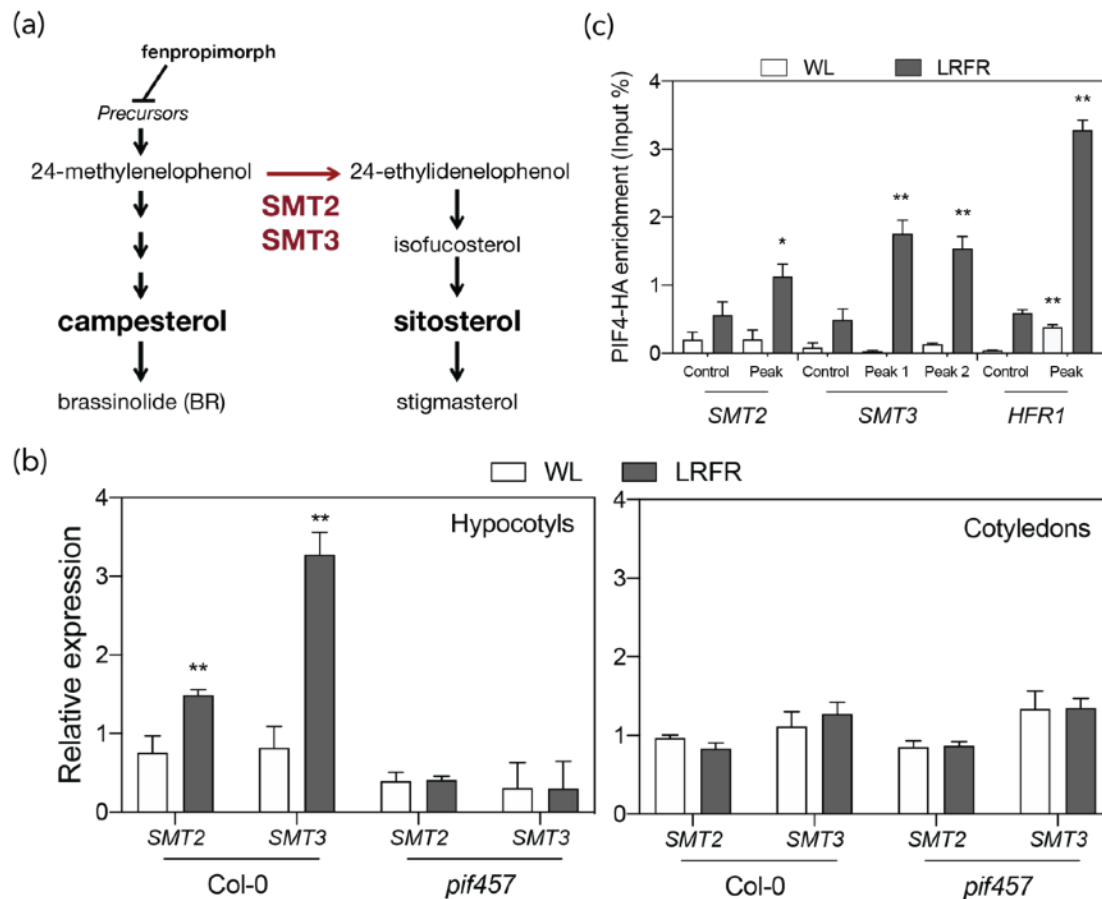


**Figure 3. PIFs regulate expression of SMT encoding genes in hypocotyls in response to LRFR treatment.**

(a) A simplified representation of sterol biosynthesis pathway in *Arabidopsis thaliana* (Carland et al. 2010). (b) Relative expression of *SMT2* and *SMT3* in hypocotyls and cotyledons of 5-d-old seedlings of indicated genotypes grown as in Fig. 2, 3h after transferred to LRFR at ZT2 obtained by RT-qPCR.  $n = 4$  (biological) with three technical replicas for each RNA sample. Data are means, error bars indicate SD. Asterisks (\*) indicates the statistical significance compared to WL (Student's T-test, \*\*  $< 0.01$ ,  $n = 4$ ). (c) PIF4-HA binding to the promoter of *SMT2* and *SMT3* evaluated by ChIP-qPCR in 10-d-old *PIF4::PIF4-HA* (*pif4-101*) seedlings either kept at WL or transferred for 5d to LRFR at ZT2. Input and immunoprecipitated DNA were quantified by qPCR using primers on 'Peak' where PIF4 binding was identified before on 5' region of each gene (Oh et al. 2012) and 'Control' primers from coding regions of each gene. PIF4-HA enrichment is presented as IP/Input and error bars show standard deviation from two to four technical replicas. Asterisks (\*) indicate the statistical significance compared to WL (Student's T-test, \*  $< 0.05$ , \*\*  $< 0.01$ ). Related to Fig. S2 & S3

brassinosteroids are also synthesised downstream of sterol biosynthesis pathway (Fig. 3a) and they are important hormones for shade-induced hypocotyl elongation (Keuskamp et al., 2011, Bou-Torrent et al., 2014, Valitova et al., 2016). Therefore, we focused on two genes coding for C-24 sterol methyltransferases (*SMT2* and *SMT3*) which are the enzymes responsible for biosynthesis of the predominant sterol in plants, sitosterol, although many other genes in the pathway are also upregulated in LRFR (Fig. 3a, S1). The loss of function mutants of *smt2* and *smt3* do not have serious growth defects despite a decrease in sitosterol and stigmasterol and an increase in campesterol (Hase et al., 2005, Carland et al., 2010). In addition, the levels of BR precursors are elevated in these mutants. These properties allowed us to conduct physiological and molecular experiments using these mutants.

We first confirmed that LRFR induces expression of *SMT2* and *SMT3* only in hypocotyls (Fig. 3a, 3b), as previously reported (Kohnen et al., 2016). This induction was lost in *pif457* mutant. Furthermore, the expression of *SMT2* and *SMT3* is unaffected in cotyledons in *pif457*, showing that PIFs specifically regulate these genes in the hypocotyl. Expressions of well-known shade marker genes were as expected as in previous publications (Hornitschek et al., 2012) (Fig. S2). Next, we checked PIF4 and PIF7 binding to *SMT2* and *SMT3* promoters in LRFR using previously reported PIF4-peaks in 5' upstream regions of in etiolated seedlings (Oh et al., 2012). We used *PIF4::PIF4-HA* and *35S::PIF4-HA* seedlings in Col-0 background grown in WL for five days and then either kept in WL or transferred to LRFR for another five days (Fig. 3c, S3c). PIF4-HA binding to the peak regions of both *SMT2* and *SMT3* was enriched only for LRFR in *PIF4::PIF4-HA* lines (Fig. 3c), whereas it was enriched for both WL and LRFR in *35S::PIF4-HA* lines (Fig. S3c). We also checked whether the binding is rapid using *PIF4::PIF4-HA* seedlings grown in WL for ten days and then transferred to LRFR for 2 hours. PIF4-HA binding to *SMT3* peaks in LRFR was significant for two independent biological replicates, whereas we detected a significant enrichment

on *SMT2* peak only in one experiment (Fig. S3a, S3b). Next, we checked whether PIF7 can bind to these peaks using *PIF7::PIF7-HA* seedlings in *pif7-2* background grown in 5d (WL) + 5d (LRFR) protocol. PIF7-HA enrichment was only significant for *SMT3* peaks, yet the enrichment was much less compared to PIF4 (Fig. S3d). Therefore, we conclude that PIFs induce *SMT2* and *SMT3* expression in hypocotyls but not in cotyledons by directly binding to their promoter regions in LRFR.

### ***SMT2* is required for LRFR-induced hypocotyl elongation**

Next, we analysed the hypocotyl elongation response of *smt2* and *smt3* mutants in LRFR. LRFR-induced hypocotyl elongation was significantly reduced in two independent alleles of *smt2*, whereas it was as the WT in the *smt3* mutant (Fig. S4a). We also did not observe a further reduction in hypocotyl elongation of the double *smt2smt3* mutant that was reported to have only trace amounts of sitosterol (Fig. 4a) (Carland et al., 2010). One characteristic phenotype of the *smt2* and *smt2smt3* mutants is the impaired cotyledon vasculature patterns (Fig. 4b). Considering that auxin and sucrose transport from cotyledons to hypocotyl is indispensable in LRFR (Keuskamp et al., 2010, de Wit et al., 2018), we tested the LRFR-induced hypocotyl elongation of *cvp2* and *cvp2cvl1* that are also severely impaired in the cotyledon vasculature (Fig. 4b). Yet, both *cvp* mutants displayed a normal hypocotyl elongation in LRFR (Fig. 3a), suggesting that the cotyledon vasculature problems of *smt2* and *smt2smt3* do not cause the impaired hypocotyl elongation. To determine whether the reduced sterol production can explain the observed hypocotyl elongation phenotype in the *smt2* mutants, we used fenpropimorph that inhibits cyclopropyl isomerase (CPI), leading to cessation of sterol biosynthesis upstream of *SMT2* and *SMT3* (Fig. 3a) (He et al., 2003). Col-0 and *smt2-1* seedlings were grown in WL for four days without fenpropimorph and then either kept in WL or transferred to LRFR in the presence of increasing fenpropimorph concentrations. Increased fenpropimorph

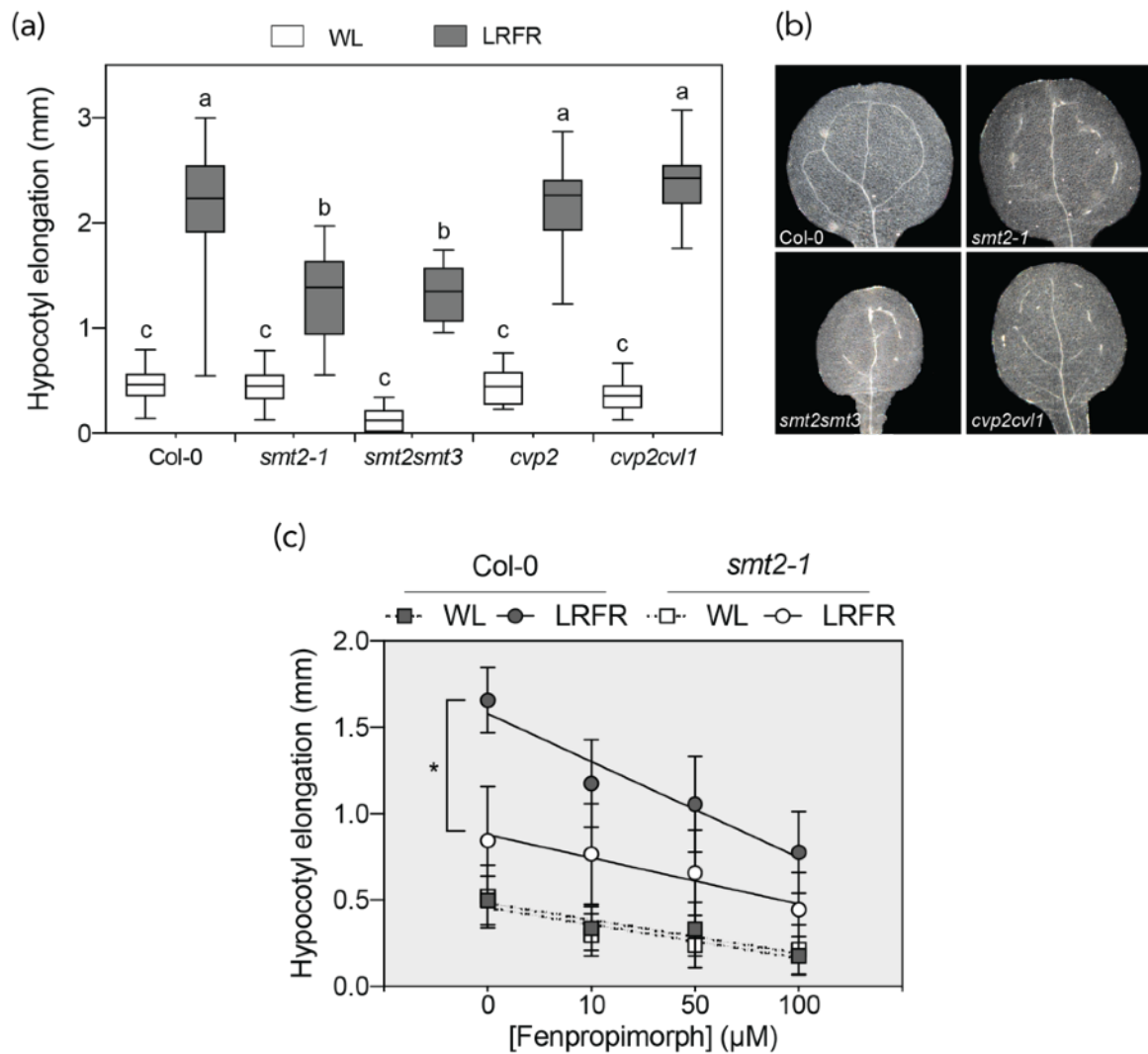


**Figure 4. *SMT2* is required for LRFR-induced hypocotyl elongation.**

(a) Hypocotyl elongation of indicated genotypes grown as in Fig. 2. Different letters indicate significant difference (two-way ANOVA with Tukey's HSD test,  $P < 0.05$ ,  $n > 12$ ). (b) Representative images of cotyledon vasculature phenotype of indicated genotypes. (c) Hypocotyl elongation of indicated genotypes as grown in (a) in presence of indicated doses of sterol biosynthesis inhibitor, fenpropimorph during the last 3 days. Asterisks (\*) indicate the statistical significance between genotypes in LRFR (two-way ANOVA,  $P < 0.05$ ). Related to Fig. S4 & S5

concentration resulted in a significantly steeper reduction in hypocotyl elongation of WT compared to *smt2-1* only in LRFR (Fig. 4c). This result supports that the *smt2* hypocotyl phenotype in LRFR is due to its reduced sitosterol production.

Levels of BR precursors downstream of campesterol increase in the *smt2* mutant (Carland et al., 2010). Therefore, we treated Col-0 and *smt2-1* seedlings with BR and confirmed that BR promotes hypocotyl elongation of both genotypes (Fig. S4b), indicating that increased BR levels in the *smt2* mutant does not correlate with the reduced hypocotyl elongation in LRFR. Furthermore, we introduced in the *smt2-1* background the WT *SMT2* coding sequence under the control of either cotyledon or hypocotyl specific promoters (*FRO6* and *GH3.17*, respectively) as well as a ubiquitous promoter *UBQ10* as a control (Fig. S5a). *UBQ10* and *GH3.17* driven expression of *SMT2* rescued the *smt2-1* hypocotyl elongation in LRFR in two independent insertion lines for each construct, whereas *FRO6* did not (Fig. S5b). It is important to note that hypocotyl elongation phenotypes of the complementation lines were not correlated with the *SMT2*-flag levels (Fig. S5c). In addition, *FRO6* lines failed to rescue cotyledon vasculature phenotype of *smt2-1*, whereas *UBQ10* and *GH3.17* driven *SMT2* complementation did (Fig. S5d). The possible explanation is that *FRO6* is not expressed in vasculature and its expression is specific to mesophyll cells (Kim et al., 2018). As we previously showed that hypocotyls of other *cvp* mutants elongate similar to WT in LRFR (Fig. 4a), we conclude that *SMT2* expression in hypocotyls is required and sufficient in LRFR-induced hypocotyl elongation.

### ***SMT2* is not required for LB-induced hypocotyl elongation**

To determine whether *smt2* mutants are generally impaired in hypocotyl elongation, we tested the *smt2* mutant in other conditions that induce hypocotyl elongation. The hypocotyl elongation for etiolated and de-etiolated seedlings in FR was normal for the both *smt2* alleles, showing that these mutants are not generally impaired in the cell elongation mechanisms (Fig. S6). Low blue light (LB) is another key component of vegetative shade. LRFR is a neighbour proximity cue that triggers elongation, while LB is a cue indicative of real shade that is accompanied by a reduction of PAR that also enhances hypocotyl elongation (Pedmale et al., 2016). Interestingly, hypocotyl elongation of neither

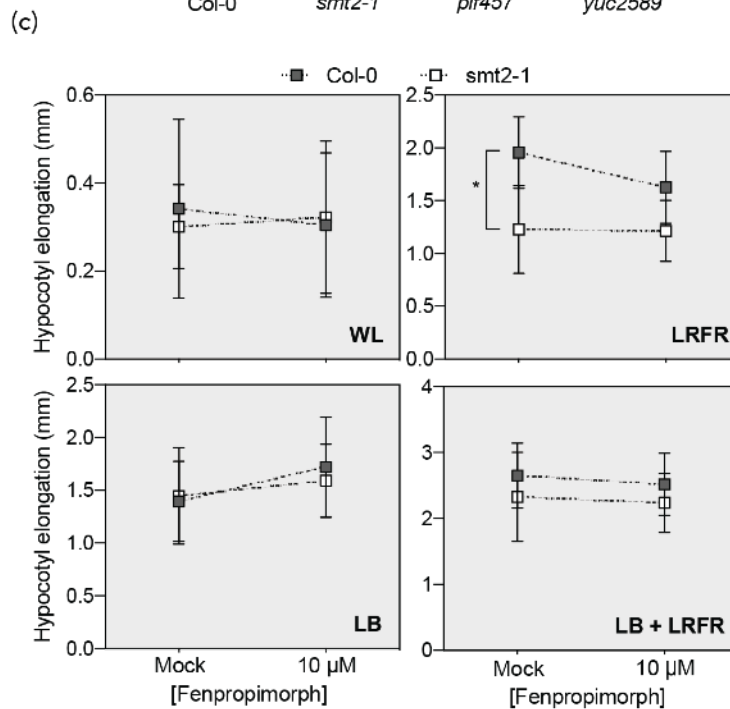
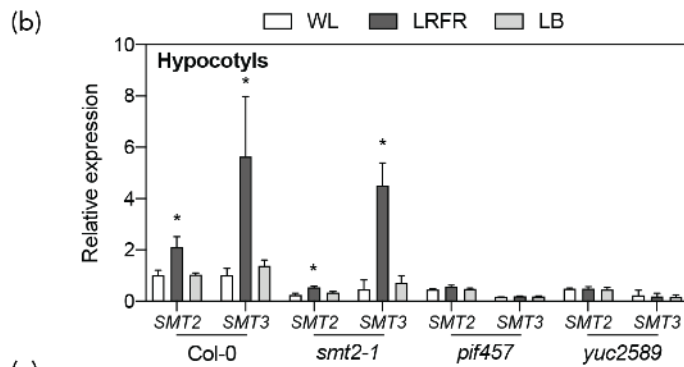
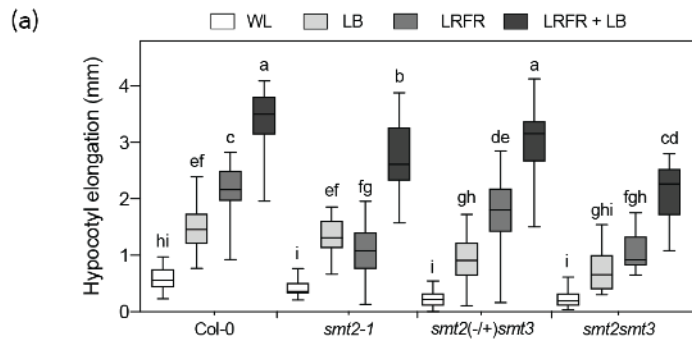


**Figure 5. *SMT2* is not required for LB-induced hypocotyl elongation.**

(a) Hypocotyl elongation of indicated genotypes grown as in Fig. 2 and transferred to the indicated light conditions for the last 3d of growth. Different letters indicate significant difference (two-way ANOVA with Tukey's HSD test,  $P < 0.05$ ,  $n > 12$ ). (b) Relative expression of *SMT2* and *SMT3* in 5-d-old hypocotyls of the indicated genotypes 3h after transferred to the indicated light conditions obtained from RNA-seq analysis. Asterisks (\*) indicate the statistical significance compared to WL (FDR  $< 0.01$ ). (c) Hypocotyl elongation of indicated

genotypes in presence of indicated doses of sterol biosynthesis inhibitor, fenpropimorph during the last 3 days. Asterisks (\*) indicate the statistical significance between genotypes (two-way ANOVA,  $P < 0.05$ ,  $n > 12$ ). Seedlings were grown as in Fig. 2. (a, b, c). Data are means; error bars indicate SD (b, c). Related to Fig. S7.

the two *smt2* alleles nor *smt3-1* in LB were altered (Fig. S7a). We also tested the effect of LB and LRFR combination on hypocotyl elongation. The results indicate

that additional LB remarkably rescues *smt2-1* hypocotyl elongation reduction observed in LRFR (Fig. 5a). Yet, the double *smt2smt3* mutant hypocotyls elongate less in LB and LB + LRFR combination compared to *smt2-1* (Fig. 5a). One possible explanation is that *SMT3* expression might be induced in LB, which may rescue hypocotyl elongation when *SMT2* is absent. Thus, we checked the expression of *SMT2* and *SMT3* after 3h of LRFR and LB treatment in hypocotyls and cotyledons of 5d-old LD-grown Col-0, *smt2-1*, *pif457*, and *yuc2589* seedlings. Surprisingly, LB did not induce *SMT* expression in hypocotyls, whereas *SMT3* expression is induced significantly in cotyledons but to a lesser extent compared to hypocotyls (Fig. 5b, S7b). These results indicate that LB does not induce sitosterol biosynthesis in hypocotyls transcriptionally. Furthermore, *SMT2* and *SMT3* expression was not induced in *pif457* and *yuc2589* hypocotyls in LRFR, indicating that auxin is required for the induction of *SMTs* in LRFR.

In order to determine whether the newly synthesised sterols are required for LB-induced hypocotyl elongation, we treated 4d-old WL grown Col-0 and *smt2-1* seedlings with fenpropimorph upon transfer to the light treatment. Fenpropimorph treatment did not cause a reduction in hypocotyl elongation in LB and LB+LRFR (Fig. 5c). As observed previously (Fig. 4c), hypocotyl elongation is reduced in Col-0 whereas *smt2-1* was not affected by 10  $\mu$ M fenpropimorph in LRFR (Fig. 5c). As LB-induced hypocotyl elongation was reduced in *smt2smt3* but was not affected in fenpropimorph, we conclude that the presence but not the new production of sitosterol is required for LB-induced hypocotyl elongation.

### **LRFR and LB induces different transcriptome changes**

In order to understand how LB and LRFR responses differ transcriptionally, we did an RNA-seq in of 5d-old LD-grown Col-0, *smt2-1*, *pif457*, and *yuc2589* seedlings treated with 3h of LB or LRFR. We used the dissected cotyledons and hypocotyls to characterise distal and local regulation of LB and LRFR, as well as functions of PIFs and auxin in these organs. Comparison of the *pif457* and *yuc2589* mutants allowed us to unravel the set of genes of which expression are

dependent on PIFs and YUCs together, only PIFs, or only YUCs. Using this comparison, we differentiated the PIF- and/or auxin-mediated molecular pathways in hypocotyl elongation. We also included *smt2-1* seedlings to test whether transcriptional differences may explain the normal and impaired hypocotyl elongation phenotype of this mutant in LB and LRFR, respectively. Last but not least, we compared the LB and LRFR transcriptomes in order to identify the similarities and differences in molecular mechanisms that drive the hypocotyl elongation in these conditions.

We first phenotypically evaluated the hypocotyl elongation of the genotypes using the growth condition that was used in RNA-seq. As previously shown, *smt2-1* hypocotyl elongation was reduced only in LRFR, whereas both *pif457* and *yuc2589* mutants were completely impaired in hypocotyl elongation in both LB and LRFR (Fig. S8).

To validate the quality of our RNA-seq data, we first used principle component (PC) analysis that showed that biological replicates of each genotype grouped closely in hypocotyls and cotyledons (Fig. S9). Next, we compared the expression profiles of 10 selected genes in the RNA-seq analysis and in quantitative RT-PCR (RT-qPCR) from an independent experiment using Col-0 (Fig. S10a). We also compared our LRFR transcriptome data to a previously reported organ-specific transcriptome data (Kohnen et al., 2016) using the matching time points (Fig. S10b). The genes, expression of which was differentially regulated in hypocotyls in our data set showed 93.5 and 90.1% overlap compared to Kohnen et al. data set for up- and down-regulated genes, respectively. However, the overlap between two data sets was lower in cotyledons. One possible reason may be the way that the cotyledons were dissected in two studies. In our method, we included the cotyledonary petioles and apical meristem in the cotyledon samples, whereas they were excluded in the previous study (Kohnen et al., 2016). These results show that our transcriptome data is in good quality.

(a)

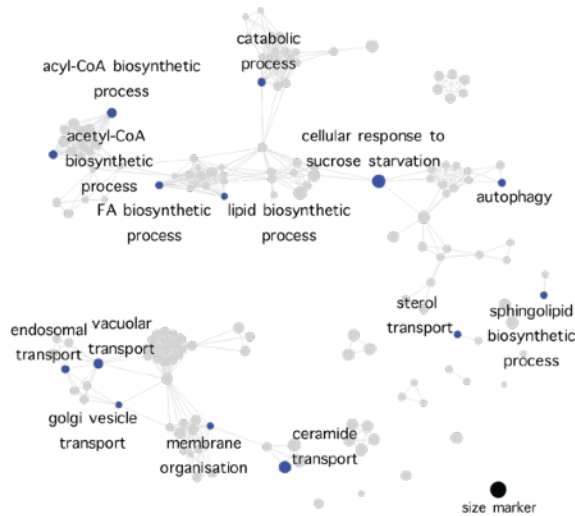
	Low Blue			
	ALL UP	ALL DOWN	FC>2 UP	FC>2 DOWN
<b>Hypocotyls</b>				
<i>Col-0</i>	1343	1520	115	431
<i>smt2-1</i>	1049	1825	102	541
<i>pif457</i>	725	1567	85	297
<i>yuc2589</i>	1075	1415	62	354
<b>Cotyledons</b>				
<i>Col-0</i>	1226	1449	130	361
<i>smt2-1</i>	727	1441	94	331
<i>pif457</i>	958	868	136	170
<i>yuc2589</i>	1121	1612	133	452

(b)

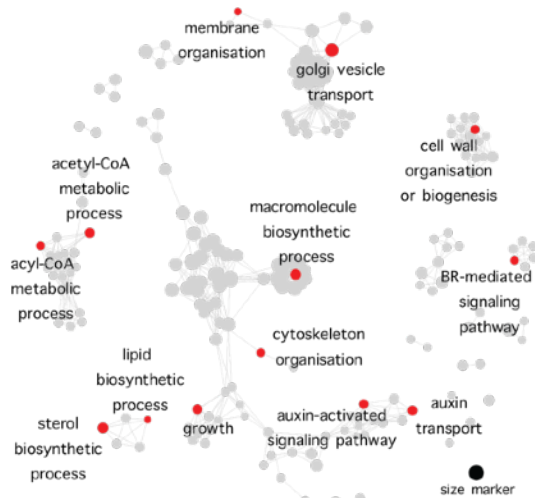
	Low Red/Far Red			
	ALL UP	ALL DOWN	FC>2 UP	FC>2 DOWN
<b>Hypocotyls</b>				
<i>Col-0</i>	2812	2626	571	750
<i>smt2-1</i>	3166	3148	861	1021
<i>pif457</i>	92	158	12	57
<i>yuc2589</i>	585	288	94	129
<b>Cotyledons</b>				
<i>Col-0</i>	1028	1054	303	238
<i>smt2-1</i>	942	1071	303	201
<i>pif457</i>	368	187	51	14
<i>yuc2589</i>	897	808	288	177

(c)

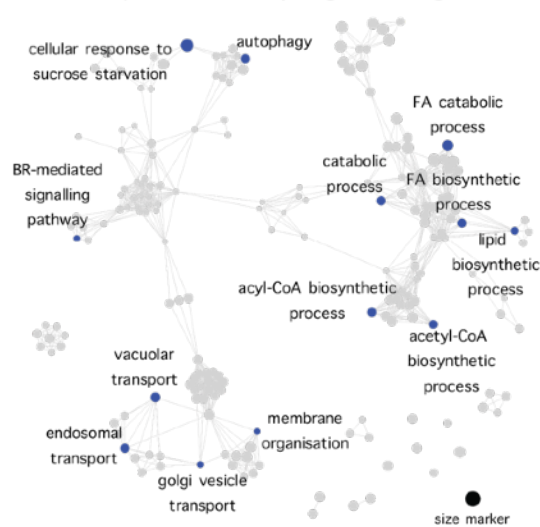
### Hypocotyl LB-upregulated genes



### Hypocotyl LRFR-upregulated genes



### Cotyledon LB-upregulated genes



### Cotyledon LRFR-upregulated genes

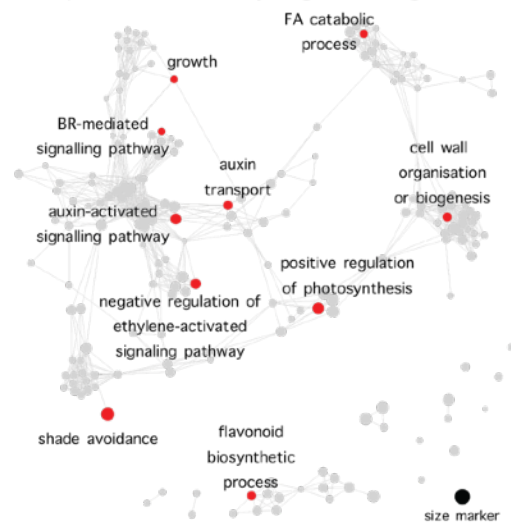


**Figure 6. LB and LRFR induces transcriptome changes in cotyledons and hypocotyls.**

Number of genes that are differentially regulated in indicated genotypes grown as in Fig. 2 and treated with 3h of (a) LB and (b) LRFR at ZT2 on day 5. The total numbers of significantly up or down regulated genes compared to WL are indicated with or without a fold change (FC) cut-off (FDR < 0.05, Benjamini Hochberg correction using whole data set together). (c) GO term enrichment analysis from the indicated gene lists. Each node indicates a significantly enriched GO term. Two terms (nodes) are connected if they share 20% or more genes. The size of the nodes indicates the regulation factor (RF) which is calculated as a function of FDR value and fold change enrichment of the corresponding GO term. Black nodes indicate a size marker with RF = 50. Only selected GO terms are annotated. *To see the full list of enriched GO terms, please download the interactive versions of (c) from [here](#). Related to Fig. S8, S9, and S10.*

Next, we defined the genes showing LB- or LRFR-regulated expression using a threshold with an adjusted P value < 0.05 (Benjamini Hochberg correction using the whole data-set together). The results showed that LRFR induces more transcriptome changes compared to LB in Col-0 hypocotyls (Fig. 6a, 6b). On the other hand, the number of differentially regulated genes was slightly higher in LB compared LRFR in Col-0 cotyledons. Furthermore, the number of genes with a 2-fold or more change fold in LRFR was higher especially for upregulated genes compared to LB in both organs. We performed a series of GO term enrichment analyses to identify biological processes that are transcriptionally regulated in LB and LRFR. For these analyses, we used all significantly upregulated genes without a FC-threshold unlike the similar studies (Kohnen et al., 2016, Pedmale et al., 2016). We reasoned that rather than a few genes that are induced more than 2-fold, significant but small induction of many genes in a particular biological process might be more important to understand the true nature of LB and LRFR transcriptional regulation. As the numbers of enriched GO terms in each gene list were higher than 100 terms (FDR < 0.05), we highlighted 8-15 terms for each organs and light conditions that we found interesting. It is

important to note that the highlighted terms are neither the most significant ones nor the ones with highest fold changes.

In our first GO term analysis, we compared the organ-specific responses in LB and LRFR-upregulated genes separately (Fig. 6c). The LB upregulated genes in both organs were enriched for terms related to starvation (e.g., cellular response to sucrose starvation), catabolic events (e.g., "catabolic process", "autophagy", and "vacuolar transport"), "lipid"- and "fatty acid (FA) biosynthetic process", and "endosomal transport" (Fig. 6c, left panel). We also noted specific GO term enrichments in LB for each organ. In hypocotyls, PM-related GO terms; "sterol transport", "ceramide transport", "sphingolipid biosynthesis" were enriched whereas "FA catabolic process" and "BR-mediated signalling pathway" were among the cotyledon-enriched GO terms (Fig. 6c, left panel). In contrast, LRFR-upregulated genes were enriched in hormone-related GO terms for both organs (Fig. 6c, right panel), which is in line with the previous reports (Kohnen et al., 2016). "Auxin transport", "auxin-activated signalling pathway", and "BR-mediated signalling pathway" were enriched in both organs, whereas "negative regulation of ethylene-activated signalling pathway" was specifically enriched in cotyledons. We noted that biosynthesis-related GO terms were present in LRFR-upregulated genes in hypocotyls for general (e.g., "macromolecule biosynthetic process"), cell wall-related (e.g., "cell wall organisation and biogenesis"), and PM-related (e.g., "lipid biosynthetic process", "sterol biosynthetic process") terms. Furthermore, "membrane organisation", "golgi vesicle transport", "acetyl-CoA"- and "acyl-CoA metabolic process" were among the GO terms shared with LB in LRFR hypocotyl-upregulated genes. These results suggest that there are shared and unique molecular mechanisms for hypocotyl elongation responses to LB and LRFR conditions.

In order to further evaluate similarities and differences between LB and LRFR-induced transcriptome changes, we compared LB and LRFR up- and downregulated genes in Col-0 hypocotyls and cotyledons (Fig. 7 and Fig. S11).

The number of common genes for both up- and downregulated gene sets were higher in hypocotyls compared to cotyledons (Fig. 7a, 7b, S11a, and S11b), suggesting more similar transcriptome regulations by LB and LRFR in the elongating hypocotyls. The GO term enrichment analysis further supported this observation. LB and LRFR common upregulated genes in hypocotyls were enriched in terms related to cellular elongation such as “cell wall organisation or biogenesis”, “BR-mediated signalling pathway”, “acetyl-CoA biosynthetic process from pyruvate”, “membrane lipid biosynthetic process”, “endocytosis”, “golgi vesicle transport”, “growth”, “cytoskeletal organisation”, and “detection of calcium ion” (Fig. 7e). Furthermore, catabolism related terms like “positive regulation of autophagy” and “vacuolar transport” were also enriched in the shared list of the common upregulated genes in hypocotyls. Considering GO terms related to catabolism in common upregulated gene lists, we saw more terms in cotyledons compared to hypocotyls, suggesting that cotyledons is the main organ for catabolic events (Fig. 7e, f). The sets for common downregulated genes were enriched in photosynthesis and electron transfer-related GO terms in both organs (Fig S11e, S11f). Some notable enriched GO terms were “photosynthesis”, “carbon fixation”, “thylakoid membrane organisation”, and “quinone biosynthetic process” in both organs; “gluconeogenesis”, “starch biosynthetic process”, and “NADH dehydrogenase complex assembly” for hypocotyls; “lipid biosynthetic process”, “glycerolphospholipid biosynthetic process”, “glycerolipid metabolic process”, and “glycolipid metabolic process” in cotyledons.

LB specifically upregulated genes in hypocotyls were enriched in GO terms related to starvation (e.g. “cellular response to sucrose starvation”) and catabolic events (e.g. “proteolysis”, “FA catabolic process” and “autophagy”) (Fig. 7c). We also observed enrichment of several catabolic process GO terms in LB specifically upregulated genes in cotyledons (Fig. 7d). LB specifically

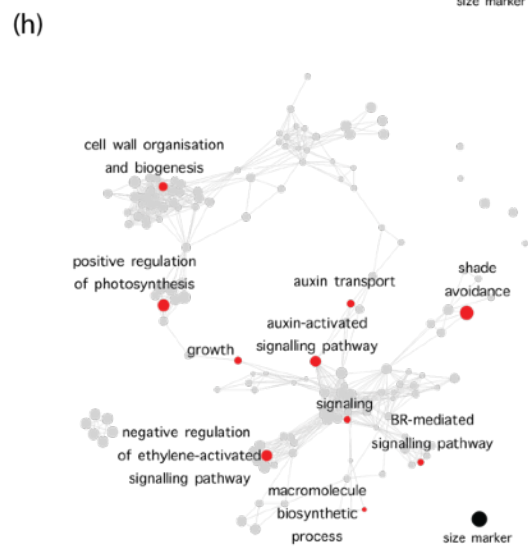
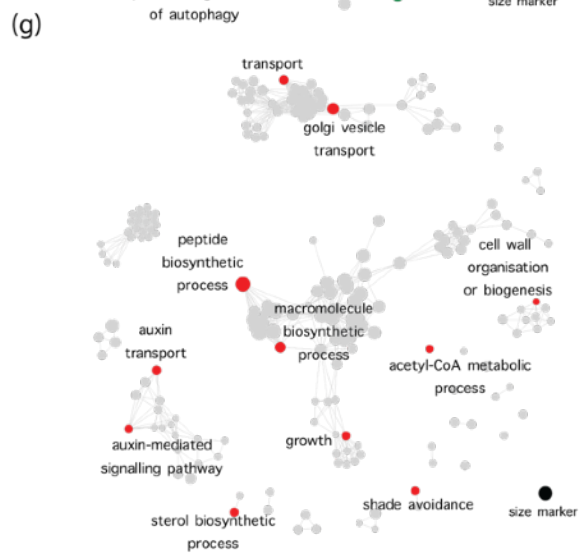
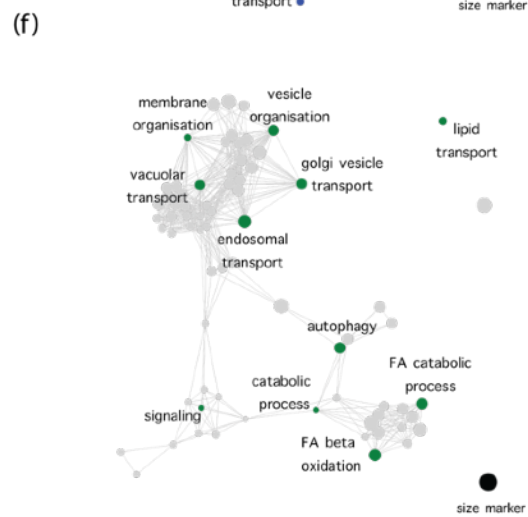
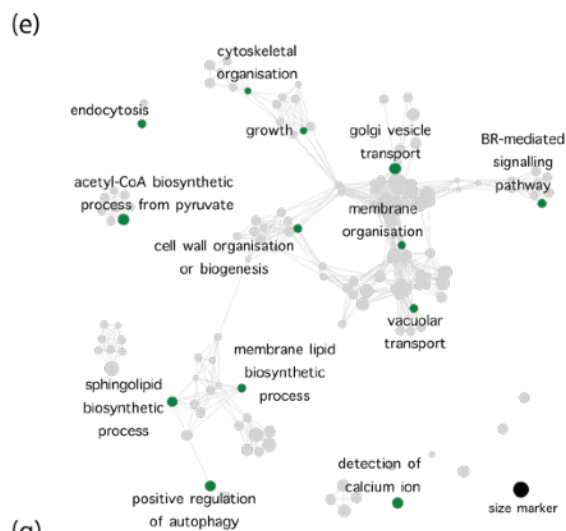
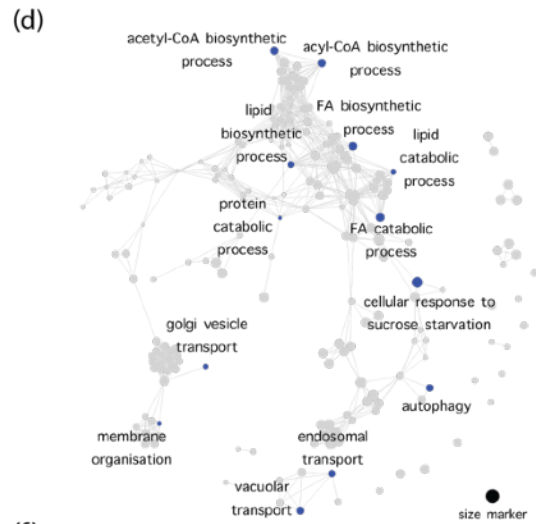
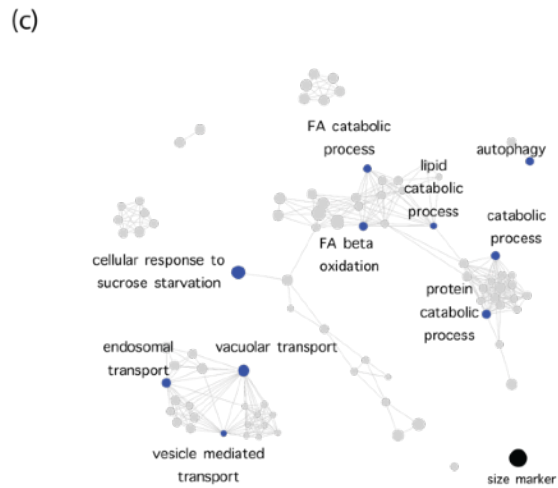
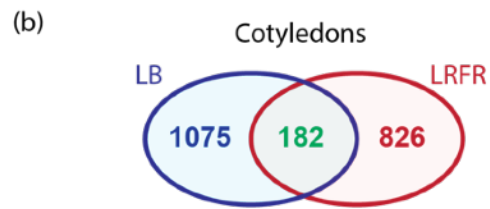
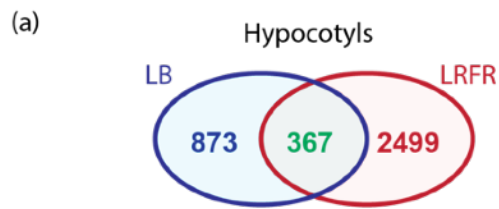


### **Figure 7. Similarities and differences LB and LRFR transcriptome.**

Venn diagrams showing the shared and specifically upregulated genes (FDR < 0.05, Benjamini Hochberg correction using whole data set together) in LB and LRFR in hypocotyls (a) and cotyledons (b) of Col-0. GO term enrichment analysis from the hypocotyl LB-specific (c), LB and LRFR shared (e), and LRFR specific (g); and cotyledon LB-specific (d), LB and LRFR shared (f), and LRFR specific (h) gene lists. Each node indicates a significantly enriched GO term. Two terms (nodes) are connected if they share 20% or more genes. The size of the nodes indicates the regulation factor (RF) which is calculated as a function of FDR value and fold change enrichment of the corresponding GO term. Black nodes indicate a size marker with RF = 50. Only selected GO terms are annotated. *To see the full list of enriched GO terms, please download the interactive versions of (c-h) from [here](#). Related to Fig. S11.*

downregulated genes in both organs were enriched in terms related to photosynthesis (e.g., "light reaction", "dark reaction", and "carbon fixation") and electron transport (e.g., "quinone"- and "plastoquinone biosynthetic process") (Fig. S11c, S11d).

In contrast to LB specifically upregulated genes, LRFR specifically upregulated genes in hypocotyls were enriched in biosynthetic processes including "peptide biosynthetic process", "macromolecule biosynthetic process", "sterol biosynthetic process", and "cell wall organisation and biogenesis" (Fig. 7g). Furthermore, we observed that hormone related GO terms were enriched in these gene sets. "Auxin mediated signalling" and "auxin transport" in both organs; whereas "BR-mediated signalling pathway" and "negative regulation of ethylene-activated signalling pathway" were additionally enriched in cotyledons (Fig. 7g, 7h). Interestingly, LRFR specifically downregulated genes in hypocotyls were enriched in several autophagy related GO terms such as "macroautophagy", "autophagosome assembly", "vacuolar organisation", and "vacuolar transport" (Fig. S11g). Although "photosynthesis, light reaction" and several terms related to chloroplasts were enriched, "carbon fixation" and "photosynthesis, dark reaction" terms were not enriched in LRFR downregulated

genes in cotyledons (Fig. S11h). We also noticed that some terms were enriched in both upregulated and downregulated gene sets especially for cotyledons. Some notable examples are auxin and photosynthesis related terms (Fig. 7h, S11h).

Altogether, GO term enrichment analyses from LB and LRFR common, LB specific, and LRFR specific gene sets indicate that LB and LRFR transcriptome responses converge in elongating hypocotyls, especially on the induction of known growth related mechanisms. One key difference between the two light treatment was the converse regulation of catabolic and anabolic events in LB and LRFR. These results suggest that LB and LRFR induce recycling and biosynthesis mechanisms, respectively to obtain new materials required for cellular elongation.

## **PIFs also induce other hormone responses and cell wall**

### **organisation in LRFR**

Next, we focused on how organ-specific transcriptome changes were in *smt2-1*, *pif457*, and *yuc2589* mutants in response to LRFR. The *smt2-1* LRFR-induced transcriptome changes were not dramatically different from Col-0 in either organ in terms of differentially regulated genes. Moreover, *smt2-1* and Col-0 samples were grouped closely in both organs in PCA (Fig. S9). These results suggest that the *smt2-1* reduced-hypocotyl elongation in LRFR is not due to transcriptome changes. As expected, *pif457* and *yuc2589* were largely incapable of responding LRFR transcriptionally. The numbers of differentially regulated genes in both mutants for hypocotyls and cotyledons were lower compared to Col-0 (Fig. 6b). It is important to note that *pif457* transcriptomic response was almost entirely gone in both organs, whereas *yuc2589* differentially regulated genes in cotyledons did not reduce dramatically. Furthermore, PCA showed that *pif457* and *yuc2589* LRFR-treated hypocotyls were grouped with WL samples but *yuc2589* cotyledons were grouped closer to Col-0 LRFR samples (Fig S9). These results are in line with Fig. 2 and previous reports indicating PIFs are required in

both organs whereas YUCCAs are mainly required for auxin production in cotyledons (Procko et al., 2014).

In order to further define the individual roles of SMT2, PIFs and YUCCAs in LRRF-induced hypocotyl elongation, we evaluated the interactions between *smt2-1*, *pif457*, *yuc2589* mutants and Col-0 and light treatments. Many genes were misregulated in LRRF between *pif457* and Col-0; and *yuc2589* and Col-0, whereas there were only a few significant misregulated genes in *smt2-1* hypocotyls (Fig. 8b). The numbers of misregulated genes in *pif457* vs. Col-0 and *yuc2589* vs. Col-0 comparisons were lower in cotyledons compared hypocotyls, indicating that PIFs and YUCCAs are more important in hypocotyl LRRF-induced transcriptome changes.

Next, we determined the PIF- and YUC-dependently and independently regulated genes in LRRF (Fig S12). As previous studies indicate that major function of PIFs is the induction of genes but not repression (Hornitschek et al., 2012, Leivar et al., 2012), we used the gene sets that were significantly upregulated in LRRF in Col-0, *pif457* and *yuc2589* in both organs (Fig S12a, b; upper panel). For 'PIF- and YUC-dependent genes', we selected the genes that are significantly misregulated in *pif457* vs. Col-0 and *yuc2589* vs. Col-0 in the LRRF vs. WL (as listed in Fig. 8b) in 2501 and 498 genes that are only upregulated in Col-0 hypocotyls and cotyledons, respectively. We identified 793 genes in hypocotyls (e.g., *XTH19*) and 121 genes in cotyledons (e.g., *GH3.3*) for 'PIF- and YUC-dependent genes' (Fig S12a, b; group *i*). We further applied two criteria to define "PIF-dependent and YUC-independent" and "YUC-dependent and PIF-independent" genes. First, the genes in these categories must be significantly upregulated in Col-0 and *yuc2589* (*pif457* for the latter) but not in *pif457* (*yuc2589* for the latter) in LRRF. Second, they also must be significantly misregulated in *pif457* vs. Col-0 (*yuc2589* vs. Col-0 for the latter) but not in *yuc2589* vs. Col-0 (*pif457* vs. Col-0 for the latter) in the LRRF vs. WL. We identified 132 genes in hypocotyls (e.g., *ERF3*) and 215 genes in cotyledons

(a) **Low Blue vs. White Light**

	ALL UP	ALL DOWN	FC>2 UP	FC>2 DOWN
<b>Hypocotyls</b>				
<i>pif457</i> vs. Col-0	0	0	0	0
<i>yuc2589</i> vs. Col-0	0	0	0	0
<i>smt2-1</i> vs. Col-0	0	0	0	0
<b>Cotyledons</b>				
<i>pif457</i> vs. Col-0	8	0	6	0
<i>yuc2589</i> vs. Col-0	1	0	1	0
<i>smt2-1</i> vs. Col-0	0	0	0	0

(b) **Low Red/Far Red vs. White Light**

	ALL UP	ALL DOWN	FC>2 UP	FC>2 DOWN
<b>Hypocotyls</b>				
<i>pif457</i> vs. Col-0	1299	1429	487	350
<i>yuc2589</i> vs. Col-0	1450	1213	524	306
<i>smt2-1</i> vs. Col-0	6	3	4	0
<b>Cotyledons</b>				
<i>pif457</i> vs. Col-0	188	191	120	133
<i>yuc2589</i> vs. Col-0	36	60	26	49
<i>smt2-1</i> vs. Col-0	0	0	0	0

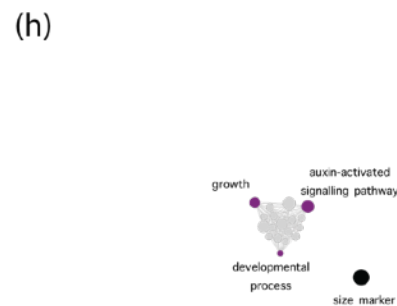
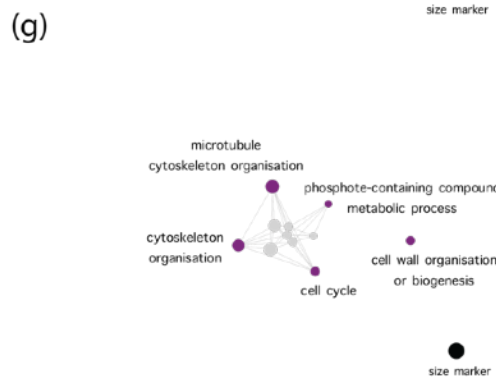
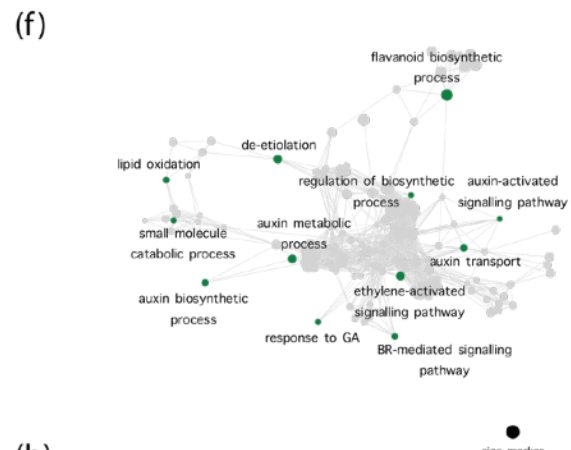
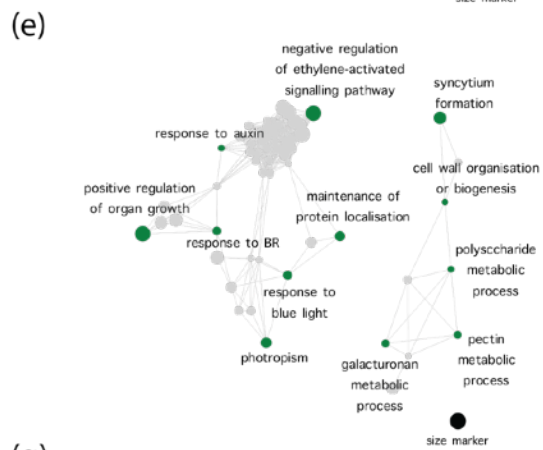
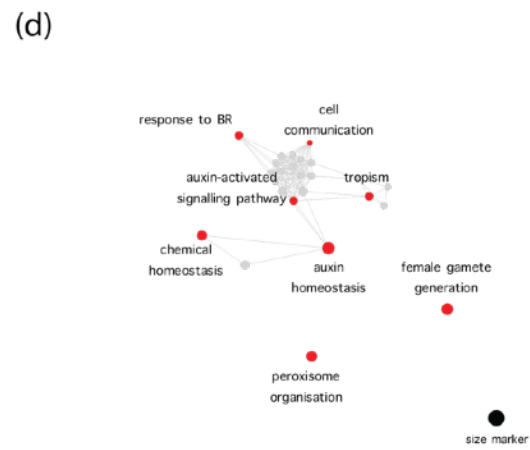
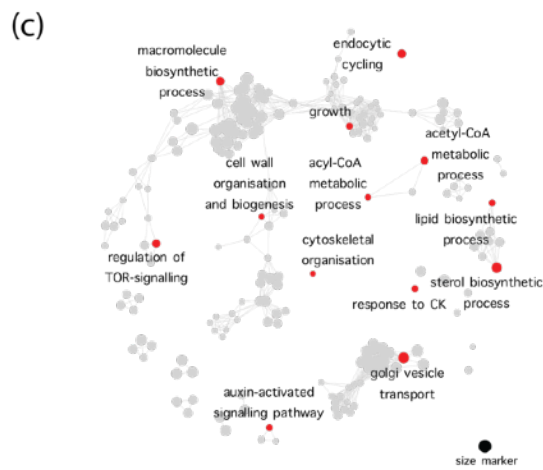


**Figure 8. PIFs induce hormone responses and cell wall organisation in LRFR.**

Number of genes that are differentially regulated in indicated comparisons in LB vs. WL (a) and LRFR vs. WL (b). The total numbers of significantly up- or down-regulated genes compared to WL are indicated with or without a fold change (FC) cut-off (FDR < 0.05, Benjamini Hochberg correction using each comparison individually). GO term enrichment analysis for “PIF and YUC dependent”, “PIF-dependent and YUC-independent”, and “YUC-dependent and PIF-independent” genes in hypocotyls (c, e, g) and cotyledons (d, f, h), respectively. Each node indicates a significantly enriched GO term. Two terms (nodes) are connected if they share 20% or more genes. The size of the nodes indicates the regulation factor (RF) which is calculated as a function of FDR value and fold change enrichment of the corresponding GO term. Black nodes indicate a size marker with RF = 50. Only selected GO terms are annotated. *To see the full list of enriched GO terms, please download the interactive versions of (c-h) from [here](#). Related to Fig. S12.*

(e.g., *AT3G54200*) for “PIF-dependent and YUC-independent genes” (Fig S12a, b; group *ii*). Despite the fact that the *yuc2589* mutant used in this study contains T-DNA insertion alleles for each *YUCCA*, the 215 genes in cotyledons included *YUC2*, *YUC8*, and *YUC9* (data not shown), confirming that PIFs induce their expression in LRFR as previously reported (Hornitshcek et al. 2012, Li et al., 2012). Surprisingly, we also found 8 genes in hypocotyls (e.g., *CSLC5*) and 15 genes (e.g., *AT5G54585*) for “YUC-dependent and PIF-independent genes” (Fig S12a, b; group *iii*). However, it is important to note that although these genes fulfil the above-mentioned statistical criteria, we observed a small fold induction for these genes in LRFR.

We used GO term enrichment analysis in order to define biological processes that are regulated by only PIFs, YUCs, or both (Fig. 8c-h). “PIF- and YUC-dependent” genes were enriched in many terms that were identified in LRFR upregulated gene sets (Fig. 8c, d). However, we also observed several terms that were not enriched in LRFR upregulated genes. Some notable examples are “regulation of TOR-signalling” for hypocotyls, “peroxisome organisation”,

“tropism”, and “female gamete generation” in cotyledons. “PIF-dependent and YUC-independent” genes were enriched in auxin, BR and ethylene response terms in both organs (Fig. 8e, f). As previously suggested (Kohnen et al., 2016, Pedmale et al., 2016), we observed many terms related to cell wall organisation such as “galacturonan metabolic process”, “pectin metabolic process”, and “polysaccharide metabolic process” in hypocotyls for this gene set (Fig. 8e). GO term enrichments in cotyledons were also in line with the previously identified roles of PIFs such as “auxin biosynthetic process”, “auxin transport”, “auxin-activated signalling pathway”, and “de-etiolation” (Fig. 8f). Finally, we also observed several GO terms directly related to growth in “YUC-dependent and PIF-independent” genes (Fig. 8g, h). The notable terms include “cytoskeletal organisation” and “cell wall organisation or biogenesis” for hypocotyls; “growth”, “developmental process”, and “auxin-activated signalling pathway” in cotyledons. These results show that PIFs locally regulate auxin and other hormone responses as well as the cell wall organisation in addition to the distal functions including auxin biosynthesis and transport in LRFR.

### **The potential roles of PIFs and YUCCAs in LB-induced hypocotyl elongation**

Interestingly, none of the mutants showed a dramatically different transcriptome profile in LB-regulated genes compared to Col-0 (Fig. 6a, Fig. S9). Furthermore, we did not observe any significant differences between any of the mutants and Col-0 in LB-regulated genes in hypocotyls, whereas there were only 8 genes that are significantly regulated between *pif457* and Col-0 in cotyledons (Fig. 8a). This was expected for *smt2-1*, as *smt2-1* hypocotyl elongation was not affected in LB (Fig. 5a, Fig S8). However, the hypocotyl elongation of *pif457* and *yuc2589* mutants was completely impaired in LB as in LRFR (Fig. S8). It is important to note that LB induces hypocotyl elongation slower compared to LRFR (Pedmale et al., 2016). Furthermore, LRFR-induced transcriptome changes become visible in both organs already after 45 minutes of light treatment, whereas 1 hour of LB

treatment does not induce major changes in transcriptome of whole seedlings (Kohnen et al., 2016, Pedmale et al., 2016). These reports suggest that LB transcriptome changes may require more time to take place compared to LRFR, which may explain why we failed to detect any significant differences between Col-0 and the mutants that do not elongate in LB. However, we were able to detect major changes in Col-0 transcriptome for both organs upon 3h of LB treatment (Fig. 6c). To visualise how LB-upregulated genes in Col-0 hypocotyls are regulated in *pif457* and *yuc2589* mutants, we did a PCA (Fig S13a, left). Interestingly, the PCA indicated that the light treatment separated all three genotypes similarly as shown by PC1, whereas genotypes are separated in two groups as WT vs. mutants on PC2. This may indicate that LB-induced hypocotyl elongation requires expression of the genes that are already misregulated in *pif457* and *yuc2589* mutants in WL. Therefore, we compared the mutants and Col-0 transcriptome in WL to investigate this hypothesis. The numbers of genes that were downregulated more than 2-fold were 348 in and 485 for the hypocotyls; 93 and 164 for the cotyledons in *pif457* and *yuc2589*, respectively (Fig. S13a, right). We used GO term enrichment analysis to define biological processes that are regulated by PIFs and YUCs in WL using genes that were downregulated more than 2-fold (Fig. S13b). Interestingly, "response to blue light" term was enriched in PIF-dependent genes but not in YUC-dependent genes. Another notable GO term that was enriched in YUC-dependent genes in both organs was "response to starvation". GO term enrichment analysis also revealed that many growth, auxin, GA, ethylene, and cell wall related terms were enriched in both PIF-dependent and YUC-dependent genes in hypocotyls. Cotyledons also showed a similar enrichment profile for terms related to hormones, with only a few cell wall-related terms. It is important to note that expression many of the hormone and cell wall related genes were not induced by LB, yet the baseline expression of each was dramatically low in *pif457* and *yuc2589* (Fig. 13c). These results show that transcriptome regulations of growth

related mechanisms, some of which are important for LB-induced hypocotyl elongation are already impaired in *pif457* and *yuc2589* mutants in WL, which may explain the LB hypocotyl elongation of these mutants to a certain extent.

### **Auxin biosynthesis, transport and response are not impaired in *smt2* mutant in LRFR**

We suspected that auxin transport might be impaired in *smt2-1* and *smt2smt3* due to the impaired cotyledon vasculature patterns (Fig. 4b). Furthermore, all sterol biosynthesis mutants upstream of 24-ethyl/24-methyl sterols showed defects in localisation of PIN auxin transporters with an altered distribution of auxin in Arabidopsis (Boutté & Jaillais, 2020). Similarly, auxin-inhibited PIN2-GFP endocytosis is reduced in *smt2smt3* roots (Carland et al., 2010). Moreover, *smt2-2* (*cvp1*) root inhibition response displayed enhanced auxin resistance in *auxin resistance1-3* (*axr1-3*) mutant background and elevated auxin response in developing embryos (Carland et al., 2010). Therefore, we checked whether auxin biosynthesis, transport and response are impaired in *smt2-1* mutant. Transcriptional activation of auxin biosynthesis was similar in Col-0 and *smt2-1*. *YUC2*, *YUC8*, and *YUC9* were induced similarly in cotyledons of both genotypes in LRFR (Fig. 9a). Next, to evaluate LRFR transcriptome response to auxin, we compared the 3h LRFR- and 2h picloram-regulated genes (Chapman et al., 2012) in hypocotyls for all the genotypes. The results showed that LRFR- and picloram-regulated genes are highly correlated for both Col-0 and *smt2-1* (Fig. 9b). The overlap was calculated from the total number of picloram genes, which was 47.3 and 51.9 % for the upregulated and 51.4 and 58.9% for the downregulated genes in Col-0 and *smt2-1*, respectively (Fig. 9b). Such an overlap was not present in *pif457* and *yuc2589*, the mutants that are known to be impaired in auxin biosynthesis in LRFR (Kohnen et al., 2016, de Wit et al., 2015, Nozue et al., 2015). Comparison of LB- and picloram-regulated genes in hypocotyls also did not show any correlation for any of the genotypes including Col-0 (Fig. S14), which is in line with previous reports (Pedmale et al., 2016). Next, we treated

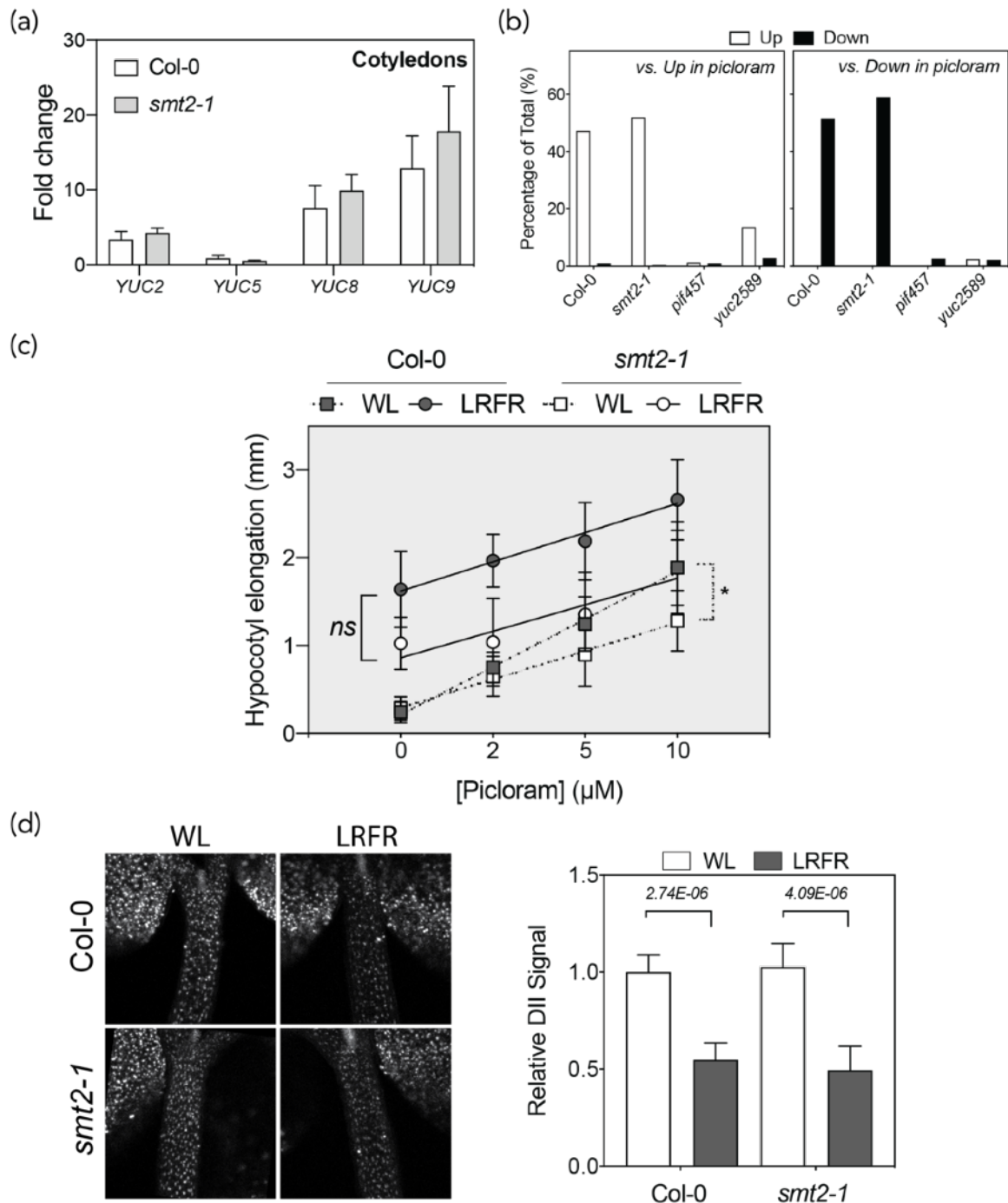


**Figure 9. Auxin biosynthesis, transport and response are not impaired in *smt2* mutant in LRFR.**

(a) Expression of *YUCCAs* in cotyledons is represented as fold change in LRFR (LRFR/WL). (b) Comparison of LRFR (3h, this study) and picloram (2h, Chapman et al., 2012) regulated genes in hypocotyls. Percentages are calculated from total number of up- or downregulated genes in picloram. (c) Hypocotyl elongation of the indicated genotypes grown as in Fig. 2 with the indicated concentrations of picloram (at ZT2 on day 5) during the last 3d with the indicated light treatments. The statistical significance between

(Figure 9 legend continues)

genotypes in WL (dashed line, \* < 0.05) and in LRFR (solid line, *ns* > 0.05) is indicated (two-way ANOVA, *n* > 12). (d) Representative images (left) and quantification (right) of the DII-VENUS signal intensity in hypocotyls of the indicated genotypes grown as in Fig. 2, either kept at WL or transferred to LRFR (at ZT2 on day 5) for 1h. Signal intensity is normalised to mean value of Col-0 in WL. Data are means; error bars indicate SD; numbers above the bars indicate P value (Student's T-test, *n* > 5). Related to Fig. S14.

Col-0 and *smt2-1* seedlings with increasing concentrations of picloram upon transfer to LRFR. Col-0 and *smt2-1* hypocotyl elongation was similar in all picloram concentrations in LRFR (Fig. 9c, solid lines). However, *smt2-1* hypocotyls elongated significantly less in WL compared to Col-0 with the increasing picloram concentration (Fig. 9c, dashed lines). These results suggest that *smt2-1* auxin response is not altered in LRFR.

Finally, we indirectly determined the auxin levels using the DII-VENUS auxin sensor (Brunoud et al., 2012) in 5d-old Col-0 and *smt2-1* seedlings 1h after transfer to LRFR. We observed a similar reduction of the DII-VENUS signal in the hypocotyls of both genotypes, indicating increased auxin levels (Fig. 7d). All together, these data indicate that auxin biosynthesis; transport and response in *smt2-1* are not altered in LRFR.

### **Sucrose transport is not altered in *smt2* mutant in LRFR**

Previously, we showed that sucrose transport from cotyledons to hypocotyls is required for LRFR-induced hypocotyl elongation (de Wit et al., 2018). Considering the cotyledon vasculature deficiency, we checked whether sucrose transport was impaired in *smt2-1*. Shulse et al. profiled RNA expression of Arabidopsis root cells in the presence and absence of sucrose in the growth medium (2019). When the sucrose is absent in the medium, the only source of sucrose for root cells is the sucrose transported from cotyledons. Therefore, we used the genes that were induced in sucrose (-) medium as a proxy for sucrose transport-related genes and compared to LRFR-induced genes in hypocotyls.

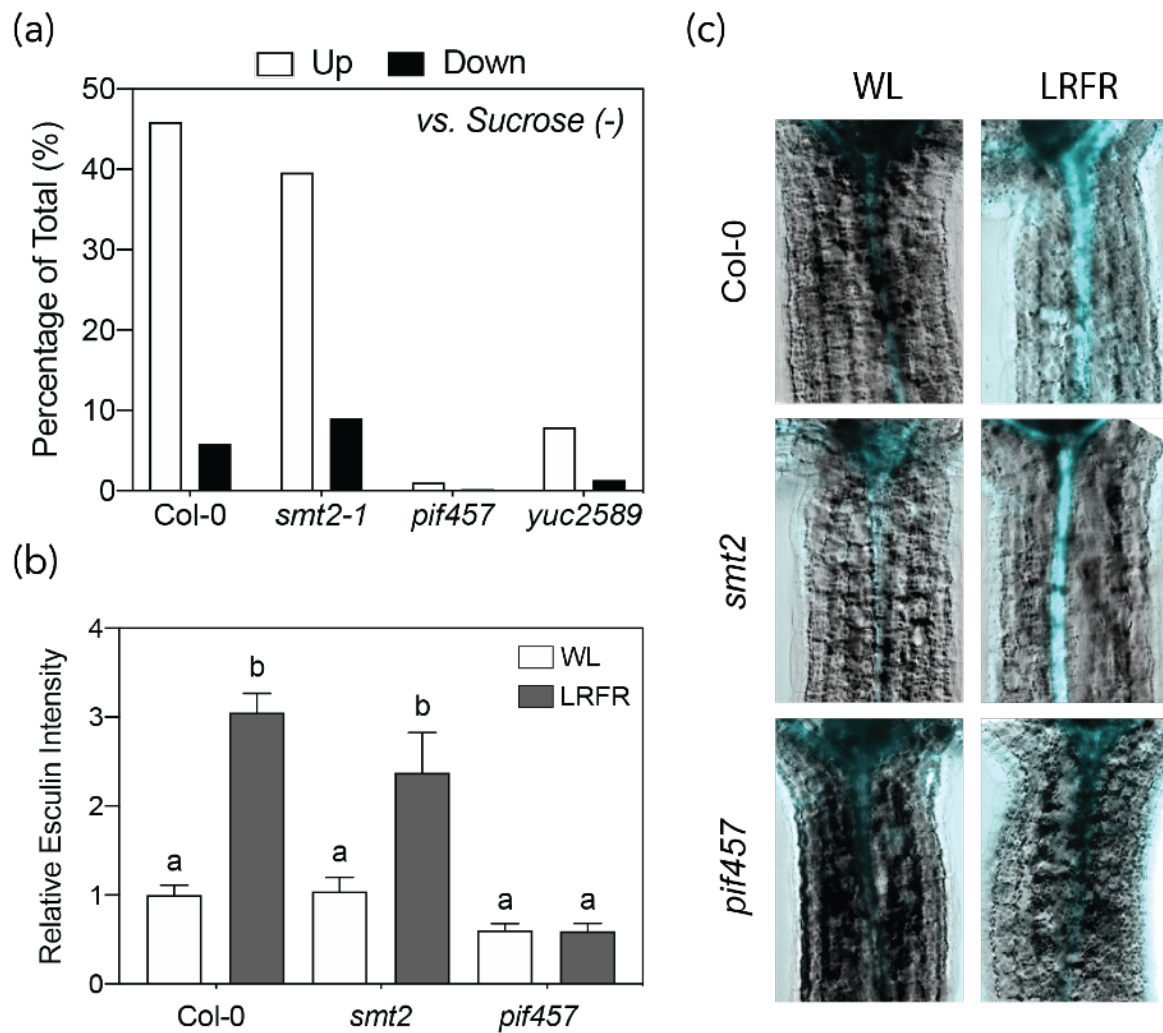


**Figure 10. Sucrose transport is not altered in *smt2* mutant in LRFR.**

(a) Comparison of LRFR (3h, this study) and sucrose (-) (Shulse et al., 2019) regulated genes in hypocotyls and roots, respectively. Percentages are calculated from total number of upregulated genes in sucrose (-). (b) Esculin signal intensity in hypocotyl vasculature signal is detected in 6d LD-grown seedlings after 150 min of LRFR treatment, last 30 min with the presence of esculin (10 mg/mL). Signal intensity is normalised to mean value of Col-0 in WL. Error bars indicate SEM; different letters indicate significant difference (two-way ANOVA with Tukey's HSD test,  $P < 0.05$ ,  $n = 4$  seedlings  $\times$  10 regions). (c) Representative images that are quantified in (b). Related to Fig. S15.

The overlap between the LRFR- and sucrose (-) induced genes were 45.9 and 39.6% in Col-0 and *smt2-1*, respectively, whereas it was only 1.0% for *pif457* and 7.9% for *yuc2589* (Fig. 10a). On the contrary, the overlaps between LRFR-repressed and sucrose (-) genes were 5.8 and 9.0% in Col-0 and *smt2-1*,

respectively. Furthermore, LB-induced and repressed genes overlapped between 4-9 % with sucrose (-) induced genes with no major correlation for any genotypes (Fig. S15a), suggesting that LB does not induce sucrose transport. Supporting this argument, GO term enrichment analysis showed that “phloem sucrose loading” was enriched in LB downregulated genes in cotyledons. To test whether phloem sucrose transport plays a role in LB hypocotyl elongation response, we measured hypocotyl elongation of sucrose transport mutants *suc2-4* and *sweet11;12* in LB and LRFR. LRFR-induced hypocotyl elongation was impaired in both mutants, as previously reported (de Wit et al., 2018). However, *sweet11;12* hypocotyls elongated as WT in LB, whereas *suc2-4* hypocotyl elongation was also impaired in LB (Fig. S15b). We conclude that sucrose is still required for LB-induced hypocotyl elongation but its transport might not be as strongly regulated in LB as in LRFR.

Next, we used esculin fluorescence dye that is used as a proxy for sucrose transport (Gora et al., 2012). To visualise sucrose transport in LRFR, after 2h of LRFR treatment we cut the cotyledons approximately from the centre perpendicular to midvein and applied a drop of esculin. We measured the esculin signal 30 min after the esculin application. The relative esculin in Col-0 and *smt2-1* hypocotyls increased similarly in LRFR, whereas it remained the same in *pif457* hypocotyls in WL and LRFR (Fig. 10b, c), which correlates with the gene expression changes in *pif457* (Fig. 10a). We conclude that *smt2-1* hypocotyl elongation reduction in LRFR is not due to reduced sucrose transport.

### **The ratio between campesterol to sitosterol in *Brassica rapa* hypocotyls does not change rapidly in LRFR**

Although we focused on SMT2 and SMT3 that regulate the ratio between campesterol and sitosterol (Fig. 3a), expression of many other genes in the sterol biosynthesis pathway were induced in LRFR in Arabidopsis hypocotyls (Fig. S1). The transcriptional regulation indicates that either LRFR changes the composition of sterols most likely for their functional roles, or it induces a total

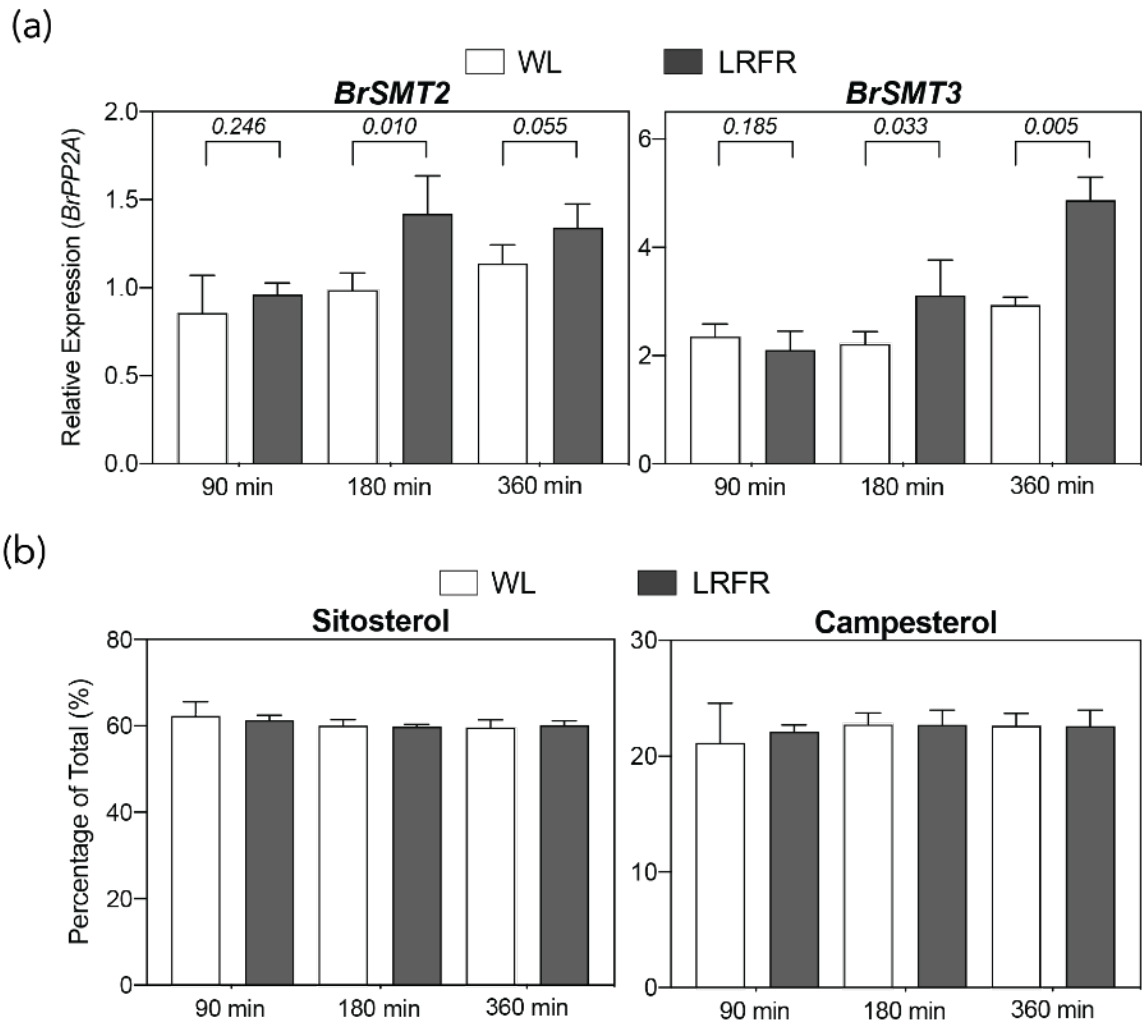


**Figure 11. Sterol composition of *Brassica rapa* hypocotyls does not change rapidly in LRFR.**

(a) Relative expression of *BrSMT2* and *BrSMT3* in 5-d-old *Brassica rapa* hypocotyls. Seedlings were grown as in Fig. 2. Gene expression values were calculated as fold induction relative to *BrPP2A*. n = 4 (biological) with three technical replicas for each RNA sample. Data are means; error bars indicate SD. Numbers above bars are P values (Student's T-test). (b) Campesterol and sitosterol percentages in total sterol pool of 5-d-old *Brassica rapa* hypocotyls. Seedlings were grown as in Fig. 2. n = 5 (biological). Data are means; error bars indicate SD. Related to Fig. S16.

increase in PM lipids including sterols for their structural roles in the elongating PM. Therefore, we measured the sterol levels to see whether LRFR changes the sterol composition. For technical reasons, we used *Brassica rapa* hypocotyls that elongate in LRFR is similar to *Arabidopsis* (de Wit et al., 2018). Furthermore, we

confirmed that *BrSMT2* and *BrSMT3* were induced in *B. rapa* hypocotyls after 3h of LRFR similarly to their orthologs in *Arabidopsis* (Fig. 11a). We also checked expression of *BrSMT1* and *BrIAA29* as a control (Procko et al., 2014). We measured sterols using GC-MS and represented relative amount of each sterol in the total sterol pool as percentages, because the fresh weight of hypocotyls increased significantly after 6h of LRFR treatment (Fig S16b). Thus, this method allowed us to detect changes in sterol composition rather than the levels. We observed that campesterol and sitosterol percentages did not change in LRFR for the tested time points (Fig. 11b). Yet, the percentage of ergosta-5,7-dienol that is a precursor for brassinosteroids downstream of campesterol, decreased, whereas an unidentified sterol increased after 3h of LRFR (Fig. S16c). Although these changes were significant, they were modest. These results suggest that LRFR induces a total increase in sterols rather than a major change in the composition.

### **Lipid profile of *Brassica rapa* hypocotyls changes in response to LRFR**

We analysed the lipid content of *B. rapa* hypocotyls more globally using untargeted lipidomics after 6h and 30h of LRFR treatment by LC-MS. In this method, we isolated and ionised the lipids, which is followed by first separation of the ions by their mass to charge ratio (i.e., MS1), which gives the putative identities for the lipid species rather than the true identities. Next, we fragmented the ions and separated the smaller ions in a second MS (i.e., MS/MS or MS2), which allowed us to detect the true identities of the lipid species. Principle component analysis (PCA) and clustering from MS/MS (MS2) detected lipid species showed that the 5 biological samples for each time point were clustered together, indicating a good data quality (Fig. 12a, b). Next, we did a term enrichment analysis of the five major lipid classes in the significantly changed lipid species in LRFR. The results indicate that the number of storage

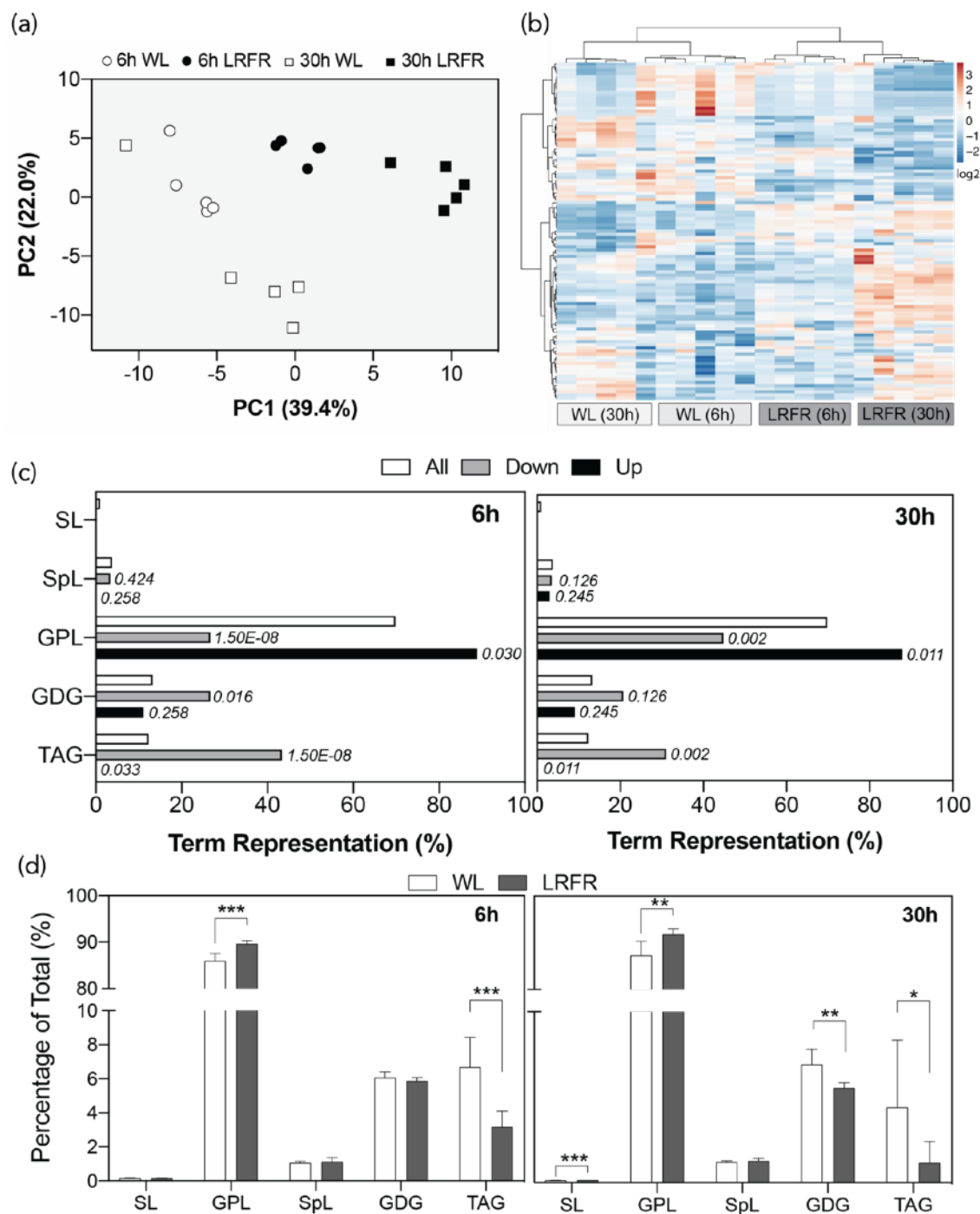


**Figure 12. Lipid profile of *Brassica rapa* hypocotyls changes in response to LRFR.**

(a) PCA of the MS/MS (MS<sub>2</sub>)-detected lipid species. PC1 and PC2 of each biological replicate (n = 5) are graphically visualised. (b) Cluster analysis and heat map representation of the MS<sub>2</sub>-detected lipid species in each biological replicate. (c) Term enrichment analysis for the main lipid classes (Sterol lipids - SL, Sphingolipids -SpL, Glycerophospholipids - GPL, Glycosyldiradylglycerols - GDG, Triadylglycerols - TAG) of significantly (Benjamini Hochberg correction (FDR) < 0.05 or FDR < 0.1 and Fold

(Figure 12. legend continues)

change (FC) > 1.5) increased (up) or decreased (down) in the MS2-detected lipid species at the indicated time points. The numbers next to each bar indicate term FDR values (Fisher's test with Benjamini Hochberg correction). (c) Lipid class abundance at indicated time points is represented as percentage of total detected lipids. Seedlings were grown as in Fig. 2. Data are means; error bars indicate SD; asterisks indicate FDR values (\* <0.1, \*\*<0.05, \*\*\*<0.01). Related to Fig. S17.

lipids (triacylglycerols - TAG) and glycosyl-diacylglycerols (GDG) that are major constituents of thylakoid membranes (Mamode Cassim et al., 2019) were significantly enriched in decreased lipid species (down), whereas a major group of PM lipids, glycerolphospholipids (GPL) were enriched in increased lipids (up) for both time points (Fig. 12c). Furthermore, GPL were underrepresented in decreased lipids whereas storage lipids were underrepresented in increased species. We observed a similar trend in MS1-detected lipid species (Fig. S18). The number of glycerolphosphoglycerol and triacylglycerol species was over- and underrepresented in increased MS1 lipid species, respectively, while glycerolphosphoglycerols were also underrepresented in decreased species (Fig. S18c). Additionally, the number of ceramide species was enriched in increased lipids after 30h of LRFR treatment. Yet, it is important to note that MS1-detected lipid species are not true identities and contains many lipids that are not found in plants. We also evaluated the changes in the level of five major lipid classes in MS2-detected lipid species (Fig. 12d). The percentage of GPL in the total lipid pool increased whereas the storage lipids decreased significantly in LRFR for both time points (Fig. 12d). The percentage of chloroplast lipids significantly decreased only after 30h of LRFR treatment. We conclude that LRFR promotes the accumulation of PM lipids in expense of storage and chloroplast lipids in *B. rapa* hypocotyls. GO term analysis using our RNA-seq data from Arabidopsis showed that terms related to biosynthesis of membrane-related lipids, such as "sterol biosynthetic process", "sphingolipid biosynthetic process", and

“membrane lipid biosynthetic process” were enriched in LRFR specific and LB and LRFR shared upregulated genes in hypocotyls (Fig. 7e, 7g); whereas photosynthesis related terms including “thylakoid membrane organisation” were enriched in the LRFR specific, LB specific, and LB and LRFR shared downregulated genes in hypocotyls (Fig. S11c, S11e, S11g). In addition, LB specific upregulated genes were enriched in many terms related to catabolism of storage lipids including “FA catabolic process” (Fig. 7c). Therefore, these results strongly suggest that LRFR modulates lipid profile of Arabidopsis and *B. rapa* hypocotyls similarly. Furthermore, LB and LRFR may share mechanisms to regulate hypocotyl lipid profiles in Arabidopsis hypocotyls.

### **LRFR decreases PM fluidity in hypocotyls**

Next, we checked whether PM fluidity changes in LRFR using the lipidomics data. The ratios of phosphatidylcholine to phosphatidylethanolamine (PC/PE), saturated to unsaturated lipids are indicators of PM fluidity (Mamode Cassim et al., 2019). An increase in PC/PE ratio indicates an increase in PM fluidity and decrease in PM order (Mamode Cassim et al., 2019). The PC/PE decreased significantly after 30h LRFR treatment (Fig. 13a), indicating a decrease in PM fluidity. We also calculated saturated to mono-, poly-, and total unsaturated ratios for PM lipids, excluding storage and chloroplast lipids. Fatty acid chains are more tightly packed as the saturation level increases. Therefore, an increase in saturated/unsaturated ratio indicates a decrease in PM fluidity and an increase in PM order. Saturated/polysaturated and saturated/unsaturated ratios increased in LRFR at both time points (Fig. 13b), indicating that LRFR promotes PM fluidity reduction in *B. rapa* hypocotyls. These results were in line with the expression profile of *FATTY ACID DESATURASE (FAD)* genes in hypocotyls and cotyledons of Arabidopsis seedlings. *FAD2*, *FAD6*, and *FAD7* expression decreased significantly in hypocotyls whereas only *FAD5* and *FAD7* expression were downregulated in cotyledons in Col-0 (Fig. 12c, S17a). The LRFR-mediated regulation of these genes was absent in *pif457* and *yuc2589*. However, their

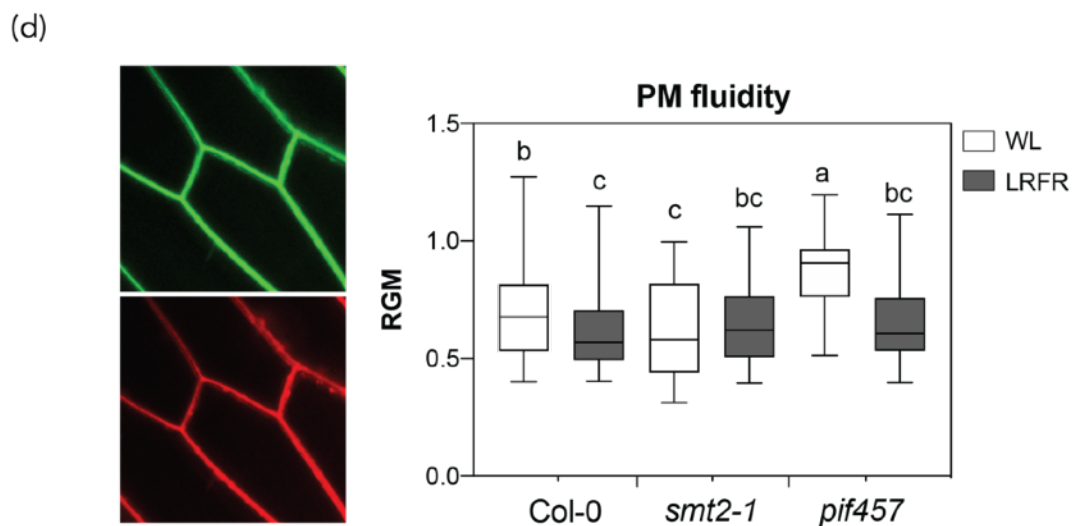
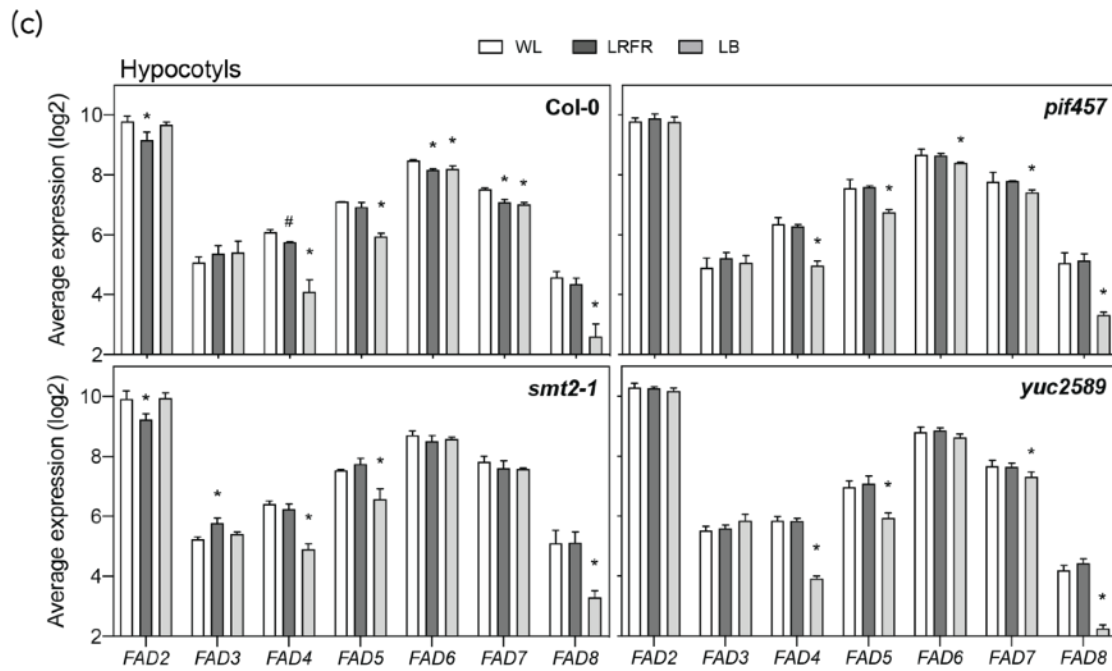
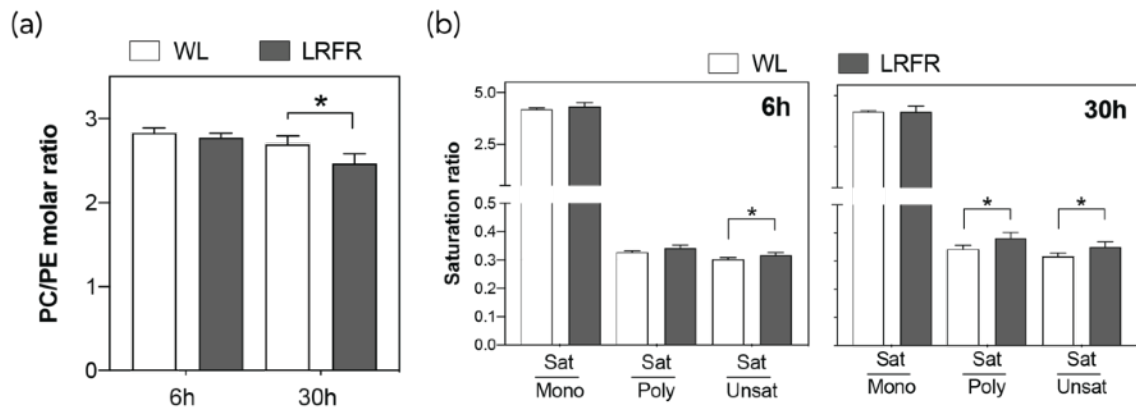


**Figure 13. LRFR decreases plasma membrane (PM) fluidity.**

(a) The ratio of phosphatidylcholine (PC) to phosphatidylethanolamine (PE) and (b) the ratio of saturated to mono-, poly- and total unsaturated MS2-detected membrane lipids in *Brassica rapa* hypocotyls. Data are means; error bars indicate SD. Asterisks (\*) indicate FDR < 0.05 with Benjamini-Hochberg correction. (c) Average expression for *FAD* family genes in hypocotyls of the indicated genotypes 3h after transferred to the indicated light conditions obtained from the RNA-seq analysis. Asterisks (\*) and hashes (#) indicate the statistical significance compared to WL (FDR value, \* < 0.05, # < 0.1). (d) The characterisation of the relative proportion of L<sub>o</sub> and L<sub>d</sub> phases of PM of indicated genotypes of *Arabidopsis thaliana* hypocotyl epidermal cells using di-4-ANEPPDHQ (2µg/mL) fluorescence dye. The RGM (for the red/green ratio of the membrane) was calculated from 7d-old seedlings grown as in Fig 2., treated with WL or LRFR for the last 3d. Different letters indicate significant difference (two-way ANOVA with Tukey's HSD test, P < 0.05, n = 9 cells from 3 seedlings x 20 membrane regions). Related to Fig. S18.

expression in *smt2-1* showed a similar trend to Col-0 in LRFR. Surprisingly, the expression of *FAD4*, *FAD5*, *FAD7*, and *FAD8* was reduced in LB significantly for both organs whereas hypocotyls also showed a reduction in *FAD6* expression. These reductions happened more drastically in LB compared to LRFR and were not dependent on PIFs and YUCCAs unlike in LRFR. We conclude that PM fluidity modifications via regulating saturation of PM lipids is a common mechanism in response to LB and LRFR, yet transcriptional regulation happens via different members of *FAD* family and do not require PIFs and YUCCAs in LB whereas they are required in LRFR. Furthermore, the transcriptional regulation of *FADs* occurs in elongating hypocotyls in LRFR whereas LB induces a more systemic change *FAD* expression in both organs.

In order to determine whether PM fluidity changes in *Arabidopsis* hypocotyls, we used the di-4-ANEPPDHQ fluorescence dye that allows to measure the relative proportion of ordered and disordered phases of PM (Mamode Cassim et al., 2019). RGM (for red/green ratio of the membrane), that is used to estimate PM fluidity, was calculated from 7d-old Col-0, *smt2-1*, and *pif457* seedlings that were

treated with WL or LRFR for the last 3d using confocal microscopy. We observed that Col-0 RGM value decreased slightly but significantly in LRFR, whereas it remained unchanged in *smt2-1*, indicating that sitosterol production is required for the RGM decrease in LRFR (Fig. 13d). However, *pif457* RGM value showed a similar trend to Col-0, suggesting PIFs are not involved in this process. We also determined the LB effect on PM fluidity with the same method. The results showed that PM fluidity also slightly decreases in hypocotyls of LB-treated seedlings yet the change was not significant (Fig. S17b). However, LRFR and LB RGM values were in the same significance group, indicating that PM fluidity change may be a common response to both light conditions with a more dramatic result in LRFR. In addition, *smt2-1* fluidity was similar in WL, LRFR, and LB, indicating that SMT2 protein is important for the regulation of PM fluidity in both LB and LRFR.

All together, three different PM fluidity indicators independently point the same conclusion about LRFR decreasing PM fluidity in hypocotyls. However, it is important to note that although significant, the changes in all three indicators were modest. Furthermore, these changes become to be apparent at late time points, especially in the di-4-ANEPPDHQ fluorescence dye measurements, while enhanced hypocotyl growth happens very rapidly in *Arabidopsis* and *B. rapa* (de Wit et al., 2018). In other words, it is highly unlikely that these changes are required for the rapid growth acceleration in LRFR.

### **Low blue light induces autophagy**

In LB, PAR decreases dramatically whereas it remains the same in LRFR. Therefore, one could expect that carbon fixation decrease in LB whereas it remains unaffected in LRFR. GO term analysis in downregulated genes in LB and LRFR showed that LB promoted the enrichment of “photosynthesis, dark reaction” and “carbon fixation” in both organs, whereas these terms were not overrepresented in LRFR (Fig. S11c-h). In line with these results, we previously showed that LRFR did not significantly decrease carbon fixation in *B. rapa*

seedlings (de Wit et al., 2018). Another striking result from our transcriptome comparison of LB and LRFR was the enrichment of catabolism and anabolism related GO terms in LB and LRFR upregulated genes, respectively (Fig. 7c-h). Thus, we hypothesised that LB may promote recycling of unused cellular material via induction of autophagy as the seedlings cannot invest on production of new material to boost the growth necessary to catch the light required for photosynthesis.

We observed the enrichment of several autophagy-related GO terms in LB upregulated genes in both organs (Fig. 7c, 7d). Next, we individually checked the expression of genes listed in autophagy-related GO categories and listed the ones that are significantly regulated in one of the organs or light treatments either in Col-0 or *smt2-1*. The expression heatmap indicates that significantly regulated autophagy-related genes in both organs were upregulated in LB, with a higher fold change in cotyledons (Fig. 14a). In contrast, the majority of significantly regulated autophagy-related genes were downregulated in LRFR in hypocotyls, as GO term analysis previously suggested (Fig. S11g). The expression pattern of autophagy-related genes in *smt2-1* was similar to Col-0 for both LB and LRFR. We also checked the expression of *AUTOPHAGY-RELATED (ATG)-8* isoforms in LRFR and LB in our RNA-seq data. ATG8A-I are isoforms of ubiquitin-fold proteins that are anchored to the developing autophagic membranes, thus a marker protein for autophagic bodies (Li & Vierstra, 2012). The expression of all, except *ATG8H* in hypocotyls and *ATG8G* in cotyledons increased after 3h LB but not LRFR in Col-0 (Fig. 14b, S19a). A similar trend was present for *smt2-1*, *pif457*, and *yuc2589* hypocotyls. In addition, the basal expression (in WL) of *ATG8B*, *ATG8C*, *ATG8E*, *ATG8F*, and *ATG8H* in hypocotyls; *ATG8C*, *ATG8D*, and *ATG8H* in cotyledons was significantly higher in *smt2-1* compared to Col-0 (Fig. 14b, S19a). In contrast, LRFR did induce expression of none of the *ATG8* members in hypocotyls, whereas *ATG8A*, *ATG8C*, and *ATG8H* expression were upregulated in LRFR in cotyledons in a PIF and YUCCA-

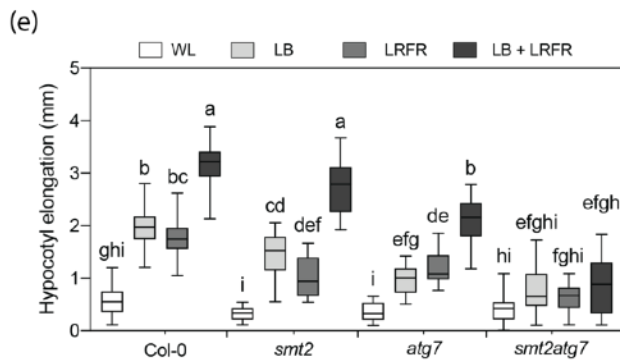
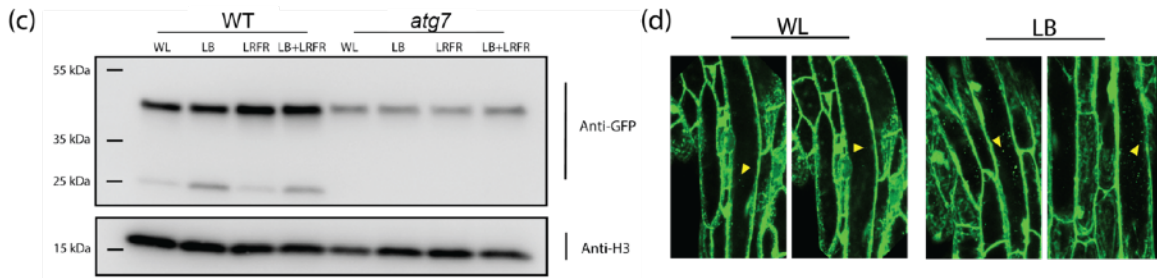
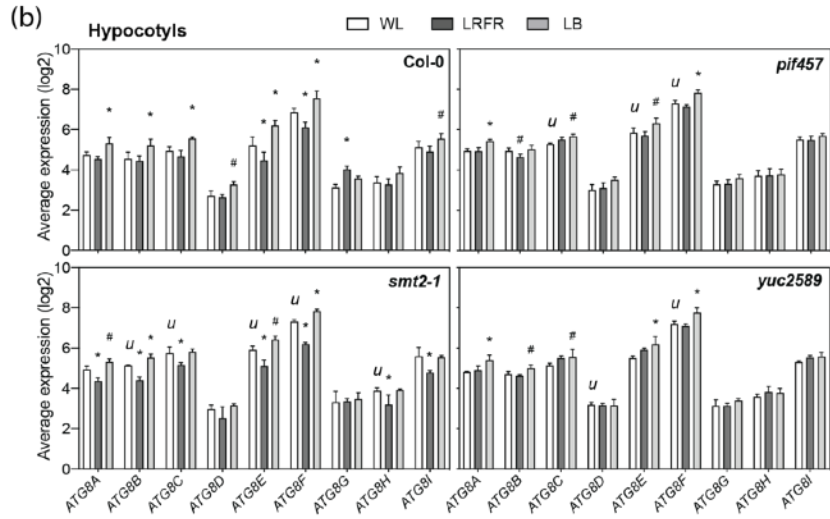
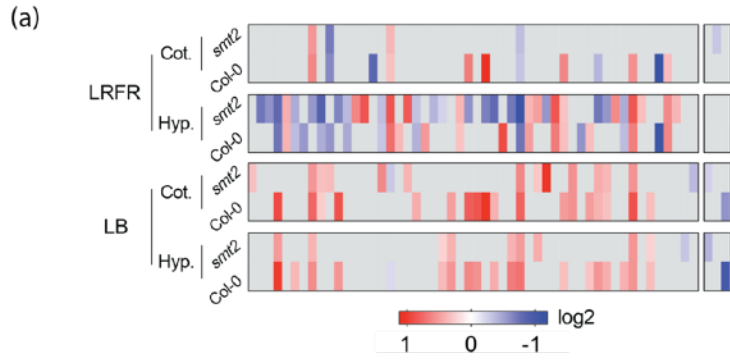


### Figure 14. Low blue light induces autophagy.

(a) Relative expression of genes annotated in the autophagy-related GO categories in Col-0 and *smt2-1* hypocotyls and cotyledons. A gene that is represented in two categories is shown only once. Genes that are significantly regulated in at least one condition (FDR < 0.1) are shown. Grey cells indicate non-significance. Last three rows indicate genes in 'negative regulation of autophagy' term. (b) Average expression for *ATG8A-I* isoforms in 5-d-old hypocotyls of the indicated genotypes 3h after transferred to the indicated light conditions obtained from the RNA-seq analysis. Asterisks (\*) and hashes (#) indicate the statistical significance compared to WL, *u* and *d* indicate up- or downregulation of basal expression in WL, respectively for mutants compared to Col-0 (FDR value, \* < 0.05, # < 0.1; *u* or *d* < 0.05). (c) ATG8-GFP and free GFP levels are detected with an anti-GFP antibody from total protein extract from 5 d old LD-grown seedlings treated at ZT2 with 8h of low blue light in presence of concanamycin (0.5  $\mu$ M). H3 was used as a loading control. (d) Petiole epidermis cells of *35S::ATG8a-GFP* in WT background as grown in (a) and treated as in (b). Yellow arrowheads indicate autophagic bodies. (e) Hypocotyl elongation of the indicated genotypes grown as in Fig 2. Elongation during the last 3 d is indicated. Different letters indicate significant difference (two-way ANOVA with Tukey's HSD test, P < 0.05, n > 12). Related to Fig. S19.

dependent manner (Fig. S19a). These results indicate that LB induces autophagy transcriptionally in both organs with a higher fold change in cotyledons.

Next, we tested whether autophagy was induced post-transcriptionally in LB using a ubiquitously expressed ATG8a-GFP (*35S::ATG8a-GFP*) line (Thompson et al., 2005). The intensity of free GFP band that shows the induction of autophagy increased in LB and LB + LRFr conditions in WT (Fig. 14c). ATG7 is an E1-activating enzyme that is required for ATG8 anchoring to autophagic membranes (Li & Vierstra, 2012), therefore we used the *atg7* mutant as a negative control for autophagy induction (Fig. 14c). In line with transcriptome data, autophagy was induced in both cotyledons and hypocotyls, indicating that it is not an organ-specific response to LB (Fig. S19b). We also detected that the number of autophagic bodies increased in petiole epidermis cells in *35S::ATG8a-GFP* line in

WT background in the presence of concanamycin (Fig. 14d). We failed to detect such a clear increase in hypocotyl epidermis cells (data not shown), possibly due to the much lower expression of *ATG8a-GFP* in hypocotyls compared to petioles. Furthermore, we also did not observe a dramatic change between WL and LB treatments in root epidermis cells (Fig. S19c). We conclude that LB induces autophagy post-transcriptionally in aerial organs of Arabidopsis seedlings with no apparent differences between cotyledons and hypocotyls.

To determine the phenotypic consequences of autophagy, we checked hypocotyl elongation of autophagy mutant *atg7* in LB, LRFR, and LB + LRFR. *atg7* hypocotyl elongation was reduced in all light conditions except WL, yet the reduction was greater in LB compared to LRFR (Fig. 14e). We hypothesised that recycling of sitosterol may explain how *smt2-1* hypocotyl elongation is not affected in LB. Thus, we analysed the hypocotyl elongation of *smt2atg7* double mutant. Remarkably, *smt2atg7* hypocotyl elongation was completely impaired in LB, LRFR, and LB + LRFR (Fig. 12e), indicating a genetic interaction between the *smt2* and *atg7* mutants. We conclude that autophagy is indispensable for LB and LRFR-induced hypocotyl elongation when sitosterol biosynthesis is impaired.

## DISCUSSION

### **PIFs induce *SMT2* and *SMT3* expression that are required for hypocotyl elongation in LRFR**

The role of PIFs in auxin production in distal organ cotyledons through induction of *YUCCA* expression are well documented in LRFR-induced hypocotyl elongation (Tao et al., 2008, Hornitschek et al., 2012, Li et al., 2012, Procko et al., 2014, Kohnen et al., 2016). We showed that PIFs bind to promoter regions of *SMT2* and *SMT3* and induce their expression in hypocotyls in LRFR (Fig. 3b, 3c). These results indicate that in addition to the previously identified distal roles in auxin metabolism, PIFs locally regulate sterol biosynthesis process in hypocotyls in LRFR.

We showed that there is a direct correlation between sitosterol production in hypocotyls and LRFR-induced hypocotyl elongation. LRFR-induced hypocotyl elongation was significantly reduced in *smt2* but not in *smt3* and we did not detect a further reduction in *smt2smt3* hypocotyl elongation (Fig. 4a, S4a). Mutants carrying null alleles of *SMT2* accumulate less sitosterol and more campesterol, yet the sterol content of *smt3* is not altered as dramatically (Hase et al., 2005, Carland et al., 2010). Sterols are one of the major components of the PM and sitosterol is the most abundant sterol in Arabidopsis (Valitova et al., 2016). The other key phenotypic difference between *smt2* or *smt2smt3* and *smt3* is the cotyledon vasculature deficiency phenotype (Fig. 4b, data not shown). Auxin and sucrose transport from cotyledons to hypocotyl are indispensable for LRFR-induced hypocotyl elongation (Keuskamp et al., 2010, Procko et al., 2014, de Wit et al., 2018). Therefore, the impaired sitosterol level or the cotyledon vasculature deficiency in *smt2* and *smt2smt3* mutant might have caused the reduced hypocotyl elongation of these mutants in LRFR. Several experiments suggest that the sitosterol production in hypocotyls is required for LRFR-induced hypocotyl elongation. First, we showed that the inhibition of sterol biosynthesis

reduces WT hypocotyl elongation more compared to *smt2-1* in LRFR but not in WL (Fig. 4c). Second, ubiquitous and hypocotyl specific complementation of *SMT2* rescue the *smt2-1* hypocotyl elongation in LRFR, whereas cotyledon specific expression does not (Fig. S5b). Thus, the phenotyping data indicate a direct correlation between sitosterol production in hypocotyls and LRFR-induced hypocotyl elongation. On the other hand, hypocotyls of other cotyledon vasculature mutants, *cvp2* and *cvp2cvl1* elongate normally in LRFR (Fig. 4a). Furthermore, auxin production; transport and response are not altered in *smt2-1* in LRFR (Fig. 9). Yet, *smt2-1* has a reduced response to picloram in WL (Fig. 9c). The regulation of auxin transport in WL and LRFR may explain this phenotypic difference. It was shown that auxin-inhibited endocytosis of PIN2 is reduced in *smt2smt3* roots (Carland et al., 2010). Yet, *PIN2* expression is very low to undetectable in cotyledon mesophyll and vasculature (Kim et al., 2018). Nagatani group showed that expression of *PIN3*, *PIN4*, and *PIN7*, coding for the main auxin transporters in LRFR-induced hypocotyl elongation, are induced in mesophyll cells upon FR treatment whereas their expression remains largely unaffected in vasculature (Kohnen et al., 2016, Kim et al., 2018). Therefore, FR-induced expression of *PINs* in mesophyll might have rescued the reduced auxin response of *smt2* mutant. Finally, sucrose transport is also not significantly affected in *smt2-1* (Fig. 10). Yet, it is important to note that although it is not significant, both the esculin signal and percentage of sucrose-related gene induction in *smt2-1* are slightly lower compared to WT (Fig. 10). Thus, sucrose transport may be slightly reduced in *smt2*. This is also somewhat expected as Kim et al. data shows that genes encoding for sucrose transporters *SUC2*, *SWEET11*, and *SWEET12* are expressed almost only in vasculature, unlike auxin transporters (Kim et al., 2018). Overall, our results indicate that the reduced hypocotyl elongation of *smt2-1* in LRFR is due to the impaired sitosterol production rather than the cotyledon vasculature deficiency and *SMT2* is primarily needed in the hypocotyl to enable LRFR-induced hypocotyl elongation.

On contrary to the *smt2* mutant, *pif457* is completely impaired in sucrose transport in LRFR (Fig. 10). In our previous work, we showed that PIF7 is important for sucrose metabolism in LRFR, but how it does so remained unanswered (de Wit et al., 2018). In line with previous reports (Kohnen et al., 2016), we showed that *pif457* is impaired in auxin biosynthesis and transport (Fig. 8e, 8f). Here we showed that sucrose-related genes are not induced in *pif457* and *yuc2589* mutant similarly, suggesting that PIFs may regulate sucrose transport in LRFR via auxin pathway (Fig. 10a). A recent report shows that auxin transcriptionally regulates sucrose transport into the rose petals (Liang et al., 2020). However, we did not observe a change in expression of sucrose transporters in our LRFR data set (data not shown), consistent with previous reports (Kohnen et al., 2016, Kim et al., 2018). These results show that although it remains unclear how, PIFs are required for sucrose transport.

### **LRFR promotes accumulation of PM lipids and degradation of storage and chloroplast lipids**

The LRFR transcriptome in hypocotyls indicates that LRFR induces expression of many genes in the sterol biosynthesis pathway as well as other PM lipids in addition to *SMT2* and *SMT3* (Fig. S1, 6c). This suggests that LRFR may induce an increase in PM lipids to provide new material to elongating PM. The model describing PM elongation in pollen tubes suggests that Golgi vesicles carry the new cell wall material together with the PM material that is often more than the requirement of PM elongation and the excess amount is recycled later via endosomal processes (Hepler et al., 2013). Consistent with this model, GO term analysis from upregulated genes in LRFR-treated *Arabidopsis* seedlings shows that “Golgi vesicle transport” and several endosomal terms are enriched in hypocotyl upregulated genes in hypocotyls (Fig. 6c, 7e, 7g). Furthermore, these terms are closely related to “membrane organisation” term indicating there are shared genes in these terms that are upregulated in shade. Therefore, we hypothesised that LRFR may modify the lipid profile of elongating hypocotyls. To

test this hypothesis, we measured composition of sterols and other lipids in *B. rapa* hypocotyls. Although we analysed Arabidopsis transcriptome, we used *B. rapa* for sterol and lipidomics analyses in order to obtain enough material for GC-MS and LC-MS measurements. We believe that this is reasonable as the two species are close relatives and hypocotyl elongation response and transcriptional regulations for both species are similar in LRFR (Fig. 11a, S16a) (Procko et al., 2014, de Wit et al., 2018).

In the sterol analysis, we normalised the sterol content to the total detected sterol pool, which represents only the changes in the sterol composition as percentages between WL and LRFR rather than the sterol levels. The results indicated that the composition of major sterols in *B. rapa* hypocotyls after 90-360 min of LRFR does not change significantly (Fig. 11b). Yet, we observed a significant decrease in ergosta-5,7 dienol percentage in 3h LRFR may indicate that seedlings invest on sterol production rather than downstream BR biosynthesis (Fig. S16c). A BR decrease in Arabidopsis seedlings treated with 4h of LRFR was also previously reported (Bou-Torrent et al., 2014). These results are consistent with a total increase in sterol levels to provide new material for the elongating PM in LRFR. Yet, it is important to note that the dynamics of sterol metabolism in *B. rapa* and Arabidopsis might be different, even though *BrSMT2* and *BrSMT3* expression are induced in hypocotyls similarly to Arabidopsis in LRFR (Fig. 11a). Furthermore, the sterol quantification method that we used is not able to quantify the free and conjugated sterols separately. Therefore, we might have missed the changes in the composition of free sterols due to the mixed quantification of free and conjugated sterols. Finally, it is possible that the time points that we selected are too early to detect a change in sterol composition.

Similar to the sterol measurement results, we calculated the percentage changes of each lipid species compared to the total detected lipid amount in the lipidomics analysis. The lipidomics analysis reveals that LRFR also mediates key

changes in lipid profile of *B. rapa* hypocotyls (Fig. 12). Both term enrichment analysis and lipid composition changes indicate that LRFR promotes accumulation of PM lipids at the expense of storage and chloroplast lipids in the total lipid pool (Fig. 12b, c). A previous study shows that photosynthesis rates decrease in tomato stems in LRFR (Cagnola et al., 2012). Consistent with this report, it seems that hypocotyls use the lipid material of chloroplast and storage lipids to supply energy and PM lipids to elongating cells. This response appears to happen relatively fast.

Our transcriptome data supports that the changes in hypocotyl lipid profiles also occur in LB-treated *Arabidopsis* seedlings (Fig. 6c). We observed that the transcriptome profile of LB and LRFR are similar in lipid organisation (Fig. 7). GO terms related to PM-lipid biosynthesis and organisation as well as breakdown of storage lipids are enriched in upregulated genes (Fig. 7c, 7e, 7g), whereas terms related to chloroplast membrane organisation are enriched in downregulated gene sets in LB and LRFR (Fig. S11c, S11e, S11g). These results suggest that the modulation of lipid profiles in elongating hypocotyls is a common mechanism for both light conditions. Lipidomics results together with microscopy and the *FAD* expression data also shows that PM fluidity in *B. rapa* and *Arabidopsis* hypocotyls significantly decreases in LRFR (Fig. 13). However, the changes in PM fluidity indicators were modest and can be detected at relatively late time points starting from 30h of LRFR treatment. LRFR promotes hypocotyl elongation very rapidly in *Arabidopsis* and *B. rapa* (Kohnen et al., 2016, de Wit et al., 2018). Although it is possible that undetectable changes in PM fluidity also occur rapidly, it is difficult to argue that these changes are required for the early growth induction in LRFR. Yet, these changes may be needed for long-term adaptations to LRFR. The decrease in PM fluidity may increase the number of lipid microdomains and slow down the lateral movements of PM proteins that are important for transport and signalling events. For example, PIN auxin transporters and cellulose synthase complexes (CSCs) are located in such

microdomains. The polarity of PINs is important for directional auxin transport to elongating cells in various conditions, including PIN3 localisation in green shade (Sasidharan et al., 2014, Armengot et al., 2016). Similarly, CSC localisation defines the orientation of growing cellulose microfibrils in newly synthesised cell wall, therefore is critically important for the polarity of cell elongation (Desprez et al., 2007, Feraru et al., 2011). Another possible function could be that PM fluidity-increase may strengthen PM to endure increasing turgor pressure of elongating cells. Yet, a study on *E. coli* PM resistance to increasing pressure indicates that the more fluid the PM, the better its endurance to increasing pressure (Casadei et al., 2002). However, to the best of our knowledge, we lack a plant study on membrane fluidity and membrane strength. Finally, it was recently suggested that membranes that are relatively rich in unsaturated fatty acids might help to take advantage of the high light available for photosynthesis in WL whereas this is not the case for LRFR, thus saturated and mono-saturated portion of fatty acids increases in LRFR (Arico et al., 2019). However, it is important to note that photosynthesis is reduced in *fatty acid desaturase (fad)* mutants not because of PM lipid saturation but due to changes in chloroplast lipid composition and saturation level (McConn & Browse, 1998). Unlike Arico et al. where they showed that the saturation increases in the whole fatty acid pool in LRFR, we directly showed that the saturation of PM lipids increases excluding chloroplast and storage lipids (Fig. 13b). Furthermore, we showed that chloroplast lipids decrease in *B. rapa* hypocotyls upon LRFR treatment and “thylakoid membrane organisation” GO term is enriched in both LB and LRFR downregulated genes in Arabidopsis hypocotyls. Fatty acids are synthesised as saturated in the majority of organisms and FADs further desaturate them later (Los et al., 2013). Thus, we argue that the changes in PM fluidity may be a side affect of the decreased photosynthesis rates. As FADs are mainly required for regulation of chloroplast lipid saturation (McConn & Browse, 1998), FAD expression may not be as important and decrease when photosynthesis rate

decreases due to the adaptations to LRFR. This may consequently cause an increase in saturation levels of other lipids, including PM lipids, leading a decrease in PM fluidity. However, it remains unclear what the biological significance of PM fluidity modifications in LRFR and further investigations are needed to unravel the true nature of these modifications.

## **The individual and combined functions of PIFs and YUCCAs in**

### **LRFR**

Previous studies show that shade- and auxin-induced genes in WT and *pif* mutants overlap to a certain extent (Tao et al., 2008, Kohnen et al., 2016, Pedmale et al., 2016), suggesting the presence of PIF-dependent but auxin-independent transcriptional changes in LRFR. Consistent with these reports, the comparison of LRFR- and picloram-regulated gene sets in hypocotyls similarly showed that only half of the LRFR-regulated genes were regulated by auxin (Fig. 9b). It was also shown that PIF4, ARF6 and BZR1 cooperatively regulate common target genes (Oh et al., 2014), suggesting that expression of some genes requires combined functions of PIFs and auxin. We spatially compared the *pif457*- and *yuc2589*-misregulated gene sets in LRFR and identified gene lists that are PIF- and YUC-dependent, PIF-dependent and YUC-independent, and YUC-dependent and PIF-independent (Fig. S12). Our results revealed that the number of PIF- and YUC-dependent genes and GO terms enriched in these gene sets are higher in hypocotyls, indicating that both PIFs and auxin are locally required for hypocotyl elongation in LRFR (Fig. S12, 8c, 8d). On the contrary, although the total number of LRFR-upregulated genes was higher in hypocotyls compared to cotyledons, the number of PIF-dependent and YUC-independent genes was higher in cotyledons (Fig. 6b, S12). In addition, the number of LRFR-regulated genes was similar in *yuc2589* and Col-0 cotyledons that also grouped closely in PCA (Fig. 6b, S9). These results are in line with the previously identified distal functions of PIFs in cotyledons for auxin production and transport (Hornitschek et al., 2012, Li et al., 2012, Kohnen et al., 2016, Procko et al., 2014).

Here we additionally showed that PIFs locally induce auxin, BR, and ethylene response and cell wall organisation related genes in hypocotyls in LRFR independent of YUCCA-mediated auxin production (Fig. 8d), as suggested in previous studies (Hornitschek et al., 2012, Hersch et al., 2014, Kohnen et al., 2016). It is important to note that our transcriptome analysis does not allow identifying auxin-dependent but PIF-independent gene sets, as PIFs are required for auxin biosynthesis. Yet, further investigations of the gene lists identified here together with previously published ChIP-seq and transcriptome data (Chapman et al., 2012, Hornitschek et al., 2012, Oh et al., 2014, Chung et al., 2020) will allow spatially defining individual and combined functions of PIFs and auxin in LRFR-induced hypocotyl elongation.

### **PIFs and YUCCAs are required in LB-induced hypocotyl elongation**

The *pif457* and *yuc2589* mutants were completely impaired in LB-induced hypocotyl elongation (Fig. S8). Previous studies also report that mutants of PIFs and auxin biosynthesis, transport and response are severely impaired in LB-induced hypocotyl elongation (Keuskamp et al., 2011, Pedmale et al., 2016, Boccaccini et al., 2020). However, transcriptome comparison revealed that there is no significant difference between these mutants and Col-0 in LB-regulated gene expression (Fig. 8a). LB-induced hypocotyl elongation and the transcriptome regulation are slower compared to LRFR (Pedmale et al., 2016). In addition, PIF4 and PIF5 protein levels increase in LB particularly toward the end of the day (Boccaccini et al., 2020). Therefore, the 3h time point that we used for RNA-seq experiment may be too early to see any major changes in LB-regulated gene expression between *pif457* and Col-0. Another study that compares LB-regulated gene expression in whole seedlings of *pif45* and Col-0 after 1h, 6h and 24h of LB treatment suggests that genes related to cell wall organisation are misregulated in *pif45* mutant after 6h of LB (Pedmale et al., 2016). However, although auxin biosynthesis, transport and signalling mutants are severely

impaired in LB-induced hypocotyl elongation, auxin responsive genes are not regulated in LB in any of the time points (Pedmale et al., 2016). We observed major changes in LB-regulated gene expression in Col-0 cotyledons and hypocotyls after 3h (Fig. 6c). Although its expression is not regulated in LB or LRFR, the loss of *TAA1* that codes for the enzyme catalysing conversion of L-Trp to IPyA prior to rate limiting step that is catalysed by YUCCAs in auxin biosynthesis pathway, results in impaired hypocotyl elongation response in both light conditions (Pedmale et al., 2016, Keuskamp et al., 2011, Tao et al., 2008). This presents a nice example where expression of a gene is required at basal levels for LB and LRFR-induced hypocotyl elongation. Previous reports show that expression of many genes including auxin related genes in *pif45* mutant even decreases in WL and these changes become steeper in low PAR compared to high PAR (Hornitschek et al., 2012). In line with this study, we showed that basal expression of many genes including hormone and cell wall related genes in WL is misregulated in similarly *pif457* and *yuc2589* mutants (Fig. S13). Therefore, we conclude that *pif457* and *yuc2589* mutants are impaired in LB-induced hypocotyl elongation that requires basal levels of auxin and PIF function. Yet, it is possible that PIF-mediated changes become more apparent and important at later time points.

## **Metabolic pathways to obtain new material for elongating**

### **hypocotyls differ in LB and LRFR**

Interestingly, LB-induced hypocotyl elongation of *smt2* is normal (Fig. 5a). We confirmed that *SMT2* and *SMT3* are not induced and the new biosynthesis of sterols was not as important in LB (Fig. 5b, c). We found these results puzzling as both LB and LRFR-induced elongation are expected to require new PM material similarly. Furthermore, combination of LB and LRFR rescued the *smt2* phenotype to a large extent, suggesting that there may be two complementary molecular mechanisms to obtain PM material in LB and LRFR.

Our transcriptome data shows that catabolism related GO terms are enriched in LB-specifically upregulated genes (Fig. 7c, d). In contrast, anabolic terms, including “sterol biosynthetic process” are enriched in LRFR-specifically upregulated genes (Fig. 7g, h). As PAR decreases in LB while it does not change in LRFR, carbon fixation is expected to slow down in LB compared to LRFR. We previously showed that LRFR does not significantly decrease carbon fixation in *B. rapa* cotyledons (de Wit et al., 2018). In line with this report, we observed that carbon fixation term is not overrepresented in LRFR-specifically downregulated genes (Fig. S11g, h). On the contrary, LB-specifically downregulated genes are enriched in “carbon fixation” whereas “cellular response to sucrose starvation” is overrepresented in LB-specifically upregulated genes (Fig. S11c, 11d, 7c, 7d). Furthermore, we observed that FA catabolism, acetyl-CoA and acyl-CoA biosynthesis and metabolic pathways are induced transcriptionally in LB, whereas “gluconeogenesis” GO term is enriched in LB downregulated genes (Fig. 7c, S11c). Therefore, it appears that LB induces lipids to be catabolised to first acyl-CoA and later acetyl-CoA that is used as a precursor for production of new material required for cell elongation, including sterols; rather than restoring as glucose via gluconeogenesis.

Autophagy recycles the unused cellular material when the resources are scarce (Li & Vierstra, 2012). Furthermore, sucrose starvation induces microautophagy in Arabidopsis root cells (Goto-Yamada et al., 2019). In our data, we showed that autophagy is induced transcriptionally in LB with a higher fold induction in cotyledons (Fig. 14a). GO terms directly related to autophagy are enriched in LB upregulated genes in both organs (Fig. 7c, 7d). In addition, expression of all genes coding for ATG8 isoforms except *ATG8H* in hypocotyls and *ATG8B* and *ATG8H* in cotyledons are significantly upregulated in LB (Fig. 14b, S19a). Later, we showed that autophagy is also induced in LB post-transcriptionally with no apparent difference between two organs using *35S::ATG8a-GFP* lines that ubiquitously express *ATG8a-GFP* (Fig. 14c, 14d, S19b). Autophagic machinery-

mediated breakdown of lipids is induced by starvation in order to obtain both energy and membrane material (Fan et al., 2019). GO term analysis also showed many lipid catabolic terms are enriched in LB-upregulated genes (Fig. 7c, 7d). Therefore, we suggest that LB-induced autophagy may provide the membrane material required for hypocotyl elongation in LB, thus can rescue *smt2* phenotype in LB and LB + LRFR. The phenotypical analysis of *atg7*, *smt2*, and *smt2atg7* remarkably supported this hypothesis (Fig. 14e). The *atg7* hypocotyl elongation was reduced more in LB, whereas *smt2* was affected more in LRFR. The combination of LB and LRFR rescued hypocotyl elongation of *smt2-1* completely and *atg7* to a large extent (Fig. 14e). However, *smt2atg7* hypocotyl elongation was completely impaired in all conditions. These results present a nice example to our hypothesis that suggests that the biosynthesis in LRFR and recycling in LB are two complementary mechanisms that enable elongation in vegetative shade.

# MATERIALS AND METHODS

## Plant material and growth conditions

We used the following *Arabidopsis thaliana* genotypes (cv Columbia-0): *FRO6::XVE::YUC3* (Chen et al., 2014), *smt2-1 (frl1)*, Hase et al., 2005), *smt2-2 (cvp1)* and *smt3-1* (Carland et al., 2010), *pif4pif5pif7* (de Wit et al., 2015), PIF7-HA line (*pif7-2/pPIF7::PIF7-3HA-tPIF7*), PIF4-HA line (*pif4-101/pPIF4::PIF4-3HA-tPIF4*) (Zhang et al., 2017), *35S::PIF4-HA (pif4-101/p35S::PIF4-HA)* (Lorrain et al., 2008), *cvp2* and *cvp2cvl1* (Carland & Nelson, 2009), DII-VENUS (Brunoud et al., 2012), *suc2-4* (Srivastava et al., 2008), *sweet11sweet12* (Chen et al., 2012), *atg7-2* (Hofius et al., 2009), *35S::ATG8a-GFP* (Thompson et al., 2005), *yuc2yuc5yuc8yuc9* is recrossed using all *yuc* alleles that are described in (Nozue et al., 2015) except *yuc5-1* (SAIL\_116\_C0). Oligonucleotides used for genotyping are listed in Table M1.

Seeds were size selected and surface-sterilised using 70% (v/v) ethanol and 0.05% (v/v) Triton X-100 for 3 min followed by 10 min incubation in 100% (v/v) ethanol. Seeds were sowed on 1/2 Murashige and Skoog medium (1/2MS) containing 0.8% (w/v) phytoagar (Agar-Agar, plant; Roth) and subsequently stratified at 4 °C for 3 day in darkness. For experiments where seedlings were grown on vertical plates the phytoagar concentration was raised to 1.6% (w/v). For all experiments, seedlings were grown in 16h/8h, light/dark photoperiod (LD) at 21 °C in a Percival Scientific Model AR-22L (Perry, IA, USA) incubator. WL was emitted from white fluorescence tubes (Lumilux cool white 18W/840) at a fluence rate of 130  $\mu\text{mol m}^{-2}\text{s}^{-1}$  and LRFRL was achieved by supplementing WL with 45  $\mu\text{mol m}^{-2}\text{s}^{-1}$  FR light (LEDs) lowering the R (640–700 nm)/FR (700–760 nm) from 1.4 to 0.2, as measured by Ocean Optics USB2000+ spectrometer. The double layer of yellow filter (010 medium yellow, LEE Filters) lowering blue light from 7  $\mu\text{mol m}^{-2}\text{s}^{-1}$  (WL) to 0.5  $\mu\text{mol m}^{-2}\text{s}^{-1}$  (LB) used to cover up the seedlings for LB

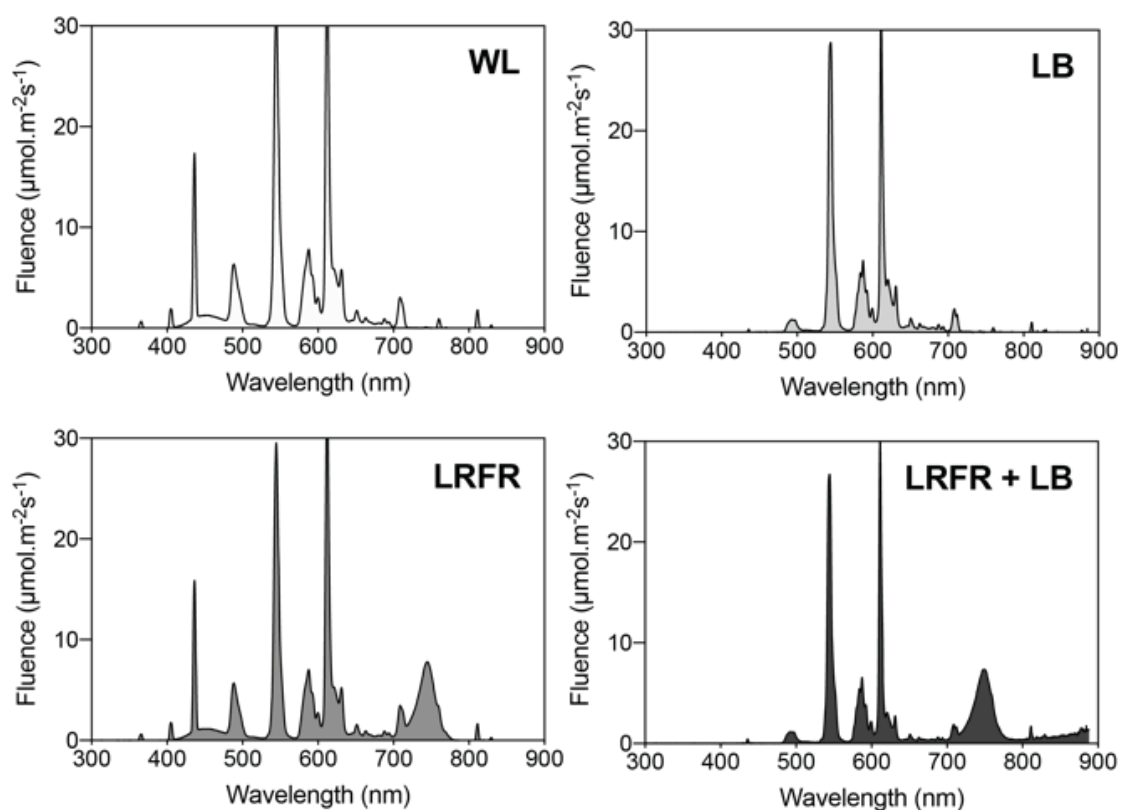


**Figure M1. Light spectra of the conditions used in this study.**

The light spectra were obtained using the Ocean Optics USB2000+ spectrometer.

treatments. The light spectra are shown in Figure M1. Unless otherwise stated, seedlings were grown for 4 days in WL and subsequently kept in WL or transferred to LB or LRFR for additional 3 days. Pharmacological treatments were done on vertically grown seedlings on nylon meshes. After 4 days in WL the seedling on nylon meshes were transferred to new plates containing the drug or the corresponding solvent and put for 3 additional days into WL or LRFR. Fenpropimorph (Carbosynth, United Kingdom, FF23264), picloram (Sigma-Aldrich, Steinheim, Germany, P5575), di-4-ANEPPDHQ (Thermo Fisher Scientific, United States, D36802), Concanamycin A (Sigma-Aldrich, Steinheim, Germany, C9705) were dissolved in DMSO (dimethylsulfoxide) and applied at the indicated concentrations in Figure legends (0.1% DMSO for mock). Estradiol (Sigma-Aldrich, Steinheim, Germany, E1024) was used at a concentration of 10  $\mu\text{M}$  and

dissolved in ethanol. Esculin (Sigma-Aldrich, Steinheim, Germany, E8250) is dissolved in H<sub>2</sub>O at 70 °C and applied immediately.

Seedlings imaging and measurements were described previously (de Wit et al., 2018)

### **Constructs cloning**

PCR amplifications were performed using Phusion® High-Fidelity DNA Polymerase (New England Biolabs, Massachusetts, USA, Cat. No. M0530). All clonings were done using In Fusion® HD Cloning kit (Takara, California, USA; Cat. No. 639649). First, GUSPlus::tOCS was cloned in *pFP100* plasmid carrying *pAt2S3::GFP* selection marker (Bensmihen et al., 2004) and the new plasmid was named as *pYI001*. *pFR06* and *pGH3.17* were cloned into *pYI001* in order to obtain *pFR06::GUSPlus::tOCS* and *pGH3.17::GUSPlus::tOCS*, respectively. *pUBQ10::SMT2-Flag::tOCS* was cloned into *pFP100*, while *pFR06::SMT2-Flag*, and *pGH3.17::SMT2-Flag* were cloned into *pYI001*. The primers are listed in Table M2. These constructs were transformed into *smt2-1* plants using *Agrobacterium tumefaciens* GV3301 strain by floral dip (Clough & Bent, 1998).

### **RNA isolation, quantitative RT-PCR and RNA-sequencing**

For RNA isolation, 5d-old seedlings were harvested in liquid nitrogen and kept in -70 °C for overnight. Next day, seedlings were covered with -70 °C cold RNAlater™-ICE (Thermo Fisher Scientific, United States, AM7030) and transferred to -20 °C for overnight. Cotyledons and hypocotyls are dissected under binocular using sharp needles on top of an ice block under a dissecting microscope and RNA isolation and reverse transcription quantitative polymerase chain reaction (RT-qPCR) reactions were performed as previously described (Kohnen et al., 2016). Oligonucleotides are listed in Table M3.

For the RNA-sequencing, RNA quality was assessed on a Fragment Analyzer (Agilent Technologies). From 40 ng total RNA, mRNA was isolated with the NEBNext Poly(A) mRNA Magnetic Isolation Module. RNA-seq libraries were then

prepared from the mRNA using the NEBNext Ultra II Directional RNA Library Prep Kit for Illumina (New England Biolabs, Massachusetts, USA). Libraries were quantified by a fluorimetric method and their quality assessed on a Fragment Analyzer (Agilent Technologies). Cluster generation was performed with the resulting libraries using Illumina HiSeq 3000/4000 SR Cluster Kit reagents. Libraries were sequenced on the Illumina HiSeq 4000 with HiSeq 3000/4000 SBS Kit reagents for 150 cycles. Sequencing data were demultiplexed with the bcl2fastq Conversion Software (v. 2.20, Illumina; San Diego, California, USA).

**Table M1. List of oligonucleotides used for genotyping**

Allele*	Collection	Name	Sequence
<i>smt2-1</i> ( <i>fr1</i> )	EMS*	YI428	TCACCATCAATCCCCGGAAA
		YI429	CTGCGTACACTTCTCCAGC
		*PCR is followed by digestion with BsaHI	
<i>smt2-2</i> ( <i>cvp1-3</i> )	EMS**	YI426	CTCTCTTTGGTCTTCCTCACTCTTCACGAAAAT
		YI427	AACCAGTAGATACCGACGGCGAC
		**PCR is followed by digestion with MsiI	
<i>smt3-1</i>	SALK_08529 2	YI430	CATGATTTTATTTTGTGAAGAAAAATG
		YI431	CCAGCTTTCTTGTTGTGAAGC
<i>cvp2-1</i>	EMS***	OM181	CGG TGT ATC CAC GGG AGT AA
		OM182	CGC TTG TTG AGA TGC AGA AT
		***PCR is followed by digestion with BsiI	
<i>cv11-1</i>	SALK_02994 5	OM183	TGA TCA GAA AAC CGT GAC TCC
		OM184	AGC ACA TTT TTG AAT TCA CCG
<i>yuc5-1</i>	SAIL_116_C O1	MT458	GAATCCAGCCGCGTAAAGTC
		AG178	GACGAGACAAGTGGTCTCTGG
<i>atg7-2</i>	GABI_655B0 6	YI444	GGAGCTTAACAAAGGGAAACG
		YI445	CGTGTAACAGTGCATTGTTGG

\**yuc2-1*, *yuc8-1*, *yuc9-1*, *pif4-101*, *pif5-3*, and *pif7-1* primers were given in Ch. 1, Table S1 (Fiorucci et al. 2019)

**Table M2. List of oligonucleotides used in cloning**

Plasmid	Target	Name	Sequence
<i>pYI001</i> ( <i>GUSPlus::tOCS</i> in <i>pFP100</i> )*	<i>GUSPlus::tOCS</i>	YI001	TCAAGCTAAGCTTGCATGCCCGGAAAATGGT AGATCTGAGGGTAA
		YI002	CCTAAAACCAAATCCAGTGGCGCTCTAGAGG TCCTGCTGA
<i>pYI006</i> ( <i>pFRO6::GUSPI</i> <i>us::tOCS</i> )**	<i>pFRO6</i>	YI011	ATCCAAGCTCAAGCTAAGCTcgatgctctcaaggcc aa
		YI012	TAGAAATTTACCCTCAGATCTACCATctttattgaatt tccacttctc
<i>pYI012</i> ( <i>pGH3.17::GUSP</i> <i>lus::tOCS</i> )**	<i>pGH3.17</i>	YI020	ATCCAAGCTCAAGCTAAGCTCATAAACATTTAC CTTTCATGG
		YI024	TAGAAATTTACCCTCAGATCTACCATtTctgaaag cagacacaacaaagc
<i>pYI046</i> ( <i>pUBQ10::SMT2</i> <i>-FLAG::tOCS</i> )*	<i>pUBQ10</i>	YI052	ATCCAAGCTCAAGCTAAGCTTCGACGAGTCAG TAATAACGGC
		YI070	AAGAGTCCATTTTCCGCGGGctagtCTGTT
	<i>SMT2-FLAG</i>	YI071	CCCGCGGAAAATGGACTCTTTAACTCTTCT T
		YI072	TATCTCATTAAAGCAGGATCCTCACTTGTGCATC GTCGTCCTTGTAATCAGAACTCTCCTCCGGT
	<i>tOCS</i>	YI056	GTGAAGGATCCTGCTTTAATGAGA
		YI002	CCTAAAACCAAATCCAGTGGCGCTCTAGAGG TCCTGCTGA
<i>pYI047</i> ( <i>pFRO6::SMT2-</i> <i>FLAG::tOCS</i> )**	<i>pFRO6</i>	YI011	ATCCAAGCTCAAGCTAAGCTcgatgctctcaaggcca a
		YI073	AAGAGTCCATctttattgaatttccacttctcagtggtg
	<i>SMT2-FLAG</i>	YI074	tcaaataaagATGGACTCTTTAACTCTTCTTCA CC
		YI072	TATCTCATTAAAGCAGGATCCTCACTTGTGCATC GTCGTCCTTGTAATCAGAACTCTCCTCCGGT
<i>pYI048</i> ( <i>pGH3.17::SMT2</i> <i>-FLAG::tOCS</i> )**	<i>pGH3.17</i>	YI020	ATCCAAGCTCAAGCTAAGCTCATAAACATTTAC CTTTCATGG
		YI075	AAGAGTCCATtTctgaaagcagacacaacaaag
	<i>SMT2-FLAG</i>	YI076	ctttcagaAaATGGACTCTTTAACTCTTCTTTCAC CG
		YI072	TATCTCATTAAAGCAGGATCCTCACTTGTGCATC GTCGTCCTTGTAATCAGAACTCTCCTCCGGT
<b>Strategy *</b>	Digestion of pFP100 with KpnI and HindIII was followed by in fusion		
<b>Strategy **</b>	Digestion pYI001 with HindIII and BglII was followed by in fusion cloning		

**Table M3. List of oligonucleotides used in RT-qPCR**

Target*	Name	Sequence
<i>SMT2</i>	YI522	TACGAGTGGGTACGACGGA
	YI523	CGCCTCTCTCAATCCCTTGG
<i>SMT3</i>	YI528	TACCAAGTGCAACGAGCCAA
	YI529	ACGTGTTTTTCATCGAACGGC
<i>HFR1</i>	SL67	TGGCCATTACCACCGTTTAC
	SL68	ACCAAACCGTGAAGAGACTG
<i>XTH19</i>	MdW27	AGTCACGTGGAGTCCCATTTC
	MdW28	AATTTGCGGGACAACTGAC
<i>PIL1</i>	MT125	TCAGACTCAGGCTACTTCTTTTACTCA
	MT126	TCCTCTATATTGCATTGCATCTTCTAA
<i>AFB1</i>	SL170	GAGCTTCTTAGGCGATGCTC
	SL171	TCAGTTCTCGCAGTTCCTTG
<i>PIF4</i>	SL63	TTCTCCTCCCACCTTCTTCTC
	SL64	AGGTTTCAGGACTGGACTTAG
<i>PIF7</i>	SL194	GAGCAGCTCGCTAGGTACATG
	SL195	GTTGTTGTTGCACGGTCTG
<i>BrSMT2</i>	YI636	GCCGAGATCTACAGGGTGTT
	YI637	TTGGATGACCTCCACGTGTT
<i>BrSMT3</i>	YI640	GATGGGTCCGATTGCGTACT
	YI641	TCCCAACAGCAGACAGAACC
<i>BrSMT1</i>	YI650	GCCAGTCAGACAAGGAAGAT
	YI651	CCTCGTCGTACACAACAGAA
<i>BrIAA29</i>	YI668	TGCATTTGACCCTGACAACG
	YI669	TGGCCAGATCCTTTTCCCAT
<i>BrPP2A</i>	YI656	AACGCCCCCGATACGAATTA
	YI657	CCACGGTCTACATAGTCACCC

\**UBC*, *YLS8*, *CPD*, *IAA29*, and *SAUR22* primers are given in Ch. 1, Table S1 (Fiorucci et al., 2019)

**Table M4. List of oligonucleotides used in ChIP-qPCR**

Target*	Name	Sequence
<i>SMT2 (peak)</i>	YI633	AGGTCCCTAGAGTGAGGGTG
	YI634	CTCCACCACCACACGTGATT
<i>SMT2 (Control)</i>	YI522	TACGAGTGGGTTACGACGGA
	YI523	CGCCTCTCTCAATCCCTTGG
<i>SMT3 (Peak 1)</i>	YI653	GGTCCTTGGGGTATCCAATTAT
	YI654	GAGTCATGCATGTGATACGACC
<i>SMT3 (Peak 2)</i>	YI659	TTTTCCCTGCCTGACCCTTG
	YI660	GCAAAAATGAAGACGGATCATGG
<i>SMT3 (Control)</i>	YI528	TACCAAGTGCAACGAGCCAA
	YI529	ACGTGTTTTTCATCGAACGGC
<i>HFR1 (Peak)</i>	PH112	ACGTGATGCCCTCGTGATGGAC
	PH113	GTCGCTCGCTAAGACACCAAC
<i>HFR1 (Control)</i>	PH126	ACGCAACAAACGAACCACAC
	PH127	AGAGCGATCGGATCAGATAG
<i>PIL1 (Peak)</i>	PH78	GAATCACGCGGCATTAC
	PH79	ACCTTCACGCCATTATTAAGAC
<i>PIL1 (Control)</i>	PL8F	GGGATGAACAATGCACCACCACAA
	PL8R	AAACACACGAAGGCACCACGAATG

\* *IAA29* control and peak primers are given in Ch. 1, Table S1 (Fiorucci et al., 2019)

#### *RNA-seq initial data analysis*

Purity-filtered reads were adapters and quality trimmed with Cutadapt (v. 1.8) (Martin, 2011). Reads matching to ribosomal RNA sequences were removed with fastq\_screen (v. 0.11.1). Remaining reads were further filtered for low complexity with reaper (v. 15-065)(Davis et al., 2013). More than 30 million uniquely mapped reads were obtained per library and reads were aligned against *Arabidopsis thaliana.TAIR10.39* genome using STAR (v. 2.5.3a) (Dobin et al., 2013). The number of read counts per gene locus was summarised with htseq-count (v.

0.9.1)(Anders et al., 2015) using *Arabidopsis thaliana*.TAIR10.39 gene annotation. Quality of the RNA-seq data alignment was assessed using RSeQC (v. 2.3.7) (Wang et al., 2012)

Reads were also aligned to the *Arabidopsis thaliana*.TAIR10.39 transcriptome using STAR (v. 2.5.3a) (Dobin et al., 2013) and the estimation of the isoforms abundance was computed using RSEM (v. 1.2.31)(Li & Dewey, 2011).

Statistical analysis was performed for genes independently in R (R version 4.0.2). All steps described here were performed separately for the samples from hypocotyls and cotyledons (except for the initial clustering of all samples together). Genes with low counts were filtered out according to the rule of 1 count(s) per million (cpm) in at least 1 sample. The number of genes retained in the analyses based on this filtering is different for hypocotyls and cotyledons. Library sizes were scaled using TMM normalisation. Subsequently, the normalised counts were transformed to cpm values and a log<sub>2</sub> transformation was applied by means of the function `cpm` with the parameter setting `prior.counts = 1` (EdgeR v 3.30.3)(Robinson et al., 2010).

Differential expression was computed with the R Bioconductor package “limma” (Ritchie et al., 2015) by fitting data to a linear model. The approach `limma-trend` was used. Fold changes were computed and a moderated t-test was applied. P-values were adjusted using the Benjamini-Hochberg (BH) method, which controls for the false discovery rate (FDR). P-value adjustment was performed globally across 8 comparisons between light conditions. All steps including p-value adjustment were performed separately for the two organs, hypocotyls and cotyledons.

### **Gene set enrichment analysis for Gene Ontology**

Gene set enrichment analysis were conducted with ShinyGO v0.61:Gene Ontology Enrichment Analysis + more (<http://bioinformatics.sdstate.edu/go/>) (Ge et al., 2020) in *Arabidopsis thaliana* using a P-value cutoff (FDR) 0.05 and 500 most significant terms to show. The networks of enriched GO categories

were visualised with R software (<https://www.r-project.org/>) using visNetwork and igraph libraries. Two terms (nodes) were connected if they share 20% or more genes. The size of the nodes indicate the regulation factor (RF) which is calculated using the formula:

$$RF=5*(\log_2(FC)+(\log_2(-\log_2(FDR))),$$

where FC and FDR represents fold change and false discovery rate, respectively.

## **ChIP-qPCR**

10d-old seedlings with the indicated light treatments at the Figure legends were harvested in liquid nitrogen. Chromatin extraction was performed as described previously (Bourbousse et al., 2018) except that samples were cross-linked only with formaldehyde. Immuno-precipitation was performed as described previously (Gendrel et al., 2005) using an anti-HA antibody (Santa Cruz Biotechnology, Inc., Dallas, TX, USA; sc-7392 X). The qPCR was done in triplicates or quadruplicate on input and immunoprecipitated DNA. Oligonucleotides are listed in Table M4.

## **Western-blot analysis**

Total protein extracts from seedlings were obtained as previously described (Galvao et al., 2019). Protein samples were separated on 4–20% Mini-Protean TGX gels (Bio-Rad, Hercules, CA, USA) and blotted on nitrocellulose membrane (Bio- Rad) using Turbo transfer system (Bio-Rad). Membranes were blocked with 5% milk overnight at 4°C or 1h at room temperature for Anti-GFP JL-8 (1:4000; Clontech, California, USA; Cat. No. 632380/632381), polyclonal H3 (1:2000; Abcam, Cambridge, UK; Cat. No.1791), Anti-FLAG M2 (1:1000; Sigma, Missouri, USA; Cat. No. F1804) antibodies before probing with horseradish peroxidase (HRP)-conjugated anti-rabbit (for H3) or anti-mouse (for anti-GFP and anti-FLAG) as the secondary antibody (1:5000; Promega, Madison, USA; Cat. No. W4011 and W4021, respectively). Chemiluminescence signal were obtained with Immobilon Western Chemiluminescent HRP Substrate (Millipore, Merck KGaA,

Darmstadt, Germany) on an ImageQuant LAS 4000 mini (GE Healthcare, Buckinghamshire, UK).

## **Microscopy and GUS Staining**

DII-Venus microscopy and image quantification were performed as indicated in (Kohnen et al., 2016).

For the membrane fluidity measurements, hypocotyls were dissected with a sharp razor from the seedlings grown as indicated in the Figure legends. All subsequent steps were done in dark. Hypocotyls were put in ice-cold di-4-ANEPPDHQ (2 mg/L) solution and vacuumed for 2 times 10 minutes. The hypocotyls were then mounted on a microscope slide with H<sub>2</sub>O and imaged immediately. The microscope used is an inverted Zeiss confocal microscope (LSM 710 INVERTED, × 40 objective with oil). di-4-ANEPPDHQ signal was detected using an Argon laser (excitation at 488 nm and band pass emission between 580 to 640 nm to visualise the total signal, 540 to 560 nm for green, 650 to 670 nm for red channel). Image stacks were acquired for every hypocotyl. The pinhole was opened to 1 Airy Units (0.9 μm section). Images were processed with ImageJ software (<http://rsb.info.nih.gov/ij>). To quantify the di-4-ANEPPDHQ signal, we selected a ROI on the plasma membrane from 20 different regions. The membrane fluidity was calculated as RGM (for the red/green ratio of the membrane).

For esculin transport assays, seedlings grown as indicated in Figure legends were treated with 2h of WL or LRFR. Then, cotyledons were cut in half and 0.5 μL of esculin dye (10 mg/mL) dissolved in 70 °C H<sub>2</sub>O was applied to the cut. Seedlings were further kept on the indicated light conditions another 30 min. For microscopy, seedlings were washed in H<sub>2</sub>O for 1 min and mounted on a microscopy slide and immediately imaged. The microscope used is an inverted Zeiss confocal microscope (LSM 710 INVERTED, × 20 objective). Esculin signal was detected using a Diode 405-30 laser (excitation at 405 nm and band pass emission between 415 to 715 nm). The pinhole was opened to maximum (14.5

Airy Units = 48.9  $\mu\text{m}$  section) to collect the maximal signal intensity. Images were processed with ImageJ software (<http://rsb.info.nih.gov/ij>). To quantify the esculin signal, we selected a ROI on the vasculature and epidermis from 10 different regions. The epidermis intensity is used as a background signal and subtracted from the corresponding vasculature intensity.

For GFP microscopy, seedlings grown as indicated in Figure legends. The microscope used is an inverted Zeiss confocal microscope (LSM 710 INVERTED,  $\times 40$  objective with oil). GFP signal was detected using an Argon laser (excitation at 488 nm and band pass emission between 505 and 550 nm). The pinhole was opened to 1.3 Airy Unit (0.9  $\mu\text{m}$  section).

The protocol for GUS staining reactions was described in (Galvao et al., 2019). Cotyledons were prepared for cotyledon vasculature imaging as described in (Carland, 2002). GUS staining and cotyledon vasculature were imaged using a dissecting microscope (Nikon SMZ1500).

### **Sterol measurements**

4 hypocotyls from 5d-old *B. rapa* seedlings per sample are pooled and frozen in liquid nitrogen immediately after fresh weights are recorded. Samples were heated for 1h in EtOH with 1% H<sub>2</sub>SO<sub>4</sub> at 85°C. Sterols were extracted in hexane. Free hydroxyl groups were derivatised at 110°C for 30 min, surplus BSTFA-trimethylchlorosilane was evaporated and samples were dissolved in hexane for analysis using GC-MS under the same conditions as described (Cacas et al., 2016). Quantification of sterols was based on peak areas, which were derived from total ion current and using cholestanol as internal standard. Each sterol was normalised to the total amount of detected sterols and presented as percentage of total.

### **Lipidomics**

4 hypocotyls from 5d-old *B. rapa* seedlings per sample are pooled and preheated isopropanol 75 °C was added immediately after fresh weights are recorded. Each sample with isopropanol was incubated at 75 °C for 15 min and

cooled to room temperature. Samples were kept at 4 °C overnight and isopropanol was first evaporated to dryness using Nitrogen steam. Lipids were extracted by the addition of 200 µL of IPA/SPLASH® LIPIDOMIX® Mass Spec Standard (92/8; v/v). This solution containing was further homogenised in the Cryolys Precellys 24 sample Homogeniser (2 x 20 seconds at 10000 rpm, Bertin Technologies, Rockville, MD , US) with ceramic beads. The bead beater was air-cooled down at a flow rate of 110 L/min at 6 bar. Homogenised extracts were centrifuged for 15 minutes at 21000 g at 4°C (Hermle, Gosheim, Germany) and the resulting supernatant was collected and transferred to an LC-MS vial.

#### *Untargeted lipidomics analysis*

Extracted samples were analysed by reversed phase liquid chromatography coupled to high resolution mass spectrometry (RPLC-HRMS) instrument (Agilent 6550 IonFunnel QTOF).

In both, positive and negative ionisation mode, the chromatographic separation was carried out on an Zorbax Eclipse Plus C18 (1.8 µm, 100 mm × 2.1 mm I.D. column) (Agilent technologies, USA). Mobile phase was composed of A = 60:40 (v/v) Acetonitrile:water with 10 mM ammonium acetate and 0.1% acetic acid and B = 88:10:2 Isopropanol:acetonitrile:water with 10 mM ammonium acetate and 0.1% acetic acid. The linear gradient elution from 15% to 30% B was applied for 2 minutes, then from 30% to 48% B for 0.5 minutes, from 48% to 72% B and last gradient step from 72% to 99% B followed by 0.5 minutes isocratic conditions and a 3 min re-equilibration to the initial chromatographic conditions. The flow rate was 600 µL/min, column temperature 60 °C and sample injection volume 2µl.

ESI source conditions were set as follows: dry gas temperature 200 °C, nebulizer 35 psi and flow 14 L/min, sheath gas temperature 300 °C and flow 11 L/min, nozzle voltage 1000 V, and capillary voltage +/- 3500 V. Fullscan acquisition mode in the mass range of 100 – 1700 m/z was applied for data acquisition while

iterative MS/MS data dependent scan acquisition mode was applied for MS/MS data acquisition.

Pooled QC samples (representative of the entire sample set) were analysed periodically (every 6 samples) throughout the overall analytical run in order to assess the quality of the data, correct the signal intensity drift (*if any, this drift is inherent to LC-MS technique and MS detector due to sample interaction with the instrument over time*) and remove the peaks with poor reproducibility (CV > 25%) (Dunn et al., 2011). In addition, a series of diluted quality controls (dQC) were prepared by dilution with buthanol:methanol: 100% QC, 50%QC, 25%QC, 12.5%QC and 6.25%QC and analysed at the beginning and at the end of the sample batch. This QC dilution series served as a linearity filter to remove the features which don't respond linearly (correlation with dilution factor is < 0.65) (Gagnebin et al., 2017).

#### *Data processing*

Raw LC-HRMS and MS/MS data was processed using MS-Dial software (Tsugawa et al., 2015)

([http://prime.psc.riken.jp/Metabolomics\\_Software/MS-DIAL/](http://prime.psc.riken.jp/Metabolomics_Software/MS-DIAL/)). Relative quantification of lipids was based on EIC (Extracted Ion Chromatogram) areas for the monitored precursor ions at the MS1 level. *Peak areas were normalised considering the sample amount (mg)*. The obtained tables (containing peak areas of detected and identified lipids by MS and MS/MS and MS only across all samples) were exported to "R" software <http://cran.r-project.org/> where the signal intensity drift correction was done within the LOWESS/Spline normalisation program (Tsugawa et al., 2015) followed by noise filtering (CV (QC features) > 30%) and visual inspection of linear response.

The amount of each lipid species was normalised to the total amount of detected lipids and presented as percentage of total.

## **Statistical analysis**

For the phenotypic analyses, the comparison of relative esculin density, and the PM fluidity, we performed two-way analysis of variance (ANOVA) (aov) and computed Tukey's Honest Significance Differences (HSD) test (AGRICOLAE package) with default parameters using R software (<https://www.r-project.org/>). For the all other comparisons including qPCR, CHIP-qPCR, relative Dll signal, sterol measurements, and lipidomics analysis, we performed Student's T-test with or without Benjamini Hochberg correction (FDR) as indicated in the figure legends. We used Fisher's test with Benjamini Hochberg correction for the term enrichment analysis for the main lipid classes.

## SUPPLEMENTARY FIGURES

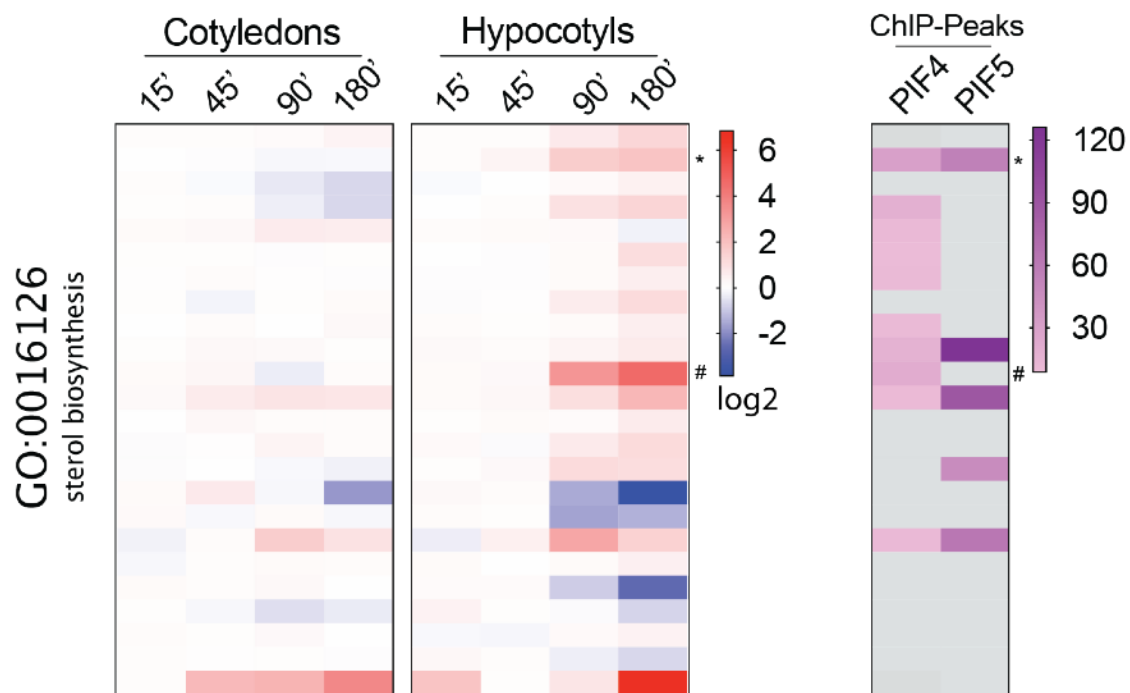


**Figure S1. Sterol biosynthesis related genes are induced in LRFR in hypocotyls.**

Relative expression (left) of genes annotated in sterol biosynthesis (GO: 0016126) in hypocotyls and cotyledons of 5-d-old seedlings after indicated times of LRFR treatment and putative binding of PIF4 and PIF5 to their promoter regions (right). Legends indicate the log2 fold change in LRFR and maximum peak height, respectively. Asterisks (\*) and hashes (#) mark *SMT2* and *SMT3*, respectively. 24 genes that are significantly regulated at 180' hypocotyl (FDR < 0.05, out of 33 annotated genes in the category) are shown (ordered according to their average expression from top to bottom). Expression data is from (Kohnen et al., 2016), PIF4 ChIP-seq data is from (Oh et al., 2012); PIF5 ChIP-seq data is from (Hornitshcek et al., 2012).

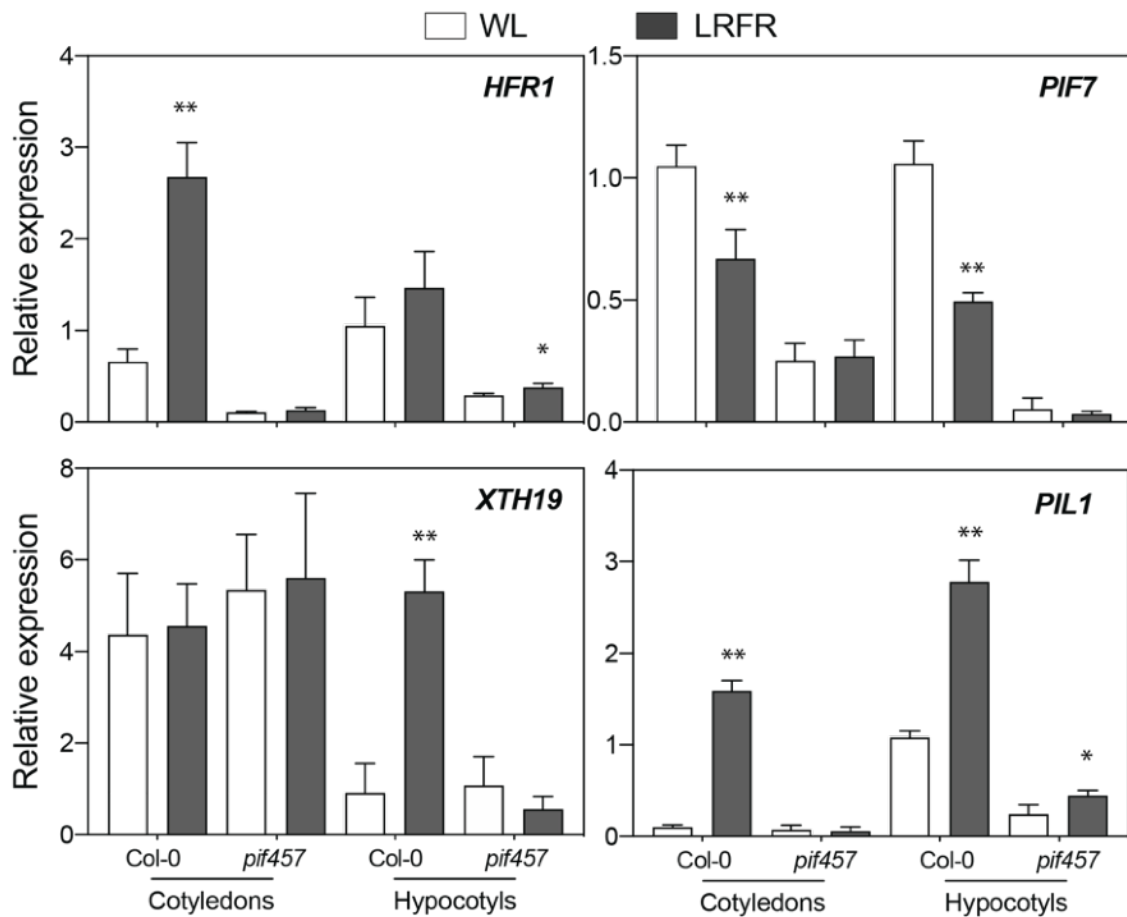


**Figure S2. Organ-specific expression of shade control genes.**

Relative expression of the indicated genes in hypocotyls and cotyledons of 5-d-old seedlings of the indicated genotypes 3h after transferred to LRFR obtained by RT-qPCR. Data are means, error bars indicate SD. Asterisks (\*) indicate the statistical significance compared to WL (Student's T-test, \* < 0.05, \*\* < 0.01, n = 3). Related to Fig. 3.

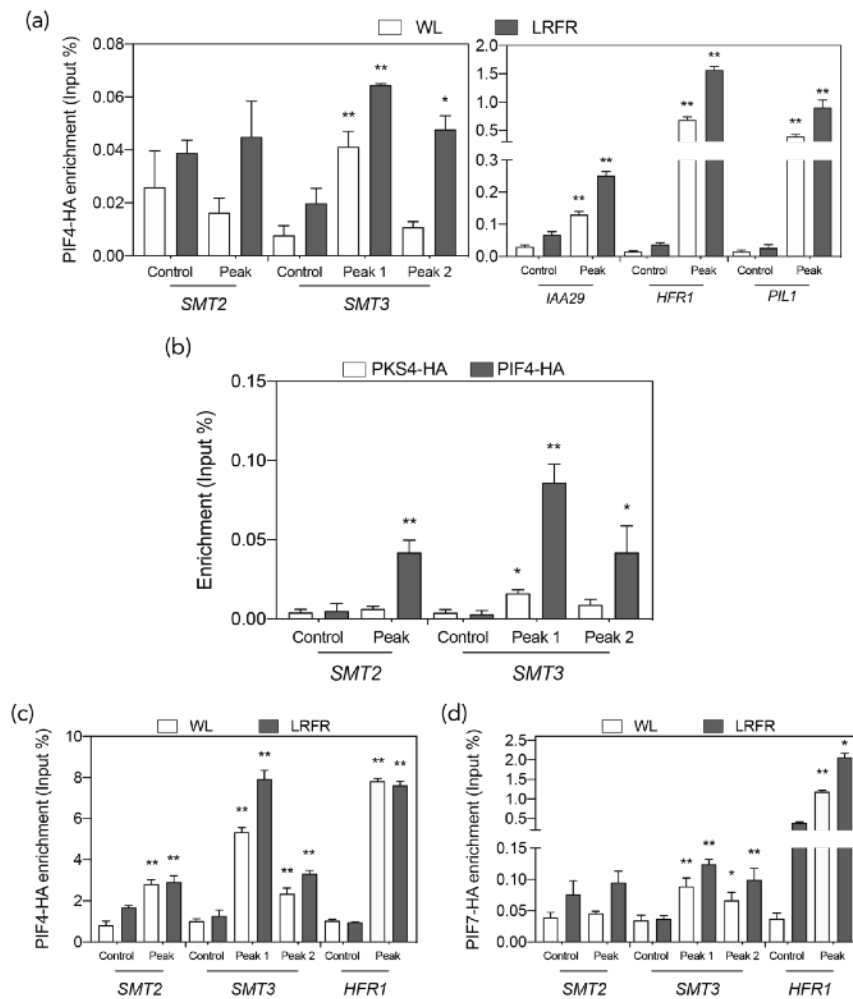


**Figure S3. PIFs bind to *SMT2* and *SMT3* promoters.**

(a) PIF4-HA binding to the promoter of indicated genes evaluated by ChIP-qPCR in 10-d-old *PIF4::PIF4-HA* (*pif4-101*) seedlings either kept at WL or transferred for 2h to LRFR at ZT2. (b) PIF4-HA and PKS4-HA (as negative control) binding to the promoter of *SMT2* and *SMT3* evaluated by ChIP-qPCR in 10-d-old *PIF4::PIF4-HA* (*pif4-101*) seedlings transferred for 2h to LRFR at ZT2 (control genes are published in Guadalupe et al. 2020). (c) PIF4-HA and (d) PIF7-HA binding to the promoter of *SMT2* and *SMT3* evaluated by ChIP-qPCR in 10-d-old (c) *35S::PIF4-HA* (Col-0) and (d) *PIF7::PIF7-HA* (*pif7-2*) seedlings either kept at WL or transferred for 5d to LRFR at ZT2. Input and immunoprecipitated DNA were quantified by qPCR using primers on ‘Peak’ where PIF4 binding was identified before on 5’ region of each gene (Oh et al. 2012) and ‘Control’ primers from coding regions of each gene. The enrichment is presented as IP/Input and error bars show standard deviation from two to four technical replicas. Asterisks (\*) indicate the statistical significance compared to control regions (Student’s T-test, \* < 0.05, \*\* < 0.01). Related to Fig. 3.

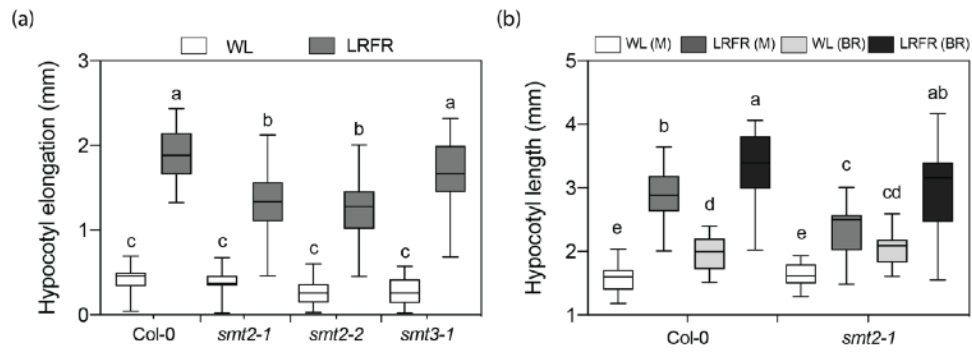


**Figure S4. Hypocotyl elongation of *smt* mutants in LRFR and in BR.**

(a) Hypocotyl elongation of the indicated genotypes grown as in Fig. 2. Elongation during the last 3 d is indicated. (b) Hypocotyl length (7d) of the indicated genotypes treated with BR (1000 nM) or mock. Seedlings were grown as in Fig. 2. Different letters indicate significant difference (two-way ANOVA with Tukey's HSD test,  $P < 0.05$ ,  $n > 12$ ). Related to Fig. 4

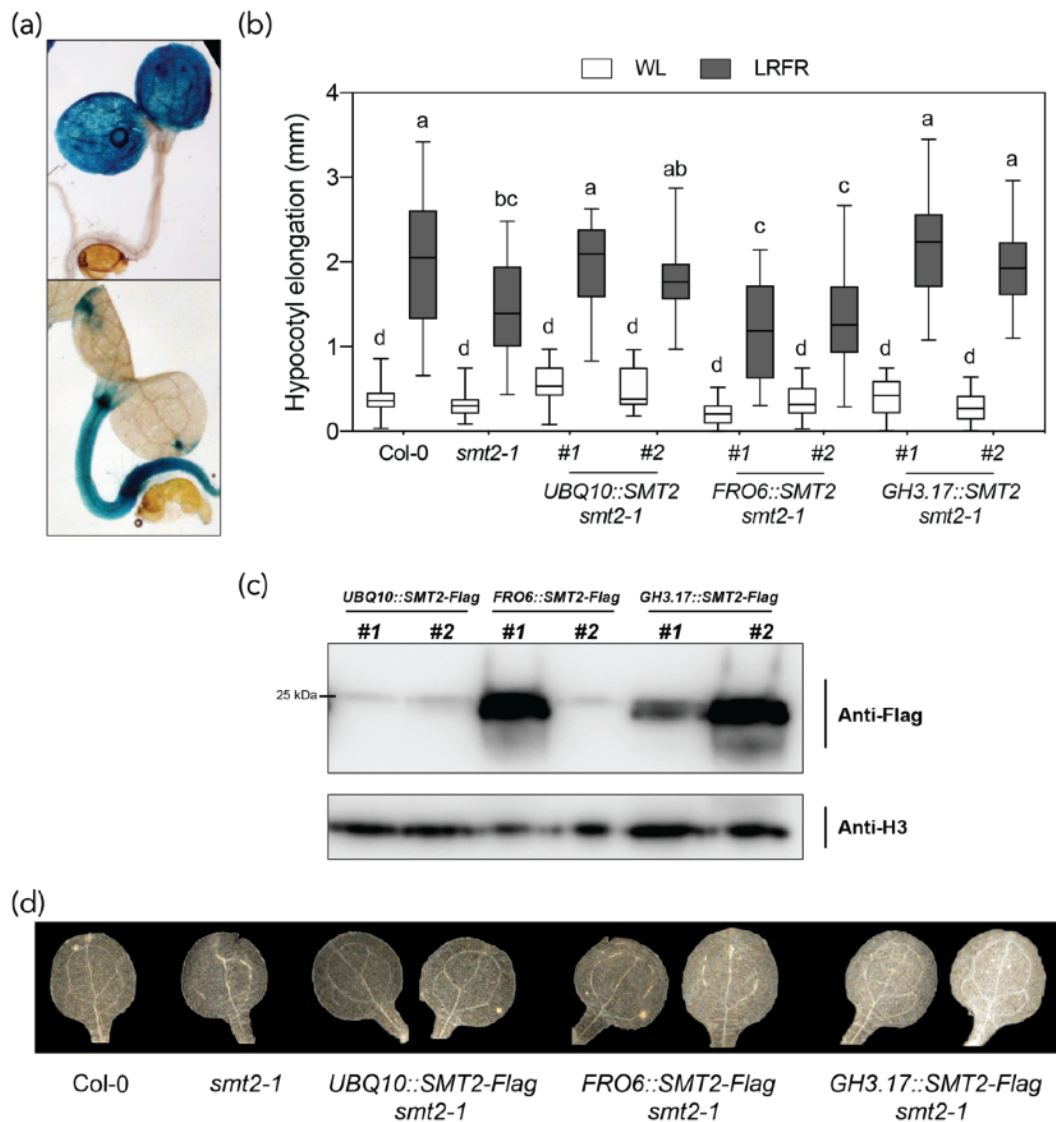


**Figure S5. Hypocotyl specific complementation of *SMT2* rescues *smt2-1* mutant hypocotyl elongation in LRFR.**

(a) GUS staining of 7d old seedlings with cotyledon specific promoter *FRO6::GUSPlus* (top) and hypocotyl specific promoter *GH3.17::GUSPlus* (bottom). (b) Hypocotyl elongation of *UBQ10::SMT2-Flag*, *FRO6::SMT2-Flag*, and *GH3.17::SMT2-Flag* in *smt2-1* background for two independent single insertion lines for each. Seedlings were grown as in Fig 2. Elongation during the last 3 d is indicated. Different letters indicate significant difference (two-way ANOVA with Tukey's HSD test,  $P < 0.05$ ,  $n > 12$ ). (c) SMT2-Flag levels are detected with an anti-flag antibody from the total protein extract from 7 d old LD-grown seedlings. H3 was used as a loading control. (d) Representative images of cotyledon vasculature phenotype of indicated genotypes and complementation lines. Related to Fig 4.

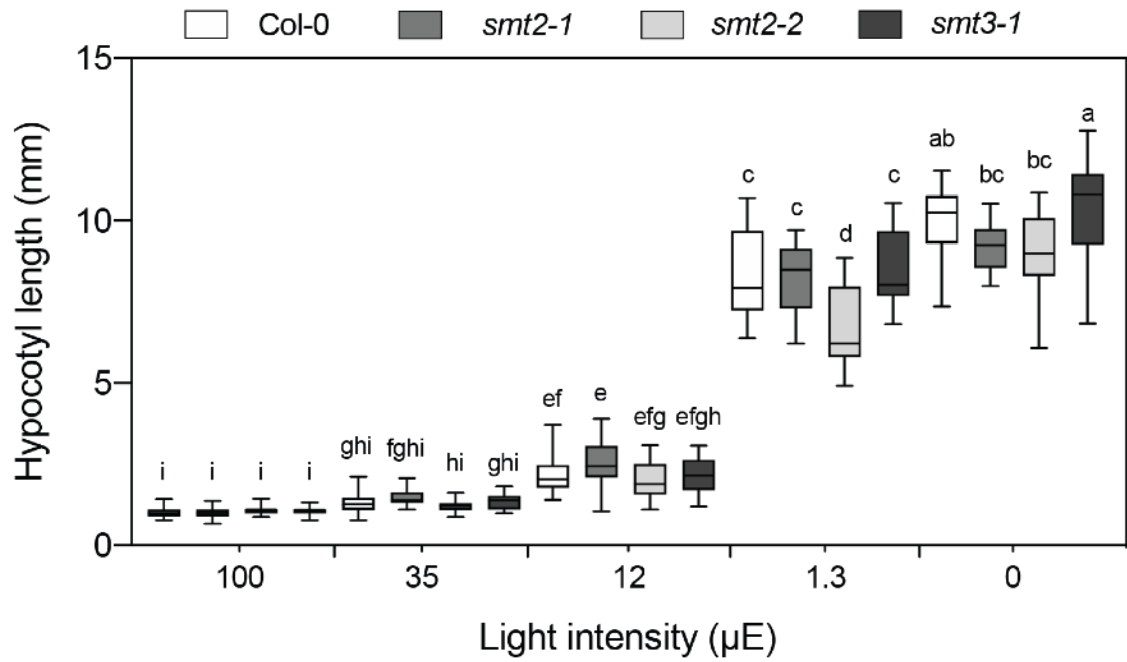


**Figure S6. Hypocotyl elongation of *smt* mutants are not impaired in cFR.**

Hypocotyl length of the indicated genotypes treated 6h with WL and then transferred to continuous FR with the indicated intensities for 4 d. Different letters indicate significant difference (two-way ANOVA with Tukey's HSD test,  $P < 0.05$ ,  $n > 12$ ).

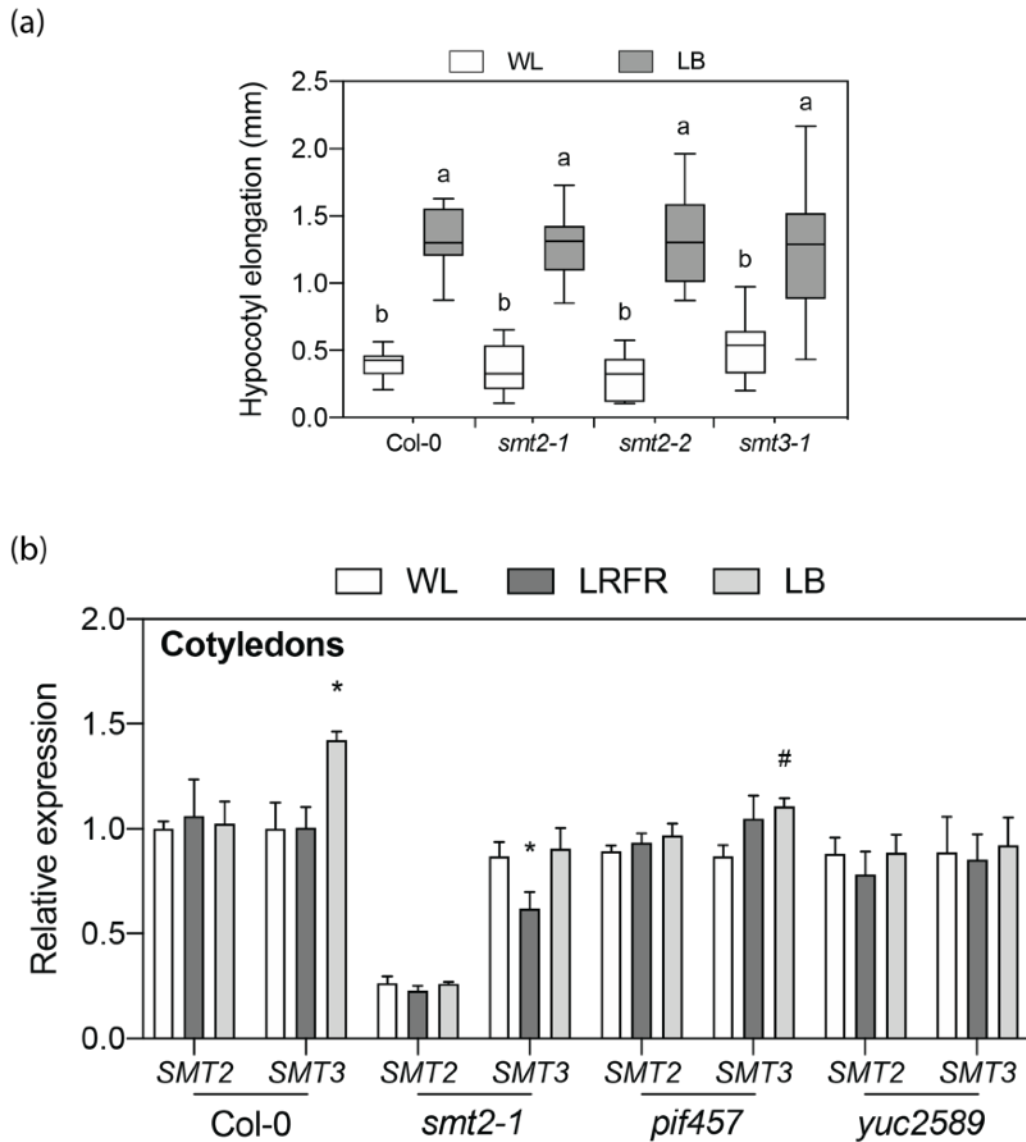


**Figure S7. Hypocotyl elongation of *smt* mutants are not impaired in LB.**

(a) Hypocotyl elongation of the indicated genotypes grown as in Fig. 2. Elongation during the last 3 d is indicated. Different letters indicate significant difference (two-way ANOVA with Tukey's HSD test,  $P < 0.05$ ,  $n > 12$ ). (b) Relative expression of *SMTs* in cotyledons of 5-d-old Col-0 seedlings 3h after transferred to LB or LRFR obtained from the RNA-seq analysis. Data are means, error bars indicate SD. Asterisks (\*) and hash (#) indicate the statistical significance compared to WL (FDR value,  $* < 0.05$ ,  $\# < 0.1$ ). Related to Fig. 5.

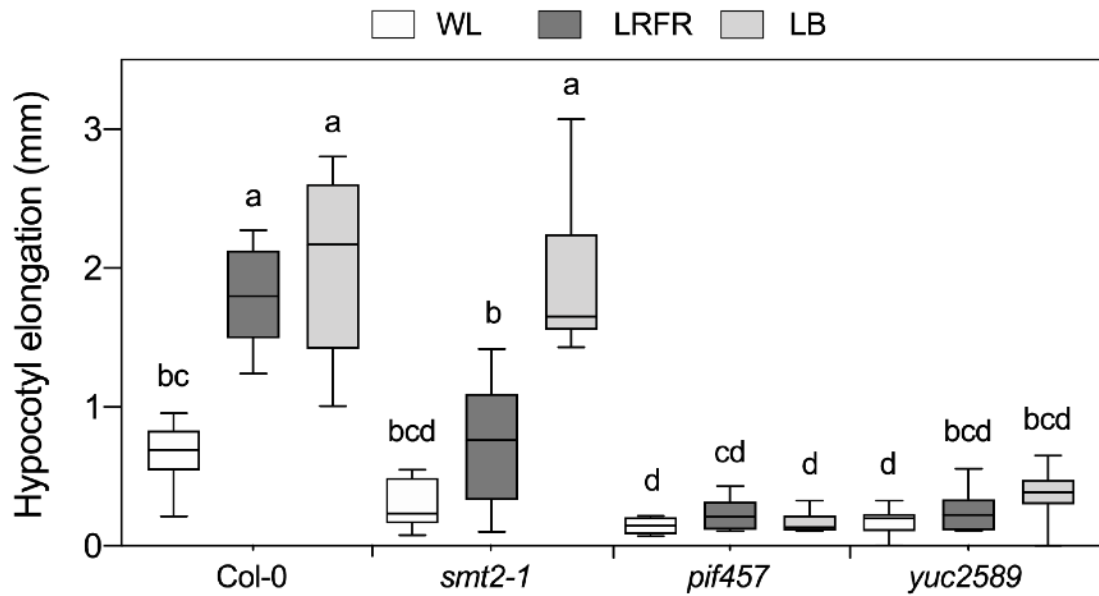


**Figure S8. Phenotypic evaluation of genotypes used in RNA-seq analysis.**

Hypocotyl elongation of the indicated genotypes grown in long days (LDs) at WL for 5 d then either kept at WL or transferred to LRFR or LB (at ZT2 on day 6) for three additional days. Elongation during the last 3 d is indicated. Different letters indicate significant difference (two-way ANOVA with Tukey's HSD test,  $P < 0.05$ ,  $n > 12$ ). Related to Fig. 6, 7 and 8.

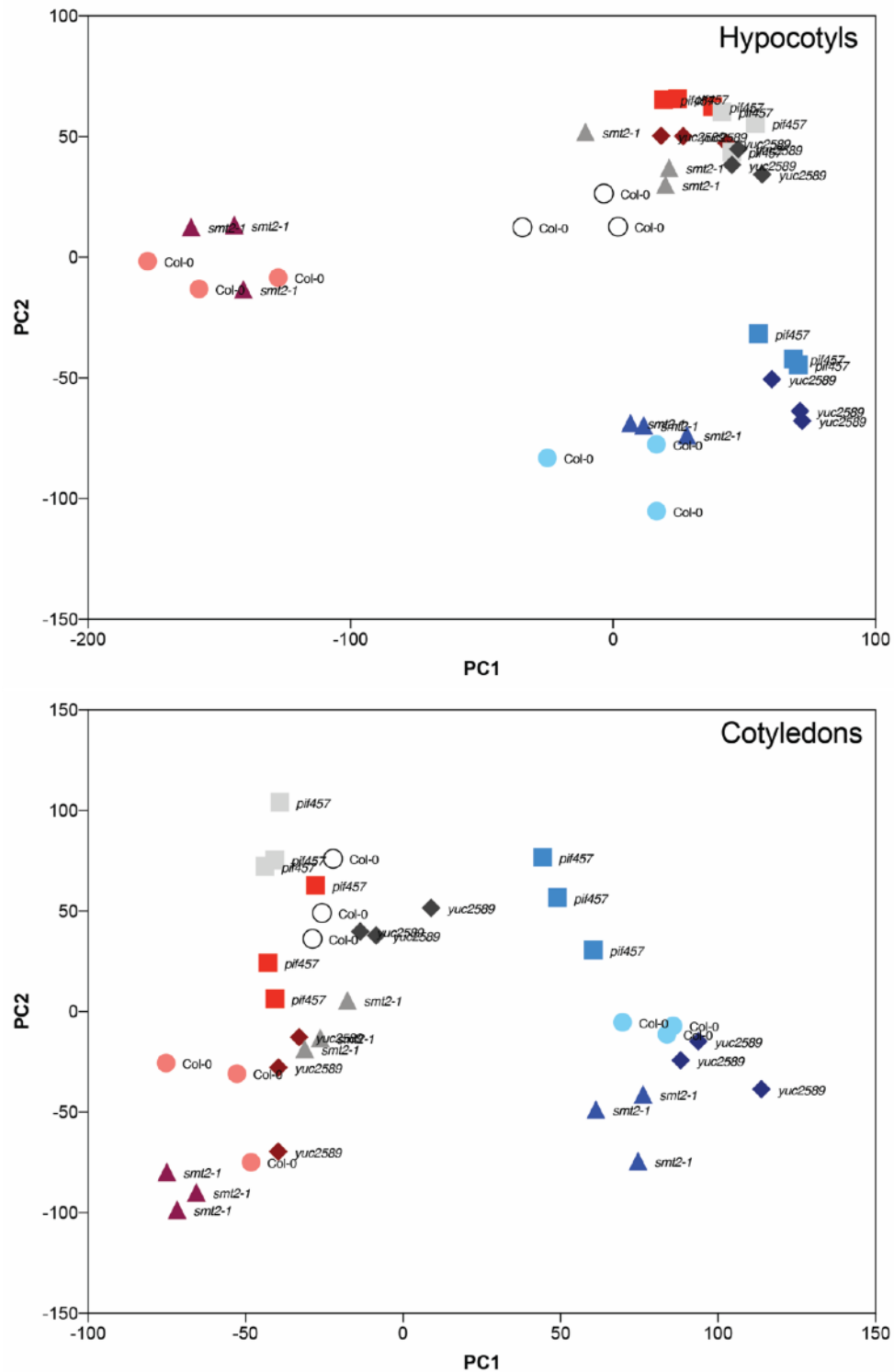
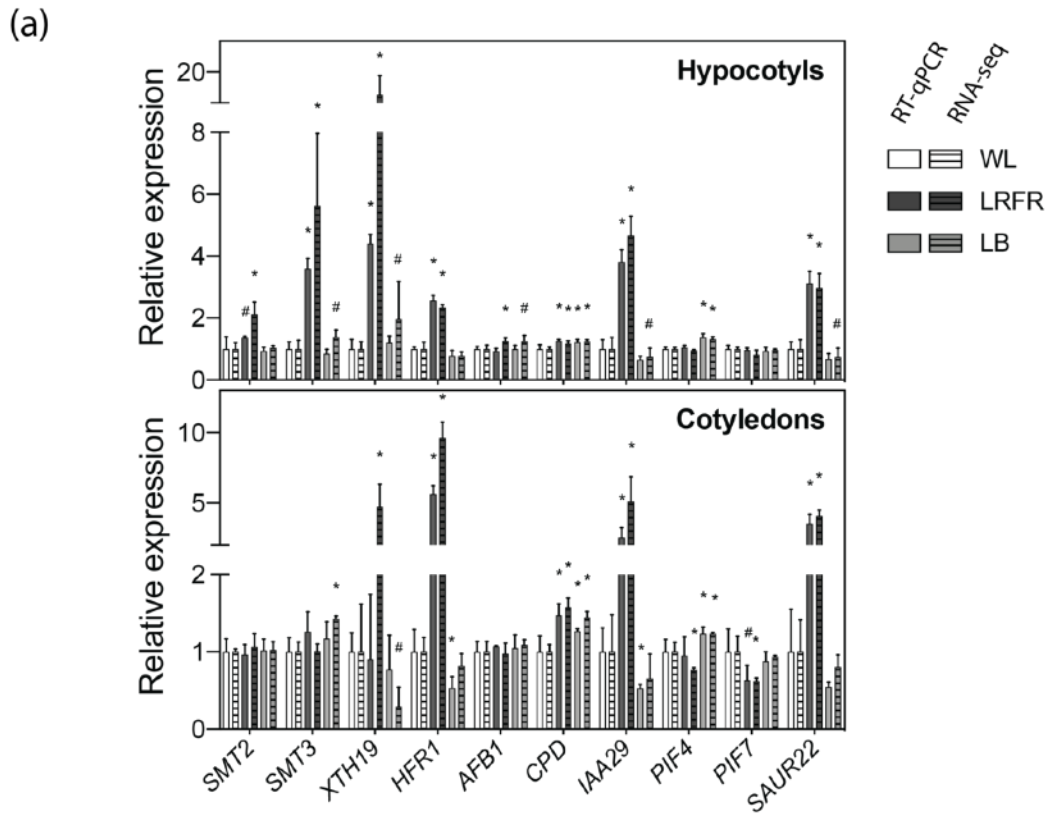


**Figure S9. Principle component analysis of hypocotyl and cotyledon transcriptomes.**

Principle component (PC) 1 and PC2 of each biological replicate ( $n = 3$ ) are graphically visualised. Grey, red and blue tones indicate WL, LRFR, and LB light treatments, respectively. [Related to Fig. 6, 7 and 8.](#)



(b)

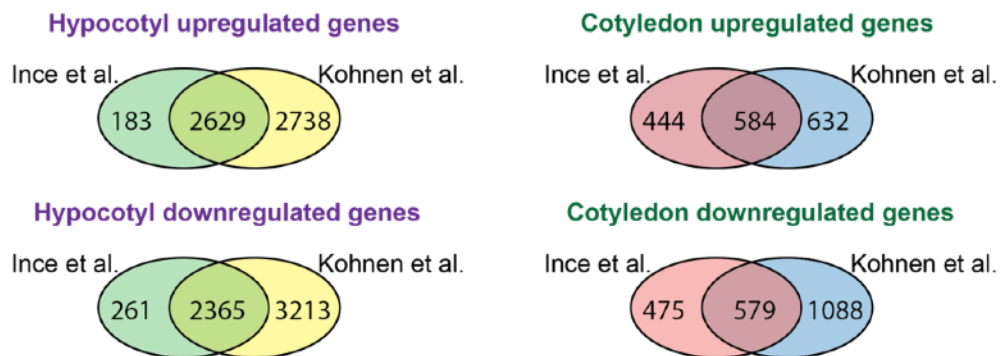


**Figure S10. Validation of RNA-seq data.**

(a) Relative expression of *SMT5* and the selected control genes in hypocotyls and cotyledons of 5-d-old Col-0 seedlings 3h after transferred to LB or LRFR. RT-qPCR results from 3 independent biological replicates are shown side by side to RNA-seq results. Data are means, error bars indicate SD. Asterisks (\*) and hashes (#) indicate the statistical significance compared to WL (Student's T-test, \* < 0.05, # < 0.1, n = 3). (b) Comparison of LRFR transcriptome obtained in this study and previously reported LRFR transcriptome in Col-0 (Kohnen et al. 2016). All significantly regulated genes are compared without any fold change cut-off (FDR < 0.05, Benjamini Hochberg correction using global adjustment). Related to Fig. 6.

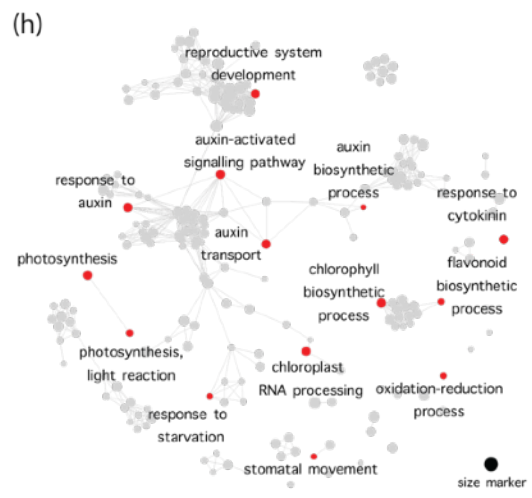
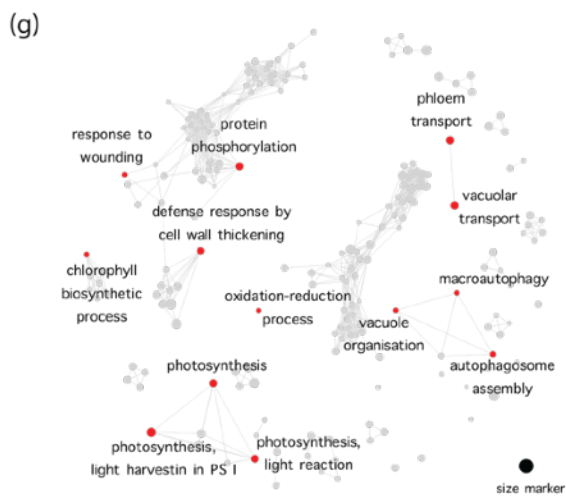
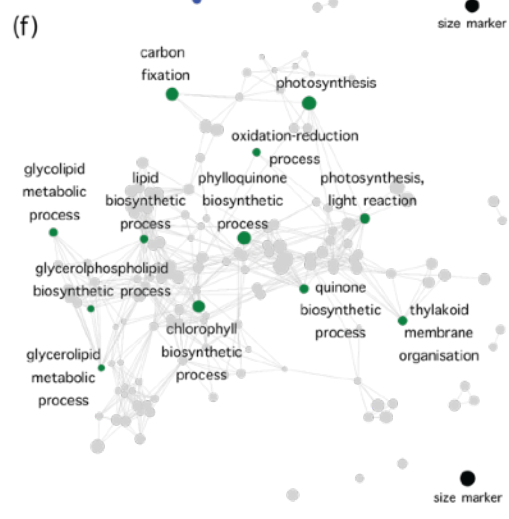
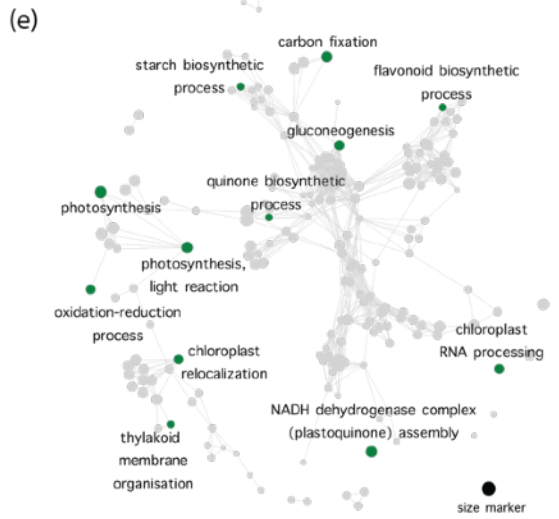
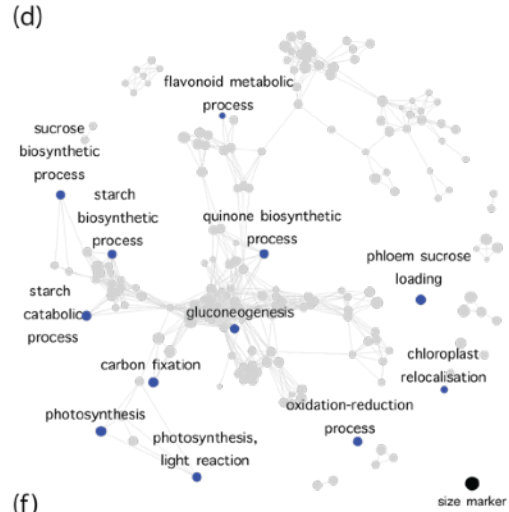
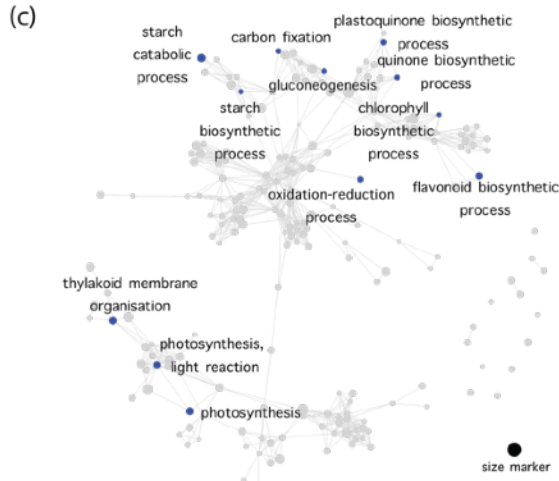
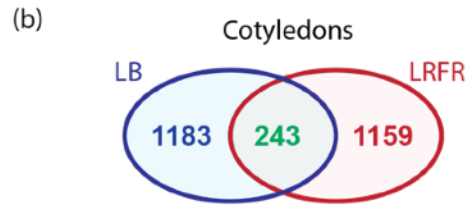
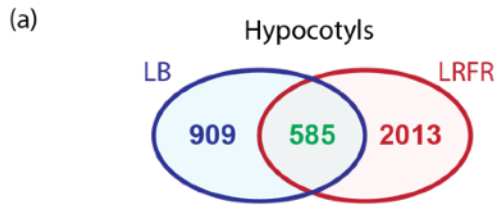


**Figure S11. Similarities and differences in LB and LRFR transcriptomes (downregulated genes).**

Venn diagrams showing the shared and specifically downregulated genes (FDR < 0.05) in LB and LRFR in hypocotyls (a) and cotyledons (b) of Col-0. GO term enrichment analysis from the hypocotyl LB-specific (c), LB and LRFR shared (e), and LRFR specific (g); and cotyledon LB-specific (d), LB and LRFR shared (f), and LRFR specific (h) gene lists. Each node indicates a significantly enriched GO term. Two terms (nodes) are connected if they share 20% or more genes. The size of the nodes indicates the regulation factor (RF) which is calculated as a function of FDR value and fold change enrichment of the corresponding GO term. Black nodes indicate a size marker with RF = 50. Only selected GO terms are annotated. *To see the full list of enriched GO terms, please download the interactive versions of (c-h) from [here](#). Related to Fig. 7.*

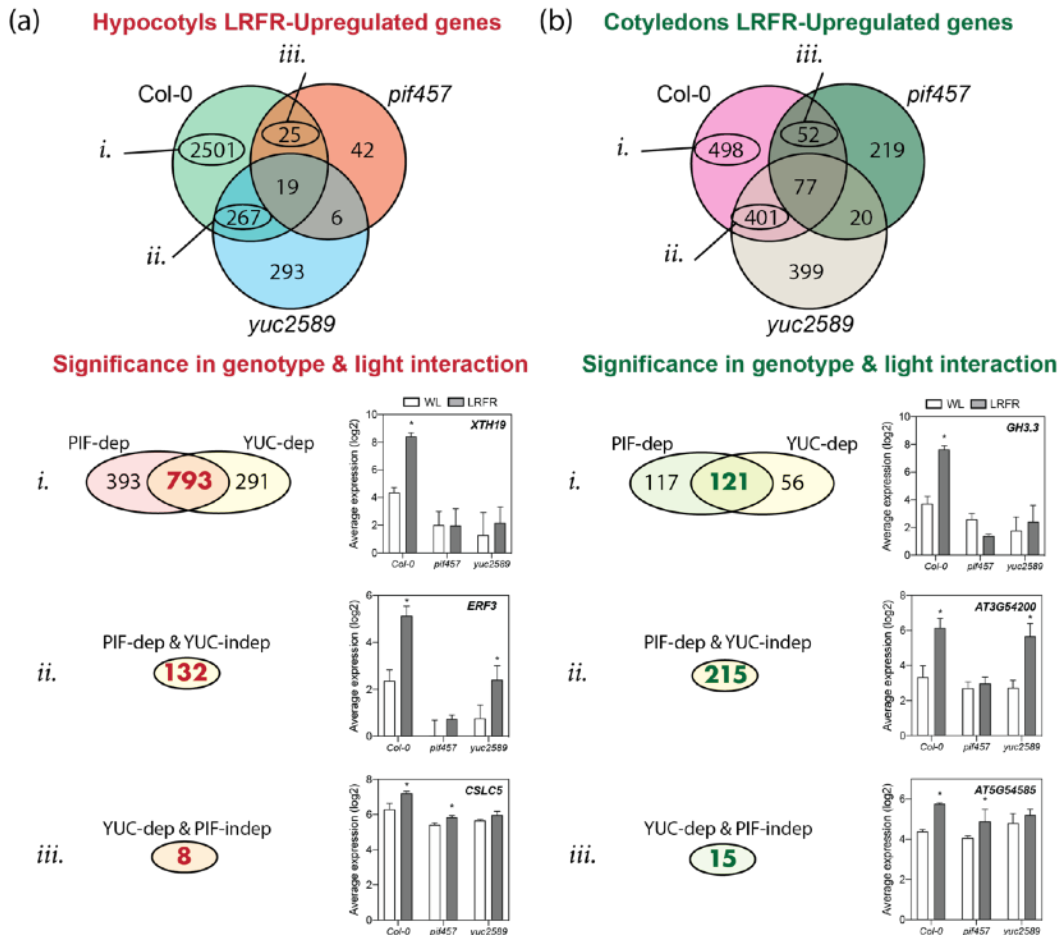
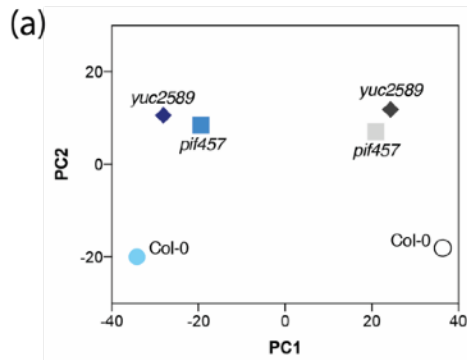


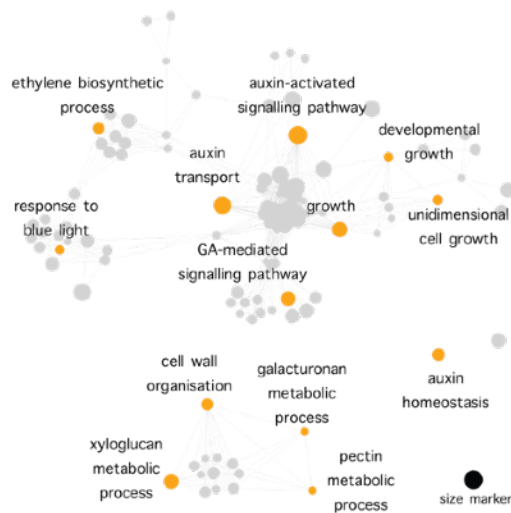
**Figure S12. Determining the PIF- and YUC- dependently and independently LRFR-regulated genes in hypocotyls.**

(a) and cotyledons (b). All significantly upregulated genes were listed using FDR values ( $< 0.05$ ) obtained from LRFR vs. WL comparison in the indicated genotypes. PIF- and YUC- dependent genes (i) were identified among the genes expression of which are significantly misregulated in *pif457* vs. Col-0 and *yuc2589* vs. Col-0 in the LRFR vs. WL (as listed in Fig. 8b). PIF-dependent and YUC-independent genes (ii) were selected using the criteria: upregulated in Col-0 and *yuc2589* but not in *pif457* in LRFR, and significantly misregulated in *pif457* vs. Col-0 but not in *yuc2589* vs. Col-0 in the LRFR vs. WL (FDR  $< 0.05$ ). YUC-dependent and PIF-independent genes (iii) were selected using the criteria: upregulated in Col-0 and *pif457* but not in *yuc2589* in LRFR, and significantly misregulated in *yuc2589* vs. Col-0 but not in *pif457* vs. Col-0 in the LRFR vs. WL (FDR  $< 0.05$ ). One example gene for each category is represented next to the corresponding Venn diagram. Data are means, error bars indicate SD. Asterisks (\*) indicate statistical significance between light treatments (FDR  $< 0.05$ ). Related to Fig. 8.

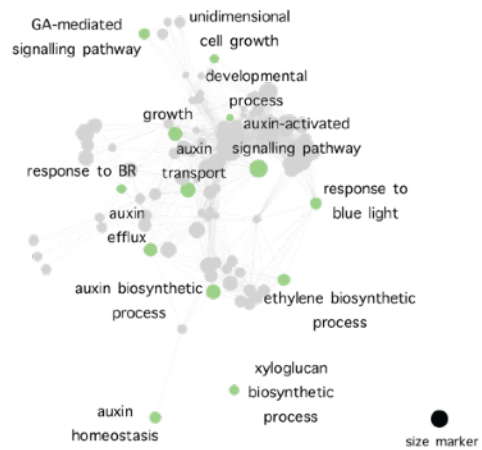


	White Light			
	ALL UP	ALL DOWN	FC>2 UP	FC>2 DOWN
<b>Hypocotyls</b>				
<i>pif457</i> vs. Col-0	900	850	36	348
<i>yuc2589</i> vs. Col-0	569	1089	92	485
<i>smt2-1</i> vs. Col-0	1040	456	80	145
<b>Cotyledons</b>				
<i>pif457</i> vs. Col-0	58	155	9	93
<i>yuc2589</i> vs. Col-0	228	234	70	164
<i>smt2-1</i> vs. Col-0	403	247	181	66

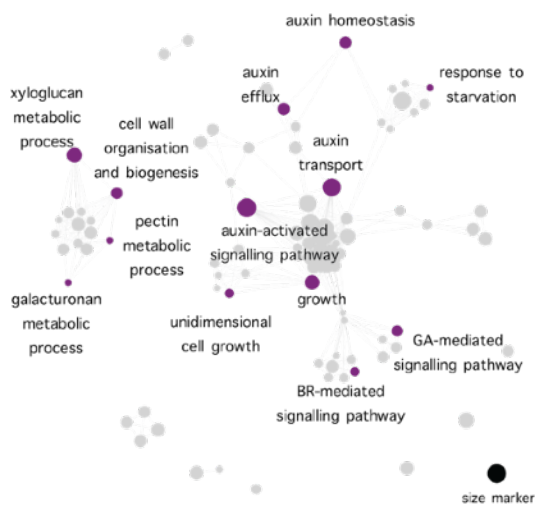
(b) **PIF-dependent genes in hypocotyls**



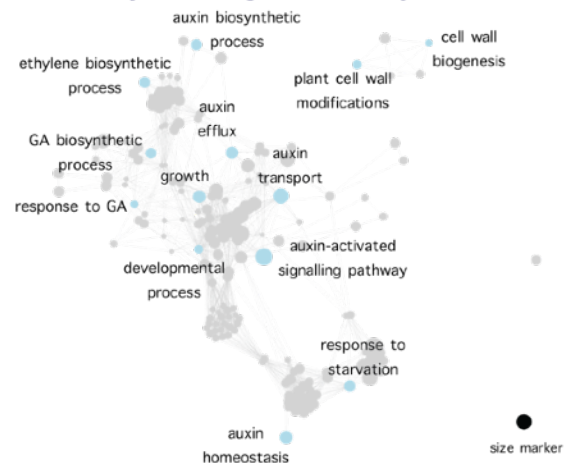
**PIF-dependent genes in cotyledons**



**YUC-dependent genes in hypocotyls**



**YUC-dependent genes in cotyledons**



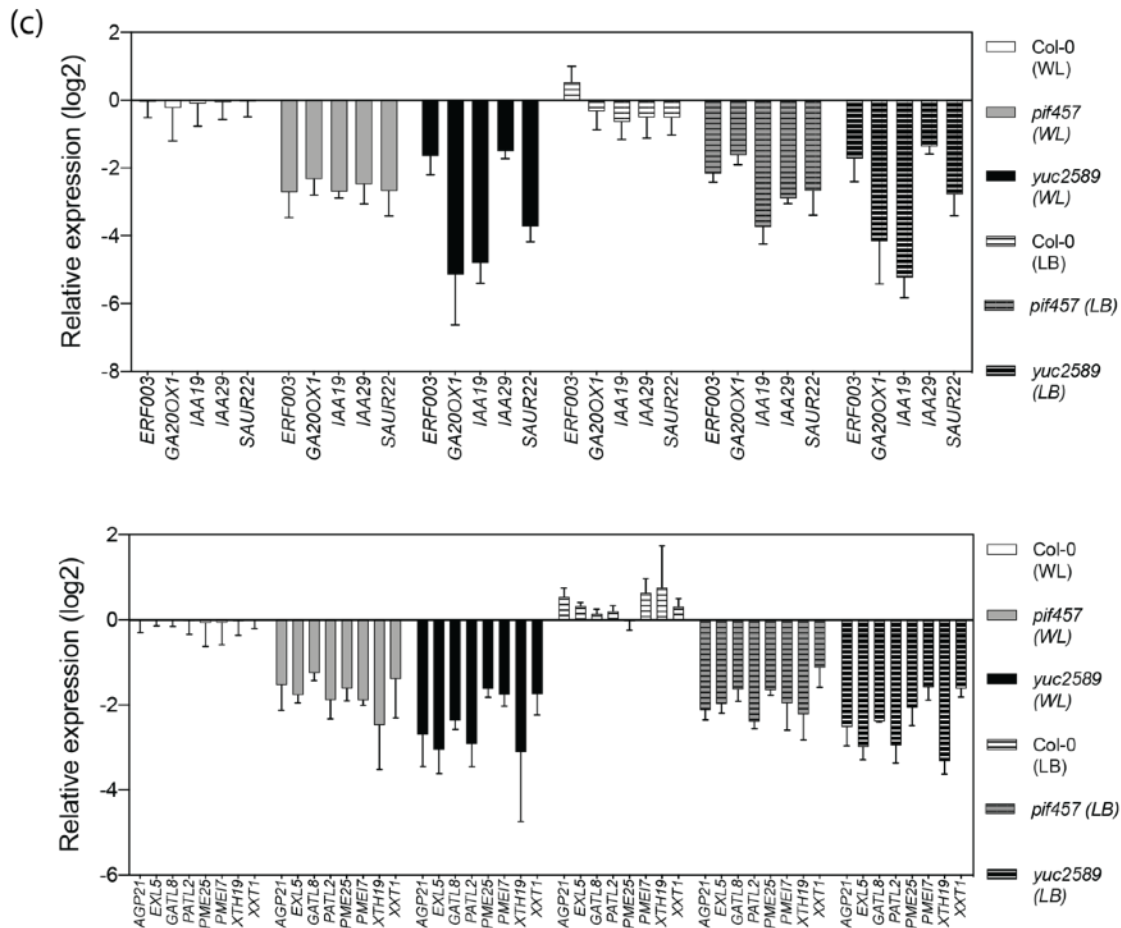


**Figure S13. Identification of transcriptome changes in mutants and Col-0 in WL.**

(a) PCA of LB-upregulated genes in Col-0 hypocotyls (left) and the number of genes that are differentially regulated in the indicated mutants compared to Col-0 in WL (right). The total numbers of significantly up- or down-regulated genes are indicated with or without a fold change (FC) cut-off (FDR < 0.05, Benjamini Hochberg correction using whole data set together). (b) GO term enrichment analysis from the indicated gene lists (FC > 2, DOWN). Each node indicates a significantly enriched GO term. Two terms (nodes) are connected if they share 20% or more genes. The size of the nodes indicates the regulation factor (RF) which is calculated as a function of FDR value and fold change enrichment of the corresponding GO term. Black nodes indicate a size marker with RF = 50. Only selected GO terms are annotated. (c) Several examples for the relative expression of hormone and cell wall related genes in WL and LB treated hypocotyls. Genes are selected from *pif457* and *yuc2589* significantly (FDR < 0.05) downregulated genes in WL. Data are means, error bars indicate SD. To see the full list of enriched GO terms, please download the interactive versions of (c-h) from [here](#).

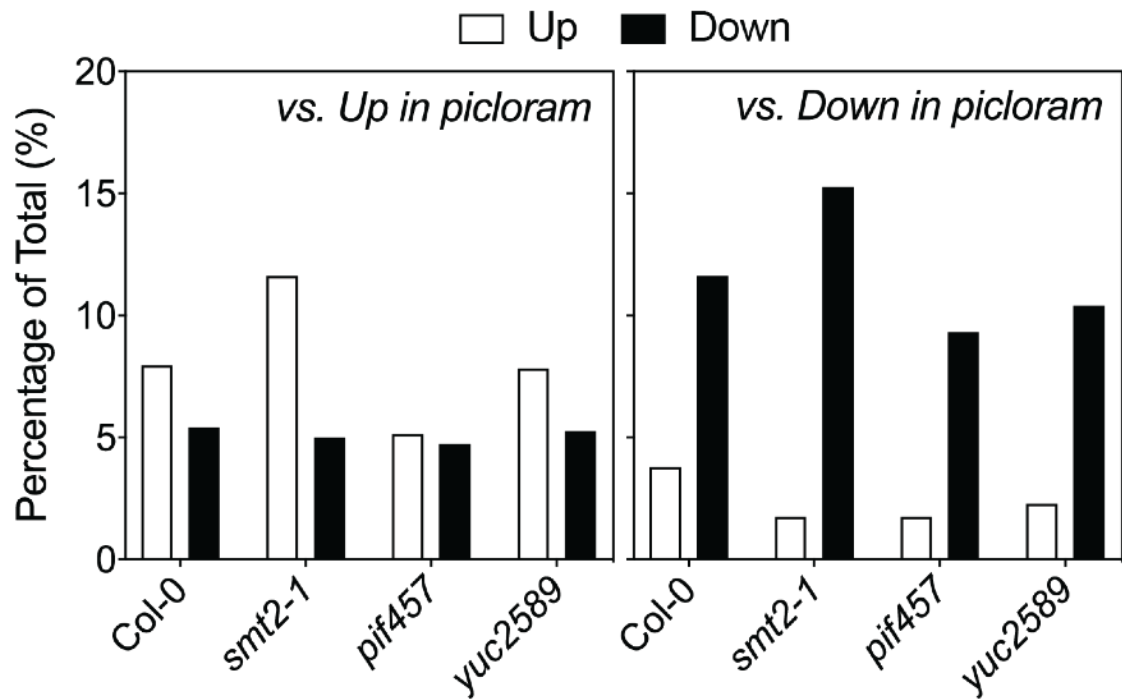


**Figure S14. Comparison of LB and picloram regulated genes in hypocotyls.**

Percentages are calculated from the total number of up- or downregulated genes in picloram. Related to Fig. 9.

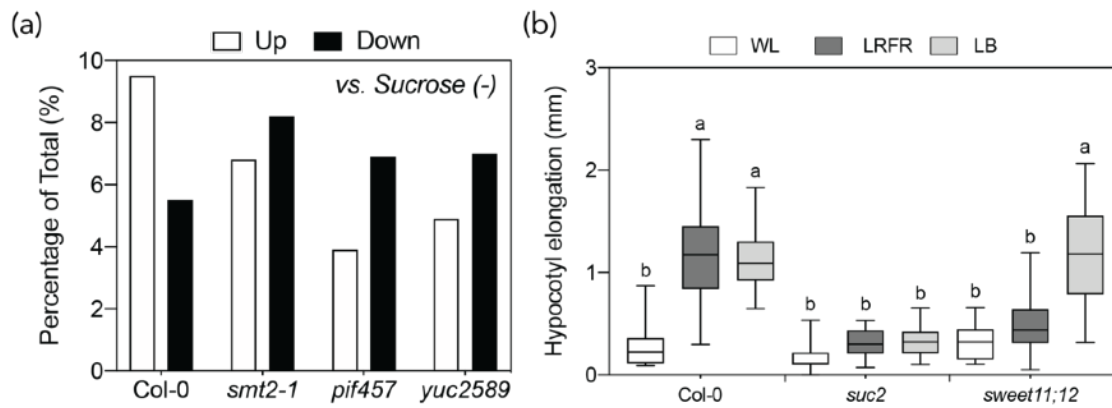


**Figure S15. Sucrose transport is not indispensable in LB light.**

(a) Hypocotyl elongation of the indicated genotypes grown as in Fig 2. Elongation during the last 3 d is indicated. Different letters indicate significant difference (two-way ANOVA with Tukey's HSD test,  $P < 0.05$ ,  $n > 12$ ). (b) Comparison of LB (3h, this study) and sucrose (-) (Shulse et al., 2019) regulated genes in hypocotyls and roots, respectively. Percentages are calculated from the total number of upregulated genes in sucrose (-). Related to Fig. 10.

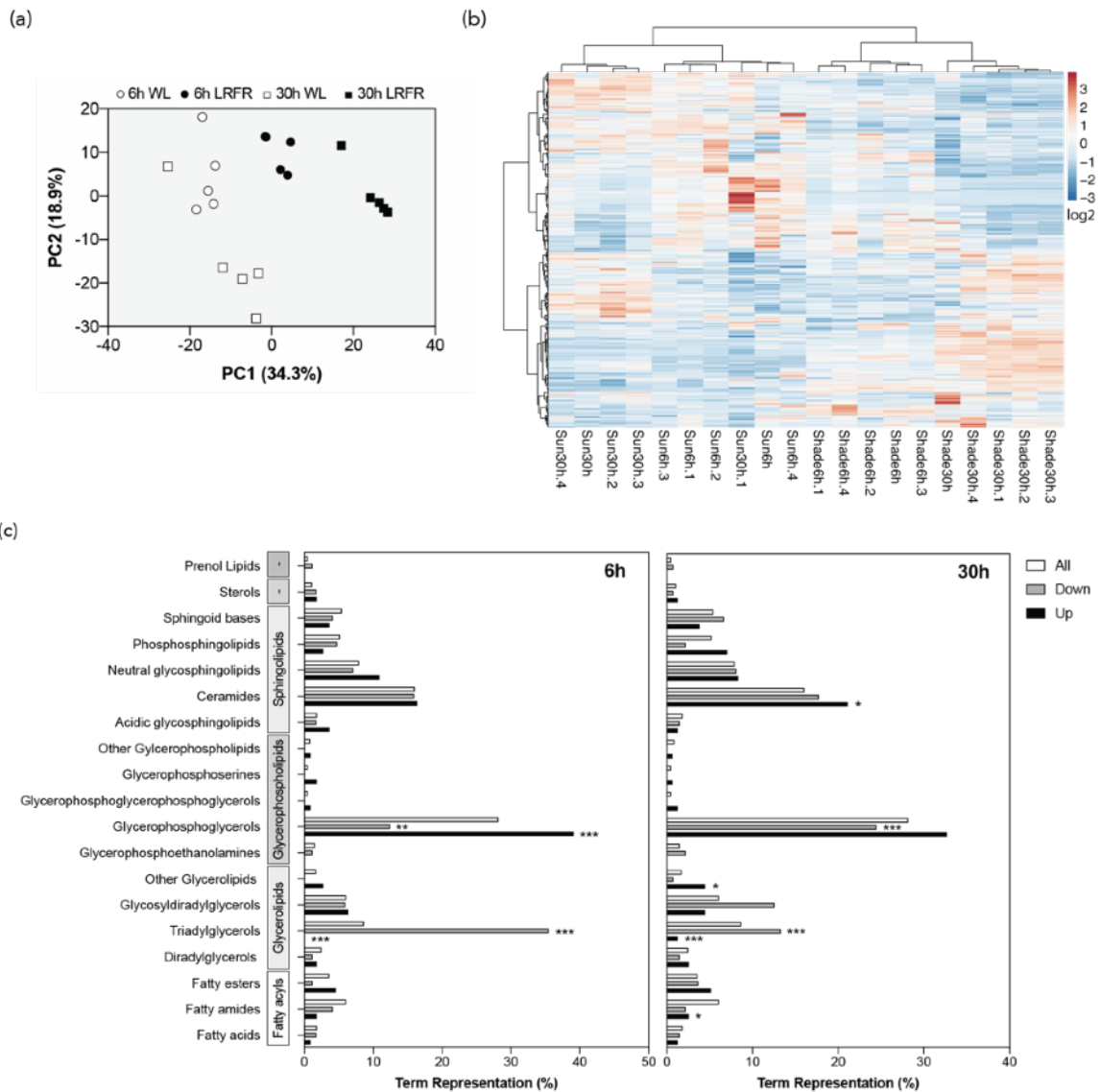


**Figure S16. Composition of other sterols and expression of control genes in LRFR in *B. rapa* hypocotyls**

(a) Relative expression of *BrSMT1* and *BrIAA29* in 5-d-old *Brassica rapa* hypocotyls. Gene expression values were calculated as fold induction relative to *BrPP2A*. n = 4 (biological) with three technical replicas for each RNA sample. (b) Fresh weight (mg) of seedlings used in sterol quantification in (c) and Fig. 11b. (c) The relative contents of indicated sterols in 5-d-old *Brassica rapa* hypocotyls. Seedlings were grown as in Fig. 2. n = 5 (biological). Data are means, error bars indicate SD (a, b, c). Numbers (a) and asterisks (b, c) (\*) above the bars indicate the statistical significance compared to control regions (Student's T-test, \* < 0.05, \*\* < 0.01). Related to Fig. 11.

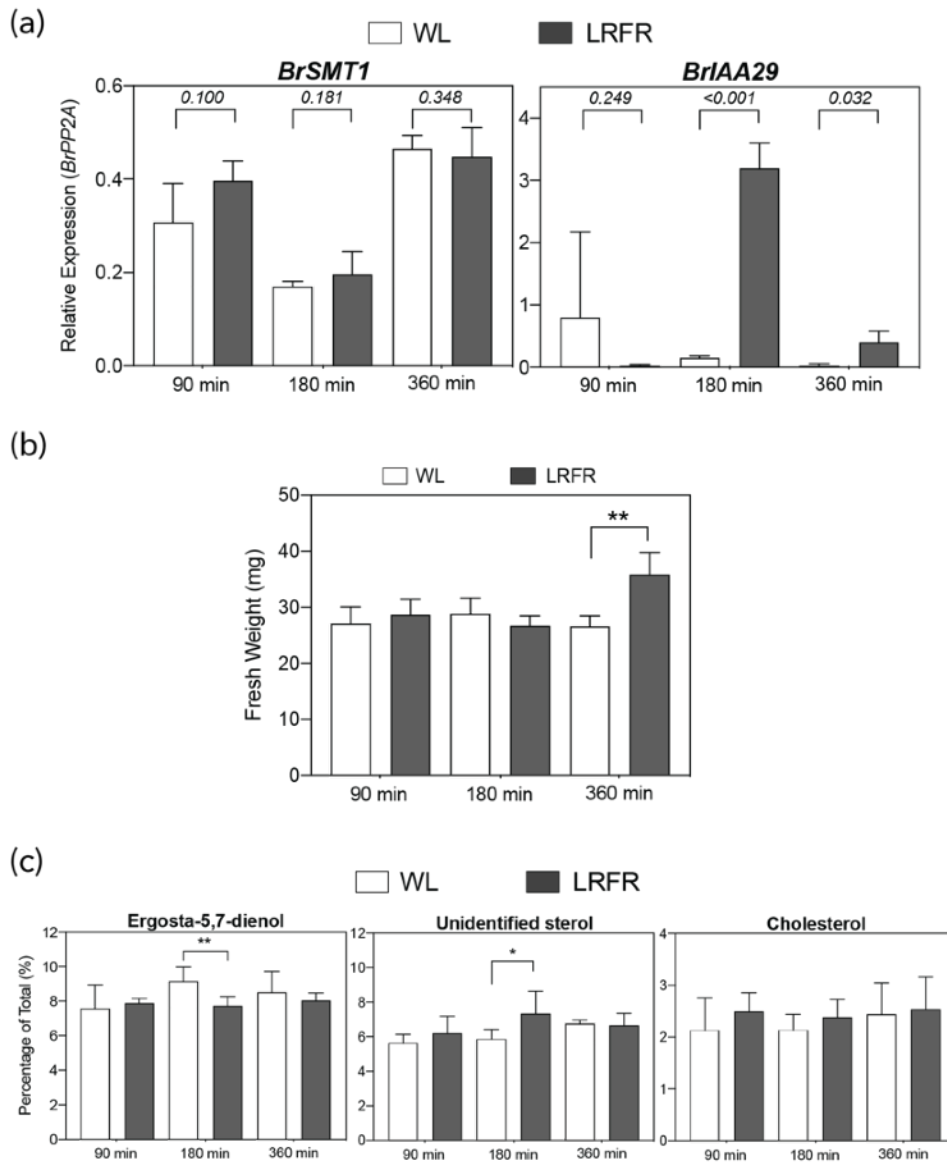


**Figure S17. Lipid profile of *B. rapa* hypocotyls changes in response to LRFR (MS1).**

(a) PCA of MS only (MS1)-detected lipid species. PC1 and PC2 of each biological replicate ( $n = 5$ ) are graphically visualised. (b) Cluster analysis and heat map representation of MS1-detected lipid species in each biological replicate. (c) Term enrichment analysis for indicated lipid classes of significantly (Benjamini Hochberg correction ( $FDR < 0.05$  or  $FDR < 0.1$  and Fold change ( $FC > 1.5$ ) increased (up) or decreased (down) in MS1-detected lipid species at indicated time points. Asterisks (\*) indicate FDR values (Fisher's test with Benjamini Hochberg correction, \*  $< 0.1$ , \*\*  $< 0.05$ , \*\*\*  $< 0.01$ ). Note that MS1-detected lipid species are not true identities and contains many lipids that are not found in plants (best hits). Related to Fig. 12.

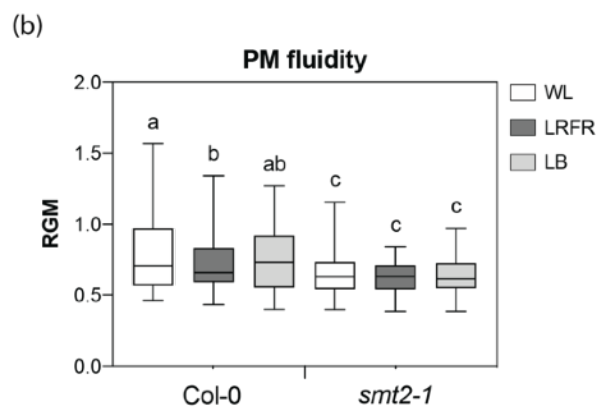
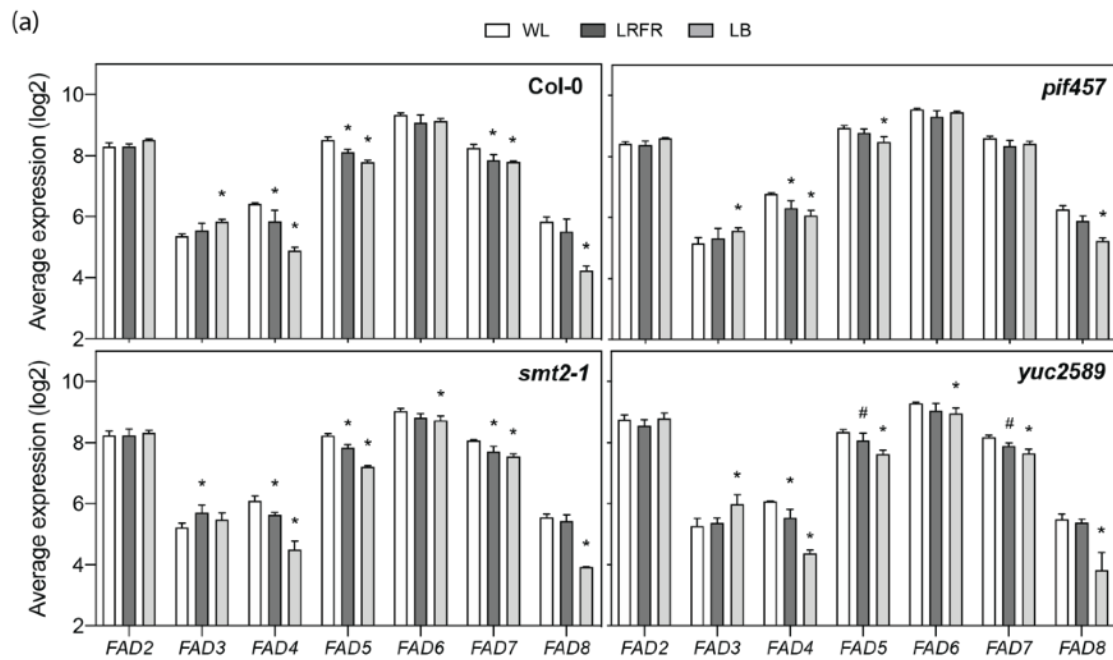


**Figure S18. LRFR expression of *FAD* family genes in cotyledons and PM fluidity in LB.**

(a) Average expression for *FAD* family genes in cotyledons of the indicated genotypes 3h after transferred to the indicated light conditions. Asterisks (\*) and hashes (#) indicate the statistical significance compared to WL (FDR value, \* < 0.05, # < 0.1). (b) The characterization of the relative proportion of  $L_o$  and  $L_d$  phases of PM of the indicated genotypes of *Arabidopsis thaliana* hypocotyl epidermal cells using di-4-ANEPPDHQ (2 $\mu$ g/mL) fluorescence dye. Seedlings were grown as in Fig 2. The RGM (for the red/green ratio of the membrane) was calculated from 7d-old seedlings. Different letters indicate significant difference (two-way ANOVA with Tukey's HSD test,  $P < 0.05$ ,  $n = 9$  cells from 3 seedlings x 20 membrane regions). Related to Fig. 13.

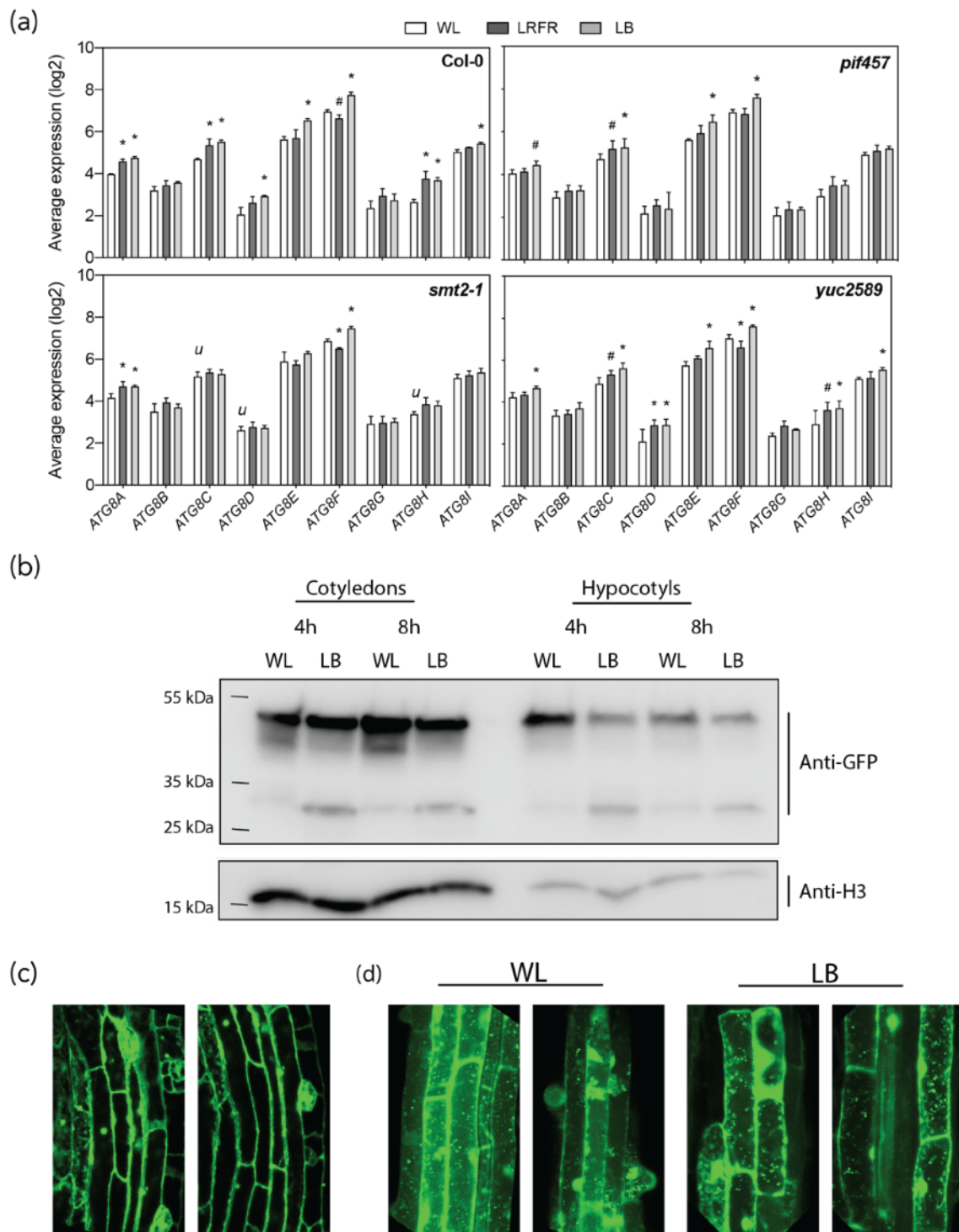


**Figure S19. Low blue light treatment induces autophagy in cotyledons and hypocotyls.**

(a) Average expression for *ATG8A-I* isoforms in 5-d-old Col-0 and *smt2-1* hypocotyls 3h after transferred to the indicated light conditions obtained from the RNA-seq analysis. Asterisks (\*) and hashes (#) indicate the statistical significance compared to WL; *u* and *d* indicate up- or downregulation of basal expression in WL, respectively for mutants

*(Figure S19 legend continues)*

compared to Col-0 (FDR value, \* < 0.05, # < 0.1; *u* or *d* < 0.05). (b) ATG8-GFP and the free GFP levels detected with an anti-GFP antibody from the total protein extract from cotyledons and hypocotyls after 4h and 8h of low blue light. (c) Petiole epidermis cells of *35S::ATG8-GFP* in the *atg7* mutant background after 8h of low blue light. (d) Root epidermis cells of *35S::ATG8-GFP* in WT background after 8h of white or low blue light. Related to Fig. 14.

## ACKNOWLEDGEMENTS

I would like to thank Sebastien Mongrand and his lab for the sterol measurements and the following discussions, Julijana Ivanisevic and her lab for the lipidomics analysis and the following discussions, Mieke de Wit, Anne-Sophie Fiorucci, Vinicius Galvao, Martine Trevisan, and Anupama Goyal for the experimental contributions (as indicated in the overview); Anne-Sophie Fiorucci for her valuable comments on the manuscript, Martina Legris, Ganesh Nawkar, Ana Lopez Vazquez, Olivier Michaud, Alessandra Boccacini, Johanna Kramer, Geoffrey Cobb for their helps and comments on the private exam presentation, Genomic Technologies Facility (GTF, Unil) for RNA-seq and initial data analysis, Christian Hardtke for providing *cvp2* and *cvp2cv11* seeds, Richard Vierstra for providing *atg7* and *35S:ATG8-GFP* seeds, Cellular Imaging Facility (CIF, Unil), Michael Knoblauch, Martina Legris, and Laure Allenbach for the technical advice on microscopy.

## GENERAL DISCUSSION AND OUTLOOK

In the present study, we investigated PIF-mediated growth responses in three different conditions with a focus on hypocotyl elongation. We identified PIF7 as a novel regulator for growth promotion in response to elevated temperature. Furthermore, we showed that LRFr increases the partition of CO<sub>2</sub> fixed in cotyledons to the elongating hypocotyls via sucrose transport, where PIFs are required. We also showed that LRFr regulates lipid composition of hypocotyls where PM lipids increase, while storage and chloroplast lipids decrease. Furthermore, sitosterol biosynthesis is required for LRFr-induced hypocotyl elongation and PIFs contribute to the process by inducing *SMT2* and *SMT3* expression in hypocotyls. PIF4 binds to promoters of both *SMT2* and *SMT3* whereas PIF7 binds to *SMT3* promoter. Our data on transcriptome of cotyledons and hypocotyls reveals interesting similarities and differences between the between LB- and LRFr-induced hypocotyl elongation. One of the key differences between LB- and LRFr-induced transcriptome is the promotion of catabolism and anabolism related processes in LB and LRFr, respectively. We further showed that autophagy is induced post-transcriptionally in LB-treated *Arabidopsis* seedlings. We conclude that cellular material required for hypocotyl elongation is obtained via new biosynthesis in LRFr whereas recycling is more important in LB-induced hypocotyl elongation.

In the first chapter, we showed that PIF7 protein levels increase rapidly when temperature elevates, whereas *PIF7* transcript levels decrease (Ch. 1, Fig. 4). Interestingly, our results indicated that both *pif4* and *pif7* mutants are impaired in elevated temperature-induced hypocotyl elongation with no apparent additive phenotype in the double mutant (Ch. 1, Fig. 1a, 1b). We first investigated whether these proteins are required to promote two essential pathways for hypocotyl elongation (e.g., auxin biosynthesis and signalling). However, we observed no indications to support this argument as transcriptional responses

including hormonal biosynthesis and signalling gene expression were similarly impaired in both mutants (Ch. 1, Fig. 2, S4). Another possible explanation is that PIF4 and PIF7 function as obligated heterodimers. PIF4 and PIF7 interact with each other as shown by Y2H assay presented in here (Ch. 1, Fig. S5) and other studies (Chung et al., 2020), as well as in mesophyll protoplasts (Kidokoro et al., 2009). However, we also showed that PIF4 and PIF7 can work independently in *phyB* mutant background (Ch. 1, Fig. S2). Furthermore, PIF7 is more important in *phyB* mediated responses to elevated temperature, whereas PIF4 functions downstream of both *phyB* and *cry1* (Ch. 1, Fig. S2) (Ma et al., 2016). These suggest that *phyB* may be involved in regulating PIF4-PIF7 synergistic functions. It was shown that PIF4 functions require *phyB*-binding APB domain (Khanna et al., 2004). Furthermore, while PIF4-OX showed a *phyB* mutant-like hypocotyl elongation, hypocotyl length of PIF7-OX was similar to WT (Khanna et al., 2004, Li et al., 2012). Therefore, I hypothesise that PIF4 may act upstream of PIF7 by inhibiting *phyB* binding to PIF7. In order to test this hypothesis, analyses of PIF4-OX and PIF7-OX lines together with the lines with the APB domain mutated (mAPB) PIF4 and PIF7 in the corresponding mutant backgrounds, as well as the crosses between those may be used. Furthermore, it remains unclear how *cry1* might be involved in PIF4-PIF7 dependent regulation of elevated temperature responses. Thus, further investigations are needed to understand whether *cry1* also interacts with PIF7. Finally, another hypothesis is that these proteins may be required to promote essential pathways that are spatially separated (e.g., cotyledons and hypocotyls). It was recently shown that epidermal expression of PIF4 is required for hypocotyl elongation in elevated temperature (Kim et al., 2020). However, it is important to note that the promoter selected to drive epidermal expression of PIF4 in this study (Kim et al., 2020) is similarly expressed in cotyledons and hypocotyls (our data set). Therefore, it remains unclear to which extent cotyledon and hypocotyl specific expression of PIF4 and PIF7 is important for hypocotyl growth promotion.

In the second chapter, we showed that LRFR-induced hypocotyl elongation is regulated by a PIF7-dependent metabolic response (Ch. 2, Fig. 5j). It was previously established that PIF4 is required for the contrasting growth phenotypes where cotyledons arrest growth and hypocotyls elongate (Khanna et al., 2004), suggesting that PIFs are involved in resource partitioning between these two organs. It was also previously shown that PIFs are required for growth promotion in response to exogenous sucrose and elevated CO<sub>2</sub> (Lilley et al., 2012). Here, we showed that sucrose transport is required in LRFR-induced hypocotyl elongation (Ch. 2, Fig. 4). As a complementary result to our paper, we showed that sucrose transport is completely impaired in *pif457* mutant in response to LRFR (Ch. 3, Fig. 10), suggesting that PIFs contribute resource partitioning via regulating sucrose transport. Comparison of sucrose (-) and LRFR-induced genes suggested that YUCCAs are required for sucrose response almost as much as PIFs (Ch. 3, Fig. 10a). Recently, it was shown that auxin transcriptionally regulates sucrose transport into the rose petals (Liang et al., 2020). Although we did not observe any transcriptional regulation on sucrose transporter genes in LRFR (data not shown), it is possible that PIF-induced auxin responses are post-transcriptionally required for sucrose transport in LRFR. Yet, this hypothesis is needed to be tested by investigating how esculin transport occurs in *yuc2589*.

In addition to their structural roles, lipids are important functionally as lipid signals in membranes. However, signalling lipids are usually low abundant phospholipids and sphingolipids (Bouttè & Jallais, 2020, Mamode Cassim et al., 2019). Since our lipidomics protocol fails to detect low abundant lipids in general, we could not further investigated whether LRFR also induces changes in the signalling lipid profiles. Furthermore, sterol derivatives have important functions in growth and development. One example is the usage of sitosterol- $\beta$ -glucoside as a primer for glucan polymerisation by CesA glucosyltransferase in cell wall extension (Valitova et al., 2016). The method that we used for sterol

quantification does not allow differentiating the levels of sterol derivatives and free sterols. Therefore, more sensitive methods for sterol quantification are required in order to further investigate the role of sitosterol in cell wall synthesis. Another key experiment would be to investigate the potential genetic interaction between *CesA* and the *smt2* mutant in LRFR.

Although PIFs bind the promoters of *SMT2* and *SMT3*, PIF-mediated induction of *SMT* genes in LRFR requires YUCCA-mediated auxin production (Ch. 3, Fig. 5b). Previously, it was shown that PIF4, auxin-response factor ARF6, and BR-signalling transcription factor BZR1 interact with each other and cooperatively regulate common target genes (Oh et al., 2014). Therefore, it is possible that *SMT2* and *SMT3* expression is regulated by a similar mechanism involving PIFs and ARF6 or other auxin response factors. Further investigations are needed to unravel the molecular interactions required for the induction of *SMT2* and *SMT3* expression. As BZR1 is also an important transcription factor in the regulation of LRFR-transcriptome, it is also necessary to investigate whether BR is required for the process.

Our transcriptome analysis from dissected *Arabidopsis* seedlings indicates that LB and LRFR induced hypocotyl elongation share several pathways that are previously shown to be involved in cell elongation (e.g., detection of calcium ion) (Fig. 7e). Although we focused on differences between these two light conditions, the further investigation of common mechanisms may give us new insights on growth in vegetative shade. Furthermore, it can reveal new functions for the shared regulators of LB and LRFR, including PIFs.

We clearly showed that the biosynthesis in LRFR and recycling in LB are two complementary mechanisms in vegetative shade using sitosterol biosynthesis and autophagy mutants (Fig. 14e). Although previous reports indicate that sucrose starvation induces autophagy and lipid breakdown occurs via autophagic machinery (Goto-Yamada et al., 2019, Fan et al., 2019), we do not know how lipids, especially sterols are recycled in LB. As SMTs would also be required for a

recycling event that breakdown lipids to sitosterol precursors, we expect that sitosterol must be recycled in a shorter circuit. Yet, the details remain unknown and further investigations are needed to understand how PM lipids are recycled in LB. One key experiment would be to check whether lipophagy is induced in LB using previously reported GFP tagged lipid droplet marker protein OLE1 in WT and *atg5* backgrounds (Fan et al., 2019). Furthermore, we still have a poor understanding on whether recycling is a broad mechanism for LB-induced responses. Analysis of other biosynthesis mutants in LRFR, LB, and LRFR+LB can help to understand the extent of recycling. Cell wall biosynthesis pathways, especially cellulose synthesis is a good candidate to test this idea, as genes coding for enzymes functioning in these processes are induced in hypocotyls in LRFR similar to *SMT2* and *SMT3* (data not shown) and mutants and drugs to inhibit these processes are already characterised (Feraru et al., 2011).

The link between LB perception and induction of autophagy is also missing in our work. We showed that PIFs do not involve in transcriptional activation of *ATG8* genes in LB. Therefore, the expression of autophagy related genes needs to be analysed in mutants of other LB-regulatory elements, starting with cryptochromes. Furthermore, we showed that LRFR also induces the expression of several *ATG8* genes but does not increase autophagy (Fig. 14b, 14c). This result indicates that induction of autophagy may be mainly regulated after transcription. These may include RNA processing, selective induction of translation from autophagy-related mRNAs, and protein modifications that leads to formation of autophagic bodies. Finally, LB-induced starvation, sucrose sensing, or TOR pathway may act as a signal for promotion of autophagic machinery. Therefore, the mutants in these pathways are needed to be screened for LB-induced hypocotyl elongation phenotypes.

# BIBLIOGRAPHY

- Ackerman-Lavert M, Savaldi-Goldstein S, 2020. Growth models from a brassinosteroid perspective. *Curr Opin Plant Biol* **53**, 90-7.
- Ahmad M, 2016. Photocycle and signaling mechanisms of plant cryptochromes. *Curr Opin Plant Biol* **33**, 108-15.
- Anders S, Pyl PT, Huber W, 2015. HTSeq--a Python framework to work with high-throughput sequencing data. *Bioinformatics* **31**, 166-9.
- Arico D, Legris M, Castro L, *et al.*, 2019. Neighbour signals perceived by phytochrome B increase thermotolerance in Arabidopsis. *Plant Cell Environ.*
- Armengot L, Marques-Bueno MM, Jaillais Y, 2016. Regulation of polar auxin transport by protein and lipid kinases. *J Exp Bot* **67**, 4015-37.
- Ayling SM, Brownlee C, Clarkson DT, 1994. The Cytoplasmic Streaming Response of Tomato Root Hairs to Auxin; Observations of Cytosolic Calcium Levels. *Journal of Plant Physiology* **143**, 184-8.
- Baluska F, Barlow PW, 1993. The role of the microtubular cytoskeleton in determining nuclear chromatin structure and passage of maize root cells through the cell cycle. *Eur J Cell Biol* **61**, 160-7.
- Bellstaedt J, Trenner J, Lippmann R, *et al.*, 2019. A Mobile Auxin Signal Connects Temperature Sensing in Cotyledons with Growth Responses in Hypocotyls. *Plant Physiol* **180**, 757-66.
- Bennett T, 2015. PIN proteins and the evolution of plant development. *Trends Plant Sci* **20**, 498-507.
- Blanco-Tourinan N, Legris M, Minguet EG, *et al.*, 2020. COP1 destabilizes DELLA proteins in Arabidopsis. *Proc Natl Acad Sci U S A* **117**, 13792-9.
- Boccaccini A, Legris M, Krahmer J, *et al.*, 2020. Low Blue Light Enhances Phototropism by Releasing Cryptochrome1-Mediated Inhibition of PIF4 Expression. *Plant Physiol* **183**, 1780-93.
- Bou-Torrent J, Galstyan A, Gallemi M, *et al.*, 2014. Plant proximity perception dynamically modulates hormone levels and sensitivity in Arabidopsis. *J Exp Bot* **65**, 2937-47.
- Bourbousse C, Vegesna N, Law JA, 2018. SOG1 activator and MYB3R repressors regulate a complex DNA damage network in Arabidopsis. *Proc Natl Acad Sci U S A* **115**, E12453-E62.
- Boutté Y, Jaillais Y, 2020. Metabolic Cellular Communications: Feedback Mechanisms between Membrane Lipid Homeostasis and Plant Development. *Developmental Cell.*
- Box MS, Huang BE, Domijan M, *et al.*, 2015. ELF3 controls thermoresponsive growth in Arabidopsis. *Curr Biol* **25**, 194-9.
- Brunoud G, Wells DM, Oliva M, *et al.*, 2012. A novel sensor to map auxin response and distribution at high spatio-temporal resolution. *Nature* **482**, 103-6.
- Cacas JL, Bure C, Grosjean K, *et al.*, 2016. Revisiting Plant Plasma Membrane Lipids in Tobacco: A Focus on Sphingolipids. *Plant Physiol* **170**, 367-84.
- Cagnola JJ, Ploschuk E, Benech-Arnold T, Finlayson SA, Casal JJ, 2012. Stem transcriptome reveals mechanisms to reduce the energetic cost of shade-avoidance responses in tomato. *Plant Physiol* **160**, 1110-9.

- Carland F, Fujioka S, Nelson T, 2010. The sterol methyltransferases SMT1, SMT2, and SMT3 influence Arabidopsis development through nonbrassinosteroid products. *Plant Physiol* **153**, 741-56.
- Carland F, Nelson T, 2009. CVP2- and CVL1-mediated phosphoinositide signaling as a regulator of the ARF GAP SFC/VAN3 in establishment of foliar vein patterns. *Plant J* **59**, 895-907.
- Carland FM, 2002. The Identification of CVP1 Reveals a Role for Sterols in Vascular Patterning. *The Plant Cell Online* **14**, 2045-58.
- Casadei MA, MañAs P, Niven G, Needs E, Mackey BM, 2002. Role of Membrane Fluidity in Pressure Resistance of Escherichia coli NCTC 8164. *Applied and Environmental Microbiology* **68**, 5965-72.
- Casal JJ, 2012. Shade avoidance. *Arabidopsis Book* **10**, e0157.
- Casal JJ, 2013. Photoreceptor signaling networks in plant responses to shade. *Annu Rev Plant Biol* **64**, 403-27.
- Casal JJ, Balasubramanian S, 2019. Thermomorphogenesis. *Annu Rev Plant Biol*.
- Casson SA, Franklin KA, Gray JE, Grierson CS, Whitelam GC, Hetherington AM, 2009. phytochrome B and PIF4 regulate stomatal development in response to light quantity. *Curr Biol* **19**, 229-34.
- Chapman EJ, Greenham K, Castillejo C, *et al.*, 2012. Hypocotyl transcriptome reveals auxin regulation of growth-promoting genes through GA-dependent and -independent pathways. *PLoS One* **7**, e36210.
- Chen LQ, Qu XQ, Hou BH, *et al.*, 2012. Sucrose efflux mediated by SWEET proteins as a key step for phloem transport. *Science* **335**, 207-11.
- Chen M, Galvao RM, Li M, *et al.*, 2010. Arabidopsis HEMERA/pTAC12 initiates photomorphogenesis by phytochromes. *Cell* **141**, 1230-40.
- Chen Q, Dai X, De-Paoli H, *et al.*, 2014a. Auxin overproduction in shoots cannot rescue auxin deficiencies in Arabidopsis roots. *Plant Cell Physiol* **55**, 1072-9.
- Chen Q, Shinozaki D, Luo J, *et al.*, 2019. Autophagy and Nutrients Management in Plants. *Cells* **8**.
- Chen X, Grandont L, Li H, *et al.*, 2014b. Inhibition of cell expansion by rapid ABP1-mediated auxin effect on microtubules. *Nature* **516**, 90-3.
- Chung BYW, Balcerowicz M, Di Antonio M, *et al.*, 2020. An RNA thermoswitch regulates daytime growth in Arabidopsis. *Nature Plants*.
- Cifuentes-Esquivel N, Bou-Torrent J, Galstyan A, *et al.*, 2013. The bHLH proteins BEE and BIM positively modulate the shade avoidance syndrome in Arabidopsis seedlings. *Plant J* **75**, 989-1002.
- Clough SJ, Bent AF, 1998. Floral dip: a simplified method for Agrobacterium-mediated transformation of Arabidopsis thaliana. *Plant J* **16**, 735-43.
- Clouse SD, 2011. Brassinosteroids. *Arabidopsis Book* **9**, e0151.
- Covington MF, Harmer SL, 2007. The circadian clock regulates auxin signaling and responses in Arabidopsis. *PLoS Biol* **5**, e222.
- Das D, St Onge KR, Voeselek LA, Pierik R, Sasidharan R, 2016. Ethylene- and Shade-Induced Hypocotyl Elongation Share Transcriptome Patterns and Functional Regulators. *Plant Physiol* **172**, 718-33.

- Davis MP, Van Dongen S, Abreu-Goodger C, Bartonicek N, Enright AJ, 2013. Kraken: a set of tools for quality control and analysis of high-throughput sequence data. *Methods* **63**, 41-9.
- De Lucas M, Daviere JM, Rodriguez-Falcon M, *et al.*, 2008. A molecular framework for light and gibberellin control of cell elongation. *Nature* **451**, 480-4.
- De Wit M, Galvao VC, Fankhauser C, 2016a. Light-Mediated Hormonal Regulation of Plant Growth and Development. *Annu Rev Plant Biol* **67**, 513-37.
- De Wit M, George GM, Ince YC, *et al.*, 2018. Changes in resource partitioning between and within organs support growth adjustment to neighbor proximity in Brassicaceae seedlings. *Proc Natl Acad Sci U S A* **115**, E9953-E61.
- De Wit M, Keuskamp DH, Bongers FJ, *et al.*, 2016b. Integration of Phytochrome and Cryptochrome Signals Determines Plant Growth during Competition for Light. *Curr Biol* **26**, 3320-6.
- De Wit M, Ljung K, Fankhauser C, 2015. Contrasting growth responses in lamina and petiole during neighbor detection depend on differential auxin responsiveness rather than different auxin levels. *New Phytol* **208**, 198-209.
- De Wit M, Lorrain S, Fankhauser C, 2014. Auxin-mediated plant architectural changes in response to shade and high temperature. *Physiol Plant* **151**, 13-24.
- Delker C, Sonntag L, James GV, *et al.*, 2014. The DET1-COP1-HY5 pathway constitutes a multipurpose signaling module regulating plant photomorphogenesis and thermomorphogenesis. *Cell Rep* **9**, 1983-9.
- Desprez T, Juraniec M, Crowell EF, *et al.*, 2007. Organization of cellulose synthase complexes involved in primary cell wall synthesis in *Arabidopsis thaliana*. *Proc Natl Acad Sci U S A* **104**, 15572-7.
- Djakovic-Petrovic T, De Wit M, Voesenek LA, Pierik R, 2007. DELLA protein function in growth responses to canopy signals. *Plant J* **51**, 117-26.
- Dobin A, Davis CA, Schlesinger F, *et al.*, 2013. STAR: ultrafast universal RNA-seq aligner. *Bioinformatics* **29**, 15-21.
- Dunn WB, Broadhurst D, Begley P, *et al.*, 2011. Procedures for large-scale metabolic profiling of serum and plasma using gas chromatography and liquid chromatography coupled to mass spectrometry. *Nat Protoc* **6**, 1060-83.
- Elander PH, Minina EA, Bozhkov PV, 2018. Autophagy in turnover of lipid stores: trans-kingdom comparison. *J Exp Bot* **69**, 1301-11.
- Ezer D, Jung JH, Lan H, *et al.*, 2017. The evening complex coordinates environmental and endogenous signals in *Arabidopsis*. *Nat Plants* **3**, 17087.
- Fan J, Yu L, Xu C, 2019. Dual Role for Autophagy in Lipid Metabolism in *Arabidopsis*. *Plant Cell* **31**, 1598-613.
- Feng S, Martinez C, Gusmaroli G, *et al.*, 2008. Coordinated regulation of *Arabidopsis thaliana* development by light and gibberellins. *Nature* **451**, 475-9.
- Feraru E, Feraru MI, Kleine-Vehn J, *et al.*, 2011. PIN polarity maintenance by the cell wall in *Arabidopsis*. *Curr Biol* **21**, 338-43.
- Findlay KM, Jenkins GI, 2016. Regulation of UVR8 photoreceptor dimer/monomer photo-equilibrium in *Arabidopsis* plants grown under photoperiodic conditions. *Plant Cell Environ* **39**, 1706-14.

- Fiorucci AS, Fankhauser C, 2017. Plant Strategies for Enhancing Access to Sunlight. *Curr Biol* **27**, R931-R40.
- Fiorucci AS, Galvao VC, Ince YC, *et al.*, 2019. PHYTOCHROME INTERACTING FACTOR 7 is important for early responses to elevated temperature in Arabidopsis seedlings. *New Phytol* **226**, 50-8.
- Foreman J, Johansson H, Hornitschek P, Josse EM, Fankhauser C, Halliday KJ, 2011. Light receptor action is critical for maintaining plant biomass at warm ambient temperatures. *Plant J* **65**, 441-52.
- Franklin KA, 2008. Shade avoidance. *New Phytol* **179**, 930-44.
- Franklin KA, Lee SH, Patel D, *et al.*, 2011. Phytochrome-interacting factor 4 (PIF4) regulates auxin biosynthesis at high temperature. *Proc Natl Acad Sci U S A* **108**, 20231-5.
- Fujii Y, Tanaka H, Konno N, *et al.*, 2017. Phototropin perceives temperature based on the lifetime of its photoactivated state. *Proc Natl Acad Sci U S A* **114**, 9206-11.
- Gagnebin Y, Tonoli D, Lescuyer P, *et al.*, 2017. Metabolomic analysis of urine samples by UHPLC-QTOF-MS: Impact of normalization strategies. *Anal Chim Acta* **955**, 27-35.
- Galvao RM, Li M, Kothadia SM, *et al.*, 2012. Photoactivated phytochromes interact with HEMERA and promote its accumulation to establish photomorphogenesis in Arabidopsis. *Genes Dev* **26**, 1851-63.
- Galvao VC, Fankhauser C, 2015. Sensing the light environment in plants: photoreceptors and early signaling steps. *Curr Opin Neurobiol* **34**, 46-53.
- Galvao VC, Fiorucci AS, Trevisan M, *et al.*, 2019. PIF transcription factors link a neighbor threat cue to accelerated reproduction in Arabidopsis. *Nat Commun* **10**, 4005.
- Gangappa SN, Kumar SV, 2017. DET1 and HY5 Control PIF4-Mediated Thermosensory Elongation Growth through Distinct Mechanisms. *Cell Rep* **18**, 344-51.
- Gendreau E, Traas J, Desnos T, Grandjean O, Caboche M, Hofte H, 1997. Cellular basis of hypocotyl growth in Arabidopsis thaliana. *Plant Physiol* **114**, 295-305.
- Gendrel AV, Lippman Z, Martienssen R, Colot V, 2005. Profiling histone modification patterns in plants using genomic tiling microarrays. *Nat Methods* **2**, 213-8.
- Gora PJ, Reinders A, Ward JM, 2012. A novel fluorescent assay for sucrose transporters. *Plant Methods* **8**, 13.
- Goto-Yamada S, Oikawa K, Bizan J, *et al.*, 2019. Sucrose Starvation Induces Microautophagy in Plant Root Cells. *Front Plant Sci* **10**, 1604.
- Gray WM, Ostin A, Sandberg G, Romano CP, Estelle M, 1998. High temperature promotes auxin-mediated hypocotyl elongation in Arabidopsis. *Proc Natl Acad Sci U S A* **95**, 7197-202.
- Grosjean K, Mongrand S, Beney L, Simon-Plas F, Gerbeau-Pissot P, 2015. Differential effect of plant lipids on membrane organization: specificities of phytosphingolipids and phytosterols. *J Biol Chem* **290**, 5810-25.
- Gruber H, Heijde M, Heller W, Albert A, Seidlitz HK, Ulm R, 2010. Negative feedback regulation of UV-B-induced photomorphogenesis and stress acclimation in Arabidopsis. *Proc Natl Acad Sci U S A* **107**, 20132-7.
- Hao Y, Oh E, Choi G, Liang Z, Wang ZY, 2012. Interactions between HLH and bHLH factors modulate light-regulated plant development. *Mol Plant* **5**, 688-97.
- Hase Y, Fujioka S, Yoshida S, Sun G, Umeda M, Tanaka A, 2005. Ectopic endoreduplication caused by sterol alteration results in serrated petals in Arabidopsis. *J Exp Bot* **56**, 1263-8.

- Hayashi K, 2012. The interaction and integration of auxin signaling components. *Plant Cell Physiol* **53**, 965-75.
- Hayes S, Sharma A, Fraser DP, *et al.*, 2017. UV-B Perceived by the UVR8 Photoreceptor Inhibits Plant Thermomorphogenesis. *Curr Biol* **27**, 120-7.
- Hayes S, Velanis CN, Jenkins GI, Franklin KA, 2014. UV-B detected by the UVR8 photoreceptor antagonizes auxin signaling and plant shade avoidance. *Proc Natl Acad Sci U S A* **111**, 11894-9.
- He JX, Fujioka S, Li TC, *et al.*, 2003. Sterols regulate development and gene expression in Arabidopsis. *Plant Physiol* **131**, 1258-69.
- Heijde M, Ulm R, 2013. Reversion of the Arabidopsis UV-B photoreceptor UVR8 to the homodimeric ground state. *Proc Natl Acad Sci U S A* **110**, 1113-8.
- Hepler PK, Rounds CM, Winship LJ, 2013. Control of cell wall extensibility during pollen tube growth. *Mol Plant* **6**, 998-1017.
- Hernandez-Garcia J, Briones-Moreno A, Blazquez MA, 2020. Origin and evolution of gibberellin signaling and metabolism in plants. *Semin Cell Dev Biol*.
- Hersch M, Lorrain S, De Wit M, *et al.*, 2014. Light intensity modulates the regulatory network of the shade avoidance response in Arabidopsis. *Proc Natl Acad Sci U S A* **111**, 6515-20.
- Hiltbrunner A, Tscheuschler A, Viczian A, Kunkel T, Kircher S, Schafer E, 2006. FHY1 and FHL act together to mediate nuclear accumulation of the phytochrome A photoreceptor. *Plant Cell Physiol* **47**, 1023-34.
- Hoecker U, 2017. The activities of the E3 ubiquitin ligase COP1/SPA, a key repressor in light signaling. *Curr Opin Plant Biol* **37**, 63-9.
- Hofius D, Schultz-Larsen T, Joensen J, *et al.*, 2009. Autophagic components contribute to hypersensitive cell death in Arabidopsis. *Cell* **137**, 773-83.
- Hornitschek P, Kohnen MV, Lorrain S, *et al.*, 2012. Phytochrome interacting factors 4 and 5 control seedling growth in changing light conditions by directly controlling auxin signaling. *Plant J* **71**, 699-711.
- Hornitschek P, Lorrain S, Zoete V, Michielin O, Fankhauser C, 2009. Inhibition of the shade avoidance response by formation of non-DNA binding bHLH heterodimers. *EMBO J* **28**, 3893-902.
- Huang H, Yoo CY, Bindbeutel R, *et al.*, 2016. PCH1 integrates circadian and light-signaling pathways to control photoperiod-responsive growth in Arabidopsis. *Elife* **5**, e13292.
- Huang X, Ouyang X, Yang P, *et al.*, 2013. Conversion from CUL4-based COP1-SPA E3 apparatus to UVR8-COP1-SPA complexes underlies a distinct biochemical function of COP1 under UV-B. *Proc Natl Acad Sci U S A* **110**, 16669-74.
- Huang X, Zhang Q, Jiang Y, Yang C, Wang Q, Li L, 2018. Shade-induced nuclear localization of PIF7 is regulated by phosphorylation and 14-3-3 proteins in Arabidopsis. *Elife* **7**.
- Huq E, Al-Sady B, Hudson M, Kim C, Apel K, Quail PH, 2004. Phytochrome-interacting factor 1 is a critical bHLH regulator of chlorophyll biosynthesis. *Science* **305**, 1937-41.
- Hwang G, Zhu JY, Lee YK, *et al.*, 2017. PIF4 Promotes Expression of LNG1 and LNG2 to Induce Thermomorphogenic Growth in Arabidopsis. *Front Plant Sci* **8**, 1320.
- Ibanez C, Delker C, Martinez C, *et al.*, 2018. Brassinosteroids Dominate Hormonal Regulation of Plant Thermomorphogenesis via BZR1. *Curr Biol* **28**, 303-10 e3.

- Iino M, Long C, Wang X, 2001. Auxin- and abscisic acid-dependent osmoregulation in protoplasts of *Phaseolus vulgaris* pulvini. *Plant Cell Physiol* **42**, 1219-27.
- Jaishy B, Abel ED, 2016. Lipids, lysosomes, and autophagy. *J Lipid Res* **57**, 1619-35.
- Jiang B, Shi Y, Zhang X, *et al.*, 2017. PIF3 is a negative regulator of the CBF pathway and freezing tolerance in Arabidopsis. *Proc Natl Acad Sci U S A* **114**, E6695-E702.
- Jung JH, Domijan M, Klose C, *et al.*, 2016. Phytochromes function as thermosensors in Arabidopsis. *Science* **354**, 886-9.
- Kaiserli E, Jenkins GI, 2007. UV-B promotes rapid nuclear translocation of the Arabidopsis UV-B specific signaling component UVR8 and activates its function in the nucleus. *Plant Cell* **19**, 2662-73.
- Keller CP, Van Volkenburgh E, 1996. Osmoregulation by Oat Coleoptile Protoplasts (Effect of Auxin). *Plant Physiol* **110**, 1007-16.
- Keller MM, Jaillais Y, Pedmale UV, Moreno JE, Chory J, Ballare CL, 2011. Cryptochrome 1 and phytochrome B control shade-avoidance responses in Arabidopsis via partially independent hormonal cascades. *Plant J* **67**, 195-207.
- Keuskamp DH, Keller MM, Ballare CL, Pierik R, 2012. Blue light regulated shade avoidance. *Plant Signal Behav* **7**, 514-7.
- Keuskamp DH, Pollmann S, Voeselek LA, Peeters AJ, Pierik R, 2010. Auxin transport through PIN-FORMED 3 (PIN3) controls shade avoidance and fitness during competition. *Proc Natl Acad Sci U S A* **107**, 22740-4.
- Keuskamp DH, Sasidharan R, Vos I, Peeters AJ, Voeselek LA, Pierik R, 2011. Blue-light-mediated shade avoidance requires combined auxin and brassinosteroid action in Arabidopsis seedlings. *Plant J* **67**, 208-17.
- Khanna R, Huq E, Kikis EA, Al-Sady B, Lanzatella C, Quail PH, 2004. A novel molecular recognition motif necessary for targeting photoactivated phytochrome signaling to specific basic helix-loop-helix transcription factors. *Plant Cell* **16**, 3033-44.
- Kidokoro S, Maruyama K, Nakashima K, *et al.*, 2009. The phytochrome-interacting factor PIF7 negatively regulates DREB1 expression under circadian control in Arabidopsis. *Plant Physiol* **151**, 2046-57.
- Kim J, Yi H, Choi G, Shin B, Song PS, Choi G, 2003. Functional characterization of phytochrome interacting factor 3 in phytochrome-mediated light signal transduction. *Plant Cell* **15**, 2399-407.
- Kim K, Jeong J, Kim J, *et al.*, 2016. PIF1 Regulates Plastid Development by Repressing Photosynthetic Genes in the Endodermis. *Mol Plant* **9**, 1415-27.
- Kim S, Hwang G, Kim S, *et al.*, 2020. The epidermis coordinates thermoresponsive growth through the phyB-PIF4-auxin pathway. *Nat Commun* **11**, 1053.
- Kim S, Mochizuki N, Deguchi A, Nagano AJ, Suzuki T, Nagatani A, 2018. Auxin Contributes to the Intraorgan Regulation of Gene Expression in Response to Shade. *Plant Physiology* **177**, 847-62.
- Kohlwein SD, 2010. Obese and anorexic yeasts: experimental models to understand the metabolic syndrome and lipotoxicity. *Biochim Biophys Acta* **1801**, 222-9.
- Kohnen MV, Schmid-Siegert E, Trevisan M, *et al.*, 2016. Neighbor Detection Induces Organ-Specific Transcriptomes, Revealing Patterns Underlying Hypocotyl-Specific Growth. *Plant Cell* **28**, 2889-904.

- Koini MA, Alvey L, Allen T, *et al.*, 2009. High temperature-mediated adaptations in plant architecture require the bHLH transcription factor PIF4. *Curr Biol* **19**, 408-13.
- Kozuka T, Kobayashi J, Horiguchi G, *et al.*, 2010. Involvement of auxin and brassinosteroid in the regulation of petiole elongation under the shade. *Plant Physiol* **153**, 1608-18.
- Kutschera U, Niklas KJ, 2013. Cell division and turgor-driven stem elongation in juvenile plants: a synthesis. *Plant Sci* **207**, 45-56.
- Lau K, Podolec R, Chappuis R, Ulm R, Hothorn M, 2019. Plant photoreceptors and their signaling components compete for COP1 binding via VP peptide motifs. *EMBO J* **38**, e102140.
- Lee CM, Thomashow MF, 2012. Photoperiodic regulation of the C-repeat binding factor (CBF) cold acclimation pathway and freezing tolerance in *Arabidopsis thaliana*. *Proc Natl Acad Sci U S A* **109**, 15054-9.
- Lee KP, Piskurewicz U, Tureckova V, *et al.*, 2012. Spatially and genetically distinct control of seed germination by phytochromes A and B. *Genes Dev* **26**, 1984-96.
- Legris M, Ince YC, Fankhauser C, 2019. Molecular mechanisms underlying phytochrome-controlled morphogenesis in plants. *Nat Commun* **10**, 5219.
- Legris M, Klose C, Burgie ES, *et al.*, 2016. Phytochrome B integrates light and temperature signals in *Arabidopsis*. *Science* **354**, 897-900.
- Leivar P, Monte E, 2014. PIFs: systems integrators in plant development. *Plant Cell* **26**, 56-78.
- Leivar P, Monte E, Al-Sady B, *et al.*, 2008. The *Arabidopsis* phytochrome-interacting factor PIF7, together with PIF3 and PIF4, regulates responses to prolonged red light by modulating phyB levels. *Plant Cell* **20**, 337-52.
- Leivar P, Tepperman JM, Cohn MM, *et al.*, 2012. Dynamic antagonism between phytochromes and PIF family basic helix-loop-helix factors induces selective reciprocal responses to light and shade in a rapidly responsive transcriptional network in *Arabidopsis*. *Plant Cell* **24**, 1398-419.
- Li B, Dewey CN, 2011. RSEM: accurate transcript quantification from RNA-Seq data with or without a reference genome. *BMC Bioinformatics* **12**, 323.
- Li F, Vierstra RD, 2012. Autophagy: a multifaceted intracellular system for bulk and selective recycling. *Trends Plant Sci* **17**, 526-37.
- Li K, Yu R, Fan LM, Wei N, Chen H, Deng XW, 2016. DELLA-mediated PIF degradation contributes to coordination of light and gibberellin signalling in *Arabidopsis*. *Nat Commun* **7**, 11868.
- Li L, Ljung K, Breton G, *et al.*, 2012. Linking photoreceptor excitation to changes in plant architecture. *Genes Dev* **26**, 785-90.
- Li N, Zhang Y, He Y, Wang Y, Wang L, 2020. Pseudo Response Regulators Regulate Photoperiodic Hypocotyl Growth by Repressing PIF4/5 Transcription. *Plant Physiol* **183**, 686-99.
- Li QH, Yang HQ, 2007. Cryptochrome signaling in plants. *Photochem Photobiol* **83**, 94-101.
- Liang T, Mei S, Shi C, *et al.*, 2018. UVR8 Interacts with BES1 and BIM1 to Regulate Transcription and Photomorphogenesis in *Arabidopsis*. *Dev Cell* **44**, 512-23 e5.
- Liang T, Yang Y, Liu H, 2019. Signal transduction mediated by the plant UV-B photoreceptor UVR8. *New Phytol* **221**, 1247-52.

- Liang Y, Jiang C, Liu Y, *et al.*, 2020. Auxin Regulates Sucrose Transport to Repress Petal Abscission in Rose (*Rosa hybrida*). *The Plant Cell* **32**, 3485-99.
- Lilley JL, Gee CW, Sairanen I, Ljung K, Nemhauser JL, 2012. An endogenous carbon-sensing pathway triggers increased auxin flux and hypocotyl elongation. *Plant Physiol* **160**, 2261-70.
- Liu H, Liu B, Zhao C, Pepper M, Lin C, 2011. The action mechanisms of plant cryptochromes. *Trends Plant Sci* **16**, 684-91.
- Liu H, Yu X, Li K, *et al.*, 2008. Photoexcited CRY2 interacts with CIB1 to regulate transcription and floral initiation in Arabidopsis. *Science* **322**, 1535-9.
- Liu Q, Wang Q, Deng W, *et al.*, 2017. Molecular basis for blue light-dependent phosphorylation of Arabidopsis cryptochrome 2. *Nat Commun* **8**, 15234.
- Liu Z, Zhang Y, Wang J, *et al.*, 2015. Phytochrome-interacting factors PIF4 and PIF5 negatively regulate anthocyanin biosynthesis under red light in Arabidopsis seedlings. *Plant Sci* **238**, 64-72.
- Locascio A, Blazquez MA, Alabadi D, 2013. Dynamic regulation of cortical microtubule organization through prefoldin-DELLA interaction. *Curr Biol* **23**, 804-9.
- Lofke C, Luschig C, Kleine-Vehn J, 2013. Posttranslational modification and trafficking of PIN auxin efflux carriers. *Mech Dev* **130**, 82-94.
- Lorrain S, Allen T, Duek PD, Whitelam GC, Fankhauser C, 2008. Phytochrome-mediated inhibition of shade avoidance involves degradation of growth-promoting bHLH transcription factors. *Plant J* **53**, 312-23.
- Los DA, Mironov KS, Allakhverdiev SI, 2013. Regulatory role of membrane fluidity in gene expression and physiological functions. *Photosynth Res* **116**, 489-509.
- Luo Q, Lian HL, He SB, Li L, Jia KP, Yang HQ, 2014. COP1 and phyB Physically Interact with PIL1 to Regulate Its Stability and Photomorphogenic Development in Arabidopsis. *Plant Cell* **26**, 2441-56.
- Ma D, Li X, Guo Y, *et al.*, 2016. Cryptochrome 1 interacts with PIF4 to regulate high temperature-mediated hypocotyl elongation in response to blue light. *Proc Natl Acad Sci U S A* **113**, 224-9.
- Mamode Cassim A, Gouguet P, Gronnier J, *et al.*, 2019. Plant lipids: Key players of plasma membrane organization and function. *Prog Lipid Res* **73**, 1-27.
- Martin G, Rovira A, Veciana N, *et al.*, 2018. Circadian Waves of Transcriptional Repression Shape PIF-Regulated Photoperiod-Responsive Growth in Arabidopsis. *Curr Biol* **28**, 311-8 e5.
- Martinez C, Espinosa-Ruiz A, De Lucas M, Bernardo-Garcia S, Franco-Zorrilla JM, Prat S, 2018. PIF4-induced BR synthesis is critical to diurnal and thermomorphogenic growth. *EMBO J* **37**.
- Mashiguchi K, Tanaka K, Sakai T, *et al.*, 2011. The main auxin biosynthesis pathway in Arabidopsis. *Proc Natl Acad Sci U S A* **108**, 18512-7.
- Mcconn M, Browse J, 1998. Polyunsaturated membranes are required for photosynthetic competence in a mutant of Arabidopsis. *Plant J* **15**, 521-30.
- Mizuno T, Nomoto Y, Oka H, *et al.*, 2014. Ambient temperature signal feeds into the circadian clock transcriptional circuitry through the EC night-time repressor in Arabidopsis thaliana. *Plant Cell Physiol* **55**, 958-76.

- Monte E, Tepperman JM, Al-Sady B, *et al.*, 2004. The phytochrome-interacting transcription factor, PIF3, acts early, selectively, and positively in light-induced chloroplast development. *Proc Natl Acad Sci U S A* **101**, 16091-8.
- Moon J, Zhu L, Shen H, Huq E, 2008. PIF1 directly and indirectly regulates chlorophyll biosynthesis to optimize the greening process in Arabidopsis. *Proc Natl Acad Sci U S A* **105**, 9433-8.
- Moriconi V, Binkert M, Costigliolo C, Sellaro R, Ulm R, Casal JJ, 2018. Perception of Sunflecks by the UV-B Photoreceptor UV RESISTANCE LOCUS8. *Plant Physiol* **177**, 75-81.
- Ni W, Xu SL, Gonzalez-Grandio E, *et al.*, 2017. PPKs mediate direct signal transfer from phytochrome photoreceptors to transcription factor PIF3. *Nat Commun* **8**, 15236.
- Nick P, Han MJ, An G, 2009. Auxin stimulates its own transport by shaping actin filaments. *Plant Physiol* **151**, 155-67.
- Nieto C, Lopez-Salmeron V, Daviere JM, Prat S, 2015. ELF3-PIF4 interaction regulates plant growth independently of the Evening Complex. *Curr Biol* **25**, 187-93.
- Nito K, Kajiyama T, Unten-Kobayashi J, *et al.*, 2015. Spatial Regulation of the Gene Expression Response to Shade in Arabidopsis Seedlings. *Plant Cell Physiol* **56**, 1306-19.
- Nozue K, Covington MF, Duek PD, *et al.*, 2007. Rhythmic growth explained by coincidence between internal and external cues. *Nature* **448**, 358-61.
- Nozue K, Harmer SL, Maloof JN, 2011. Genomic analysis of circadian clock-, light-, and growth-correlated genes reveals PHYTOCHROME-INTERACTING FACTOR5 as a modulator of auxin signaling in Arabidopsis. *Plant Physiol* **156**, 357-72.
- Nozue K, Tat AV, Kumar Devisetty U, *et al.*, 2015. Shade avoidance components and pathways in adult plants revealed by phenotypic profiling. *PLoS Genet* **11**, e1004953.
- Nusinow DA, Helfer A, Hamilton EE, *et al.*, 2011. The ELF4-ELF3-LUX complex links the circadian clock to diurnal control of hypocotyl growth. *Nature* **475**, 398-402.
- Oh E, Kim J, Park E, Kim JI, Kang C, Choi G, 2004. PIL5, a phytochrome-interacting basic helix-loop-helix protein, is a key negative regulator of seed germination in Arabidopsis thaliana. *Plant Cell* **16**, 3045-58.
- Oh E, Zhu JY, Bai MY, Arenhart RA, Sun Y, Wang ZY, 2014. Cell elongation is regulated through a central circuit of interacting transcription factors in the Arabidopsis hypocotyl. *Elife* **3**.
- Oh E, Zhu JY, Wang ZY, 2012. Interaction between BZR1 and PIF4 integrates brassinosteroid and environmental responses. *Nat Cell Biol* **14**, 802-9.
- Oh J, Park E, Song K, Bae G, Choi G, 2020. PHYTOCHROME INTERACTING FACTOR8 Inhibits Phytochrome A-Mediated Far-Red Light Responses in Arabidopsis. *Plant Cell* **32**, 186-205.
- Oravec A, Baumann A, Mate Z, *et al.*, 2006. CONSTITUTIVELY PHOTOMORPHOGENIC1 is required for the UV-B response in Arabidopsis. *Plant Cell* **18**, 1975-90.
- Pacin M, Legris M, Casal JJ, 2013. COP1 re-accumulates in the nucleus under shade. *Plant J* **75**, 631-41.
- Paradez A, Wright A, Ehrhardt DW, 2006. Microtubule cortical array organization and plant cell morphogenesis. *Curr Opin Plant Biol* **9**, 571-8.
- Park E, Kim Y, Choi G, 2018. Phytochrome B Requires PIF Degradation and Sequestration to Induce Light Responses Across a Wide Range of Light Conditions. *The Plant Cell*.

- Park E, Park J, Kim J, Nagatani A, Lagarias JC, Choi G, 2012. Phytochrome B inhibits binding of phytochrome-interacting factors to their target promoters. *Plant J* **72**, 537-46.
- Park YJ, Lee HJ, Ha JH, Kim JY, Park CM, 2017. COP1 conveys warm temperature information to hypocotyl thermomorphogenesis. *New Phytol* **215**, 269-80.
- Pedmale UV, Huang SC, Zander M, *et al.*, 2016. Cryptochromes Interact Directly with PIFs to Control Plant Growth in Limiting Blue Light. *Cell* **164**, 233-45.
- Penfield S, Josse EM, Halliday KJ, 2010. A role for an alternative splice variant of PIF6 in the control of Arabidopsis primary seed dormancy. *Plant Mol Biol* **73**, 89-95.
- Perchorowicz JT, Raynes DA, Jensen RG, 1981. Light limitation of photosynthesis and activation of ribulose biphosphate carboxylase in wheat seedlings. *Proc Natl Acad Sci U S A* **78**, 2985-9.
- Pham VN, Kathare PK, Huq E, 2018. Phytochromes and Phytochrome Interacting Factors. *Plant Physiol* **176**, 1025-38.
- Pierik R, Cuppens ML, Voeseek LA, Visser EJ, 2004. Interactions between ethylene and gibberellins in phytochrome-mediated shade avoidance responses in tobacco. *Plant Physiol* **136**, 2928-36.
- Pierik R, Djakovic-Petrovic T, Keuskamp DH, De Wit M, Voeseek LA, 2009. Auxin and ethylene regulate elongation responses to neighbor proximity signals independent of gibberellin and della proteins in Arabidopsis. *Plant Physiol* **149**, 1701-12.
- Ponnu J, Riedel T, Penner E, Schrader A, Hoecker U, 2019. Cryptochrome 2 competes with COP1 substrates to repress COP1 ubiquitin ligase activity during Arabidopsis photomorphogenesis. *Proc Natl Acad Sci U S A*.
- Procko C, Burko Y, Jaillais Y, Ljung K, Long JA, Chory J, 2016. The epidermis coordinates auxin-induced stem growth in response to shade. *Genes Dev* **30**, 1529-41.
- Procko C, Crenshaw CM, Ljung K, Noel JP, Chory J, 2014. Cotyledon-Generated Auxin Is Required for Shade-Induced Hypocotyl Growth in Brassica rapa. *Plant Physiol* **165**, 1285-301.
- Pucciariello O, Legris M, Costigliolo Rojas C, *et al.*, 2018. Rewiring of auxin signaling under persistent shade. *Proc Natl Acad Sci U S A* **115**, 5612-7.
- Qiu Y, Li M, Kim RJ, Moore CM, Chen M, 2019. Daytime temperature is sensed by phytochrome B in Arabidopsis through a transcriptional activator HEMERA. *Nat Commun* **10**, 140.
- Qiu Y, Li M, Pasoreck EK, *et al.*, 2015. HEMERA Couples the Proteolysis and Transcriptional Activity of PHYTOCHROME INTERACTING FACTORs in Arabidopsis Photomorphogenesis. *Plant Cell* **27**, 1409-27.
- Qiu Y, Pasoreck EK, Reddy AK, *et al.*, 2017. Mechanism of early light signaling by the carboxy-terminal output module of Arabidopsis phytochrome B. *Nat Commun* **8**, 1905.
- Rayle DL, Cleland RE, 1992. The acid growth theory of auxin-induced cell elongation is alive and well. *Plant Physiol* **99**, 1271-4.
- Reed JW, Wu MF, Reeves PH, *et al.*, 2018. Three Auxin Response Factors Promote Hypocotyl Elongation. *Plant Physiol* **178**, 864-75.
- Ren H, Gray WM, 2015. SAUR Proteins as Effectors of Hormonal and Environmental Signals in Plant Growth. *Mol Plant* **8**, 1153-64.
- Ritchie ME, Phipson B, Wu D, *et al.*, 2015. limma powers differential expression analyses for RNA-sequencing and microarray studies. *Nucleic Acids Res* **43**, e47.

- Ritz T, 2011. Quantum effects in biology: Bird navigation. *Procedia Chemistry* **3**, 262-75.
- Rizzini L, Favory JJ, Cloix C, *et al.*, 2011. Perception of UV-B by the Arabidopsis UVR8 protein. *Science* **332**, 103-6.
- Robinson MD, McCarthy DJ, Smyth GK, 2010. edgeR: a Bioconductor package for differential expression analysis of digital gene expression data. *Bioinformatics* **26**, 139-40.
- Roig-Villanova I, Bou J, Sorin C, Devlin PF, Martinez-Garcia JF, 2006. Identification of primary target genes of phytochrome signaling. Early transcriptional control during shade avoidance responses in Arabidopsis. *Plant Physiol* **141**, 85-96.
- Roig-Villanova I, Bou-Torrent J, Galstyan A, *et al.*, 2007. Interaction of shade avoidance and auxin responses: a role for two novel atypical bHLH proteins. *EMBO J* **26**, 4756-67.
- Sakuraba Y, Jeong J, Kang MY, Kim J, Paek NC, Choi G, 2014. Phytochrome-interacting transcription factors PIF4 and PIF5 induce leaf senescence in Arabidopsis. *Nat Commun* **5**, 4636.
- Sasidharan R, Chinnappa CC, Staal M, *et al.*, 2010. Light quality-mediated petiole elongation in Arabidopsis during shade avoidance involves cell wall modification by xyloglucan endotransglucosylase/hydrolases. *Plant Physiol* **154**, 978-90.
- Sasidharan R, Keuskamp DH, Kooke R, Voeselek LA, Pierik R, 2014. Interactions between auxin, microtubules and XTHs mediate green shade-induced petiole elongation in Arabidopsis. *PLoS One* **9**, e90587.
- Sellaro R, Yanovsky MJ, Casal JJ, 2011. Repression of shade-avoidance reactions by sunfleck induction of HY5 expression in Arabidopsis. *Plant J* **68**, 919-28.
- Shalitin D, Yang H, Mockler TC, *et al.*, 2002. Regulation of Arabidopsis cryptochrome 2 by blue-light-dependent phosphorylation. *Nature* **417**, 763-7.
- Shalitin D, Yu X, Maymon M, Mockler T, Lin C, 2003. Blue light-dependent in vivo and in vitro phosphorylation of Arabidopsis cryptochrome 1. *Plant Cell* **15**, 2421-9.
- Shatz O, Holland P, Elazar Z, Simonsen A, 2016. Complex Relations Between Phospholipids, Autophagy, and Neutral Lipids. *Trends Biochem Sci* **41**, 907-23.
- Shi H, Shen X, Liu R, *et al.*, 2016. The Red Light Receptor Phytochrome B Directly Enhances Substrate-E3 Ligase Interactions to Attenuate Ethylene Responses. *Dev Cell* **39**, 597-610.
- Shin AY, Han YJ, Baek A, *et al.*, 2016. Evidence that phytochrome functions as a protein kinase in plant light signalling. *Nat Commun* **7**, 11545.
- Song Y, Yang C, Gao S, Zhang W, Li L, Kuai B, 2014. Age-triggered and dark-induced leaf senescence require the bHLH transcription factors PIF3, 4, and 5. *Mol Plant* **7**, 1776-87.
- Sorin C, Salla-Martret M, Bou-Torrent J, Roig-Villanova I, Martinez-Garcia JF, 2009. ATHB4, a regulator of shade avoidance, modulates hormone response in Arabidopsis seedlings. *Plant J* **59**, 266-77.
- Soy J, Leivar P, Gonzalez-Schain N, *et al.*, 2016. Molecular convergence of clock and photosensory pathways through PIF3-TOC1 interaction and co-occupancy of target promoters. *Proc Natl Acad Sci U S A* **113**, 4870-5.
- Spartz AK, Ren H, Park MY, *et al.*, 2014. SAUR Inhibition of PP2C-D Phosphatases Activates Plasma Membrane H<sup>+</sup>-ATPases to Promote Cell Expansion in Arabidopsis. *Plant Cell* **26**, 2129-42.

- Srivastava AC, Ganesan S, Ismail IO, Ayre BG, 2008. Functional characterization of the Arabidopsis AtSUC2 Sucrose/H<sup>+</sup> symporter by tissue-specific complementation reveals an essential role in phloem loading but not in long-distance transport. *Plant Physiol* **148**, 200-111.
- Stavang JA, Gallego-Bartolome J, Gomez MD, *et al.*, 2009. Hormonal regulation of temperature-induced growth in Arabidopsis. *Plant J* **60**, 589-601.
- Steer MW, Steer JM, 1989. Pollen tube tip growth. *New Phytologist* **111**, 323-58.
- Stepanova AN, Robertson-Hoyt J, Yun J, *et al.*, 2008. TAA1-mediated auxin biosynthesis is essential for hormone crosstalk and plant development. *Cell* **133**, 177-91.
- Stephenson PG, Fankhauser C, Terry MJ, 2009. PIF3 is a repressor of chloroplast development. *Proc Natl Acad Sci U S A* **106**, 7654-9.
- Sun J, Qi L, Li Y, Chu J, Li C, 2012. PIF4-mediated activation of YUCCA8 expression integrates temperature into the auxin pathway in regulating arabidopsis hypocotyl growth. *PLoS Genet* **8**, e1002594.
- Sun TP, 2008. Gibberellin metabolism, perception and signaling pathways in Arabidopsis. *Arabidopsis Book* **6**, e0103.
- Takahashi K, Hayashi K, Kinoshita T, 2012. Auxin activates the plasma membrane H<sup>+</sup>-ATPase by phosphorylation during hypocotyl elongation in Arabidopsis. *Plant Physiol* **159**, 632-41.
- Tan ST, Dai C, Liu HT, Xue HW, 2013. Arabidopsis casein kinase1 proteins CK1.3 and CK1.4 phosphorylate cryptochrome2 to regulate blue light signaling. *Plant Cell* **25**, 2618-32.
- Tao Y, Ferrer JL, Ljung K, *et al.*, 2008. Rapid synthesis of auxin via a new tryptophan-dependent pathway is required for shade avoidance in plants. *Cell* **133**, 164-76.
- Tavridou E, Schmid-Siegert E, Fankhauser C, Ulm R, 2020. UVR8-mediated inhibition of shade avoidance involves HFR1 stabilization in Arabidopsis. *PLoS Genet* **16**, e1008797.
- Teale WD, Paponov IA, Palme K, 2006. Auxin in action: signalling, transport and the control of plant growth and development. *Nat Rev Mol Cell Biol* **7**, 847-59.
- Tilbrook K, Arongaus AB, Binkert M, Heijde M, Yin R, Ulm R, 2013. The UVR8 UV-B Photoreceptor: Perception, Signaling and Response. *Arabidopsis Book* **11**, e0164.
- True JH, Shaw SL, 2020. Exogenous Auxin Induces Transverse Microtubule Arrays Through TRANSPORT INHIBITOR RESPONSE1/AUXIN SIGNALING F-BOX Receptors. *Plant Physiol* **182**, 892-907.
- Tsugawa H, Cajka T, Kind T, *et al.*, 2015. MS-DIAL: data-independent MS/MS deconvolution for comprehensive metabolome analysis. *Nat Methods* **12**, 523-6.
- Turner S, Kumar M, 2018. Cellulose synthase complex organization and cellulose microfibril structure. *Philos Trans A Math Phys Eng Sci* **376**.
- Valitova JN, Sulkarnayeva AG, Minibayeva FV, 2016. Plant Sterols: Diversity, Biosynthesis, and Physiological Functions. *Biochemistry (Mosc)* **81**, 819-34.
- Vandenbussche F, Vriezen WH, Smalle J, Laarhoven LJ, Harren FJ, Van Der Straeten D, 2003. Ethylene and auxin control the Arabidopsis response to decreased light intensity. *Plant Physiol* **133**, 517-27.
- Verbancic J, Lunn JE, Stitt M, Persson S, 2018. Carbon Supply and the Regulation of Cell Wall Synthesis. *Mol Plant* **11**, 75-94.
- Vineyard L, Elliott A, Dhingra S, Lucas JR, Shaw SL, 2013. Progressive transverse microtubule array organization in hormone-induced Arabidopsis hypocotyl cells. *Plant Cell* **25**, 662-76.

- Wang L, Hart BE, Khan GA, Cruz ER, Persson S, Wallace IS, 2020. Associations between phytohormones and cellulose biosynthesis in land plants. *Ann Bot* **126**, 807-24.
- Wang P, Mugume Y, Bassham DC, 2018a. New advances in autophagy in plants: Regulation, selectivity and function. *Semin Cell Dev Biol* **80**, 113-22.
- Wang Q, Barshop WD, Bian M, *et al.*, 2015. The blue light-dependent phosphorylation of the CCE domain determines the photosensitivity of Arabidopsis CRY2. *Mol Plant* **8**, 631-43.
- Wang Q, Liu Q, Wang X, Zuo Z, Oka Y, Lin C, 2018b. New insights into the mechanisms of phytochrome-cryptochrome coaction. *New Phytol* **217**, 547-51.
- Wang Q, Zuo Z, Wang X, *et al.*, 2016. Photoactivation and inactivation of Arabidopsis cryptochrome 2. *Science* **354**, 343-7.
- Wang ZY, Bai MY, Oh E, Zhu JY, 2012. Brassinosteroid signaling network and regulation of photomorphogenesis. *Annu Rev Genet* **46**, 701-24.
- Won C, Shen X, Mashiguchi K, *et al.*, 2011. Conversion of tryptophan to indole-3-acetic acid by TRYPTOPHAN AMINOTRANSFERASES OF ARABIDOPSIS and YUCCAs in Arabidopsis. *Proc Natl Acad Sci U S A* **108**, 18518-23.
- Wu J, Wang W, Xu P, *et al.*, 2019. phyB Interacts with BES1 to Regulate Brassinosteroid Signaling in Arabidopsis. *Plant Cell Physiol* **60**, 353-66.
- Xie L, Yang C, Wang X, 2011. Brassinosteroids can regulate cellulose biosynthesis by controlling the expression of CESA genes in Arabidopsis. *J Exp Bot* **62**, 4495-506.
- Xu F, He S, Zhang J, *et al.*, 2018. Photoactivated CRY1 and phyB Interact Directly with AUX/IAA Proteins to Inhibit Auxin Signaling in Arabidopsis. *Mol Plant* **11**, 523-41.
- Yang C, Xie F, Jiang Y, Li Z, Huang X, Li L, 2018a. Phytochrome A Negatively Regulates the Shade Avoidance Response by Increasing Auxin/Indole Acidic Acid Protein Stability. *Dev Cell* **44**, 29-41 e4.
- Yang X, Montano S, Ren Z, 2015. How Does Photoreceptor UVR8 Perceive a UV-B Signal? *Photochem Photobiol* **91**, 993-1003.
- Yang Y, Liang T, Zhang L, *et al.*, 2018b. UVR8 interacts with WRKY36 to regulate HY5 transcription and hypocotyl elongation in Arabidopsis. *Nat Plants* **4**, 98-107.
- Yeh KC, Lagarias JC, 1998. Eukaryotic phytochromes: Light-regulated serine/threonine protein kinases with histidine kinase ancestry. *Proceedings of the National Academy of Sciences* **95**, 13976-81.
- Yu M, Cui Y, Zhang X, Li R, Lin J, 2020. Organization and dynamics of functional plant membrane microdomains. *Cell Mol Life Sci* **77**, 275-87.
- Yu X, Klejnot J, Zhao X, *et al.*, 2007. Arabidopsis cryptochrome 2 completes its posttranslational life cycle in the nucleus. *Plant Cell* **19**, 3146-56.
- Yu X, Sayegh R, Maymon M, *et al.*, 2009. Formation of nuclear bodies of Arabidopsis CRY2 in response to blue light is associated with its blue light-dependent degradation. *Plant Cell* **21**, 118-30.
- Zhang Y, Liu Z, Chen Y, He JX, Bi Y, 2015. PHYTOCHROME-INTERACTING FACTOR 5 (PIF5) positively regulates dark-induced senescence and chlorophyll degradation in Arabidopsis. *Plant Sci* **237**, 57-68.
- Zhang Y, Pfeiffer A, Tepperman JM, *et al.*, 2020. Central clock components modulate plant shade avoidance by directly repressing transcriptional activation activity of PIF proteins. *Proc Natl Acad Sci U S A* **117**, 3261-9.

- Zhao Y, Christensen SK, Fankhauser C, *et al.*, 2001. A role for flavin monooxygenase-like enzymes in auxin biosynthesis. *Science* **291**, 306-9.
- Zhong S, Shi H, Xue C, *et al.*, 2012. A molecular framework of light-controlled phytohormone action in Arabidopsis. *Curr Biol* **22**, 1530-5.
- Zhu J-Y, Oh E, Wang T, Wang Z-Y, 2016. TOC1–PIF4 interaction mediates the circadian gating of thermoresponsive growth in Arabidopsis. *Nature Communications* **7**.
- Zuo ZC, Meng YY, Yu XH, *et al.*, 2012. A study of the blue-light-dependent phosphorylation, degradation, and photobody formation of Arabidopsis CRY2. *Mol Plant* **5**, 726-33.